Sediment transport in meandering river channels with overbank flow

by
Thomas Buckland Bryant

University of Bristol

A dissertation submitted to the University of Bristol in accordance with the requirements of the degree of Doctor of Philosophy in the Faculty of Engineering

Department of Civil Engineering

December 1999

Word Count: 54,862

Abstract

The purpose of this investigation is to increase understanding of the behaviour of flow and sediment transport in two stage meandering channels with mixed grain mobile beds.

The author conducted a large-scale physical model test at Hydraulics Research Wallingford (UK), in association with a team of investigators. The experiment formed part of a ten-year experimental program examining two-stage channels. Earlier tests in the program examined straight and meandering two stage channels, initially with fixed beds and subsequently with mobile beds of uniform grain size.

The reported tests were performed at bankfull and two overbank depths, with first smooth and then rough floodplains. Three dimensional flow velocities were measured using an ADV probe over the bed in a mobile state. Innovative techniques devised by the author for the automated collection and processing of data are presented. Bedload transport was measured using a scaled down Helley Smith sampler. A further investigation into vegetative floodplain roughness was also performed

Measurements of primary and secondary velocities are presented and discussed. Recorded discharges are compared with those obtained via the F* approach and the James and Wark predictive method. Discrepancies are explained and a new predictive method based on momentum transfer proposed.

The effects of overbank flow on the global sediment transport rates are examined.
The rates and grading curve of sediment transport are calculated using the Ackers White, van Rijn and Engelund and Hansen Equations and compared with the measured results. The reasons for the variation between measured and predicted transport rates are postulated and an improved method for the application of current models to sediment transport problems in this context is suggested. In addition the experiments provide a valuable data bank for the training and calibration of numerical models.

Dedication and acknowledgements

The author would like to gratefully acknowledge the help, generosity, patience, wisdom and supervision he has received from Professor Robert H. J. Sellin and Dr John H. Loveless, over the course of this research.

I am also indebted to the co-investigators on the project, Dr Richard Hey and Dr Peter Wormleaton for their advice and support and to my friend and colleague Sarah Catmur for sharing the experimental burden.

Many thanks to the staff at H R Wallingford in particular Mary Johnstone for helping to run the facility and to Dr Roger Bettesss for his excellent direction and good humour.

I would also like to thank my other colleagues and friends who shared my time at Bristol University. Thanks especially to Catherine Wilson and Damion Debski for their friendship and advice in the preparatory stages. Writing up has been greatly aided and enlivened by the support and camaraderie in 1.20 Queens Building. In particular thanks to Daniel Fox, Mike Walkden, Ahmed Musa Siyam and the invaluable Dr Breac MacLeod

Finally I would like to dedicate this work to my wife Dr Hannah Bryant for her constant physical and emotional support and her belief in me.

Authors Declaration

I declare that the work in this dissertation was carried out in accordance with the Regulations of the University of Bristol. The work is original except where indicated by special reference in the text and no part of the dissertation has been submitted for any other degree.

Any views expressed in the dissertation are those of the author and in no way represent those of the University of Bristol.

The dissertation has not been presented to any other University for examination either in the United Kingdom or overseas

SIGNED:  DATE: 7th June 2000

Table of Contents

Notation

The following list is broken down into the following sub-lists:
Hydraulic Geometry, Sediment Properties, Flow Parameters and Sediment Transport Parameters.
Notation specific to particular theories is presented in the relevant section under the name of the theory.

Hydraulic geometry of meandering natural bed two stage channels

λ	meander wave length
ω	angle of main channel flow to floodplain at crossover
θ	angle of main channel flow to floodplain slope
A	cross sectional area
AR	aspect ratio of deeper main channel
B	top width of deeper main channel
H	average depth of flow in deeper main channel, = A_{1V}/B
h	hydraulic mean depth of main channel, = A_{bf}/B
R	hydraulic radius
r	sinuosity
S	bed slope of main channel
S_0	longitudinal bed slope of main flood plain/Valley
S/r	longitudinal bed slope of meandering deeper main channel
W_m	width of meander belt
Wt	total floodplain width
WR	width ratio (Wm/Wt)
S_s	cotangent of main channel side slope (Horizontal/Vertical)

Sediment Properties

d_i	sieve diameter of ith percentage passing, i = 50 if no subscript is present
σ_g	standard deviation of sediment sample g
sf	shape factor
ρ_s	sediment density
s	ratio of specific mass of solid phase to fluid phase
γ_s	specific weight of sediment

Fluid Flow Parameters

α	energy coefficient
β	momentum coefficient
τ_b	bed shear

υ	kinematic viscosity
C	Chezy coefficient
f	Darcy friction factor
Fr	Froude number
g	gravitational constant
K_s	equivalent sand grain roughness
n	Manning's coefficient
n'	Manning's coefficient including bend losses
Q	discharge
q	discharge per unit width
Re	Reynolds Number
Re*	Grain Reynolds Number
S	main channel gradient
S_0	floodplain gradient
u,v,w	point velocity in x,y and z directions respectively
u^*	point shear velocity
U*	channel shear velocity
U*'	grain shear velocity
U*''	form shear velocity
X	displacement down floodplain
x	displacement down main channel
Y	horizontal displacement across floodplain normal to the floodplain slope
y	horizontal displacement across main channel normal to the channel bank
z	vertical displacement from floodplain level

F* Approach

F*	actual measured discharge/theoretical discharge
DR	relative depth of flood plain compared with main channel (H - h)/H

James and Wark Method

C_{sl}	length coefficient for expansion and contraction losses, zone 2H
C_{ssc}	side slope coefficient for contraction loss, zone 2H
C_{sse}	side slope coefficient for expansion loss, zone 2H
C_{wd}	shape coefficient for expansion and contraction losses, zone 2H
c	coefficient in equation for zone 1H adjustment factor
F_1	factor for non-friction losses in zone 2H associated with main channel geometry
F_2	factor for additional non-friction losses in zone 2H associated with main channel sinuosity

f'	ratio of floodplain and main channel Darcy Weisbach friction factors
K	coefficient in equation for zone 1H adjustment factor
K_e	factor for expansion and contraction losses in zone 2
K_c	contraction coefficient
m	coefficient in equation for zone 1 adjustment factor
W_{2H}	width of zone 2

Momentum transfer method

F_{mt}	The force equivalent to the transfer of momentum between main channel and floodplains

Floodplain Roughness

A_i	the projected area of the i th plant in the streamwise direction.
C_D	the drag coefficient for vegetation
C_O	the orifice coefficient
d	diameter of rods
F_{drag}	the drag force
F_{ROD}	the form drag of the rods per unit length of the channel
F_t	total drag per unit length of channel
f_t	overall friction factor
n_i	Manning's roughness coefficient pertaining to variable i
N	number of rods per unit channel length
p	the percentage of openings in the hedgerow (porosity)
r	number of rods in each row.
S_g	slope caused by the bed roughness
S_h	slope caused by the resistance of the hedges
S_t	total slope
V_i	the average approach velocity to the i th plant
V	approach velocity.
z	flow depth

Greek Symbols

β	blockage coefficient
Δ_1, Δ_2	cross stream and streamwise spacing of roughness rods
ϕ	roughness strip spacing

Sediment transport parameters

General

C_v	sediment concentration by volume
d	sediment size

d_*	non-dimensional sediment size
D	depth of flow
τ_*	Shields stress (dimensionless)
τ_{scr}	Shields critical shear stress
τ_{cr}	critical stress

Ackers - White

A_{gr}	threshold of mobility
C_{gr}	coefficient in transport formula
F_{gr}	sediment mobilisation parameter
G_{gr}	dimensionless transport rate
m	exponent of transport formula
n_{gr}	a transitional parameter varying from 1.0 for fine sediments to 0 for
coarse	material

Engelund and Hansen

ϕ	dimensionless sediment discharge

van Rijn + Hiding Functions

d_a	scaling size
d_g	*sediment geometric mean particle size*
$\tau_{scr,i}$	Shields critical shear stress for fraction i
$\tau_{cr,i}$	Critical stress for fraction i

Subscripts

bf	bankfull
calc	calculated
meas	measured
1H, 2H	zones 1 and 2 with horizontal division lines
1V, 2V	zones 1 and 2 with vertical division lines
3l, 3r	zone 3 on the left and right floodplain

Table of Figures

List of Tables

1. Introduction: Sediment Transport in Meandering river channels with overbank flow

1.1. The river system: A wide ranging overview of the river system with discussion of systems approach vs. reductionist approach

Scientific study involves controlled observation of nature to discover the patterns, which describe its behaviour. In the speciality of civil engineering, we are concerned with quantifying those patterns and using our observations to inform safe design.

Nature is rarely simple. In the case of the river, there are multiple layers of systems of variables, all of which affect the river's behaviour. Overbank flow increases this diversity of influences, the qualities of the floodplain as well as those of the main channel becoming factors in the river's behaviour.

In order to unravel some of the variables to which this study is exposed, the following introduction examines the river considering the importance of the various subsystems present. This context is important if the tools that are developed from the work are to be of any benefit when faced with real world problems rather than the simplicity of the laboratory.

1.1.1. The physical system

The variables in a river system include water discharge (Q), Sediment Discharge (Q_s), Channel Width (B), flow depth (D), Mean velocity (U) hydraulic radius (R), channel slope (S) and friction factor (F). Whether or not these are dependant or independent variables, depends to some extent on the period over which the river is being studied.

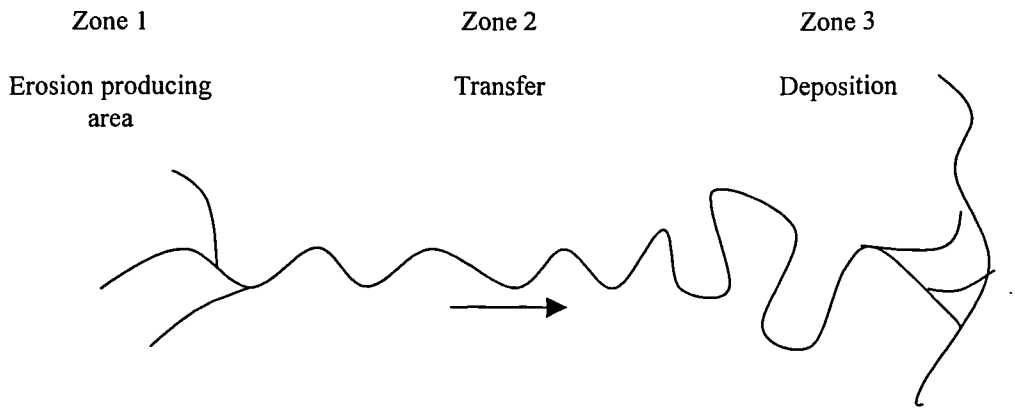

Figure 1.1 The Fluvial system (after Schumm, 1977)

The pattern of river development shown above is common to all rivers to some extent. The watershed is the major source of water and sediment, the transfer zone, carries this load to the sea or lake where it is deposited as a delta at the mouth of the river.

The diagram shows that there is stark difference between the different channel forms. Considerable work has been done to identify the thresholds at which rivers change their planform. Examples are given in Lane (1957) and Leopold and Wolman (1957). It has been proposed that for a river system to reach equilibrium, its transport capacities for water and sediment, must be equal to the rate at which these are supplied. In order to achieve this balance the river must change its slope and hence its planform.
The bankfull flow is generally considered to determine the course of a river. This is the inbank flow with the highest potential to transport sediment. The sediment carrying capacity of overbank flow is considered to be mainly absorbed by the rough floodplain. These processes will be explored in considerably greater depth in the rest of this thesis

1.1.2. The chemical and biological systems

The river system creates a habitat suitable for an abundance of life. A good supply of water insures the growth of vegetation, assuming temperature and soil conditions are agreeable. This growth however can effect the river. For example, trees can prevent bank erosion and by shadow prevent the growth of algae instream. In Indian rivers the growth of water hyacinth is a major problem, blocking waterways, increasing flow resistance and making navigation impossible. In remote regions such as British Columbia, studies have highlighted the importance of inbank wood in channel stability. River restoration regularly consists of returning large woody debris to river channels to minimise scour and enhance bank stability.

In Britain, Sellin (1997) has shown a significant seasonal variation of Manning's n in the River Blackwater, attributed to vegetation growth.
Flood plain vegetation is also important. Plants on flood plains vary according to the frequency and duration with which they are flooded. Their flow resistance is also important in the calculation of flood duration.

The river system also provides a natural habitat for many faunas. With the exception of the beaver, which changes its environment more than any other creature save mankind, the river is something that is lived with. Flooding provides a natural culling in some areas, providing a strong and healthy controlled population

1.1.3. Civilisation: The economic and social system

The river system was central to the growth and development of many societies, our attitude to and use of river systems has changed over time. This subject is explored here very briefly.

Human requirements of rivers

The use of rivers for food, water and washing is something that early man shared with many animals. With the development of boat building, rivers became transport routes, important for trade, and exploration of new areas. The development of agriculture meant that rivers became a source of irrigation and, in some cases, fertilisation from sediment washed onto the floodplain. Later, industries developed, such as the wool

industry which require large quantities of water. Power plants also frequently require big water intakes. The river system has also been used as a waste disposal system, carrying factory and human waste to the sea. The recent increase in leisure time experienced by many in the western world has increased the demand for recreational space.

Human problems with rivers

The two major problems with rivers are that they provide a natural boundary and that they flood unpredictably causing problems that will be explored later.

Human response to the river system

Both human requirements and problems have varied in importance throughout the development of civilisations.

The benefits of a river as a transport route and problems as a boundary mean that due to the heavy cost and thus relative scarcity of bridges and fords, a river crossing became an ideal place for a garrison and a market town. The problem of building on a flood plain was unavoidable and thus the first flood defences were built. Dams have been built as flood defences, water storage, for irrigation and latterly recreation.

The development of river transport led to increased canalisation of rivers. Agriculture also encouraged the straightening and deepening of streams to increase space and to reduce flooding. An increasing ability to change the environment has hastened these changes.

Fluvial response to intervention

The river system, physical, biological and social, is responsive to change. The changes that man has made have had mixed effects. Predicting and providing for the effects is the job of the river engineer.

Building on flood plains has reduced the absorbency of the ground, thus vastly increasing the speed with which the water reaches the river system, worsening flooding.

Canalisation has reduced the habitat of some animals and locks have made the passage of fish impossible. In some cases, such as the cut-offs on the Mississippi, the river has reverted to its original course. Some river works need regular and costly maintenance. Changes in flow velocity have also altered habitats for plants and animals.

Water transport has become less important as roads have improved and the development of motor transport has made the industrial use of canals unfeasible.

Introduction of large amounts of waste into the river system has reduced its use as a source of clean water and a habitat.

Heightened awareness of the problems of pollution, advances in farming efficiency, drastic reduction in the use of rivers for transport, and the desire for more recreational space, all promote the need for river restoration. Whilst the majority of industrialised countries' rivers are ugly and inhospitable places, there behaviour as deepened straight channels is reasonably predictable. Just as major work on natural rivers may

have unwanted effects, the removal of concrete banks and deepened bottoms of our rivers must be carried out with caution and work done to predict the effects of such action.

1.2. Aspects of the river system specific to this project

1.2.1. Meandering channels.

The work presented in this thesis is specific to meandering channels. Referring to Figure 1.1, the meandering planform is common to natural rivers in the central section of the river system. The regions through which they run are generally of low slopes and frequently are the most suitable for human habitation. They are thus of great interest to the engineer. Straightening of rivers has been performed in many areas to improve navigation routes or to increase land space. Some of the most dramatic consequences of this policy have occurred on the Mississippi where the river reinstated its meandering path at great economic cost. Due to the naturally meandering nature of rivers, the cost of maintaining a straight channel is high. Often the only way to do so is to build fixed beds and banks, which are environmentally damaging. Even these measures may be insufficient.

1.2.2. Overbank flow

Overbank flow occurs when a river level rises above the bankfull level and spills out onto the floodplain. In natural rivers this tends to occur every one to two years. The financial costs of flooding in the UK are substantial. The flooding in the Midlands in April 1997 caused an estimated £40M of damage. Efforts to reduce this bill have included deepening channels, building levies and construction of artificial two stage channels.

1.2.3. Sediment transport

Due to the danger involved in taking reliable measurements during floods, little is known on the effects of overbank flow on sediment transport rates and river morphology. The behaviour of sediment under such conditions is of interest in the consideration of dam sedimentation, design of water intakes, floodplain replenishment and the release of toxins.

1.3. A model of the required complexity: justification for building a river model and investigation of how realistically processes are simulated

A review of this kind brings to light a wide range of variables affecting a system and helps set in context the results from a model test in which only a selection of these variables are present.

The experiment described and analysed in this thesis is the most recent in a series of tests performed on two stage channels over the past 15 years. These experiments have all contributed to our knowledge of two stage channel hydraulics, however, the relative simplicity of earlier models have not fully described the system.

The model presented examines two stage flow at large scale over a natural bed shape which is responsive in terms of form and sediment transport to the applied flow. As such it is the simplest model available that effectively models the majority of the important variables.

1.3.1. The EPSRC Flood Channel Facility

The EPSRC flood channel facility (FCF) has provided a national centre for flood channel research since it was constructed at Hydraulics Research Wallingford in 1987. The original aim of the facility was to investigate the hydraulic behaviour of rivers and flood attenuation channels when the flow is in an out of bank condition. The investigation has been conducted through three test programs:

Series A: Unidirectional flow in straight prismatic channels with flood plains.

Series B: Flow in meandering channels with floodplains.

Series C: flow in straight and meandering channels with mobile beds.

The size of this experiment avoids many of the scale effects traditionally associated with hydraulic models. The fixed bed channels of the A and B tests were necessary for examination of the fundamental flow behaviour in the two stage channels. However the fixed bed condition is a significant simplification of the mobile bed condition found in most rivers. The transition in the series C tests has significantly increased the complexity of the model including factors such as bed movement, bed forms and time, which were not previously important. The tests described here used mixed grain sediment introducing processes such as lateral sediment sorting and armouring.

The large scale, natural bed shape and mobile boundary make this model perhaps the most complex fundamental river model ever constructed.

1.4. Description and aims of the Series C mixed grain channel tests

The official aims and objectives of the Series C channel tests were as follows.

1.4.1. Aims

"To advance our understanding of the hydraulic behaviour of two-stage river channels and the interaction with mobile bed material." The special aspect of the project is that it concentrates on meandering channels with fixed banks. The industrial significance of these aims is that this project will also aim to provide a design guide with which UK Civil Engineers may make more reliable prediction of overbank flow on river flood-plains

1.4.2. Objectives

The following specific points relate to both bankfull and overbank flow conditions and mixed grain size sediments in a meandering mobile bed channel and they indicate milestones or criteria by which success in a project may be assessed.

- To determine the sediment transport rates and conveyance in each test configuration. (Bristol/QMW/UEA)

- To establish internal flow structures.(Bristol)
- To determine the effect of flood-plain geometry / roughness on the discharge and sediment transport regime.(QMW/UEA)
- To determine the conditions under which bed sediment is deposited on the river flood plain.(Bristol)
- To investigate the introduction of an engineered channel (with reduced flood plain area) over a part of the FCF channel length. (Bristol/QMW/UEA)

1.5. Position of Author with respect to the experiments in terms of time and role

The period of experimentation commenced 6 months into the author's three year contract and lasted for 15 months. The initial 6 months were largely concerned with finding and testing sediment for use in the flume. As a result the majority of the theoretical work has taken place during and subsequent to the experimental work. The author worked on the model with a colleague from another university. The experiments have been divided roughly according to who did the work, however, some overlap was inevitable.

1.5.1. The scope of this thesis

The literature review in Chapter 2 is founded in the theoretical concepts of hydrodynamics and hydraulics. These concepts are then developed to a study of sediment transport, flow in curved channels, overbank flow and flow through vegetation, the four areas of study which overlap in the subject of meandering mobile bed river channels with overbank flow.

Chapter 3 explores the development of the experimental design, commenting on scale and applicability to real river systems.

In Chapter 4, the results from the experiments are presented namely the variation in velocity distribution, bedform, water surface slope and rate of sediment transport with varying flow depth and floodplain roughness.

Chapter 5 explores the flow structure and conveyance in relation to previous tests and the theoretical and empirical predictive methods developed from them. Namely the F* approach and the James and Wark method. A new method developed by the author is also presented based on the transfer of momentum between floodplain and main channel

In Chapter 6 the bulk sediment transport in the channel is compared with that predicted using conventional formulae. Reasons for the discrepancies are examined and new approaches proposed.

The major conclusions from the work are summarised in Chapter 7.

2. Meandering mobile bed river channels with overbank flow and mixed grain sediments: A literature review

2.1. Introduction

As the title of this thesis suggests, the subject under consideration is one in which a number of different lines of research are brought together. These are, the study of hydrodynamics, the more practical application of those theories in river hydraulics, the study of sediment transport with mixed grain sediment as well as the flow resistance properties of floodplain vegetation. Whilst these disciplines are closely interrelated the various processes have historically been divorced in order to obtain elements suitable for the application of the scientific method.

This literature review is presented in a number of sections. The first section introduces the basic hydrodynamic theories on which the study of river flow and sediment transport is based. The next section considers the application of those theories to basic straight fixed bed river channels and to roughened floodplains. At this juncture enough hydraulics has been explored to be able to approach the majority of work on sediment transport. This forms the second part of the chapter. The third section is dedicated to an investigation of the more complex hydrodynamic and sedimentological issues associated with meandering overbank flow on which the research presented in the rest of this thesis is based.

2.2. Hydrodynamics in Rivers

Studies of basic fluid mechanics are based on the concept of an elementary mass or particle of fluid. The fundamental principles, which are used in the solution of problems, are the conservation of mass (the continuity equation) and the conservation of momentum (the Navier-Stokes equations). The derivation of these equations are treated in depth in textbooks such as Schlichting (1968).

Viscosity refers to the resistance to motion in a fluid resulting from shear or friction between the molecules. The introduction of viscosity to Euler's equations for frictionless flow by which we obtain the Navier Stokes equations gives a correct description of fluid flow. However, the equations are sufficiently complex to make an analytical solution very difficult to reach for in real flow scenarios. For this reason, a large proportion of work on fluid flow relies on experimental data or semi-empirical formulae

2.2.1. Laminar and turbulent flow.

By experiment, Osborne Reynolds in 1883 distinguished two flow regimes in liquid, laminar and turbulent. Using dye injected into a pipe, Reynolds found that at low flow velocities, the dye moved in a straight line with the fluid, this behaviour is now known as laminar flow. The velocity was steadily increased, and at a critical velocity, the dye stream became rapidly diffused across the pipe due to turbulence in the flow. Reynolds also observed that laminar flow was restored at a lower velocity than that at which it had broken down, thus there is an upper and lower limit to the critical velocity. This lower limit has generally proved to be the more important in pipe design as it gives the level at which any

turbulence entering the system will be always be damped out by laminar flow. In hydraulic models where it is important to be operating in turbulent flow conditions the upper limit is more important. In laminar flow the agitation of water particles occurs only on a molecular level. Hence the motion appears to be along parallel paths on a macroscopic level. The shear is completely described by the equation,

$$\tau = \mu \frac{du}{dz} \qquad (2.1)$$

where μ is the kinematic viscosity.

The flow is very stable and the viscosity quickly damps down disturbances in the flow.

Turbulent flow is the normal condition for rivers. In this case, the fluid has lost its laminar structure and inertia forces are dominant. Fluid particles collide randomly, causing continual mixing throughout the fluid.

Reynolds generalised his observations using the dimensionless term now referred to as the Reynold's Number.

$$Re = ul\rho/\mu \qquad (2.2)$$

where l is a characteristic length, for example, pipe diameter or depth in a stream.

Re can be considered as the ratio of the inertial forces to the viscous forces in the flow.

2.2.2. Analysing Turbulence

Interaction between the flow and solid objects such as the banks of a river as well as interaction between flows of different speeds generate turbulence. Defining turbulence precisely is difficult. Tennekes and Lumley (1972) however, produced the following list, describing features of turbulent flow.

1. Irregularity or randomness in time and space.
2. Diffusivity or rapid mixing.
3. High Reynolds number
4. Three Dimensional vorticity fluctuations.
5. Dissipation of the kinetic energy of the turbulent fluctuations.
6. Turbulence is a continuum phenomenon even at the smallest scales.
7. Turbulence is a feature of fluid flows, not a property of the fluids themselves

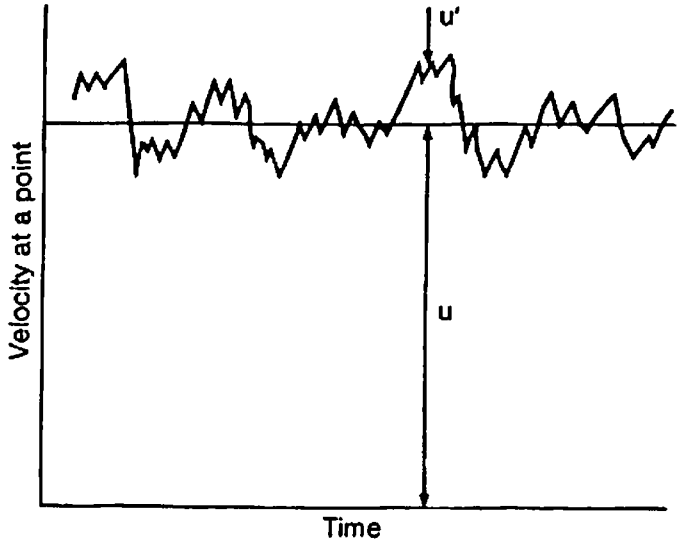

Figure 2.1 Schematic of velocity in turbulent flow

Fluid particles in turbulent flow are observed to travel in randomly moving fluid masses of varying size, called eddies. At a point in the flow, this behaviour can be described as "a rapid and irregular pulsation of velocity about a well defined mean value", thus at any time $u=\overline{u}+u'$. This is described in Figure 2.1. The rms of u' indicates the violence of the turbulent fluctuations in that direction, giving the magnitude of the turbulent fluctuation above the mean value. The relative turbulence is given by rms $u'/\overline{u}$. Turbulent intensity is usually proportional to mean velocity and scale is related to water depth.

2.2.3. Boundary layer theory

An expression for the shear stress in turbulent flow can be found by considering the transfer of momentum between imaginary fluid layers in the flow.

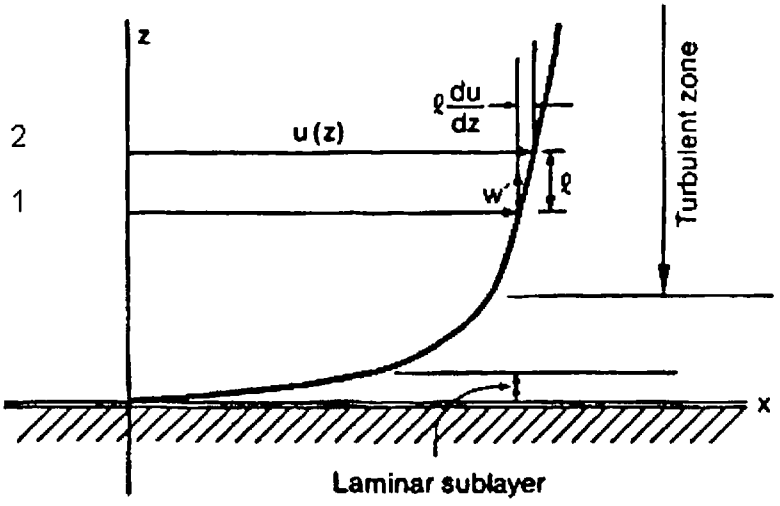

Figure 2.2 Velocities in boundary layer

Consider Figure 2.2. At point 1 the average velocity is u and at point 2, u + Δu. The distance between the points is *l* and the velocity gradient over this distance is given by du/dz if *l* is small. The vertical turbulent velocity w between the layers, is responsible for the transfer of particles travelling at u + Δu moving into the slower layer travelling at u, and vice versa. This has the effect of slowing down the faster moving layer and increasing the speed of the slower moving layer, effectively creating a shear stress between the layers.

Written in the same form as the expression for laminar flow, this behaviour was described by Bousinesq in 1877 as

$$\tau = \varepsilon \frac{du}{dz} \qquad (2.3)$$

The eddy viscosity is a property of the turbulent flow, not of the liquid. This is problematic as it is not constant with displacement. The expression may be more generally written

$$\tau = (\varepsilon + \mu)\frac{du}{dz} \qquad (2.4)$$

to include the transitional region where both laminar and turbulent effects are active.

Reynolds confirmed that the product of the fluctuating velocities in the streamwise and cross stream directions gave the mean shear stress in turbulent flow that could be written as $\tau = -\rho\overline{u'w'}$. This is now known as the Reynolds stress.

Prantl introduced the concept of a mixing length in order to relate turbulent velocities to the general flow characteristics. He postulated that turbulent fluctuations could move small aggradations of particles from one region of velocity to another across a distance *l*, the mixing length. The particles experience a change in velocity due to this transition u'. Prantl postulated that *Δu*, occurring over distance *l* was proportional to u'. and w'. i.e. $ldu/dz \propto u'$ and $ldu/dz \propto w'_y$

Considering Reynolds term for shear stress, this becomes

$$\tau = \rho l^2 \left(\frac{du}{dz}\right)^2 \qquad (2.5)$$

Von Karman suggested the relationship $l = \kappa z$ to relate the mixing length to the distance from the boundary. The resulting equation is

$$\tau = \rho(\kappa z)^2 \left(\frac{du}{dz}\right)^2 \qquad (2.6)$$

The linear relationship of *l* to distance from the boundary is confirmed by experiment.

2.2.4. Shear Velocity

To this point shear in a viscous fluid has been described in terms of the shear stress τ. It is dimensionally convenient to describe shear in terms of the shear velocity, u_*.

Where $$u_* = \left(\frac{\tau_o}{\rho}\right)^{0.5} \quad (2.7)$$

And τ_0 is the boundary shear.

This description of fluid shear will be used throughout the remaining text.

Subsitituting Equation 2.7 into Equation 2.6 we obtain

$$\kappa z \frac{du}{dz} = u_* \quad (2.8)$$

Integrating this equation results in the basic form of the boundary layer equation.

$$\frac{u}{u_*} = \frac{1}{\kappa} \ln z + C \quad (2.9)$$

The evaluation of the constants in this expression depends on the conditions at the fluid boundary. Boundaries are characterised as hydraulically smooth where a sublayer of laminar flow exists, as hydraulically rough where the flow is fully turbulent to the wall and transitional were the sublayer does not completely cover all the roughness elements.

2.3. Basic Hydraulics

2.3.1. Categorisation of river flow

Open channel flow is often defined by the changes that occur in the depth and velocity of flow with respect to time or distance. 'Steady flow' describes conditions where the flow rate does not change with time. If fluctuations in flow depth do occur with time, the flow is termed 'unsteady'.

Uniform flow, describes a condition where the flow depth does not change along the channel length; i.e. bed slope and water slope are equal. Non uniform is the term used when changes in depth do occur with distance

Flow may be steady and non uniform, if flow is added or removed, at a constant rate, at points along the stream. Uniform flow however, only ever occurs in practise if the flow is steady.

		Steady	Unsteady
		dD/dt = 0	dD/dt ≠ 0
Uniform	dD/ds= 0	Only achieved in practice in long straight flumes	Theoretically possible but of no practical relevance
Non-Uniform	dD/ds≠00	Can occur if the supply and flows joining and leaving a system are all steady	The common state for most natural river systems

Table 2.1 Categorisation of open channel flow (D = depth of flow)

Uniform flow is very rare in natural channels; it is however an integral assumption in many flow analyses and is the condition which most laboratory studies aim to emulate. Even in a laboratory channel however real uniform flow is only achieved in a long straight flume. In order to be able to use formulae designed for uniform flow in more complex scenarios, the rules must be relaxed.

Non-uniform flow can be further subdivided into gradually varied flow, e.g. water flowing into a reservoir, and rapidly varied flow, e.g. a hydraulic jump. Gradually varied flow can be approximated to normal flow at a section.

2.3.2. Channel shear stress

The channel shear stress is derived by balancing the weight of water in the down stream direction, for a unit length of channel. This may be written $w_s = \rho g A s$, where A is the cross sectional area and S is the water surface slope against the resistance due to the channel perimeter, $\text{resistance} = \tau_b P$, where P is the wetted perimeter and τ_b the bed shear stress.

$$\textit{Thus } \tau_b = \rho g \frac{A}{P} S \qquad (2.10)$$

2.3.3. Uniform flow formula

The basic design tool used by engineers for establishing the relationship between flow depth and discharge are the uniform flow formulae. They relate the discharge to basic variables in river flow such as slope, flow depth channel roughness, geometry etc. Three formulae have achieved widespread use. The simplest and earliest is the Chezy relationship, derived by balancing the flow resistance forces with the force due to the weight of flow.

$$U = C(RS)^{0.5} \qquad (2.11)$$

Where C is the empirically determined Chezy coefficient. Manning's equation has been found to vary less with depth than Chezy's and is given by

$$U = \frac{1}{n} R^{2/3} S^{1/2} \qquad (2.12)$$

Tables relating n and C to surface types and pictures of channels may be found in Chow (1959) and other text books. Significant criticisms have been levelled at both of these formulae. The constants are not dimensionless and vary with depth, particularly in the case of vegetated channels. They also account for a wide range of varying energy losses. The Darcy Weisbach equation, originally developed from pipe flow goes some way to answering these objections. Darcy f is given by

$$f = \frac{4\tau_b}{\frac{1}{2}\rho U^2} \qquad (2.13)$$

Where τ_0 is the shear stress at the boundary given by ρgRS. Substituting this value for τ_0 we obtain

$$U = \left(\frac{8gRS}{f}\right)^{1/2} \qquad (2.14)$$

This formula has a relatively sound theoretical basis and f is non-dimensional, however as flow resistance is not simply a function of bed shear it is still depth dependent.

2.3.4. Methods for attributing roughness values to main channels

A range of methods for calculating the roughness of river channels from observation and data collection have been suggested. One simple method involves matching a river channel with a photograph of a river of known roughness. More advanced methods based on the size of sediment in the channel and the sinuosity will be dealt with later in this chapter.

2.4. Floodplain roughness

The preceding section outlined the basic method by which the resistance of river channels is usually determined. The following section considers the calculation of floodplain roughness which is an integral part of the calculation of overbank flows.

2.4.1. The Soil Conservation Service Method

Cowan (1956) developed a procedure for calculating open channel 'n' values based on summing the resistance due to a number of factors and multiplying by a further factor to account for meandering. The Soil Conservation Service (1963) adopted this formula and produced a table of appropriate values. Aldridge and Garret (1973), may be used to adjust the formula for use on floodplains as shown.

$$n = (n_b + n_1 + n_2 + n_3 + n_4)m \qquad (2.15)$$

where

n_b = a base value of n for the flood plain's natural bare soil surface,

n_1 = a correction factor for the effect of the surface irregularities on the floodplain,

n_2 = used to describe resistance due to the variation in the shape and size of a river channel and hence not applicable to the wide floodplain cross section, assumed to equal 0.0,

n_3 = a value for obstructions on the floodplain,

n_4 = a value for vegetation on the floodplain, and

m = a correction factor for sinuosity of the flood plain equal to 1.0 as flow across the flood plain is assumed straight.

Values of n_b are given in Table 1 - Aldridge and Garret (1973), values of n_{1-3} can be found in table 3 of the same source. Typical values of n_4 for different flood plain types are available from a number of sources: natural channels - Barnes (1967), crops - Ree and Crow (1977), Arizona vegetation - Aldridge and Garret (1973), heavily vegetated floodplains - Acrement and Schneider (1989)

Example of the soil conservation service method

A firm soil floodplain n_b = 0.025-0.032, with a few rises and dips n_1 = 0.001-0.005, obstructions occupying 20% of the cross sectional area n_3 = 0.02 - 0.03. The floodplain is covered in turf grass, hence n = 0.05 - 0.1 for flow half the height of the vegetation and n_4= 0.001-0.01 for flow greater than three times the height of the vegetation. Using these values in Equation 2.15 gives a total n value of n = 0.096 - 0.161 for flow half the height of the vegetation and a total n value of n = 0.047 - 0.071 for flow greater than three times the vegetation height.

This equation provides a logical method for determining the flood plain roughness with increasing flow depth. It can be seen however, that a wide range of possible n values can be obtained using this method and that their selection is open to personal interpretation, particularly n_4. For flow over the same floodplain according to this method, n may vary by a factor of 4. It is also unclear whether Cowan's assumption of additive roughness is applicable in all cases. On floodplains where ground vegetation is sufficiently dense to reduce the near bed velocity to very low levels, the roughness contributed by the bed would be significantly less than it would have been had the plants not been present.

2.4.2. Matching Photographs

A second method of determining Manning's n values for a channel, proposed by the U.S. Geological Survey, is based on the photographs presented in Barnes (1967). After training, results suggest that engineers may be able to estimate the roughness of a channel to +/- 15% comparing the channel in question with similar images of channels of known roughness viewed through a three dimensional imager. The method has been extended to floodplains by Acrement and Schneider (1989) and is recommended to give a ball park figure on which to base an estimation of roughness for a particular floodplain.

2.4.3. Rigid non-submerged roughness

Petryk and Bosmajian (1975) developed a relationship between depth and Manning's n for vegetation of known density. The analysis is based on the assumptions that the vegetation is non-submerged, that the velocities are sufficiently low to prevent plant bending and changes in the projected area, and that the plants are evenly spaced.

The force on an individual plant is given by

$$F_{drag} = C_D \rho g A_i \frac{V_i^2}{2g} \qquad (2.16)$$

where F_{drag} = the drag force, C_D = the drag coefficient for vegetation, V_i = the average approach velocity to the i th plant and A_i the projected area of the i th plant in the streamwise direction. The average boundary shear force is given by

$$F_b = \rho g R S L \qquad (2.17)$$

The slope, S, is calculated using the Manning equation with a value of n for the soil surface

Rearranging and summing the forces gives

$$\sum F = \rho g A L S - C_D \rho g \sum A_i \frac{V^2}{2g} - \rho g V^2 n_b^2 \left(\frac{P}{A}\right)^{1/3} P L = 0 \qquad (2.18)$$

Implicit in this arrangement is the assumption that the water surface slope is equal for the vegetation and the bed, which is reasonable if the vegetation is evenly distributed.

Petryk and Bosmajian use data sets provided by Ree (1958) and Ramser (1929) to verify their results. These data sets consist of plots of Manning's n and vegetation density with depth. Entering the data for vegetation density into the equation gives good results for Manning's n. The paper gives correlations for wheat, sorghum, cotton, and four vegetated channel conditions. In order to determine the roughness of a new channel the user must determine the value of $C_D \Sigma A_i/(AL)$ as a function of height. The vegetation density may be found indirectly by analysis of previous floods. The paper outlines the path from finding flow values from the flood and using these to estimate the vegetation density. A direct method, appropriate to heavily wooded flood plains, is to measure the projected area of vegetation in a representative sample section of the floodplain and to extend this data to the rest of the flood plain covered in similar vegetation.

The methods above are all described in detail in Acrement and Schneider (1989) and examples are given.

2.4.4. Rigid, non-submerged, incremental roughness.

The assumption that the water surface slope is equal for the vegetation and the bed is reasonable if the vegetation is evenly distributed. In the case of fields and hedges this clearly is not the case as a large proportion of the head loss occurs when the flow passes through the hedge. Klaassen and Zwaard (1973) performed a two dimensional experimental study at full scale to investigate this condition. Flow through a hedge is given by

$$q = C_O p A \sqrt{2g\left(\Delta h + \frac{V^2}{2g}\right)} \qquad (2.19)$$

Where: q = the discharge in m^3s^{-1}, C_O = the discharge coefficient, p = the percentage of openings in the hedgerow (porosity)

The velocity V is the mean velocity upstream of the hedgerow. Rearranging gives

$$C_O p = \sqrt{\frac{1}{1+\left(\frac{2g\Delta h}{V^2}\right)}} \qquad (2.20)$$

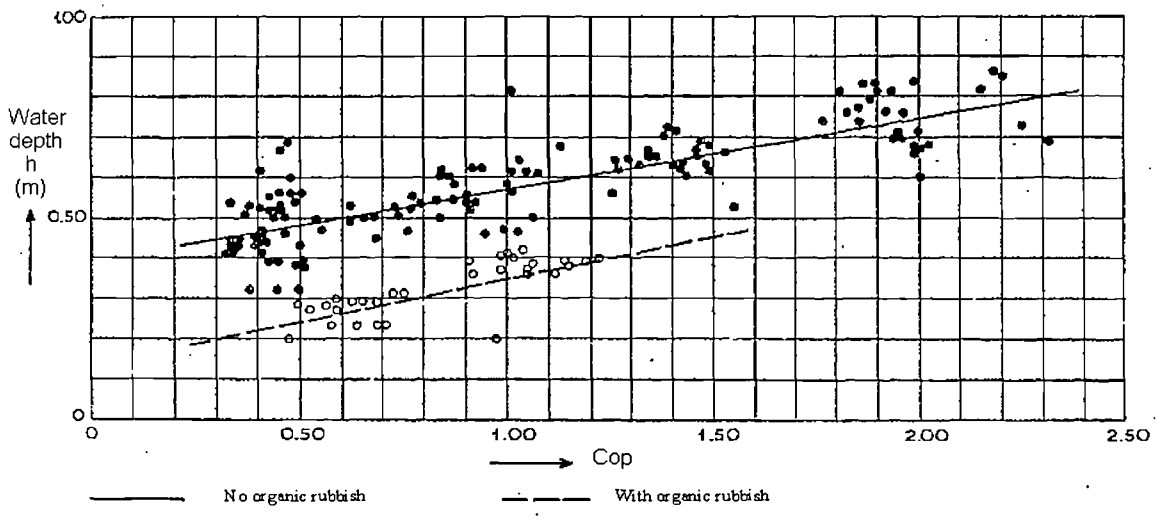

Figure 2.3 Experimental relationship between h and μp for the hedges tested (after Klaasen and Zwaard, 1974)

The authors plot a graph of C_0p against water depth h, showing an increasing value of C_0p with depth. The proposed method for calculating roughness is based on the assumption that the energy gradient of a flow path crossing the hedges is composed of a gradient S_s caused by the surface roughness and a gradient S_e caused by the elemental resistance of the hedges. Thus the total gradient is given by

$$S_t = S_s + S_e \qquad (2.21)$$

Substituting Manning's equation into this formula gives

$$n_t^2 = n_s^2 + \frac{R^{4/3}}{2gd}\left(\frac{1-C_O^2p^2}{C_O^2p^2}\right) \qquad (2.22)$$

2.4.5. Rigid, submerged, incremental roughness

Klaassen and Zwaard (1985) expanded this analysis to over-topped hedges

Considering the hedge as a short crested weir, the discharge over the hedge is given by

$$q = m_0(h-H)\sqrt{2g\left(h+u^2/2g\right)} \qquad (2.23)$$

where q = flow over the hedge per unit width ($m^3/s/m$), H = hedge height.

The total discharge is then given by

$$q_t = q_0(h=H) + q_w = M.h\sqrt{2g\left(h+u^2/2g\right)} \qquad (2.24)$$

where

$$M = \left[\left(C_D p\right)_{h=H}.\frac{H}{h} + m_0.\left(\frac{h-H}{h}\right)\right] \qquad (2.25)$$

This equation is valid assuming that the flow over the hedge is not affected by the flow through it and vice versa. Experimental verification showed that the flow through the hedges had minimal effect on the flow over the hedges and a value of 1.00 is generally applicable for the weir coefficient.

2.4.6. Flexible roughness

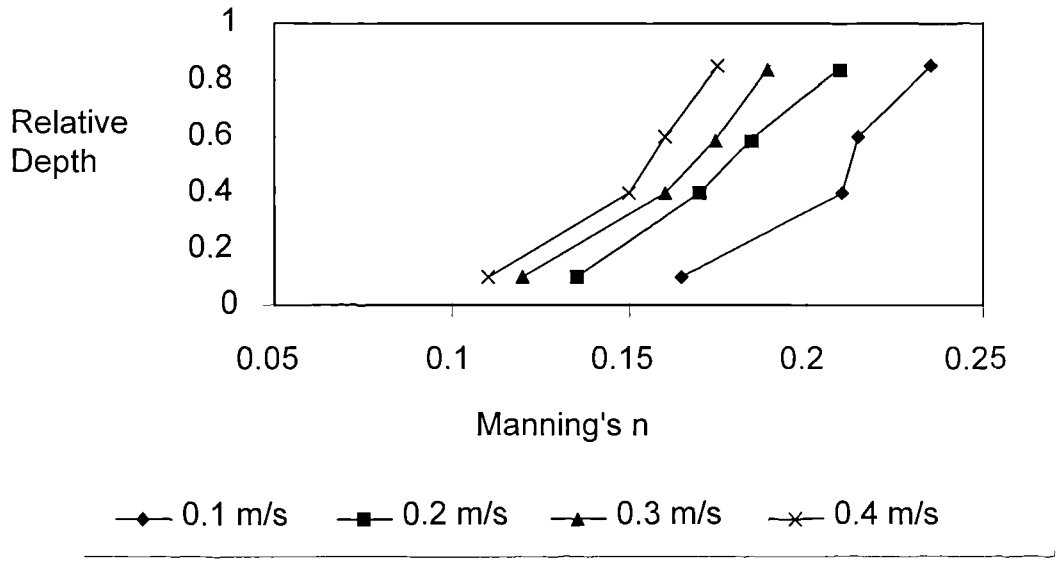

Figure 2.4 Relationship Between Manning's n, Mean Velocity and relative depth of submergence (after Fathi-Maghadam and Kouwen, 1997)

Figure 2.4 shows the variation with flow depth and velocity for a non-submerged pine stand. It can be seen that the value of Manning's n varies between 0.11 and 0.24 with flow depth and velocity.

Introducing the flexibility of vegetation into a resistance formula introduces a further degree of complexity. The resistance is now a function of the flow velocity and plant stiffness as well as the depth of flow and plant density.

By dimensional analysis of variables the roughness is found to be a function of the variables shown below.

$$C_D = f\left(\frac{A}{a}, \frac{h}{z}, \frac{\rho U^2 A_i}{EA_s}, \frac{U^2}{gy_n}, \frac{\rho Uz}{\mu}\right) \qquad (2.26)$$

Where C_D is the discharge coefficient, A the momentum absorbtion areas, a is the horizontal area of vegetation canopy, h is the height of vegetation, z is the flow depth, E is the plant stiffness and A_s the stem area.

Fathi-Maghadam and Kouwen (1997) proceed on the assumptions that the vegetation is a "non-uniform, randomly distributed and densely vegetated array of roughness". In a less densely populated area, flow paths through the vegetation may exist which would cause errors in the analysis.

Further assumptions are that the surface shear on the ground is negligible compared to plant drag and that the flow depth is equal to or less than the maximum height of vegetation.

By further assuming that the resistance is independent of Froude and Reynolds numbers, on the basis that the flow is subcritical and fully turbulent, and multiplying dimensionless variables for drag coefficient, momentum absorbing area and flow depth, Fathi-Maghadam and Kouwen (1997) obtain the following theoretical expression

$$C_D \frac{A}{az} h = f_4\left(\frac{\rho U^2 A_i}{EA_s}\right) \qquad (2.27)$$

However, there is not as yet sufficient experimental evidence to evaluate the form of f_4.
An alternative approach taken by Rahmeyer (1998) was to perform a regression analysis of the dimensionless groups, in this case including the Reynolds number and removing Froude number, as flow is subcritical. The analysis was based on results from 21 test series. For submerged flow C_D is given by

$$C_D = 0.202\left(\frac{A}{a}\right)^{-0.631}\left(\frac{h}{z}\right)^{0.328}\left(\frac{\rho U^2 A_i}{EA_s}\right)^{-0.247}\left(\frac{\rho U z}{\mu}\right)^{-0.156} \qquad (2.28)$$

Both sets of research show that flow resistance decreased with an increase in velocity and decreased with an increase in depth. Flow resistance also decreased with an increase in plant flexibility and a decrease in plant density.

2.4.7. Summary of methods

The following methods are ordered in terms of increasing complexity, accuracy and expense. Acrement and Schneider (1989) recommend the use of the first two methods to achieve ball park figures before further analysis.

Method	Data Required	Advantages	Disadvantages
Experience and intuition	Site visits Photographs	Quick	Requires experience open to errors of judgement
Photo Matching	Site visits Photographs	Quick and widely used - gives a ball park figure for any conditions	No variation with water level.
Use of tabled n values	More detailed information on vegetation type density season etc	Systematic, familiar	Accuracy is deceptive
Rigid roughness formula	Estimation of variation of plant density with depth, appropriate value of C_D	Gives variation with depth	Only applicable to limited conditions: low velocity i.e. no bending
Hedge roughness	C_D value for hedge type	Accounts for flow through hedges	Calibration required
Flexible roughness formula	C_D and EI for all plant types present Estimation of density	The most accurate method for flexible vegetation in a high velocity flow	Only applicable to densely packed vegetation. Each variety requires costly and time consuming experimental analysis

Table 2.2 Summary of methods for predicting vegetative resistance to flow

2.5. Behaviour of loose boundary channels

2.5.1. Historical Background

The phenomenon of sediment transport has been observed for thousands of years. The driving force behind investigations has been to limit or prevent the silting or scouring of rivers or canals. As early as 1 BC Chang observed in Chhien Han Shu that fast water flow will cause scour of a riverbed. The first recorded attempt to study sediment transport in Europe was made by Guglielmini (1690,1697). He wrote " a stream widens and deepens in proportion to the violence of motion which erodes and carries away the earth that forms its sides and bottom". In other writing he shows an appreciation of equilibrium between erosive capacity and bed resistance.

In 1786 Du Buat showed clear recognition of the equilibrium between boundary shear and gravity force. He expressed this in the equation

$$\tau_b P = \gamma A S_0 \qquad (2.29)$$

This equation was used as the basis to an early bed load formula.

Brahms (1873) took critical velocity for the onset of movement as being proportional to the one-sixth power of the weight of the original particles.

He related the boundary shear to the square of the velocity. Equating these two concepts gives an equation relating the critical shear to the particle shape. Throughout the 19th century the criteria for incipient motion was that of a critical shear stress proportional to the linear size of the bed material and in equilibrium with the gravity given in the above equation.

2.5.2. Approach to reviewing the material

Following on from these early investigations the subject of sediment transport has been investigated by many different researchers in a large number of countries resulting in a wide variety of different formulae. In view of the sheer quantity of material available, it is considered unnecessary and unhelpful to include references to all the available theories. Therefore, in this review the author has tried to outline the major arguments in the development of sediment transport and illustrate these with commonly known formulae. Having studied the general history of the development of sediment transport theory the Ackers-White, Engelund and Hansen and van Rijn formulae are presented in more detail, as they will be used later in the thesis. This section is prefaced by considering the properties of sediment in fluid and the resistance to flow from bedforms both of which form a necessary grounding for a study of sediment movement. The section is concluded by an examination of the attempts to deal with the problems of mixed grain size sediment transport and the uses of such formulae in models that this research will hopefully inform.

Finally it should be mentioned that transport of bed load material is the primary focus of this work. As suspended load adds significantly to the scope of the study it is mentioned only in passing. This is a reflection on the time and space available to the author rather than its importance as a transport process.

2.5.3. Sediment properties

The phrase "sediment properties" commonly refers to the size, shape, density, angle of repose and fall velocity of a sediment particle, and the distribution of such properties in a sediment sample. Other properties such as chemical composition are not commonly considered in sediment transport calculations.

Of particular interest in the study of sediment properties are deviations from the assumption of a collection of equally sized spheres often employed in the derivation of sediment transport formulae.

Sediment size and size distribution

The size of sediment particles is an important factor in determining their mobility and the associated hydraulic roughness they generate when situated on a boundary.

There are a number of commonly accepted ways of describing the size of a particle, frequently in terms of an equivalent sphere. The common forms are as follows:

Nominal diameter, the diameter of a sphere having the same diameter of a particle.

Sieve diameter, the diameter of a sphere equal to the length of the side of a square sieve opening through which the given particle will just pass.

Sedimentation diameter which is a sphere having the same specific weight and the same terminal velocity as a particle in the same fluid under the same conditions and

Fall diameter The diameter of a sphere having a specific gravity of 2.65 and the same terminal velocity as the particle when each is allowed to settle in distilled water a 24°C.

Generally size distribution analysis on a sample splits it into a number of different fractions with an upper and lower bound for each fraction based on the diameter of the grain relevant to the method of analysis. For example if sieving is used them it will be the sieve diameter.

Assuming that we have performed sieve analysis on a sediment sample we may present it in a number of ways.

Visualisation of mixed grain sediment distributions

There are two basic ways in which sediment distribution data can be presented: the histogram and the cumulative frequency diagram.

The histogram method of description has the advantage of showing clearly the position of a distribution peak, however it has disadvantages. From one sediment sample we can obtain a range of different histogram shapes depending on the chosen sieve sizes. The discrepancies are reduced as the intervals between the sieve sizes become smaller.

The cumulative frequency diagram has the advantage over the histogram of being independent on the distribution of the sieve sizes used. However as observed by Bagnold (1980) it is not a good way of presenting a particle distribution as it is considerably harder to judge the slope of a curve than the height of a histogram. Krumbein (1934) presented a cumulate frequency diagram as a histogram by using the gradient of the cumulative frequency diagram, thus obtaining the best of both methods.

Scales

Investigators have suggested three scales:

A linear plot of frequency vs. diameter

The phi scale (log-linear = normal distribution)

A hyperbolic distribution (log-log = hyperbolic distribution)

Wentworth 1922 proposed a sediment scale where the base unit was 1 mm and all other grades follow by dividing or multiplying by two. The advantages of this method were that sediments could be graded in convenient units along a continuous curve. It was also used for grading material as sand, gravel, boulders etc.

Based on the Wentworth scale, Krubein 1934 described the phi scale as $\varphi = -\log2(d)$ where d is in mm. Dyer (1986) shows that a typical uniform beach sand is skewed toward the finer end of the range. By plotting against a log curve however, we obtain a log normal distribution so that the distribution may be described in terms of a mean and standard deviations.

Bagnold (1980) argues that the natural frequency of sediment grain size is also logarithmic. When the frequency diagram is plotted on these axes the curve approximates to a hyperbola and not a parabola, as would be the case of the distribution was log normal. A method of statistical description of this system is provided.

Application to the problems of sediment transport

In sediment transport formulae relating to rivers the phi scale is rarely used. Instead representative diameters tend to be favoured. For example, d_{50} refers to the grain size of which 50% of the sample is finer. In cases of mixed sediments a number of representative size fractions may be chosen and the calculation weighted by the proportion of the streambed covered in the fraction of interest.

In the determination of the standard deviation of mixed grain sediment needed for determination of hiding functions the standard deviation is frequently described by the formulation

$$\sigma = (d_{84}/d_{16})^{0.5}$$

This is clearly highly sensitive to the values of the upper and lower quartiles. A series of more consistent approaches have been suggested based on the phi scale. The method used for determination of the standard deviation in this thesis is that proposed by McCammon (1963)

$$\sigma = 2^{-(\phi 70 + \phi 80 + \phi 90 + \phi 97 \quad \phi 3 - \phi 10 - \phi 20 - \phi 30)} \qquad (2.30)$$

Investigation into the nature of sediment is more advanced in coastal engineering than river engineering. The disciplines appear to share common ground which the author has not had time to explore fully.

Shape factor

The shape of a sediment particle has a significant affect on its angle of repose and fall velocity and is hence of importance in sediment transport. Shape factor is commonly described by:

$$SF = \frac{c}{(ab)^{1/2}} \qquad (2.31)$$

Where a, b and c are respectively the lengths of the longest, intermediate and shortest mutually perpendicular axes of the particle.

2.5.4. Bedform properties

Consideration of the role of bed forms in the hydraulics of mobile bed channels is vital for accurate assessment of boundary roughness and bedload sediment transport. This section considers the steps towards determining the bed roughness of an alluvial bed with a view to determining the skin friction at the bed. Summaries of the subject may be found in Chang (1988), Raudkivi (1998), and Yalin (1979). Effects of water temperature, and detailed investigation of upper regime flows are not covered in this study as they were not of importance in the experiments on the flood channel facility.

Classification and characteristics of bed forms

Simons and Richardson (1964) divided bedforms into categories of lower, transitional and upper flow regimes in order of increasing velocities or stream power. The distinctions were made on the basis of similarities in form, resistance to flow and sediment transport

Flow Regime	Bed Form	Bed Material Concentration (ppm)	Mode of Sediment Transport	Type of Roughness	Phase Relation Between Bed and Water Surface
Lower regime	Ripples	10-20		Form	Out of phase
	Ripples on dunes	100-1200	Discrete	Roughness	
	Dunes	200-2000	Steps	Predominates	
Transitional zone	Washed out dunes	1000-3000	____	Variable	____
Upper Regime	Plane Beds	2000-6000	Continuous	Grain	In Phase
	Antidunes	Above 2000		roughness	
	Chutes and pools	Above 2000		predominates	

Table 2.3 Classification of Bed Forms and their Characteristics (After Simons et al., 1965)

A description of each of these bed types is found in Figure 2.5.

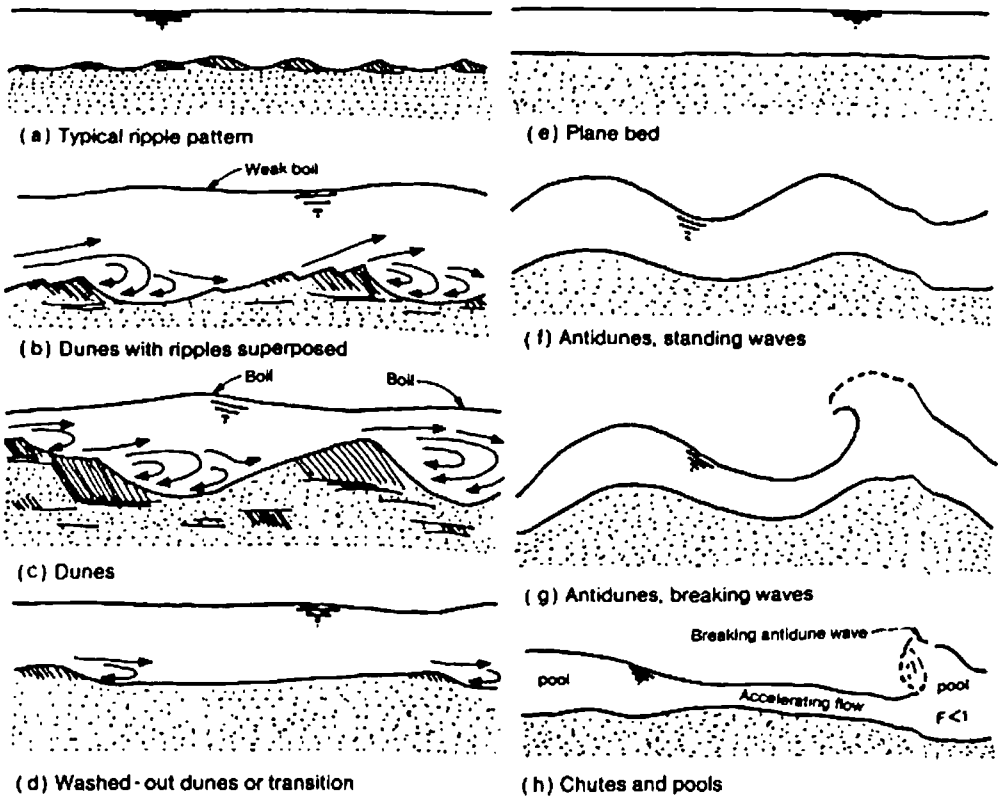

Figure 2.5 Idealised bedforms in alluvial channels (after Simons et al., 1966)

2.5.5. Empirical investigations of skin friction and velocity profiles over bed forms

Raudkivi (1962) reports results from experiments conducted in a clear sided tilting and recirculating flume 2.5m long 75mm wide and 150mm deep containing a sand bed 1520mm long and 375mm deep. Experiments were conducted in conditions as close as possible to uniform flow and the wall effect treated by the Vanoni and Brooks (1952) method. This method was found to be adequate by comparing results for shear velocity with those of a plane sand bed. A ripple bed was formed in the sediment and the velocity profiles measured. The sand ripples were replaced with a galvanised metal replica and the measurements repeated, scatter in the velocity readings was within four percent of the readings over the sand bed. The resultant shear stress distribution is shown in Figure 6.1.

It is clear from the experiment that the shear stress varies over the bed form structure and that the velocity profile is a function of the distance along the bed form.

Smith and McLean (1977) collected field data form a series of dune forms in the Colorado River. Taking velocity profiles at a large number of longitudinal intervals along each dune they spatially averaged the data over one wavelength using the bed level as a datum. The authors presented this data as a log depth vs. normalised velocity plot and suggested that the spatially averaged velocity profile should be divided into upper and lower zones, describing the grain and form roughness respectively. Each zone being described by a log linear plot. The authors assume an expression for the height of the internal boundary

layer, formed downstream of a bed feature and use this as the matching height between the two profiles. Using an expression for the form roughness incorporating a drag coefficient and an extension of Nikuradsee's expression for roughness height the authors obtain an expression for the ratio of grain to form roughness in terms of the bed roughness height, von Karman's constant and the bed form dimensions and drag coefficient.

2.5.6. Bed form predictors

Bed form predictors have been proposed by van Rijn (1984) and others and are summarised in Chang (1988). A more recent procedure based on the work of van Rijn is presented by Bennet (1995).
The prediction of bedforms is important if a better understanding of the flow resistance caused by bedforms and the variation in resistance mechanisms with bedform type is to be obtained.
Despite extensive theoretical studies on the prediction of bed form an acceptable relationship has yet to be determined. Most theoretical models employ a two dimensional flow assumption. A recent approach by Cheong (1998) is an example of a number of studies based on a 2D grid that models the turbulent structures over a dune.
This study concentrates on the empirical methods developed particularly with respect to the lower regime and transitional flows, which are present in the flood channel facility.

From flume data on a sand bed, Simons and Richardson (1964) developed a graphical system of bed form prediction, plotting stream power against median fall diameter. The resultant chart is relatively complicated and covers a limited range of particle size
This approach has subsequently been revisited by a number of authors using alternative prediction parameters. Froude number approaches are unsatisfactory for lower regime flows as dunes and ripples occur in closed conduit flow and can be shown to be independent of free surface effects.

van Rijn(1984c) based his classification on the rate of bed load sediment transport. The terms are those given in his 1984 sediment transport formula

$$d^* = d\left[\frac{(\rho_s - \rho)g}{\rho\upsilon^2}\right]^{1/3} \qquad (2.32)$$

$$T = \frac{\tau'_b - \tau_c}{\tau_c} \qquad (2.33)$$

where τ_c is obtained from the shields curve and τ'_b is taken from the equation below

$$U'_* = \frac{g^{1/2}}{C'}U = \frac{g^{1/2}}{18\log(12R_b)/(3d_{90})}U$$

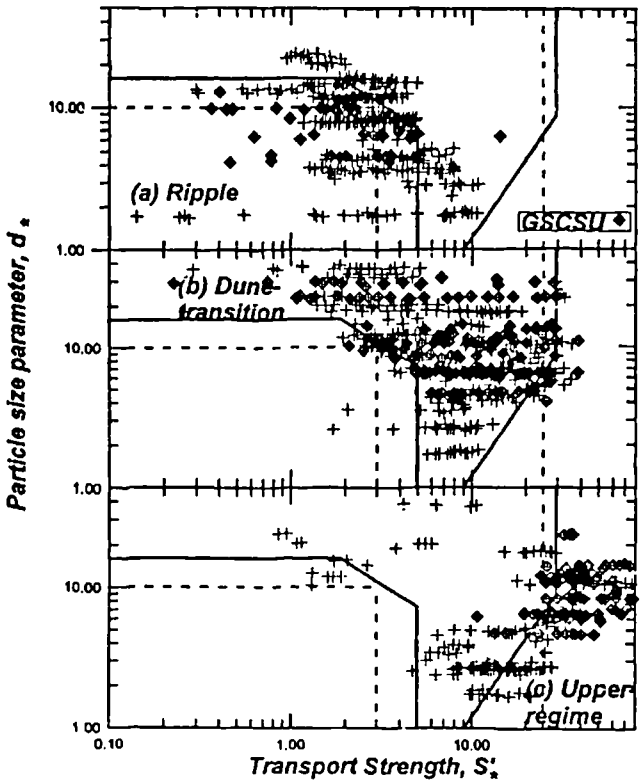

Figure 2.6 Bedform prediction diagram (After Bennet 1995)

van Rijns approach was refined by Bennet (1995). The assumptions behind this development are examined in the section on bed roughness

Bed form dimensions

A discussion of the dimensions of bedforms is found in Yalin (1972), van Rijn (1984c) being a widely used approach.

The effect of water temperature is not considered in this thesis but is highly significant in the determination of bed form shape and alluvial roughness due to the change in the fall velocity of sediment with temperature. In regions with large temperature changes between summer and winter, the bedform regime has been observed to change from dunes to antidunes over the seasons considerably altering the channel roughness.

2.5.7. Effect of mixed grain sediment

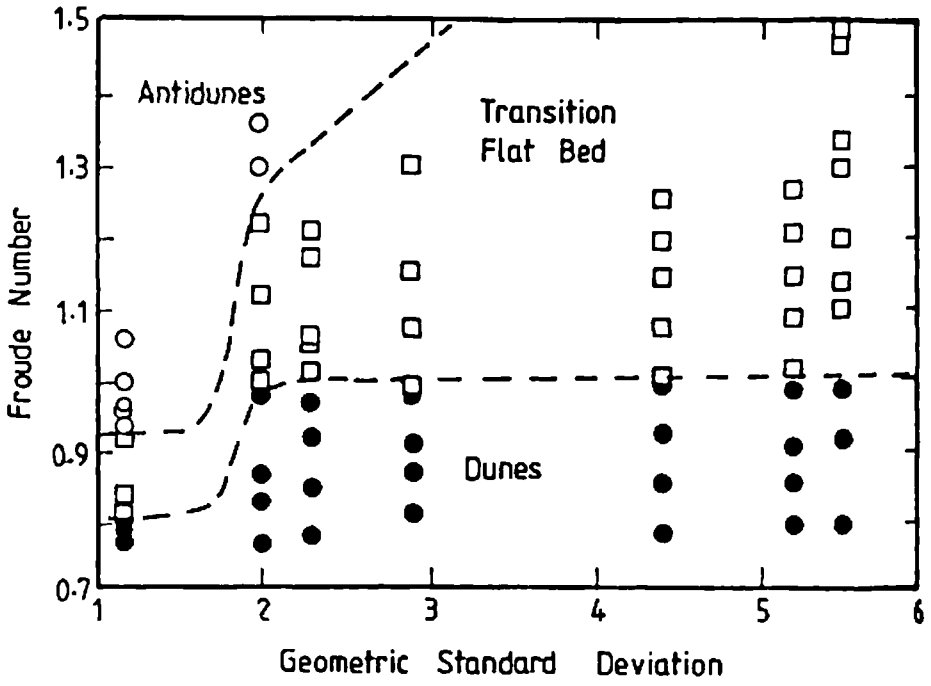

Figure 2.7 Bedform prediction for mixed grain sediments (after Chiew 1991)

One of few studies investigating bedforms in mixed grain sediments is presented by Chiew (1991) This study explores the formation of bed features in nonuniform sediments. Chiew performed experiments in a recirculating flume using a range of sediments. He found that the amount of sediments on the bed surface influenced the size of the bed features. At low velocities, the availability of fine sediment particles on the bed surface controls the size of the bed features. It was noted that the finer portion of the bed sediment in transport formed the bed features, while the coarser sediment particles formed the underlying armour layer. At high velocities, when all grains were mobile, antidunes did not form for Froude numbers exceeding unity, because of the presence of a pavement or dynamic armoured layer near the surface of the bed. No antidunes were observed in the experiment for geometric standard deviations of the bed sediment exceeding 2.3. In the study the bed feature is a transition flat bed when the Froude number exceeds unity.

2.5.8. Determination of bed form roughness

The forms of flow resistance equation given by Chezy and Manning for fixed bed flumes will clearly require modification or replacement for use in alluvial rivers as a single resistance coefficient is no longer adequate for expressing the range of possible energy losses. A number of improvements have been developed, that proposed by Einstein and Barbarossa (1952) is possibly the first. The method employed by Engelund and Hansen in their sediment transport formula is widely used. The development of computer models has created a need for formulations suitable for computer code. Brownlies' (1983)

model fulfils this purpose and forms the theoretical basis of the SAM river modelling package used in Chapter 3 for assessing the suitability of sediment for the Flood channel facility.

Einstein and Barbarossa

Einstein and Barbarossa (1952) proposed an alluvial channel stage discharge predictor, for the lower bedform regime. They introduced a concept of dividing resistance into grain resistance and form resistance as two additive quantities. This may be written in terms of the slope, hydraulic radius or bed shear stress, S= S'+S'' or R= R' +R'' or $\tau = \tau' + \tau''$. Writing the Manning-Stricker equation in terms of R' and U'* the grain shear velocity, they obtained

$$\frac{U}{U'^*} = 7.66\left(\frac{R'}{d_{65}}\right)^{1/6} \qquad (2.34)$$

where $U'^* = (gR'S)^{1/2}$. Similar formulations were proposed for cases that were not fully rough using the transitional formula.

They determined the value of form shear velocity, U''*, by presenting a graphical relationship between U/U''* and the intensity of shear on representative particles,

$$\psi'_{35} = (\rho s - \rho/\rho) d_{35}/R'S \qquad (2.35)$$

This method has been criticised by Yalin (1972) on the basis that it suggests that the friction factor is a function of a single dimensionless variable.

Englund

Engelund (1967) subsequently employed the principle of roughness separation. Considering the expansion losses over a dune he obtained an expression for the head drop over one wavelength or the slope associated with form roughness

$$S'' = \frac{\Delta H''}{\lambda} = \frac{\alpha}{2}\frac{h^2}{\lambda D}F^2 \qquad (2.36)$$

where F is the Froude number and λ is a constant. Assuming the divided slope concept

$$S = S' + \frac{\alpha}{2}\frac{h^2}{\lambda D}F^2 \qquad (2.37)$$

Multiplying throughout by $\gamma R/(\gamma_s - \gamma)d$, replacing depth D by the hydraulic radius R, and assuming $\tau' = \gamma RS' = \gamma R'S$, Engelund obtains expressions for the bed shear given by

$\tau^* = \tau'_* + \tau''_*$

Where

$$\tau'_* = \frac{\gamma R' S}{(\gamma_s - \gamma)d} \qquad (2.38)$$

and

$$\tau_*'' = \frac{\alpha}{2}\frac{\gamma h^2}{(\gamma_s - \gamma)d\lambda}\mathbf{F}^2 \qquad (2.39)$$

The grain roughness is once again based on the assumption that a traditional expression based on a grain hydraulic radius will give the value of U'*.

$$\frac{U}{U'^*} = \frac{U}{(gR'S)} = 6+2.5\ln\left(\frac{R'}{2.5d}\right) \qquad (2.40)$$

Engelund and Hansen (1967) applied these expressions to data obtaining a series of expressions in terms of τ'. Using a trial value of D' or R' the stage for a particular discharge may be found by iteration.

Brownlie

Brownlie (1983) used an alternative method in his stage discharge predictor intended for convenient use in computer models. The formula computes flow depth and bed regime, given q, S, temperature and sediment properties (ρ_g,s,d_μ and σ_g assuming log-normal distribution). Its unique feature is that bed forms treated as large grains.

The method uses the following dimensionless groups

$$\frac{RS}{d_\mu} = \frac{(\rho_S - \rho)}{\rho}\tau_* = F\left(\frac{q}{\left(gd_\mu{}^3\right)^{1/2}}, S, \sigma_g\right) \qquad (2.41)$$

Thus shear stress (RS) is related to sediment properties, discharge and slope. Fully turbulent flow is assumed and thus Reynolds number is not present.

Brownlie uses the Manning Strickler formula to describe the flow over the bed, where $n = d^{1/6}/25.7$ is substituted into the Manning equation to give

$$\frac{U}{U_*} = a\left(\frac{R}{d}\right)^{1/6} \qquad (2.42)$$

Substituting D, the grain diameter with k_d, an equivalent roughness to simulate the presence of dunes, and rearranging gives

$$\frac{(\rho_S - \rho)}{\rho}\tau_* = a^{-0.6}\left(\frac{k_d S}{d_\mu}\right)^{0.1}\left(q^* S\right)^{0.6} \qquad (2.43)$$

where $q^* = q/(gd_\mu{}^3)^{1/2}$.

As the shear stress is shown not to be strongly dependant on the dune roughness (k_d) it is assumed that an exact definition is not a critical factor in the prediction of τ*.

Hence it is assumed that k_d/d_μ is proportional to the undetermined powers of q* and S, since the dune height in relation to sediment size is a direct function of the power expenditure represented by q.S.

$$\frac{k_d}{d_\mu} \propto q_*{}^x S^y \qquad (2.44)$$

The effect of a non-uniform bed material is considered by using σ_g raised to an unknown power. Substituting these assumptions into 2.56 leads to

$$\frac{(\rho_S - \rho)}{\rho}\tau_* = w\left(q^* S\right)^x S^y \sigma_g{}^z \qquad (2.45)$$

by taking logarithms of both sides of this equation the constants were obtained by regression analysis from a large set of data. They give lines for the upper and lower regime. The regression line for the upper regime is given by

$$\frac{R}{d_\mu} = 0.3724(q_*)^{0.6539} S^{-0.2542}\left(\sigma_g\right)^{0.1050} \qquad (2.46)$$

and for the lower regime it is

$$\frac{R}{d_\mu} = 0.2836(q_*)^{0.6248} S^{-0.2877}\left(\sigma_g\right)^{0.08013} \qquad (2.47)$$

The method is based on a large amount of data from flume and field studies. Data is taken over a wide range of values

Variable	Upper limit	Lower limit
Mean diameter d_μ	2.8 mm	0.088 mm
flow rate per unit width	40 $m^3/s/m$	0.012$m^3/s/m$
Slope S	3.7 x 10-2	3.0 x 10-6
Hydraulic Radius R	17m	0.025m
Temperature T	63°C	0°C

Table 2.4 Range of variables in Brownlie's stage discharge predictor

Determination of flow regime and hence depth, is based on forces of bed sediment particles, to which bed deformation is related.

Dimensionless parameters used in the analysis are: grain Froude number, F_g, d_μ/δ,S and σ_g.
F_g represents the square root of the ratio of drag force on a particle to its immersed weight.

$$F_g = \frac{U\rho^{1/2}}{\left[(\rho_S - \rho)gd\right]^{1/2}} \qquad (2.48)$$

The ratio of mean grain size to boundary layer

$$\frac{d_\mu}{\delta} \quad \textit{Where } \delta = 11.6\nu/U_*' \tag{2.49}$$

The variable U_*' is the shear velocity given by the upper flow regime, i.e. when no dunes are present.

Plotting F_g against S on a log-log plot it can be said that above a slope of 0.006 only the upper regime exists. Below this value the division line is given by

$$F_g = F_g' = 1.74S\text{-}1/3 \tag{2.50}$$

Where F_g' is the value along this line. There are however some examples of lower regime that fall above this line and some examples of upper regime that fall below it.

The final part of the analysis concerns the overlap of this line. This refinement is achieved by studying the effects of temperature; viscosity has so far been ignored in the analysis.
As the temperature of water rises the viscosity is reduced; hence a particle has a higher fall velocity at a higher temperature. If a point is close to the transitional boundary this change in temperature can cause a dramatic change in bed form resistance.
Transitional data is plotted on a log-log chart of F_g/F_g' against d/δ. Above a threshold of $d/\delta>2$ temperature effects may be considered unimportant. Below this value the upper limit of F_g/F_g' for the lower regime flow and the lower limit of F_g/F_g' for the upper regime flow are functions of d/δ. These relationships are given below. The transitional region lies between them.
Lower flow regime

$$\log\frac{F_g}{F_g'} = \begin{cases} -0.2026 + 0.07026\log\frac{d}{\delta} + 0.9330\left(\log\frac{d}{\delta}\right)^2 \; for \; \frac{d}{\delta} < 2 \\ \log 0.8 \; for \; \frac{d}{\delta} > 2 \end{cases} \tag{2.51}$$

Upper flow regime

$$\log\frac{F_g}{F_g'} = \begin{cases} -0.02469 + 0.1517\log\frac{d}{\delta} + 0.8381\left(\log\frac{d}{\delta}\right)^2 \; for \; \frac{d}{\delta} < 2 \\ \log 1.25 \; for \; \frac{d}{\delta} > 2 \end{cases} \tag{2.52}$$

2.5.9. Incipient motion

Incipient motion refers to the conditions under which a sediment grain becomes mobile. Many bed load formulae contain some expression for incipient motion. The incipient motion of a particle is generally considered to be a function of the shear stress and the submerged weight, and fall velocity of the particle.

2.5.10. Sediment Transport Theory

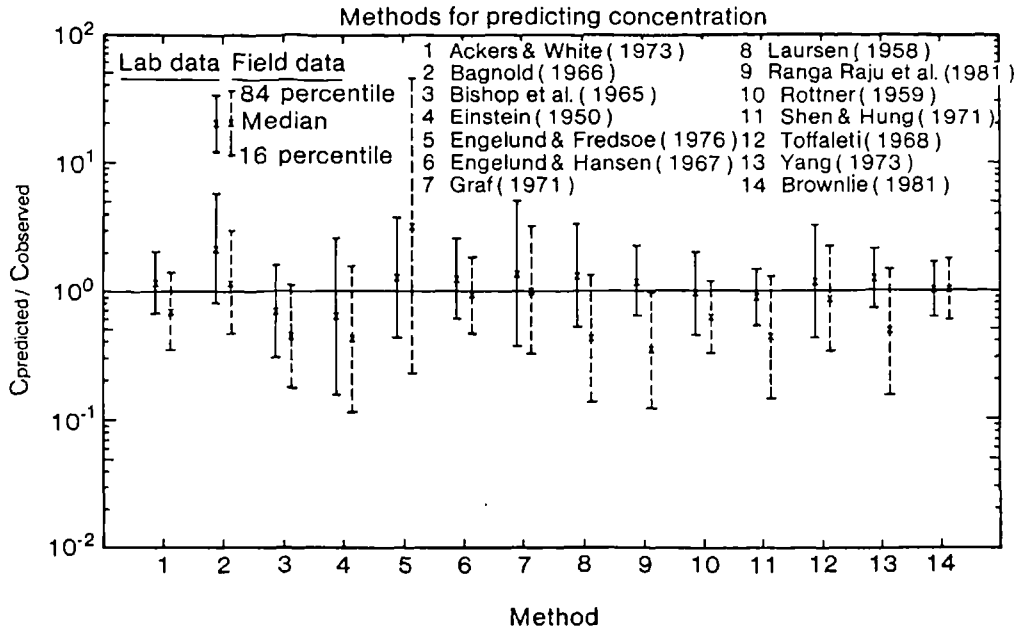

Figure 2.8 Comparison of methods for predicting sediment concentration, after Brownlie (1981). Median and 16th and 84th percentile values are based on the approximation of a log normal distribution of errors

A large number of sediment transport theories have been devised by investigators over the last 100 years with limited success. Figure 2.8 shows a comparison of results from a selection of these formulae. The figure shows that even the best formulae do not reliably predict sediment transport within a factor of two of the measured rate of transport. There are many discussions of which of these sets of formulae is the most acceptable. See for example, Raudkivi (1998), Yang (1996) or Chang (1988). It is generally considered that no single transport theory is suitable for all applications.

The following section, by way of introduction, contains description of three fundamental early works of sediment transport theory. Du Buoys equation was the first theoretical formula and introduced the concept of excess shear stress, Shields major contribution was a study of the conditions of incipient motion and Bagnold introduced the concept of stream power. He also divided bed load and suspended load according to their transport mechanisms. A further transport concept not mentioned is that of Einstein (1950) and others based on probabilistic concepts.

Transport formulae have subsequently been improved, as more data became available for empirical fitting. The Ackers White , the van Rijn and the Engelund and Hansen equations have been chosen for use in the analysis of sediment transport in Chapter 6, as: they are based on similar flow characteristics to those found in the FCF flume, they have been widely used and they have been shown to give consistent results.

Du Buoys theory

Du Boys (1877) produced the first theoretical bedload formula. His concept rested on the hypothesis that the channel bed consisted of a number of layers of sediment, each with a thickness equal to the particle diameter. He postulated that these layers would move across one another until the excess shear stress from the flow was taken up in friction between the moving layers.

This concept has been criticised on the basis that the verifying experiments were conducted in a small flume with a limited particle size range. With a mixed grain sediment this behaviour is certainly not observed. Whilst the assumptions on which his theory rests are flawed Du Buoy's equation continued to be used until Shields in 1936.

Shields' approach

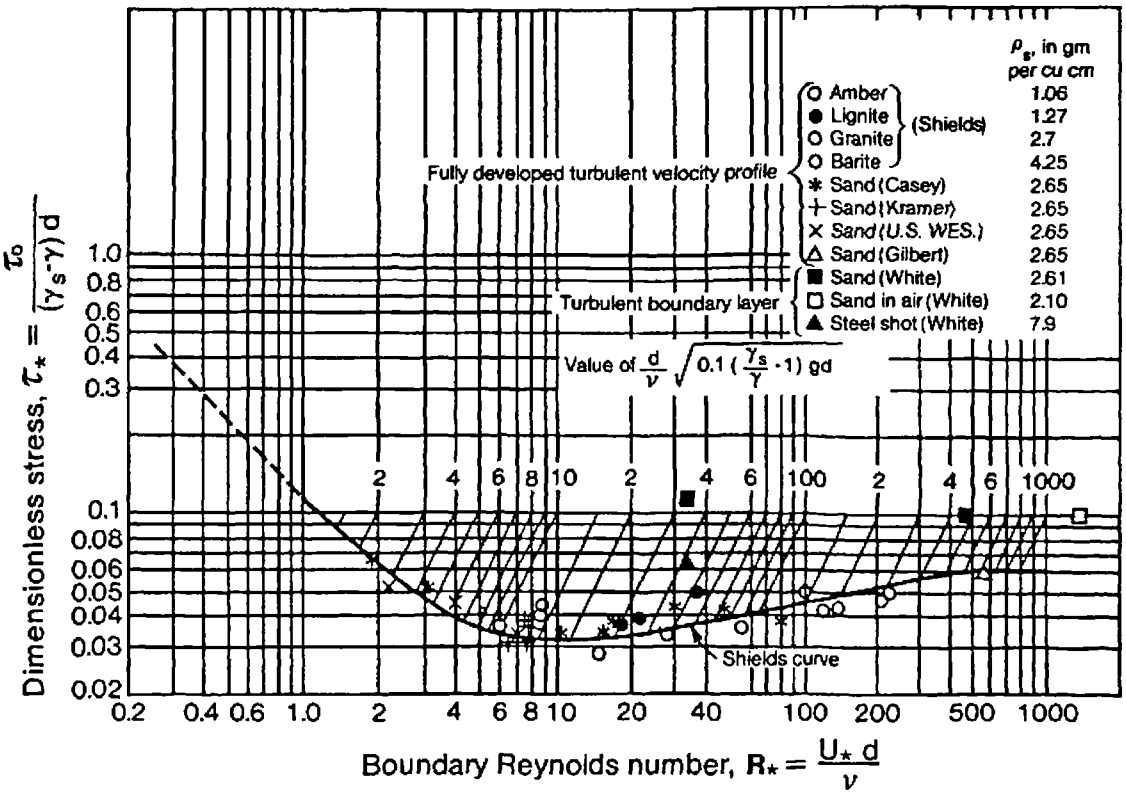

Figure 2.9 Shields diagram for incipient motion (Shields 1936)

Figure 2.9 shows "the Shield's curve" relating the dimensionless shear stress to the Boundary Reynolds number at the point of incipient motion. Shields diagram is based on empirical results for uniform sediments. He measured flow conditions with sediment transport greater than zero and then extended that relationship to find the conditions at incipient motion. The diagram has been used extensively in subsequent work, for example the van Rijn Theory.

The Bagnold, Stream power theory.

By 1966 there were a very large number of sediment transport theories in which the value of sediment load had been based on discharge, mean velocity, tractive force and rate of energy dissipation. Bagnold (1966) identifies the absence of agreement on these theories or even a study comparing them. He attributes this proliferation of ideas to "the lack of any sound and indisputable quantitative basis of reasoning compatible both with the facts and with the laws of nature."

The stream power theory is based on physical principles. Bagnold avoids uncertainties over turbulence effects on the flow resistance, such as those involved with boundary roughness, form drag and sediment transport, by considering tractive force and mean flow velocity as independent. These quantities must be found by the user of the formula using appropriate theory.

Bagnold's theory is based on the following essential features of granular flow.

1. The motion is a shearing motion wherein successive layers of solids are sheared over one another.
2. An impelling or tractive force, applied in the direction of motion, is necessary to maintain the motion.
3. The array of solids is immersed in some pervading fluid, either a liquid or a gas, and the fluid is also under shear.
4. The solids are heavier that the fluid, and are therefore pulled downward toward a lower boundary or bed.
5. In steady continuing motion the forces acting on every layer of solids must be in statistical equilibrium.

Bagnold implies from the above, the existence of an upward supporting stress. The magnitude of this upward stress, must necessarily therefore be equal to the immersed weight of the solids. Whether this applies in the case of a rolling or sliding particle is unspecified.

The presence of this upward force demands a source. Two mechanisms for applying an upward force to the sediment are explored.

The first considers the transfer of momentum from solid to solid, by continuous or intermittent contact. Over a period of time the weight of the uplifted particle is precisely equal to the mean upward flux of momentum per unit time.

The second source of upthrust is by the transfer of momentum from one mass of fluid to another and thence to the otherwise unsupported solid. Bagnold uses the example of a non-buoyant balloon, which may be kept aloft by drifting from one current of rising air to another. If this were to happen indefinitely the excess weight of the balloon would be precisely equal to the mean upward flux of momentum transferred to it. The point is made that continued support by this mechanism requires the continual maintenance of upward fluid currents whose effects exceed those of downward fluid currents.

The maintenance of these forces is attributed to the shearing motion which is in turn maintained by the applied tractive force. In the case of the solids, this is a shearing between solid layers and in the case of the fluid transmitted stress, a shearing between fluid layers, causing turbulent fluctuations.

The formula is restricted to the following conditions.

1. Steady open channel gravity driven liquid flow.
2. Unlimited availability of transportable solids.
3. The concentration of transported solids, by immersed weight, is sufficiently small that the contribution of the tangential gravity pull and the solids to the applied tractive stress can be neglected.
4. The system considered is defined as statistically steady and as representative, not of conditions at a single cross section, but of average conditions along a length of channel sufficient to include all repetitive irregularities of slope, cross section, and boundary.

These conditions are loosely applicable to laboratory flumes modelling steady flow and some natural rivers. Conditions 1 and 4 are likely to cause problems in the flood channel facility as the conditions at individual sections are of interest. Condition 2 is clearly problematic as only a small section of the flume (the main channel) has a mobile bed in which an armour layer is likely to form, reducing the availability of sediment.

The theoretical basis of Bagnold's theory

Bagnold divides the bed load and suspended load according to their support mechanism. For each form of transport he equates the work done in moving the sediment to the available "stream power, τU" for moving the sediment, calculating the efficiency of the process. Some or all of these concepts are inherent in the following theories.

The Ackers White sediment transport theory

The introduction to the Ackers White 1973 paper acknowledges that total shear stress alone is unsuitable as a predictor for bedload sediment transport. The problem with this approach being that the majority of natural streams contain bed forms and thus a significant amount of shear stress is due to non-transporting form loss. In formulae that do use bed shear as their basis it is necessary to make the distinction between form loss and transporting shear. Small errors in this calculation can result in large errors in the calculation of transporting power.

Ackers and White thus adopt the stream power theory in which sediment transport is related to the power available per unit bed area.

The analysis is split into an investigation of the transport of coarse grains along the bed as bed load $\tau' U$ and then fine grains supported by turbulence, as suspended load, τU. A transitional region is identified where both processes are at work. All equations are established on physical principals and then combined to form non-dimensional groups. Extensive flume data is used to find the coefficients linking these equations.

The general non-dimensional form of the transport function is

$$G_{gr} = C\left[\left(F_{gr} - A_{gr}\right)/A_{gr}\right]^{m} \qquad (2.53)$$

Where Fgr is a non dimensional expression of the sediment mobility and A_{gr} is an empirically determined sediment movement threshold condition. The mobility term is given by,

$$F_{gr} = \frac{U_*^{n} U_*^{(n-1)}}{\sqrt{[g(s-1)d]}} \qquad (2.54)$$

where

$U_* = gDS$ and

$$\frac{U}{U_*'} = 5.66 Log\left(\frac{10D}{d}\right)$$

U_*' is the grain shear velocity and U_* is the total shear velocity. The empirically determined exponent n, describes the mechanism by which the grains are transported. Grains are considered to move either by a bed load process, a function of the grain shear velocity, or as a suspended load process, a function of the total shear, or to be found in a transitional region where both processes are active.

The problem of obtaining the tractive force is overcome by the assumption that the relationship between velocity, depth and grain size is constant regardless of bedform. Hence the user need only determine the main stream velocity.

The non dimensional transport rate G_{gr} is given by

$$G_{gr} = \left(\frac{Qs}{Q}\frac{D}{d}\right)\left(\frac{U^*}{U}\right)^n \qquad (2.55)$$

Where Qs is the volume of sediment transport

The empirically derived parameters, n, m, A_{gr} and C are all functions of the dimensionless grain size.

$$D_{gr} = D\left[\frac{g(s-1)}{\upsilon^2}\right]^{1/3} \qquad (2.56)$$

The values of the parameters have been recalculated and appear in Ackers 1993 as

for D_{gr}>60 (coarse sediment, D>2mm

$$n = 0 \qquad (2.57)$$

$$A_{gr} = 0.17 \qquad (2.58)$$

$$m = 1.78 \qquad (2.59)$$

$$C = 0.025 \qquad (2.60)$$

for 1<Dgr<60 (transitional and fine sediments,0.06<D<2 mm)

$$n = 1.00 - 0.56 \log D_{gr} \qquad (2.61)$$

$$A = 0.14 + 0.23/\sqrt{D_{gr}} \qquad (2.62)$$

$$m = 1.67 + 6.83/D_{gr} \quad (2.63)$$

$$\log C = -3.46 + 2.79 \log D_{gr} - 0.98(\log D_{gr})^2 \quad (2.64)$$

The formula was originally derived for single sized or closely graded sediments and hence no account is taken of the observed phenomena of hiding and exposure in a mixed grain sediment.

In order to calculate the sediment transport:

1. The dimensionless grain number must be obtained from Equation 2.56
2. The parameters C, n, A and M may now be calculated from Equations 2.57 -2.64
3. The values of F and G can now be calculated from Equations 2.54 and 2.53 respectively
4. Finally the sediment transport rate Q_s may be obtained from Equation 2.55

2.5.11. Engelund and Hansen

Engelund and Hansen (1967) developed a function to be applied to lower regime gravel bed rivers based on the stream power theory. It is unusual in containing no expression for critical shear. The sediment transport equation is given by:

$$f'\varphi = 0.1(\tau_*)^{5/2} \quad (2.65)$$

with

$$f' = \frac{2gRS}{U^2} \quad (2.66)$$

$$\varphi = \frac{q_s}{\gamma_s\left[(s-1)gd^3\right]^{1/2}}, \qquad \tau_* = \frac{\tau_0}{(\gamma_s - \gamma)d} \quad (2.67)$$

substituting Equations 2.66 and 2.67 into Equation 2.65 gives Equation 2.68

$$\frac{Q_s}{Q} = 0.05\left(\frac{s}{s-1}\right)\frac{US}{\left[(s-1)gd\right]^{1/2}}\frac{RS}{(s-1)d} \quad (2.68)$$

Equation 2.66 can now be used to calculate the sediment transport rate.

Mixed grain sediment

An important aspect of the work presented in this thesis is the treatment of mixed grain sediment. The majority of formulae describing sediment transport are derived from the assumption of uniform grain size, however mixed grain sediment is found in a large proportion of rivers and thus demands attention. Transport of a sediment containing a range of sediment sizes is significantly more complex than the transport of a single grain size. This is for two reasons, firstly the variation in the availability of different fractions for transport and secondly because the sediment sizes interact; smaller sizes becoming less mobile and larger sizes becoming more mobile.

In 1950 Einstein was the first to approach the problems associated with mixed grain sediment. This study was continued by several researchers (Laursen 1958 and Egiazaroff 1965). The majority of work on the topic has been concentrated in the period following the development of computer models designed to predict the change in bed form due to engineering construction.

The simplest approach to dealing with mixed grain sediment is to divide the sediment into a number of fractions and calculate the transport rate of each fraction. The calculated rates must then be weighted to give the actual transport of each fraction.

Laursen (1958) developed a uniform grain formula based on excess shear stress, the ratio of shear velocity to fall velocity and the ratio of sediment size to depth. He surmised that the scatter around the plot of his relationship when applied to mixed sediments was caused by the non-uniformity of the grain, and thus introduced the relationship

$$C_{mix} = \sum p_i C_i \qquad (2.69)$$

Where C_i is sediment concentration and p_i is the percentage by weight of the mixture represented by grain size d_i.

Subsequent researchers for example Ackers (1993) have suggested that it would be more appropriate to use the percentage area of each sediment size present on the bed.

This type of equation has been applied to many other relationships subsequently (for example Yang 1973), often for the purpose of obtaining the grain size distribution rather than to improve the predictive ability of the equation. This method is used later in Chapter 6 with the transport equations.

It is readily apparent that this approach does not take account of the interaction between small and large grains but simply accounts for their availability. It is also unclear what depth of sediment is appropriate for use in determining the proportions.

Einstein's sediment formula is based on probability, the expression for the particle mobility is given by

$$\psi_* = \left(\frac{\beta^2}{\beta_*{}^2}\right)\psi \quad where \ \psi = \frac{\rho_s - \rho}{\rho}\frac{d}{R'S} \qquad (2.70)$$

The β term introduced a "hiding function" into his 1942 expression (Einstein 1950), to account for the effect of large grains "hiding" smaller grains.

The calculation of the rates of different sediment size fractions in a mixed grain sediment is explored by Pender (1995) in which the availability and interaction of different sized fractions in a sediment mixture are considered. He proposes and evaluates two new hiding functions. Both concepts introduce a factor to the critical Shields stress to account for the mixed grain effect.

The first method that Pender proposes is based on the concept that one sediment size in a mixture moves at the same rate as it would in a uniform grained bed of that sediment diameter. This sediment diameter

is known as the scaling size. Scaling size has been found to be a function of the grading curve and the flow conditions. The value of ε_i, the hiding function, is a function of this scaling size.
The new critical shear may be obtained from, $\tau_{cr,i}=\varepsilon_i\tau_{scr,i}$. Where $\tau_{scr,i}$ is the critical Shields stress for sediment size d_i. The second method proposed is a development of Parker's concept that all particles in a mixture have the same mobility as the mean grain size. The new critical shear may be written,

$$\tau_{cr,i} = \tau_{scr,g}\varepsilon_i \qquad (2.71)$$

where subscript g refers to the median grain size. The evaluation of the second hiding function is again based on the grading curve and the flow conditions in terms of the standard deviation and the Froude number in the following way.

$$\varepsilon_j = \frac{\left(d_i/d_g\right)^{-0.105}}{\sigma_g^{\alpha}} \qquad (2.72)$$

Where, by regression analysis from laboratory data.

$$\alpha = 4.198-2.548\sigma_g+0.192\sigma_g^2+0.275Fr-7.488Fr^2+2.490\sigma_g Fr$$

The Froude number $Fr = U/(gR)^{0.5}$

The standard deviation $\sigma_g = (d_{84}/d_{15})^{0.5}$

The standard deviation may be made less sensitive to local fluctuations in the sediment profile by adopting the phi scale and using an empirical fit such as that given by McMannon in Equation 2.34. This method has been used in the calculations in Chapter 6.

The results of Pender's experiments suggest that the hiding function based on equal mobility performs significantly better than that based on a scaling size. However, the results still appear to be weighted toward the smaller sediment sizes, particularly after long experimental runs. Pender's calculation for sediment transport rate is based on the van Rijn sediment transport equations which are given below.

2.5.12. van Rijn (1984)

van Rijn defines bed and suspended load according to Bagnold. Bedload motion is dominated by gravity forces and consists of rolling, sliding and saltating whilst suspended load is supported by turbulent bursts. This division is made on the grounds that transport below the maximum saltation height for a particle can be termed bed load. Bed load transport is therefore defined as $q_b = u_b\delta_b c_b$ where u_b = particle velocity, δ_b = maximum saltation height and c_b = particle concentration.
New relations are defined for the particle characteristics u_b and δ_b and a term for concentration of the bed load is obtained using these proposed relation ships and empirical bed load data to obtain a transport equation.
van Rijn modified his original equations which were based on stream power and excess shear stress for simplicity to obtain Equations 2.90 and 2.91 for bed load and suspended load respectively. Here the sediment transport rate is based solely on the mean stream velocity. Equations 2.88 and 2.89 are similar to those derived by Laursen for adjusting the equations for mixed grain transport.

$$q_s^* = \sum_{i=1}^{n} \beta_i q_{s,i}^* \qquad (.2.73)$$

$$q_b^* = \sum_{i=1}^{n} \beta_i q_{b,i}^* \qquad (2.74)$$

$$\frac{q_{s,i}^*}{uhb} = 0.012 \left(\frac{u - u_{cr,i}}{\sqrt{[g(s-1)d]}} \right)^{2.4} \left(\frac{d}{h} \right) d_*^{-0.6} \qquad (2.75)$$

$$\frac{q_{b,i}^*}{uhb} = 0.005 \left(\frac{u - u_{cr,i}}{\sqrt{[g(s-1)d]}} \right)^{2.4} \left(\frac{d}{h} \right)^{1.2} \qquad (2.76)$$

Where β is the proportion of each fraction

In order to apply these equations it is necessary to calculate the critical velocity which is related to the critical shear velocity by the equation

$u_{cr,i} = u_*'_{cr,i}\, C/(\sqrt{g})$

where $u^*'_{cr,i}$ is calculated from Equations 2.86 and 2.87

2.5.13. Sediment transport computational models

Morphological models describe the response of a river to a change in flow or sediment conditions with time. This thesis is not intended to cover the development of such a model however the subject is included here because the integral concepts of such models are useful when considering the morphological changes in riverbeds when the flow leaves the main channel. It is also envisaged that the work in this thesis will eventually aid the development of such models, which rely on accurate calculation of mixed grain sediment transport.

A morphological model generally contains expressions for calculation of the hydraulic behaviour of the river system and further expressions, explaining the sediment movement. The equations for determination of the hydraulic behaviour of streams have attained a high degree of accuracy, at least for inbank flows. Models describing bed material movement however, are considerably more complex, particularly for mixed grain sediment. Parker (1978) summarised the problem "Rivers and canals with perimeters composed of non cohesive sand and silt have self formed active beds and banks. Thus, they provide an interesting fluid flow problem for which one must determine the container as well as the flow".

A morphological flow model must determine when a bed is stable, when it will erode and when sediment will deposit. In order to model these processes over a period of time, it is necessary to consider the gradation in grain size of the bed material. As smaller grains are generally more mobile and move faster

than larger grains, the bed material will tend to become coarser during a period of net erosion. As bed stability is highly dependent on the grain size of the material, the bed will eventually reach a level where the flow is deep enough and the bed coarse enough to reach equilibrium conditions. This coarsening of the bed material is termed sorting and is clearly only applicable to mixed grain sediments.
For each control section the model must keep account of the quantity of grains in each size fraction of bed material represented. This account is adjusted, for each iteration, by calculation of the proportion of each grain size fraction moving using a sediment transport formula. It is clear that accurate calculation of the rate of transport of each sediment size fraction is crucial to the success of this process.
In order to apply these equations a depth over which the bed material gradation is considered constant is chosen, this is usually termed the active depth.

Numerous programs have been written which used alternative expressions for sediment transport rate, armouring, sorting and active depth. Examples of such programs are as follows: HEC-6 (1977) is still widely used and is relatively simple. Bettess and White (1981) is based on the Ackers-White (1973) sediment transport theory with a correction of mixed grain sediments and the authors are available for comment. Rahuel et al (1989), has been used subsequently by Pender and Li (1994) and gives a fully coupled solution, setting itself out as a benchmark against which other less computationally expensive methods may be used.

Active depth

All of the programs considered deal with the problem of mixed grain sediments by designating an active depth, first introduced by Bayazit (1975). This is a region immediately below the surface of the river bed in which the bed sediment gradation is considered constant.
In HEC -6 this depth is the layer of material between the bed surface and a hypothetical depth at which no transport will occur. This equilibrium depth is calculated by combining Einstein's mobility function ψ with Manning's and Strickler's equations. They are combined to give an expression for depth of

$$d = d_e = \left(\frac{q}{10.21 D^{2/3}} \right)^{6/7} \qquad (2.77)$$

Where d_e is the equilibrium depth.
To account for mixed grain sizes, an expression is derived to account for the depth of scour required to produce enough coarse material to armour the bed. The gradation curve is split into sections and the equilibrium depth calculated for each grain size until a depth is found that is below the current bed level. The scour depth may then be calculated as the sum of the volumes represented by the grain size fractions smaller than that fraction. If no sediment diameter is found to have an equilibrium depth below the current level, i.e. the smallest sample will armour the bed, the scour will not occur.
Subsequent issues of HEC-6 have recognised that this method for deriving the armour layer tends to give an active layer that is too thick in sand bed rivers. This dampens hydraulic sorting.

Borah (1982) proposes a similar relationship given by

$$E_m = \frac{1}{1-p}\frac{d_L}{\sum_{i=L}^{i}\beta_i} \qquad (2.78)$$

in which p = bed sediment porosity; L = the smallest sediment size class whose particles are immobile; d_L = characteristic diameter of size class L and β_i = fractional representation of size class i in the mixed layer. Researchers examining armour layers have always recognised that these layers consist of a full range of grain sizes and thus this equation is only justified on its ability to predict global behaviour.

Bettess and White (1981) suggest a physical justification of the active depth term in their program by equating it to the bedform height H, stating that at least this height may be considered mixed. Rauel (1989) examines these arguments in terms of time-scale. In a very short time scale, then the mixed layer can only consist of a thin layer of particles at the surface that may be immediately entrained by the flow. If a longer time period is selected i.e. the time for a ripple or dune to traverse its own wavelength is chosen then the use of bedform height as an active depth seems justified. In the very long term the active depth may be considered as in the HEC - 6/ Borah model to be equal to the depth of material eroded or deposited. I.e., there is an asymptote at the level of the equilibrium bed.
Rahuel et al proposed a more complex model of the active layer to account for these processes based on Karim and Kennedy (1981). The thickness of the active layer is taken to be equal to the bedform height, which in turn is given by

$$E_m = c_d h_m \qquad (2.79)$$

Where h_m is the mean water depth and c_d is a coefficient taken to be a constant between 0.10 and 0.20. In a depositing stratum the layer accumulated is periodically "emptied" to form the inactive bed.
In an eroding bed Borah's 1982 formulation and the Karim and Kennedy (1981) formulations are used, the smallest depth being selected. Clearly as the bed gets closer to an armoured condition Borah's equation will be preferred.
These concepts may be useful in consideration of the formation of a natural formed channel from a float screeded bed. The process is considered in qualitative terms in Chapter 4.

In the analysis of the results the concepts of active depth, armouring and grain sorting will be considered and in order to inform future developments of such models. Clearly, an important issue in meandering streams, not considered in these models is the issue of lateral grain sorting. One way of investigating the effects of lateral grain sorting and the changes in depth and velocity around a meander bend is to use a three-dimensional flow model. In order to run a three-dimensional model successfully however, a large quantity of data is required which often may exhaust the resources of the modeller. Ways of adjusting a one-dimensional model to account for the three dimensional processes at work are extremely valuable. These possibilities will be considered later in this review.

2.6. Meandering flow

Introduction

Summarising the discussion in Chapter 1, a river system tends to consist of three stages. The first stage is an upland source region characterised by steep slopes, high erosion and sediment transport, and braided river forms. The second stage is a transfer zone in which sediment transport is carried at a shallower slope through river channels characterised by their meandering planform and the third stage a depositional delta at the mouth of the river.

The meandering river form is a consistent feature of rivers in the areas of most economic value and is thus of great interest.

The cause of meandering has long been a source of controversy. Lane's (1955) relationship of balance suggests that slope is a function of the flow rate, the rate of sediment transport and the median grain size. If this is the case then a consideration of the different erosive and depositional characteristics of rivers can be used to explain meandering forms. In a river containing excess sediment the river takes on a braided form and deposition tends to be uniformly distributed over the valley steepening the whole floodplain. In a river in which there is a shortage of sediment the morphological response is a confined channel. As armouring of the bed material generally prevents massive degradation of the valley the river tends to erode the channel walls and a meandering planform results. The process continues until the flow is insufficiently powerful to cause further erosion.

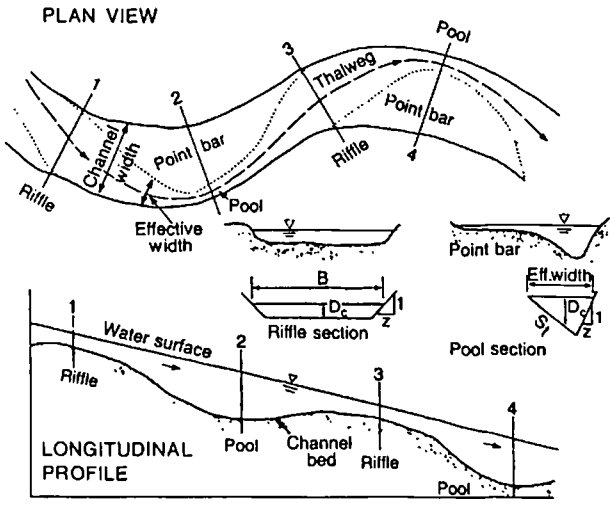

Figure 2.10 Meandering channel at low flow (After Chang 1988)

Figure 2.10 shows a typical meandering channel of a similar form to the Series C model. The position of the thalweg and the shape of the point bars are appropriate to a bankfull flow. This part of the literature review is concerned with the flow processes particularly those relating to bed shear transverse slope and

grain size distribution in a meandering channel of this type. Once these processes are understood, we can make headway with an examination of the effect of overbank flow on these processes.

When considering flow in curved channels the two-dimensional assumptions made for flow in relatively straight channels are no longer applicable. Fluid flowing around a bend experiences centripetal acceleration causing superelevation at the outer bank, much like coffee stirred in a mug; there is a radial slope on the water surface. The velocity profile in viscous flow above a surface was examined in Section 2.2.3. As the velocity increases with distance from the bed the centripetal acceleration near the water surface where the flow is fastest will be stronger than that experienced by flow near the bed. This imbalance results in helical flow, or secondary circulation around a bend. The strength of the secondary circulation is a function of the variation in streamwise velocity with depth. In a meander sequence it is clear that the secondary circulation will be strongest around an apex reducing towards the crossover and reversing at the next apex. These secondary currents are partially responsible for the variation in sediment size across the channel and the transverse channel slope. A quantitative understanding of these processes is necessary if we are to calculate accurately the passage of sediment movement in a meandering channel.

Basic equations for flow in curved channels may be derived by considering the small element of flow shown in Figure 2.11. The derivation presented here can be found in a similar form in textbooks such as Chang (1988) and Schlichting (1968). We assume subcritical flow and a hydrostatic pressure distribution. Bank effects are neglected on the basis of wide shallow flow. Δs, Δr and Δz give the dimensions of the block of fluid in the streamwise, radial and vertical directions respectively.

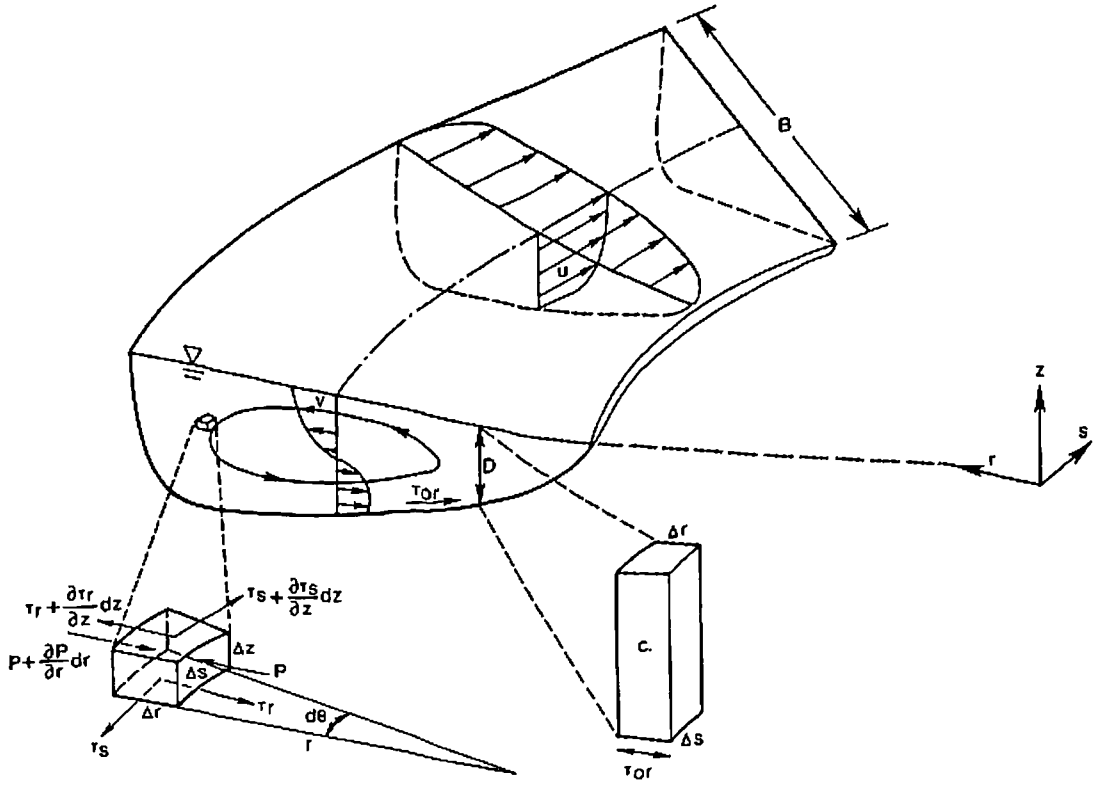

Figure 2.11 Definition Sketch for flow in a curved channel

For the element in velocity field U, Newton's law of momentum states

$$dF = dm\frac{DU}{Dt} \tag{2.80}$$

Where F is the force vector and dm is the mass of the fluid element

The Velocity vector may be written in vector notation

$$U = ui_s + vi_r + wi_z \tag{2.81}$$

The acceleration DU/Dt from the right hand side of Equation 2.80 may be written in polar cylindrical co-ordinates as

$$a_s = \frac{DU}{Dt} = \frac{\partial u}{\partial t} + u\frac{\partial u}{ds} + v\frac{\partial u}{\partial r} + w\frac{\partial u}{\partial z} + \frac{uv}{r} \tag{2.82}$$

and

$$a_r = \frac{Dv}{Dt} = \frac{\partial v}{\partial t} + u\frac{\partial v}{ds} + v\frac{\partial v}{\partial r} + w\frac{\partial v}{\partial z} - \frac{u^2}{r} \tag{2.83}$$

Where the first term on the left hand side gives the change in velocity with respect to time and the central three terms the change with respect to displacements in the s, r and z directions respectively. The final term gives the acceleration due to the circular motion.

The force term on the left hand side of Equation 2.80 consists of the surface pressure - due to the super elevation and the surface shear due to viscosity.

In the *tangential direction* the force consists of the tangential component of fluid weight $\rho g S_r \Delta s \Delta r \Delta z$ and the shear force on the element. This shear force is given by the difference in shear stress on the upper and lower boundaries of the fluid cell multiplied by the area of action, dr ds. With reference to the diagram this may be written

$$\left[\left(\tau_s + \frac{\partial \tau_s}{\partial z}\right) - \tau_s\right] dsdr = \frac{\partial \tau_s}{\partial z} dsdrdz \qquad (2.84)$$

Assuming that the banks make no contribution and substituting Equation 2.84 and the terms for fluid weight and shear force into Equation 2.83 gives

$$\frac{\partial u}{\partial t} + u\frac{\partial u}{ds} + v\frac{\partial u}{\partial r} + w\frac{\partial u}{\partial z} = -\frac{uv}{r} + gS + \frac{1}{\rho}\frac{\partial \tau_s}{\partial z} \qquad (2.85)$$

In the *radial direction* there is a net pressure force across the section due to the super elevation. This can be written

$$\left[P - \left(P + \frac{\partial P}{\partial r} dr\right)\right] dsdz = -\rho g S_r dsdrdz \qquad (2.86)$$

where S_r is the transverse water surface slope. In a similar way to Equation 2.87 the radial shear may be written

$$\left[\left(\tau_r + \frac{\partial \tau_r}{\partial z}\right) - \tau_r\right] dsdr = \frac{\partial \tau_r}{\partial z} dsdrdz \qquad (2.87)$$

Thus substituting the radial shear and pressure terms and the radial acceleration given in Equation 2.83 into Equation 2.81 gives

$$\frac{\partial v}{\partial t} + u\frac{\partial v}{ds} + v\frac{\partial v}{\partial r} + w\frac{\partial v}{\partial z} = \frac{u^2}{r} - gS_r + \frac{1}{\rho}\frac{\partial \tau_r}{\partial z} \qquad (2.88)$$

and the continuity equation is given by

$$\frac{\partial v}{\partial r} + \frac{\partial v}{ds} + \frac{\partial w}{\partial z} + \frac{v}{r} = 0 \qquad (2.89)$$

Neglecting the bed resistance and assuming that the pressure force associated with the transverse surface is balanced by the centrifugal force, for a column of water of height D we can write

$$\int_0^D \frac{u^2}{r} \rho dsdrdz - \rho g S_r dsdrdz = 0 \qquad (2.90)$$

and hence

$$S_r = \frac{\int_0^D u^2 dz}{gr} = \frac{C_r U^2}{gr} \qquad (2.91)$$

Where C_r is a correction factor. If we assume that the correction factor C_r is equal to 1 we can obtain a term for the super elevation between inner and outer bank, r_1 and r_2.

$$\Delta Z = \int_{r1}^{r2} S_r dr = \int_{r1}^{r2} \frac{U^2}{gr} dr = \frac{\overline{U}^2 B}{gr_c} \qquad (2.92)$$

The equations of motion derived above may justifiably be simplified for further analysis. If the flow is steady then dv/dt = 0 and du/dt = 0. For fully developed flow, which rarely occurs in a meandering stream we can also write δu/δs = 0 and δv/δd = 0. In addition, v and w are small in comparison to u in a wide channel and hence the equations of motion may be written:

$$gS + \frac{1}{\rho}\frac{\partial \tau_s}{\partial z} = 0 \qquad (2.93)$$

and

$$\frac{u^2}{r} - gS_r + \frac{1}{\rho}\frac{\partial \tau_r}{\partial z} = 0 \qquad (2.94)$$

Integrating Equation 2.90 over the distance from the bed to depth z gives $\tau_s = \rho g S(D-z)$and Equation 2.91 gives the distribution of τ_r, the radial shear stress along the vertical. Adopting semi empirical theories of turbulence we may write τ_s and τ_r in terms of eddy coefficients

$$\tau_s = \varepsilon \frac{\partial u}{\partial z} \text{ and } \tau_r = \varepsilon \frac{\partial v}{\partial z} \qquad (2.95)$$

Taking an expression for the variation of stream velocity U along the vertical, U= f(z), we can find a value for eddy viscosity from the streamwise terms Equations 2.109 and 2.111. This value can then be inserted into the transverse term Equation 2.96 - assuming that turbulence is isotropic. Integration over the flow depth results in an expression for v as a function of z.

2.6.1. Boundary shear stress

Boundary shear stress is clearly of great interest in the calculation of sediment transport in a meandering stream. Two approaches have been made to calculating the transverse boundary shear stress in a curved flow field. One consists of calculations based on the variation in the transverse velocity profile with depth, the other, proposed by Falcon-Ascanio and Kennedy (1983) and presented here, uses momentum considerations on a vertical fluid element.

The streamwise velocity profile is given by

$$\frac{u}{U} = \frac{1+m}{m}\left(\frac{z}{D}\right)^{1/m} \qquad (2.96)$$

Where

$$m = \kappa\left(\frac{8}{f}\right)^{1/2} \qquad (2.97)$$

The radial acceleration varies with the square of the streamwise velocity over the depth ($a_r = u^2/r$). This method assumes that the vertical shear stresses are small because of the small radial velocity element. The pressure forces are not considered, as they will pass through the centroid of the element. Taking moments about the centroid of the block of fluid we obtain a term due to the variation in streamwise velocity over the depth and a counter moment due to the force on the element due to bed shear

$$\frac{1}{2}D\tau_{0r}dsdr = \rho\int_0^D \frac{u^2}{r}\rho\left(z-\frac{D}{2}\right)dsdrdz \qquad (2.98)$$

This may be simplified to give

$$\tau_{0r} = \frac{2\rho}{rD}\int_0^D u^2\left(z-\frac{D}{2}\right)dz \qquad (2.99)$$

Substituting the velocity profile obtained above and integrating we get

$$\tau_{0r} = \frac{1+m}{(2+m)m}\rho\frac{D}{r}U^2 \qquad (2.100)$$

Transverse bed slope and grain size distribution

In order to complete a calculation of sediment transport the gradation of sediment size must be known. Falcon - Ascianio and Kennedy (1983) went on to consider the variation in slope and grain size across the river section. They argued that the value of lateral shear stress could be related to the weight of the active layer of grains on the bed slope

$$\tau_{0r} = z_b(1-\lambda)(\rho_s-\rho)g\sin\beta \qquad (2.101)$$

where λ is the porosity and β is the bed slope z_b, the active layer thickness was obtained from work by Karim (1981) and found to be given by

$$z_b = d\frac{U_*}{U_{*c}} \qquad (2.102)$$

where $d = d_{50}$, U_* is given by $U_* = U/(f/8)^{1/2}$ is the local shear velocity and U_{*c} is the critical shear velocity based on critical Shields stress

$$U_{*c} = \left(\frac{\tau_c}{\rho}\right)^{1/2} = \left(\frac{\rho_s - \rho}{\rho} g d \tau_{*c}\right)^{1/2} \qquad (2.103)$$

Where τ_{*c} is the critical shields stress.

Substituting the expression for bed shear (Equation 2.101) and the expression for the thickness of the active layer into Equation 2.103 gives

$$S_t = \sin\beta \approx \frac{dD}{dr} = \frac{D}{r}\mathbf{F}_d \frac{(8\tau_{*c})^{1/2}}{1-\lambda} \frac{1+f^{1/2}}{1+2f^{1/2}} \qquad (2.104)$$

Where S_r is the transverse bed slope and $\mathbf{F}_d$ the particles densimetric Froude number given by

$$\mathbf{F}_d = \frac{U}{\left\{\left[(\rho_s - \rho)/\rho\right] g d\right\}^{2/2}} \qquad (2.105)$$

This equation has been supported by experimental evidence

$$S = S_c \frac{r_c}{r} \qquad (2.106)$$

$$U(r) = \left[\frac{8}{f} g S D(r)\right]^{1/2} = \left[8 S_c \frac{r_c}{r} \frac{g D(r)}{f}\right]^{1/2} \qquad (2.107)$$

$$\frac{1}{D^{1/2}} - \frac{1}{D_c^{1/2}} = \left[\frac{1}{r^{1/2}} - \frac{1}{r_c^{1/2}}\right] \frac{(8\tau_{*c})^{1/2}}{1-\lambda} \frac{1+f^{1/2}}{1+2f^{1/2}} \left\{\frac{8 S_c r_c g}{f g\left[(\rho_s - \rho)/\rho\right] d}\right\}^{1/2} \qquad (2.108)$$

2.6.2. Odgaard Approach

Odgaard (1984) pursued a method similar to Falcon Ascanio obtaining an equation for the bed slope given below. His basic assumptions in the derivation of this equation was that the size of the stationary particles forming the bed at any point are the size of the particles that are just about to move in the longitudinal direction by rolling about their point of support. The justification given is that if $\tau_0' > \tau_c$ then $\tau_0' - \tau_c$ is primarily used on particles and only occasionally diverted to the bed.

$$\sin\beta = \frac{D}{r} \frac{U^2}{\left[(s-1) g d_{cr}\right]^{1/2}} \frac{1+m'}{m'(2+m')} \qquad (2.109)$$

where α is the projected area - volume ratio for a particle normalised by that for a sphere, $s = \rho_s/\rho$ is the specific gravity of the particle whose motion is impending; and m' is the reciprocal of the velocity exponent for grain roughness. The value of m' is related to the critical Shield shear stress as follows.

$$m' = \kappa \frac{U^2}{\left[(s-1)g d_{cr} \tau_{*c}\right]^{1/2}} \qquad (2.110)$$

The transverse variations of U d_{cr} and m' are needed in order to apply this equation. The following equations are presented with reference to the channel centre line

$$\frac{U}{U_c} = \frac{m'}{m'_c}\left(\frac{D}{Dc}\right)^{1/2}\left(\frac{r_c}{r}\right)^{1/2} \qquad (2.111)$$

Using the Strickler formula in which n varies with grain size to the power 1/6 as a precedent m' is assumed to vary with the relative depth D/d to the $^1/_6$ power

$$\frac{U}{U_c} = \left(\frac{dc}{d}\right)^{1/6}\left(\frac{D}{D_c}\right)^{2/3}\left(\frac{r_c}{r}\right)^{1/2} \qquad y \qquad (2.112)$$

Using a semi empirical approach Odgaard(1982) related the distribution of grain size to the displacement from the centreline of the channel and change in depth of flow from the centreline depth

$$\frac{d}{d_c} = \left(\frac{D}{D_c}\right)^{5/3}\left(\frac{r_c}{r}\right)^{3/2} \qquad (2.113)$$

This formula can then be substituted into equation y to give

$$\frac{U}{U_c} = \left(\frac{D}{Dc}\right)^{7/18}\left(\frac{r_c}{r}\right)^{1/4} \qquad (2.114)$$

Using this approach, the transverse slope and grain size distribution may be calculated.

2.6.3. Regime Theory and planform prediction

The work performed by Lane (1955) and other early researchers to find the stable width and slope of loose boundary canals has been extended to obtain predictive equations describing the planform and channel properties of a meandering channel. The prediction of the stable depth, width, slope and other channel properties is important if meandering river channels are to be reintroduced with success. It is also important to be able to estimate the effects of reducing the sediment load in a stream due to the introduction of a weir or dam or other engineering works.

Most researchers agree that the river form is a function of the sediment laden flow and the material through which it is transported.

There are five relations that may be used in describing this form.

1. The flow continuity equation Q=UA
2. A stage discharge relationship, such as Manning's equation
3. An equation for the sediment transport rate

4. The equation for minimum stream power per unit length
5. The equation for minimum stream power per river reach.

The first three of these relations have already been explored in some depth. The last two require further explanation here.

Regime theory concerns the equilibrium state of the river or the state of stable geometry. Sediment entering the channel at the top of the reach is carried through without deposition and further channel erosion does not occur. This is expressed in the concept of minimum stream power, the rate of work done by the flow being just sufficient to prevent further deposition. This concept has been in existence for many years and stated in various differed ways. Chang (1979a) states that for given constraints the necessary and sufficient condition of equilibrium in a mobile channel occurs when the stream power per unit channel length γQS is a minimum. As discharge Q is a given parameter, the river will tend toward a minimum slope S.

This concept is illustrated below.

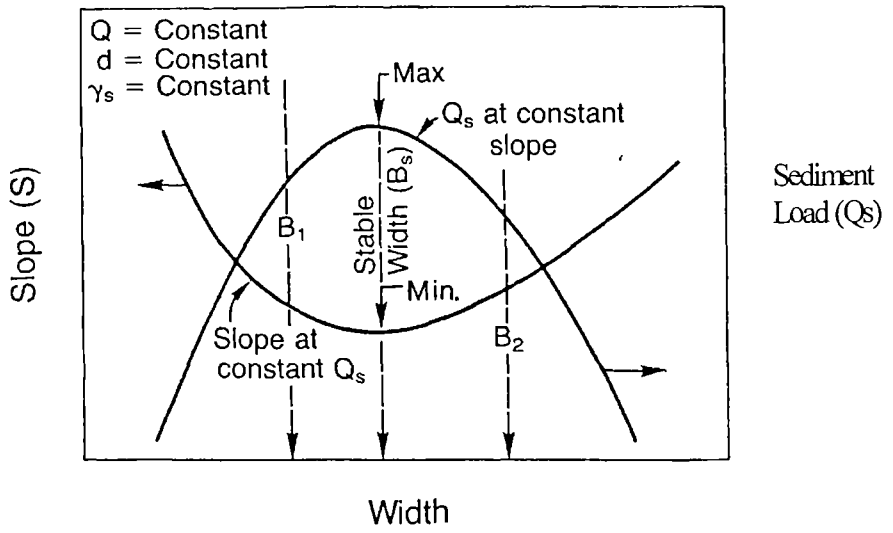

Figure 2.12 The minimum stream power diagram after Chang (1988)

Consider a straight channel with vertical walls. For a constant sediment load and water discharge, there is a channel width at which the slope is a minimum. Similarly for a constant slope there is a width at which the sediment transport is maximum. This width is shown in the diagram above. In a straight channel, the slope can only be varied by massive valley degradation or aggradation. Meandering reduces the channel slope. The maximum sediment transport may therefore occur in a meandering stream

Additional complexity is introduced by a meandering planform as the results of the experiments of Onoshi et al. (1976) show. The investigators identified the absence of scientific information available for transferring knowledge derived for straight streams to meandering rivers. They conducted a series of mobile boundary experiments in large-scale flumes, one straight and one meandering. The tests were conducted with a sediment of D_{50} = 0.25mm and a standard deviation of 1.4. The flume was allowed to

run for 70 to 90 hours in order to establish equilibrium. Onishi et al. observe that the meandering nature of the flow causes secondary currents, which have two important effects on the sediment. Firstly the secondary currents at the apex are directed downward at the out side of the bend, increasing the fall velocity there and they are directed upward at the inside of the bend reducing the fall velocity and hence increasing the mobility. The second affect of secondary currents is the creation of a point bar. This introduces variation into the flow depth and hence the velocity field.

These two mechanisms were considered by Onishi et al. to counteract each other. They observed that the majority of sediment movement occurred around the outside of the bend and thus the increase in fall velocity slowed the sediment rate. The variation in the velocity field was observed to increase it. These tests on loose boundary, straight and meandering channels showed the meandering channel to be more efficient at transporting sediment than a straight one. The researchers concluded that this resulted from the increased mobility of sediment non-uniformity of channel velocity, which outweighed the negative effect of the reduction in mobility at the apex.

It is also useful to consider the minimum stream power over a channel reach given by

$$P = \int_L \gamma Q S dx$$

Where P is the total stream power over reach length L and x is the co ordinate in the flow direction. This is satisfied by all uniform flow conditions.

These five relationships are satisfactory for a straight channel. However as shown by Onishi et al (1976) above, the variation in bed shape caused by secondary currents must also be considered in meandering streams. And additional relationship describing channel shape is also required.

Using these relationships Chang (1984a) constructs a model for a reach of a sand bed channel.

The approach to modelling the channel planform properties is broken down into the following steps.

1. Identification of the independent or controlling variables
2. Application of the relations described above to those variable and
3. Computation of the resulting channel geometry

The independent variables selected by Chang are the water discharge and sediment inflow and there respective properties. These are determined by the watershed and the valley slope, which over the time scale that we are considering may be taken as fixed.

Dependent variables include flow velocity, channel width, flow depth, channel slope and radius of curvature. Chang makes the important caveat that the material through which the channel is following is homogenous and that the effects of vegetation are not considered.

Chang uses Du Bouys to predict sediment transport. Engelund's (1977) relationship to consider alluvial bed forms and Odgaard (1982) to describe transverse bed slope. These equations could be interchanged with others.

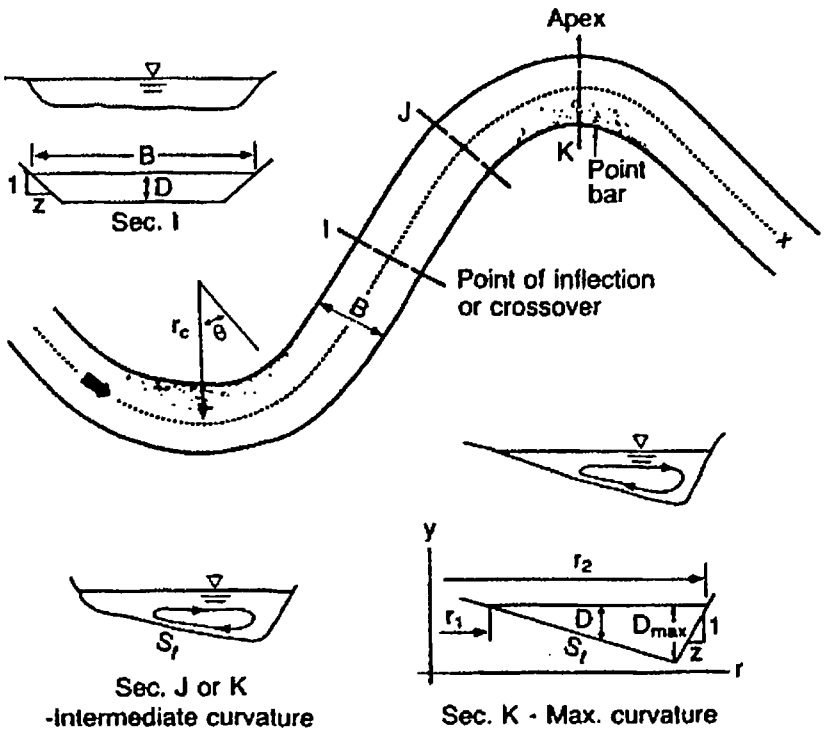

Figure 2.13 Control sections used in planform prediction model, after Chang 1988

Entering the dependent variables into a program and iterating to a solution for sections IJK shown in the diagram Chang obtains regime channel dimensions for each of the three sections. The remaining condition is that the three sections should exist along the same river reach and hence have the same minimum energy. This is achieved by adjusting the angle of the channel side slope. This is observed to vary in a natural channel. The meander geometry is adjusted in such a way that the minimum power is kept constant along the reach.

2.7. Compound channels

The work presented so far in this chapter has concentrated on inbank flow, either in straight channels or meandering channels. The remainder of this review will consider the work done on river channels in the overbank condition. MacLeod (1997) and Wilson (1997) have conducted comprehensive reviews of the subject. A summary of these reports is proffered and more weight is given to the limited amount of material that can be related to sediment transport in meandering streams.

2.7.1. The rationale behind research into compound channels

A compound channel is formed when the flow down a river exceeds its bankfull capacity and spreads out onto the floodplains. Whilst the flood plains provide a natural storage area for floodwaters, they are also flat fertile lands, attractive for farming and housing. Also, historically, towns have developed around river crossings, where trade was concentrated. For these reasons mankind has for many years been interested in constricting the areas in which rivers flood. Traditionally rivers have been deepened and straightened increasing the inbank flow. However as rivers naturally meander this is expensive. It changes natural habitats and has serious environmental consequences. Compound channels can provide an environmentally sensitive, low maintenance solution. Their implementation is hindered by lack of knowledge and predictive equations for the flow and sediment transport behaviour in such streams. The development of reliable design formula would increase their usage.

Early study of compound channels was prompted by the failure of traditional discharge prediction methods to accurately predict discharge.

2.7.2. Discharge prediction methods

The single channel method in which the two-stage channel is treated as a single unit unsurprisingly gives misleading results. Manning's n appears to drastically reduce when overbank flow occurs due to a discontinuity in the hydraulic radius; the wetted perimeter increases rapidly for a small increase in flow depth. In reality, the resistance actually increases.

An improvement on the single channel method is the divided channel method. Here the channel is divided by lines of theoretically zero shear stress, and treated as separate zones. Variations of this method include treating the division lines as part of the wetted perimeter and increasing their roughness to simulate the interaction losses.

The difficulty of accurately predicting these losses is the major focus in the study of discharge capacity in open channels. As current methods rely heavily on field calibration at present, excessively conservative designs are the only way to insure that flooding is prevented. Other influences such as the resistance of vegetation are considered elsewhere in this review.

2.8. Straight compound channels

Straight compound channels are very infrequently natural phenomena. However they have been used in a range of flood relief schemes and result from overbank flow in artificially straightened rivers. Thus, they are of significant engineering interest. A detailed review of the subject can be found in Wark (1993). Important developments are discussed below as they introduce some of the concepts relevant to the meandering compound channels.

Sellin (1964) investigated the interaction between floodplain flow and main channel flow in straight compound channels. He established that large eddies formed over the channel banks introducing slower floodplain flow into the main channel and faster main channel flow onto the floodplain. This interaction introduced greater resistance to the flow than would occur if flood plain and main channel were treated as separate units.

Tamai et al. (1986) investigated the nature of these eddies, stating their importance in drawing up fine sediment onto the floodplain and in exchanging momentum from main channel to floodplain. Using flow visualisation techniques they showed that the fundamental cause of the eddies, was the shear layer between the fast main channel and slow floodplain flows. They also identified the presence of periodic upward swirls caused by the interaction between horizontal surface eddies and eddies on the main channel bed.

Tominga et al. (199?) used a laser Doppler anemometer to show the behaviour of secondary currents in straight flumes. They found that floodplain and main channel flows were separated by a strong upflow from the channel edge directed toward the main channel. They quantified the shear on this junction plain as the shear stress on the flood plain bank plus the shear stress on the floodplain bed less the force of the floodplain flow calculated using the energy slope. This compared well with the results however the variables in the equation are hard to measure. On a quantitative basis, they found that the secondary currents in the main channel were greatly affected by the floodplain flow and that main channel momentum transferred onto the floodplain significantly increased the floodplain shear.

Further tests have been conducted investigating phenomena such as relative flow depth, channel width, relative roughness between main channel and floodplain, and variations in the side slope of the main channel. These variables were examined in the experimental program known as Series A conducted at the flood channel facility HR Wallingford. UK. Studies were performed of boundary shear and investigations into the energy loss mechanisms associated with overbank flow.

This work was summarised by Ackers (1991). Ackers based his predictive method on two main parameters: coherence and DISADF. Coherence is defined as the ratio of conveyance calculated by treating the channel as a single unit to that calculated by treating it as separate zones.

DISADF is defined as the ratio of actual discharge capacity of a straight compound channel, Q divided by the theoretical discharge Q_{th}. (The sum of the discharge in the two zones indicated by the vertical division lines at the top of the two banks.)
The results showed three zones of interaction dependant on the interaction mechanisms.
Ackers work has been criticised because it is a largely empirical system without an adequate theoretical foundation.

A second way of calculating the resistance of compound channels is the lateral distribution method (LDM) developed by Knight and Shiono (1989). It is based on the depth integrated Navier-Stokes equations. This equation models the exchange of turbulence between vertical strips in the cross section. By adjusting the eddy coefficient for the various zones the equation can be solved numerically to predict flow depth. Again calibration is necessary which limits the predictive capacity of the method.

As the data presented in this thesis is related to meandering compound channels, the following comments are intended only to set the work on meandering compound channels in some historical context.

2.9. Meandering compound channels.

A meandering compound channel is formed when river flow exceeds the bankfull capacity of a meandering stream. The resulting hydrodynamic situation is highly complex and has primarily been investigated in laboratories. Field data is difficult to obtain because overbank flows are generally of short duration and taking measurements is inconvenient and dangerous. Water level data has been obtained at some field sites using an automatic data logger. Velocity readings and shear stress measurements required for sediment transport have not been obtained.

The Series B tests were the precursor to the Series C test series of which the tests presented in this thesis form a part. The aim of the Series B was to examine the flow behaviour in a compound meandering channel and to obtain from them the knowledge for effective flow prediction methods. The test channels were modelled in smooth concrete. The effects of the following parameters on flow behaviour were investigated: The relative depth and roughness of flood plain and main channel, aspect ratio and sinuosity of the main channel and the width of the floodplain. The range of values explored in these parameters is given in the top two rows of Table 2.5. The planform details of the Series B channel are given in Figure 2.14. A similar channel was modelled at a sinuosity of 2.043.
Stage discharge measurements were taken for a range of channel forms. Bed shear and point velocity measurements were also taken in a selection of the tests.

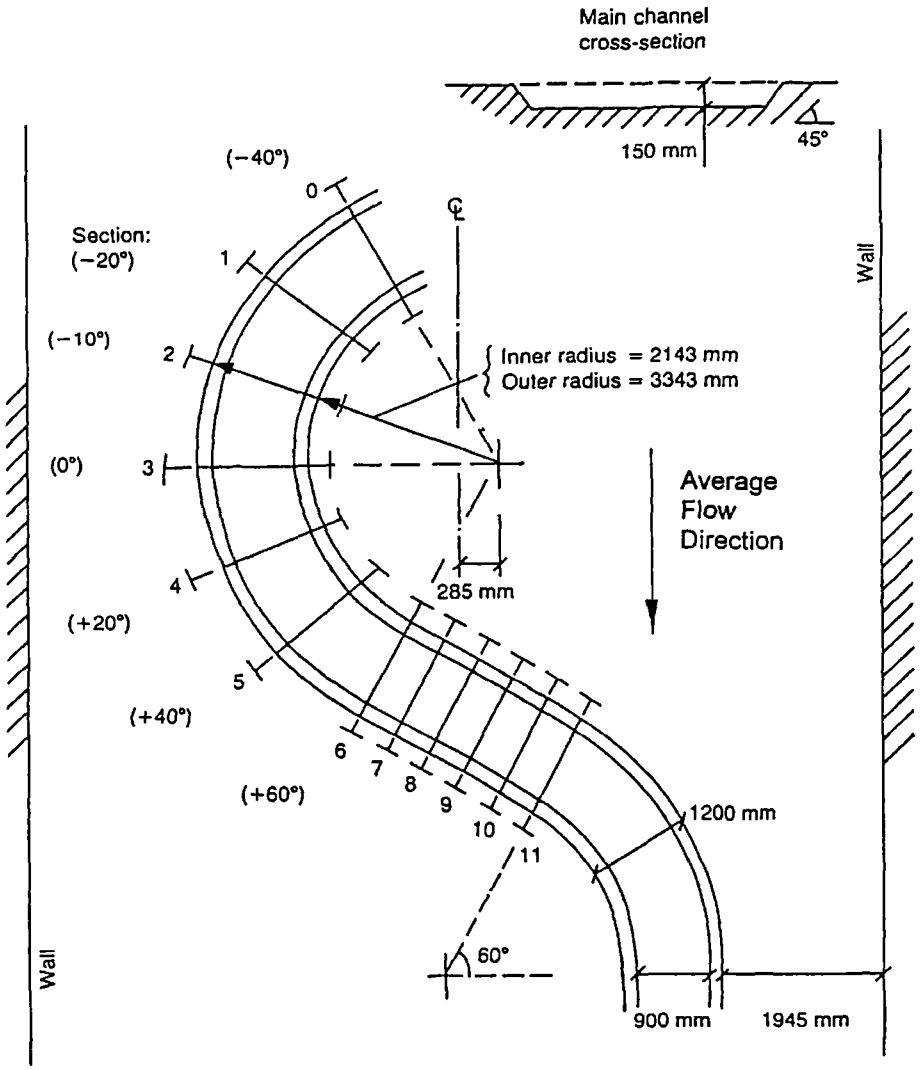

Figure 2.14 Plan view of the Series B showing location of measuring sections

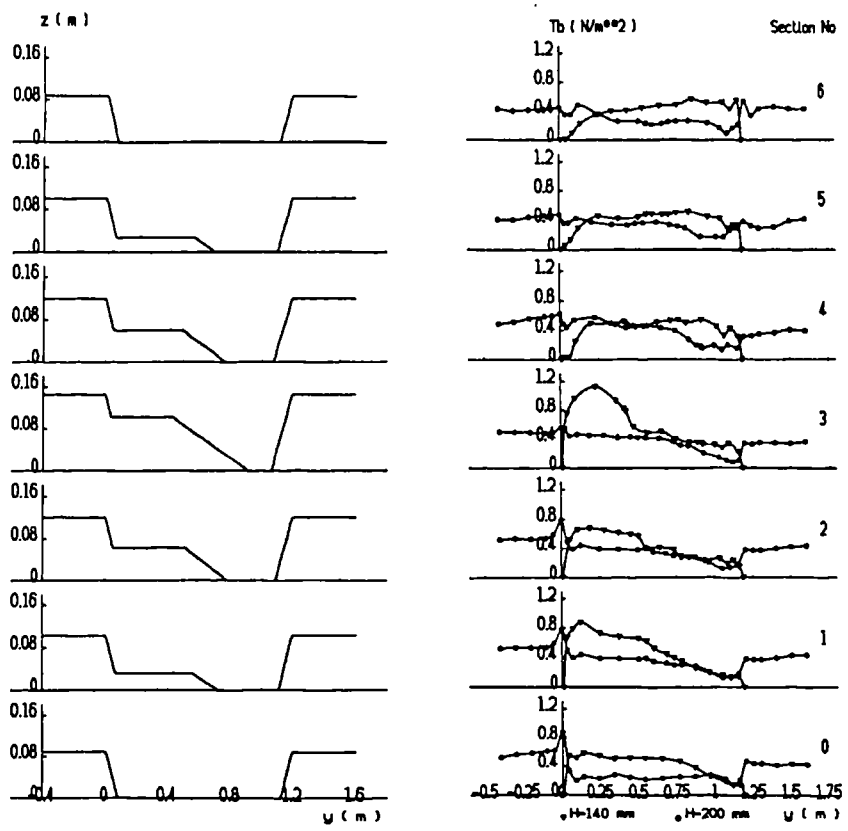

Figure 2.15 Comparison of Channel Geometry of the Flood Channel Facility, Series B, Natural Bedform test (Sinuosity 1.37) with the lateral shear distribution for inbank (140mm) and overbank (200mm) flows

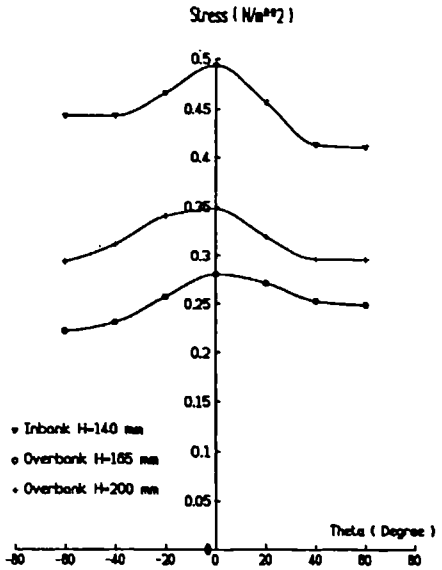

Figure 2.16 Sectional Average Shear Stress along Main Channel (after Knight 1992)

2.9.1. Boundary shear in compound channel flows

The effects of overbank flow on boundary shear are particularly pertinent to sediment transport. Knight et al 1992, recorded boundary shear using a Preston tube for the natural channel form at inbank and overbank flows. Regrettably, measurements were only taken on the smooth floodplain tests.
The average cross-sectional boundary shear for the 1.374 sinuosity channel is shown in Figure 2.16. The x-axis displays the angle between the main channel and the floodplain. Figure 2.15 shows the variation of shear stress across the main channel for the inbank and overbank flows in the 1.37 sinuosity channel.
It should be noted that the shear distribution illustrated is appropriate to the channel when overbank flow first commences. If the bed were to change shape in response to the changing patterns of shear then the shear pattern would also change.

2.9.2. Flow structure

The flow structure is also important in the determination of sediment transport behaviour. The point velocity measurements from the Series B tests are presented by Sellin Ervine and Willetts (1993) and explored in more detail in Sellin and Willetts (1996). The main observations from the analysis are summarised in Figure 2.17 below.

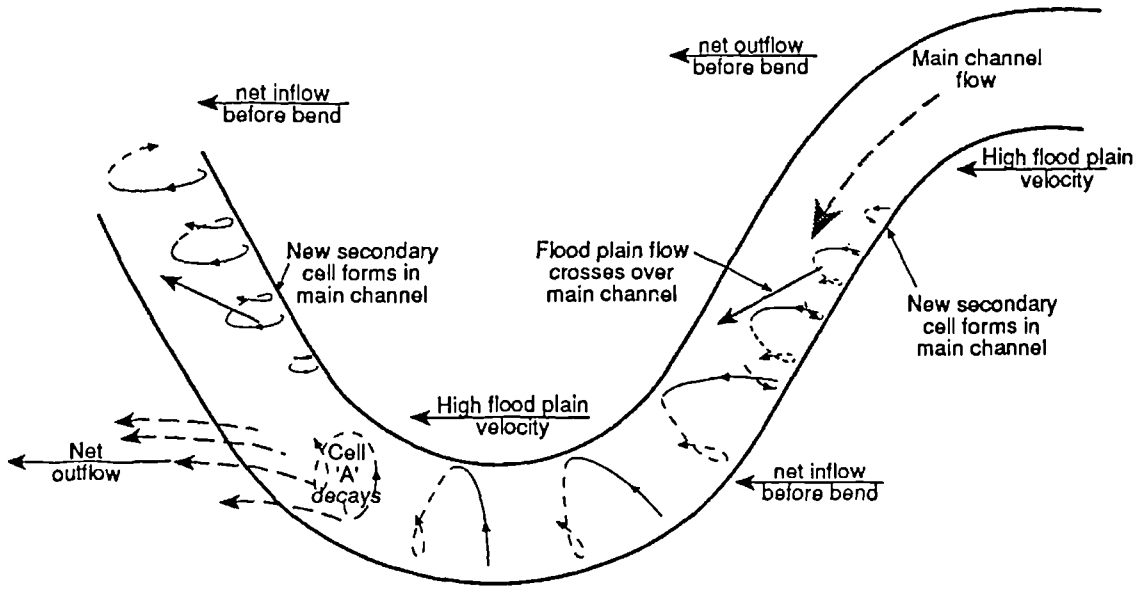

Figure 2.17 Representation of Important Flow Mechanisms within Flooded Meandering Channels

The flow effects illustrated are for the smooth floodplain test. The figure shows that at the crossover the fast flow from the floodplain crosses the main channel at an angle. Some flow passes over the main channel whilst some is entrained by the strong secondary flow cell induced by the overbank flow. This cell is maintained into the following apex, reversing the familiar inbank secondary flow structure.

2.9.3. Discharge prediction methods.

Two predictive methods are described in this section, the empirical F* method and the semi-empirical James and Wark method based on energy considerations. In Chapter 5, these predictive methods are tested against the data collected and a new method of prediction is proposed. The importance of discharge prediction is twofold. As well as accurately predicting the stage it is important to have a method of prediction the effect of overbank flow on flow velocities and shear stress in the main channel discharge to be able to model sediment transport. The efficacy of methods in situations involving a mobile bed and rough floodplains will be closely connected to how well the flow structures are modelled.

2.9.4. The F* approach

The F* approach is an extension of the DISADF method proposed by Ackers for the straight channel work. As it is a development of a straight channel method it can only be applied at the apex where all flow is in the same direction. F* is defined as

$$F^* = \frac{\text{actual measured discharge}}{\text{theoretical discharge based on skin friction only } (Q_1 + Q_2 + Q_3)} \quad (2.115)$$

Where the Q1, 2, 3, shown in Figure 2.18, are calculated in the following way. Q1 is calculated from Manning's equation using the meandering channel bed slope and the bed friction characteristics of the main channel. If the channel does not change form during the overbank flow period this may be thought of as the bankfull flow. Q2 is calculated for the areas shown using the floodplain slope and roughness and the floodplain wetted perimeter excluding the main channel width. This is equivalent to deepening the section of flow over the floodplain to include the section of flow above the main channel. Q3 is computed using the roughness and width and depth of flow on the floodplain outside the meander belt.

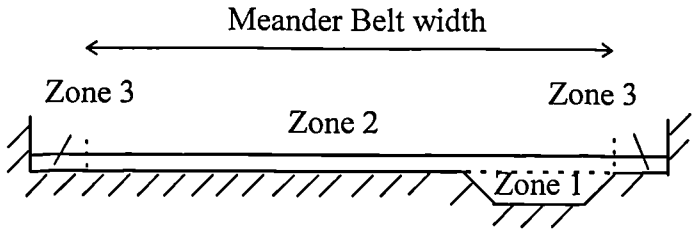

Figure 2.18 Description of zones in the F method*

The value of F* reflects the level of interaction losses between main channels and floodplain. As F* reduces from unity interaction losses become more important.

The parameters investigated in the Series B channel are shown in Table 2.5.

Case Study	Depth ratio (DR)	Sinuosity r	Aspect Ratio (AR)	Cross Section (CS)	Roughness ratio (RR)	Width ratio (Wm/Wt)	Floodplain slope (x 10^{-3})(8)
SERC Series B	0-0.6	1.374	8.0-13.5	Trapezoid - natural	1.0-3.0	0.6-1.0	0.996
SERC Series B	0-0.6	2.04	13.5	Natural	1.0-3.0	0.86-1.0	1.02
Aberdeen	0-0.55	1.41	3.48	Trapezoid	1.0	0.83	1.0
Aberdeen	0-0.55	2.06	3.48	Trapezoid	1.0	0.83	0.62
Glasgow	0-0.5	1.277	6.7	Rectangular	1.0	0.83	1.0
Cork	0-0.44	1.25	4.0	Rectangular	1.0	0.642	1.0
U.S.Army	0-0.38	1.17-1.57	3.0-5.0	Trapezoid	1.0-2.0	0.31-0.91	1.0
Toebes - Sooky	0-0.5	1.13	5.5	Rectangular	1.0	0.40	1.6

Table 2.5 Range of parameters for Meandering Compound flow model studies (after Ervine et al *1993)*

For the range of variables tested the investigators found that the conveyance was always less that that predicted by calculation from the bed resistance. In some circumstances interaction could make up to half the flow resistance.

F* reduces and the hence the interaction effects created under the following conditions:

1. increasing main channel sinuosity
2. decreasing aspect ratio
3. decreasing model scale
4. decreasing available floodway beyond the meander belt
5. in the transition from natural to trapezoidal channel.

F* was found to increase to near unity with relative flow depth when the floodplains were rough and exhibited a double minima when they were smooth.

2.9.5. The James and Wark method

The James and Wark method was based on the observation of flow mechanisms already examined from the Series B tests. It has a semi-physical basis rather than being purely empirical. However, the range of data collected in the Series B tests limits its applicability.

The method calculates the flow in several zones based on Figure 2.18 except that zone 3 is split into zones 3 and 4. The assumption for calculation of these zones is that they have negligible effect on and are negligibly affected by, the flow within the meander belt. The flow in zone 1 is calculated using the boundary roughness and the Soil Conservation Service Method for roughness adjustments in meandering flows in a linearised form.

From empirical data the Soil Conservation Service Method (1963) is given by

$n'/n = 1.0$ for $s<1.2$

$n'/n = 1.15$ for $1.2 < s < 1.5$

$n'/n = 1.30$ for $s > 1.5$ *(2.116)*

To overcome discontinuities this equation was linearized by Wark (1993) to become

$n'/n = 0.43s + 0.57$ for $s<1.7$

$n'/n = 1.30$ for $s > 1.5$ *(2.117)*

This is adjusted by a factor accounting for the overbank flow.

This is the greater of

$Q1' = 1.0\text{-}1.69y'$ *(2.118 a)*

or $Q1' = my' + Kc$ *(2.118 b)*

where $m = 0.0147\ B^2/A + 0.032\ f' + 0.169$

$c = 0.0132\ B^2/A - 0.302s + 0.851$

$K = 1.14 - 0.136f'$

$y' = y^2/[A/B]$

$f' = f_2/f_1$

For rough floodplains at low floodplain depths the first adjustment factor is appropriate however this becomes negative at higher depths. The second adjustment factor only affects very high overbank flow or very smooth floodplains. Therefore this relationship should be treated with caution.

The calculation of flow in zone 2 is based on observations of expansion and contraction losses in flow over a slot and the roughness of the floodplain. A full discussion of the validity of this method is provided in Macleod (1996).

2.10. Conclusions from Chapter 2

The following points are considered most pertinent to the work:

- Inbank channels are attributed a roughness parameter, either Manning's n or Chezy's C that has dimensions and is not constant with depth. The equations strictly only apply to uniform flow, which rarely occurs in practice. Any formulae in which these parameters are used are subject to the resultant inaccuracy.
- For vegetated floodplains the use of n or an equivalent as a roughness parameter is less appropriate as n varies strongly with depth as well as plant density and stiffness, the time of year and the length of inundation. Using a single value of roughness can lead to errors in Manning's n of up to a factor of 4 or greater.
- Research has been conducted into improved formulae for the calculation of vegetative roughness, for dense vegetation and for incremental roughness such as hedges. Application of these formulae however requires collection of significant quantities of field data.

- Improved calculation of floodplain flow is a prerequisite to improved calculation of flow interaction between main channel and floodplain.
- Study of flow over bed forms shows that the vertical velocity profile above a bedform changes considerably between crest and trough. It is unclear at which point along the form the shear velocity is most closely related to the sediment transport rate.
- The best sediment transport formulae are shown to be incapable of reliably predicting sediment transport rate to better than a factor of 2 of the actual value. This is in part due to assumptions in the formula which fail to accurately describe the processes occurring at the bed and partly due to the variation in flow properties across channels. These issues are considered in more detail in Chapter 6.
- The subject of compound channels has been studied extensively for 35 years the primary focus being the resistance due to flow interaction between the floodplain and main channel flows.
- The F* approach to categorising interaction losses in meandering channels has shown that interaction losses decrease as the floodplain side walls become of shallower slope and with increased floodplain roughness.
- Of the methods available for prediction of flow rates in meandering two-stage channels the James and Wark method has been found to predict flow rates most accurately. However, the model is based on a limited set of data and incorporates a single value for Manning's n for the floodplain roughness. The division method which suggested incorporating a horizontal division line at the bankfull level, may not be the most appropriate for rough floodplains where the floodplain flow velocity is much lower than that of the main channel.
- The study of mixed grain sediment transport in a meandering two-stage channel has not previously been investigated by physical model, to the knowledge of the author. Therefore the effects of such a boundary on overbank flow are unknown save by conjecture.
-

3. The Flood Channel Facility Series C (meandering mobile bed with mixed grain sediment) testing program: Experimental design

3.1. Introduction

The specific aims and objectives of the test series are laid out in the introduction to this thesis. This section describes the experimental design used to meet those aims and objectives and the reasoning behind the design approach.

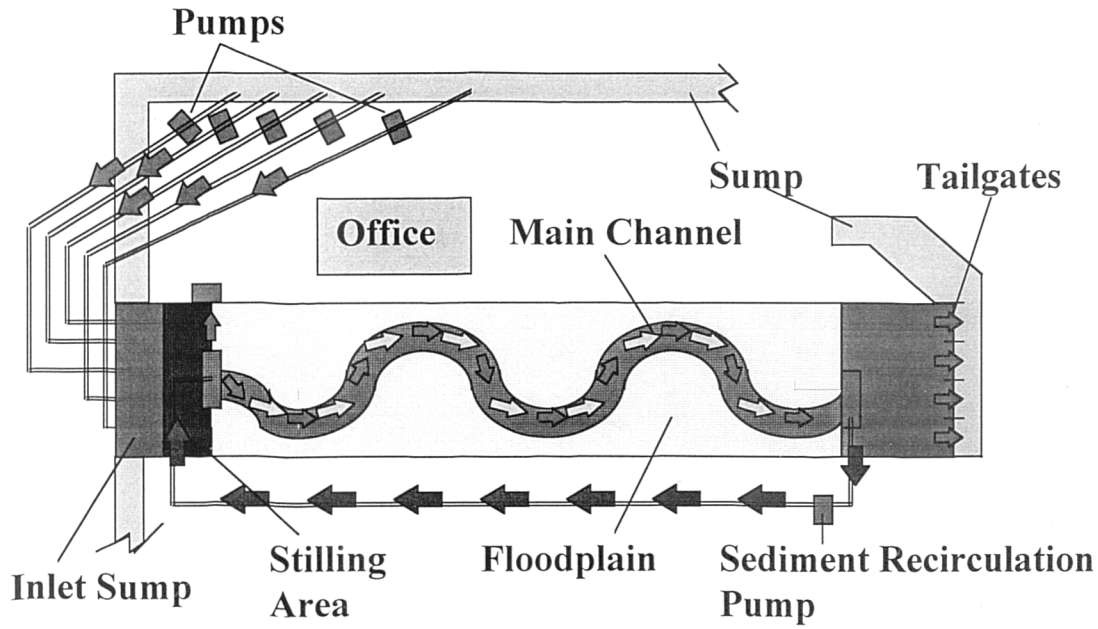

Figure 3.1: Schematic Illustration of the flood channel facility

3.2. Description of flood channel facility

The flume measures 56m in length and 10 m in width. The recirculating flow is provided by a number of pumps, drawing from a common sump, with a maximum discharge of $1.08m^3s^{-1}$. Water slope is controlled by the tailwater level, which is in turn fixed by a row of adjustable overshoot weir plates. The configuration used on the Series C tests on meandering mobile bed channels with overbank flow, conducted between February 1997 and May 1998 is described below.

3.3. Choice of Channel Dimensions

3.3.1. Scale

The aims of the experiment described differ in some ways from those of many physical models; the model is not of an actual river but intended to represent a typical upland meandering stream with a coarse sand to fine gravel bed. The aim being to look at the general effect on sediment transport of the

interaction between floodplain and main channel flows during flooding, rather than the processes of a real stretch of river associated with a specific design. The chosen sediment for the model was a coarse sand with a distribution curve shown in Figure 3.7. This size and density of sediment is appropriate to viewing the channel as a prototype scale model, in which a range of flow conditions may be examined that would be very difficult to test in nature. The extension of the results to larger scales is examined below.

Validation of the model for overbank flows

Limited work has been done on modelling overbank flow in a stream with a mobile bed which means that direct comparisons with field results are not possible. However it has been proposed that if a hydraulic model correctly models sediment processes at a particular flow condition then results obtained at different flow conditions will also be correct (French 1986). This assumption has been successfully used in model development by researchers such as Fargue as early as 1875 and Reynolds 1885 and was the principal behind models up to the middle of the 20th century. A number of sets of data from mobile bed meandering rivers have been obtained for inbank flows (Thorne 1983) and theories to support them. If the bed forms obtained in the model are similar to those found in the field the model may be treated with confidence.

Scaling up the results

In theoretical approaches to scaling, the dimensionless parameters, Fr_s and Re*, the grain Froude and Reynolds numbers are often used to describe the conditions at the surface of a sediment bed. These quantities may be plotted against one another to obtain the Shields curve Figure 2.9. If the model and prototype value of Fr_s and Re* are equal and the channel roughness condition is equivalent then the bed may be considered accurately modelled. Einstein and Barbarossa (1950) present such an approach to modelling the river. If strict grain Reynolds number scaling is applied however it is necessary to change the density of the sediment. Using the method proposed by Einstein and Barbarossa and assuming the model to be at a scale of 1:5 results in a sediment specific gravity in the prototype of 5.4. This is clearly unsatisfactory.

As the transport process of most interest is the bedload and the scale of the model is such that Re*>100 the requirement that Re* be equal in model and prototype can be relaxed, Gerig (1980). This is because the Shields curve is approximately constant where Re*>100. Gerig proposes a scaling scheme where the ratio between grain Froude numbers is kept constant and the roughness condition is equivalent in model and prototype,

$$Fr_{g_R} = 1 \text{ when } \frac{Y_R^2}{\mathrm{L}_R d_R \alpha_R} = 1$$

and

$$\text{Roughness condition } \frac{L_R^3}{\mathrm{H}_R^4 d_R} = 1$$

where L_R is the longitudinal scale ratio, Y_R the horizontal ratio, d_R the grain size ratio and α_R the ratio of submerged particle density.

If α_R is taken as constant then $L_R = H_R = d_R$. This limits the direct extension of the sediment transport results to streams of a similar breadth depth ratio and of larger sediment to that found in the channel. This sort of river is not uncommon. There is also the question of varying bedform regime with Shear Reynolds number which increases with shear velocity and sediment size. These issues have not been fully addressed for mixed grain sediments and require further analysis before the results are applied quantitatively to large systems, however preliminary experiments supported by Chiew (1991) suggest that antidunes are suppressed in mixed sediments.

3.3.2. Slope

The slope has been selected to be similar to those found in real rivers with active bed load transport. The chosen slope is 1/550.

3.3.3. Planform and Aspect ratio

The available floodplain length is 44m. A sine generated planform meandering channel was moulded into the floodplain as shown in Figure 3.3 and Figure 3.3 the horizontal geometry of the channel was devised by investigators from Newcastle and Birmingham universities. This figure is repeated in appendix 5 for easy reference. The side walls are vertical at the outside of the apex and 45° to the vertical at the inside of the apex. The walls are 45° to the vertical on either side of the cross-over section, with a smooth transition in between. The top width of the channel is 1.60m and the sinuosity is 1.344, the valley wavelength is 14.963m thus the channel consists of $1^1/_2$ wavelengths and entrance and exit sections. The moulded channel is on average 0.75m deep. The bottom 150mm is filled with a gravel drainage layer and a land drain pipe. This section is covered by a membrane to stop fines before the sediment is laid on top and screened to a depth of 150mm below bankfull.

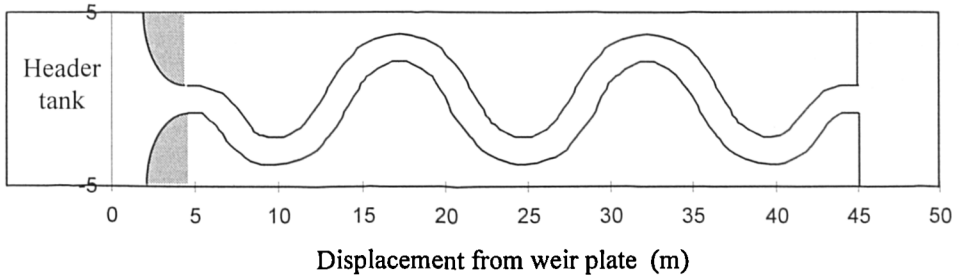

Figure 3.2 Series C: Planform of Flood Channel Facility

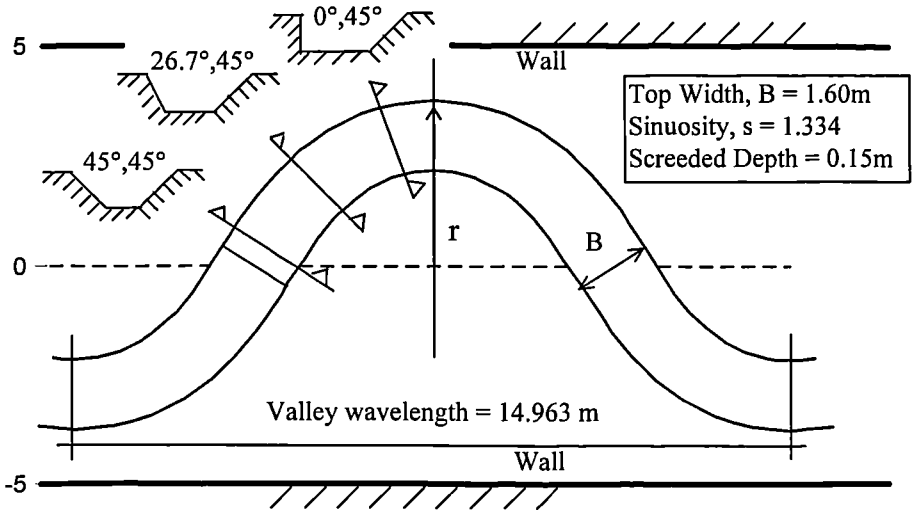

Figure 3.3 Plan view of one wavelength of the Flood Channel Facility: Series C Mixed grain configuration with wide floodplains

3.3.4. Justification for the planform shape

The planform of a river model must be of similar form to natural river channels. The river should have a width to depth ratio similar to those found in reality if the importance of secondary flows is not to be overestimated Yalin(1972). The sinuosity should be similar to that found in upland meandering rivers and the channel sides should be of natural slope. A number of characteristic features of natural meandering rivers are outlined in Chapter 2. The values relevant to the Flood Channel Facility Series C test are given below

Characteristic		**Length (m)**
Meander wavelength	λ_m	14.963
Meander amplitude	a_m	7.62
Bend Radius	R_c	3.00
Channel top width	B_c	1.6
Average depth	h_a	0.15

Table 3.1 Characteristic values for the series C channel

Comparison with the typical relationships found by Leopold et al (1960) give the following results. The most significant deviation is in the relationship between meander amplitude and channel width.

Observed relationship	**Series C geometry (m)**	**Formula (m)**
$\lambda_m = 10.9B_c^{1.01}$	14.963	17.52216
$a_m = 2.7B_c^{1.1}$	7.62	4.527889
$\lambda_m = 4.7R_c^{0.98}$	14.963	13.79357
$R_c = 2.4B_c$	3.00	3.84

Table 3.2 Comparion of Series C characteristic values with the Leopold et al (1960) Formula

Ervine and Ellis (1987) also compiled a set of ratios where the relationship between radius of curvature and channel width is furthest from the accepted mean.

Ratio	Value from series C channel	Observed mean Value
λ_m / B_c	9.351875	10
a_m/λ_m*	0.509256	0.5
λ_m / R_c	4.987667	4.6
R_c/B_c	1.875	2.4

Table 3.3 Comparison of series C characteristics with ratios noted by Ervine and Ellis (1987)

*when $5>B_c/h_a>20$ and $h_a = A_c/B_c$

In general, the channel fits the requirements tolerably well.

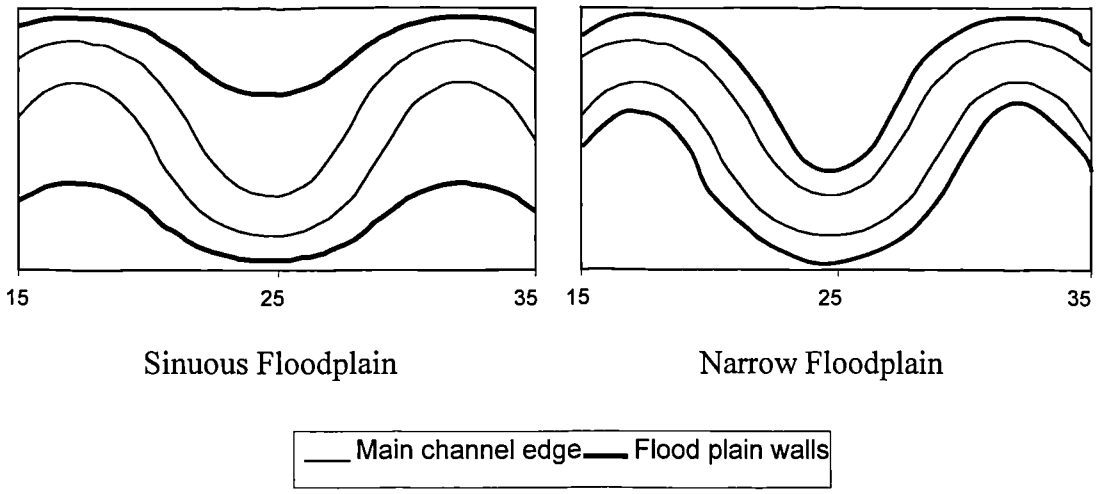

Figure 3.4 Engineered floodplain forms

In order to establish the effects of changes on the flood plain form, some tests were performed with sinuous or narrow floodplain walls as shown in Figure 3.3. The walls were built at an angle of 30° to the floodplain

3.4. Fabrication of the main channel

The Channel was constructed in the steel basin in the following manner.

The channel consists of a $1^1/_2$ meander wavelength test section with a distorted entrance and exit section. The test section was built first, using a $^1/_2$ wavelength template. This was positioned with reference to the centreline of the flume. Breeze block walls were built inside the edge of the template to floodplain level

to retain fill. The floodplain was given a smooth surface finish at the floodplain slope of 1:550. The entrance and exit sections were added when the main section was complete.

The channel walls were screeded to the vertical at the outside of the apex and changed to a 45° angle at the centre line (See Figure 3.2). Form templates were removed before drying. All surfaces were given a smooth finish.

3.5. Sediment selection

3.5.1. Selection objectives

The choice of sediment for the mixed grain tests was based on a number of factors, including quality and consistency of material and the results of both physical and computer tests. The conditions to which the desired material had to comply are outlined below.

1. The smaller fractions should move onto the flood plain when the river is in flood.
2. All fractions should move under maximum flow conditions.
3. Bed forms in the sediment should be minimal if present.
4. Sediment transport should be largely confined to bed load.

Calculations based on the dimensions of the channel at Wallingford suggest that at the initial screeded depth, the maximum shear velocity would be approximately 0.05ms^{-1}. Using the Ackers White sediment transport formula, this suggests that at a mean grain size of 1 - 2 mm all the sediment would be in motion. The calculations are presented in section 0.

3.5.2. Selection Procedure

A large number of samples were collected from different quarries and sieved to obtain grading curves. The quarries producing suitable material could be divided into two categories; those supplying unprocessed material to the building trade direct from the quarry and those supplying high quality sieved sand for use in water filters etc. The latter proved prohibitively expensive and seemed unlikely to produce the plane bed specified by condition 3. Two samples were chosen for further analysis each having a well distributed grain size. One was grade M (medium) and the other grade C (coarse).

3.5.3. Initial Laboratory tests

Both sediments were tested under straight flume conditions at Bristol University.

Tests were carried out in the 7.5 x 0.5 x 0.3m flume. The flume was levelled to a slope of 0.0183, mirroring the apex slope in the flood channel facility. The first 2m of the flume were roughened with enkamat® to develop the flow. A 50mm thickness of sediment was poured on the bottom of the flume and levelled with a float.

Velocity Profiles were taken for both sediments at flows corresponding to initial sediment motion and the point when all grains were in motion. Vertical profiles were taken at the centre of the flume and horizontal profiles, 10 mm above the bed. All readings were taken using a Nixon Probe.

Readings of flow rate for each flow were made using a V-notch weir

Results

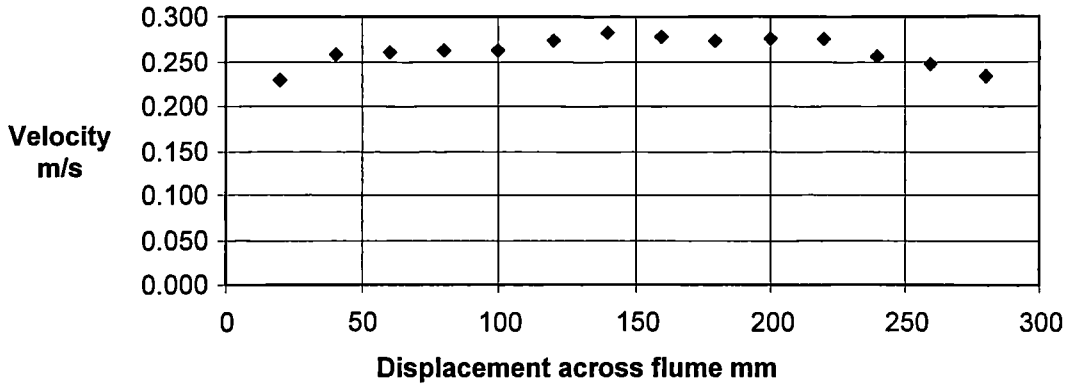

Figure 3.5 Horizontal velocity profile in tilting flume

The horizontal profile shown in Figure 3.5 showed a relatively consistent velocity profile over the centre of the flume which meant that the vertical profile taken at the centre could be expected to show a reasonable value for the central band of the flow. The slow velocities at the sides of the flume are illustrated in the sediment deposition. Large grains are collected at the side of the flume where the velocities are too slow to move them. However smaller grains may still be winnowed out. As this side strip of large grains develops, the roughness increases and the flow becomes still slower reinforcing the effect.

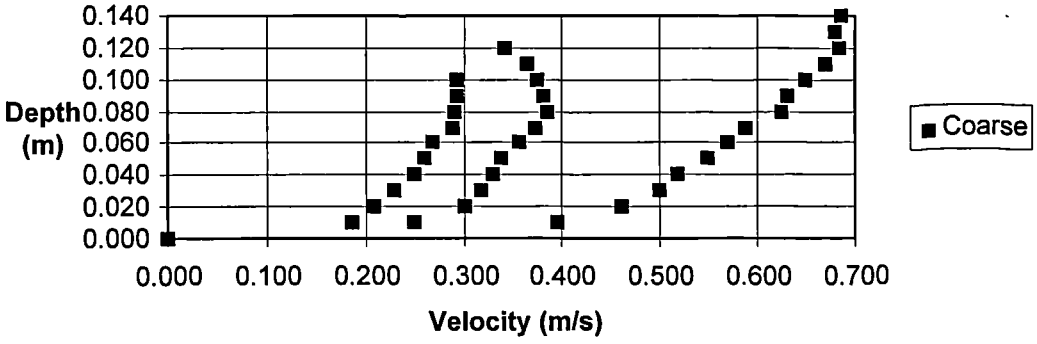

Figure 3.6 Vertical velocity profiles at increasing discharge rates

The shear velocity u_* was selected as the value on which comparisons will be made between estimated Wallingford conditions and those under which the preliminary tests have been performed.

The shear velocity on the flume bed at incipient motion was calculated using two methods, one based on the velocity profile, the other based on the depth slope product using the method proposed by Vanoni and Brookes (1952) to account for the influence of the side walls. The results for each method are shown in the table below.

Condition	u_* (Velocity Profile)	u_* (Vanoni and Brookes)
Initial movement	0.037	0.035
All Fractions in Motion	0.046	0.041

Table 3.4 Values of shear velocity for incipient motion in the medium sediment

Condition	u_* (Velocity Profile)	u_* (Vanoni and Brookes)
Initial movement	0.033	0.046
All Fractions in Motion	0.038	0.048

Table 3.5 Values of shear velocity for incipient motion in the coarse sediment

The results show that in most cases the two methods agree reasonably well. As would be expected the values obtained using the velocity profile are slightly lower than those obtained from the depth slope product approach due to minor bedform roughness described later. The calibration of the probe and the presence of sediment in the flow may affect velocities recorded using the propeller meter.

Bedforms

The remaining condition is that imposed by the bed forms. The coarse sediment formed dunes 400 - 700 mm long in the 7.5m long x 0.3m wide flume. Their vertical height reached about 5mm which would be acceptable in the Wallingford channel. The medium sediment formed ripples about 10mm apart in some sections of the flume, these were confined to a height of about 5mm. Given the much larger bed forms that occur in single size materials of grain sizes present in the sample, it is concluded that the mixed grain sizes suppressed the formation of large bed forms in each case.

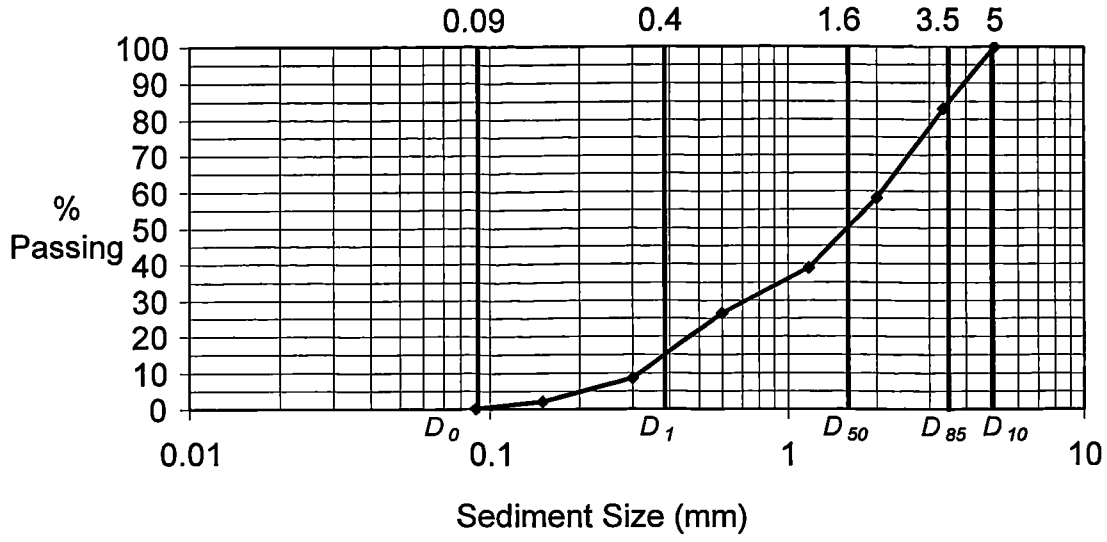

Figure 3.7 The sediment distribution curve for the sediment used in the series C mixed grain tests

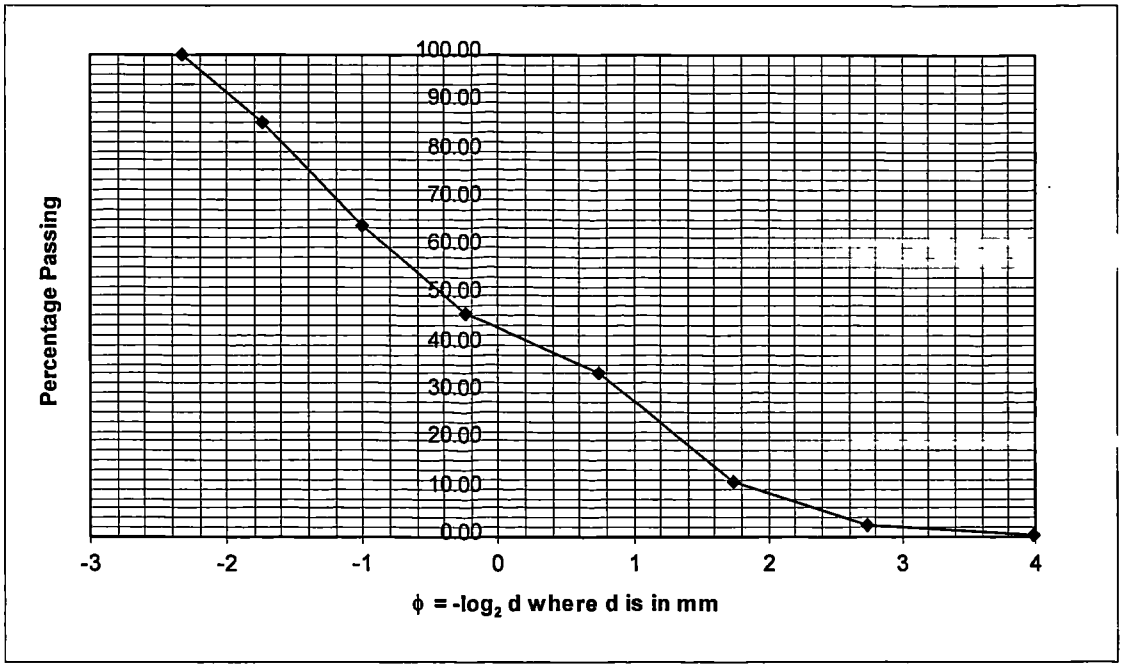

Figure 3.8 Distribution of chosen sediment on the phi scale

Satisfactory results were obtained for both sediments. The coarser fraction was selected. Tests using the SAM program, which incorporates Brownlie's bedform predictor, also indicated suppressed bedforms in the coarse fraction under likely conditions in the FCF.

3.5.4. Trial of the chosen sediment in the flood channel facility

The final test of sediment suitability was a trial of the sediment in the flood channel facility. The sediment was found to produce large stable bedforms in the positions in the channel expected in a natural river. Sediment moved in long flat dunes across this stable geometry and thus the dunes did not dominate the flow behaviour. Sediment sorting was observable over the channel width and tended to accumulate in

dead zones behind the point bar. Thus the sediment acceptably modelled the behaviour of sediment in a real river.

3.5.5. Sediment Return system

As shown in Figure 3.1, a sediment return system was used in the model. The sediment fell into a hopper on reaching the end of the flume and was returned up a pipe and re-entered the flow at the top end. A smooth concrete entrance was constructed so that the flow had enough energy to pick up the sediment and return it to the system. Tests showed that material below 0.2mm in diameter travelled over the hopper in suspension. As this represented only a very small section of the sediment distribution, it was considered as wash load.

The relative merits of sediment feed and recirculation systems are considered in Parker (1995) but not discussed further here.

3.6. Selection and calibration of material for roughening the floodplain

Floodplain roughness has been simulated in many ways during the era of hydraulic modelling. Previous tests on the flood channel had been performed either using a smooth concrete floodplain with Manning's $n \approx 0.012$ or roughening rods, with a Mannings $n \approx 0.02$-0.04. These experiments had been criticised on the basis of failing to model the highly roughened floodplain surfaces found in nature. In the series C experiments a method was desired which would create very high floodplain roughness.

Expanded aluminium of the type used for plastering has previously been attached flat to roughen surfaces. In the current test vegetative material on the floodplain was simulated using expanded aluminium sheets, cut and folded to form 100mm high roughening strips of triangular cross section. These were placed perpendicular to the flow at 500 mm centres.

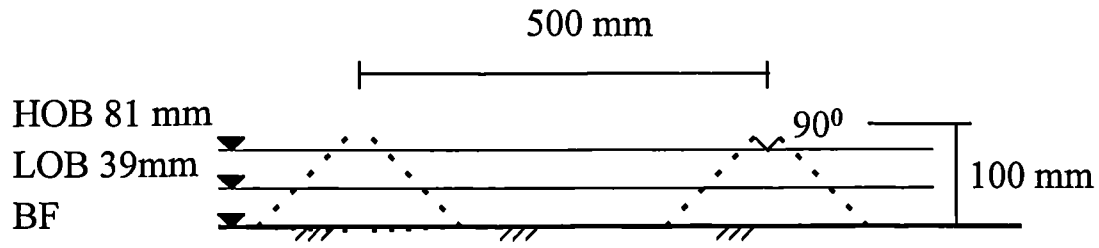

Figure 3.9 Schematic illustration of the aluminium roughness strips used on the floodplain

The sections were tested in the same tilting flume as the sediment samples. Tests were performed at a range of flow depths and frame spacings. The results in terms of variation of Manning's n with depth are given in Figure 3.10.

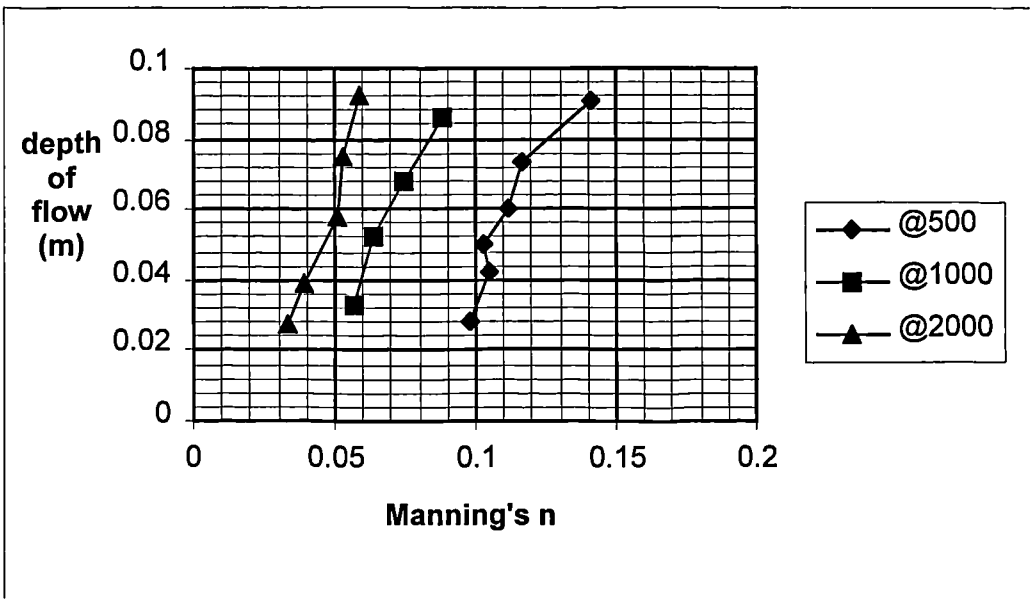

Figure 3.10 Variation of Manning's n with depth for roughness strips at three spacings

This form of roughness was found to have the following advantages:-

- Versatile - the spacing can be changed to produce different roughnesses
- Versatile - height can be varied to give submergence if required
- Cheap to use; easy to manufacture
- Access onto floodplain still possible along the gaps
- No large wakes which persist downstream
- When placed across main direction of floodplain fall they would be most correct for highest floods

A method has been devised by the author, based on the concept of flow through an orifice, for obtaining roughness values for this form of floodplain roughness at any depth and spacing. This method is compared with that obtained for the rod roughness used in previous tests in Appendix 2: Simulating vegetative roughness in physical models.

3.7. Instrumentation and Measurements

Reading Positions

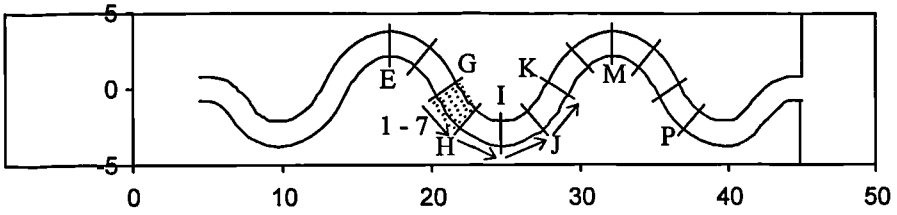

Figure 3.11 Measuring positions: Velocities G - K, Bed profiles G, G1 - J7, K - N, Water surface slope E - P

Datum pins, set level with the concrete flood plain, were positioned at each 1/8th of a wavelength down the main channel and ascribed letters starting from A at the first Apex. Measurements were confined to

the sections E to P to allow for entrance and exit effects. For more detailed measurements these divisions were divided into eight subdivisions i.e. G, G1, G2...G7, H. This measurement system and nomenclature was common with the uniform grain tests.

The facility is equipped with an instrument bridge, running on horizontal rails mounted on the sides of the flume. The bridge supports a carriage which can be moved across the channel, to which a bed profiler, automated traverser system and point gauge are connected.

3.7.1. Water Levels

All tests were conducted at uniform flow. Stilling wells were found impractical as sediment blocked the entrances; hence readings were taken with a point gauge attached to the carriage on the main bridge. At bankfull and all subsequent tests measurements were taken relative to the datum pin on the right hand side of the channel. Water levels were recorded from E to P inclusive and a regression line drawn through all points. Uniform flow was accepted when the slope at the regression line was equal to the floodplain slope divided by the sinuosity of the main channel. On overbank tests the water levels on the top and bottom of the floodplain were recorded and the tailgates adjusted to give an initial slope before readings were taken on the main channel.

This procedure was common to all tests in the FCF mixed grain series C and to the previous work on uniform grain sediment.

3.7.2. Sediment Sampling

Total Load.

The rate of total sediment movement was measured continuously for six hours during each test. Two collection trays were placed side by side under the return system at the top of the channel. The sediment return was directed into one tray for five minutes. The return system flow was then directed into the second tray and the sediment in the first tray weighed wet and emptied into the channel. The empty tray was then returned, thus allowing continuous sampling.

Local Bedload Measurement

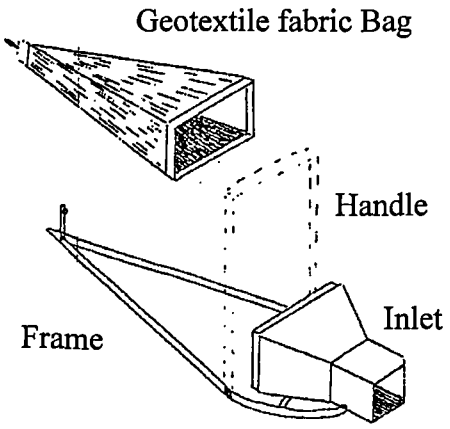

Figure 3.12 Helley Smith Bedload Sampler

After experiments on two designs and a range of scales, a scaled down (1:3.75) Helley Smith type sampler was chosen to measure local bedload transport. Dimensions are given in Appendix 5. Zhou & Zou (1997) identified the following requirements of a bedload sampler:

- When the sampler is set on the riverbed, the interference of water flow should be the minimum, especially near the entrance.
- The effect of sediment size and transport rate on the sampling efficiency should be minimised. Calibration should be performed.
- The Sampler should be simple in its design, firm in its structure, easy in its operation and maintenance and should have sufficient weight.
- The intake velocity at sampler entrance should be close to natural velocity.

These conditions were met adequately by the chosen sampler.

Samples were taken at 100 mm intervals across the channel at five sections (K - O). The measurement duration was five minutes. The samples were subsequently oven dried and graded by wet sieving.

3.7.3. Bed Profile Measurements

Bed formation was measured using a Hydraulics Research bed profiler and photogrammetry. The profiler was used to record profiles at $^1/_8$th wavelength sections from G to O, with detailed measurement from G - K, as shown. The step width was 25mm. The bed surface form was also recorded using photogrammetric techniques (performed by Lane, 1998). The two methods correlate extremely well.

3.7.4. Velocity Measurements

Floodplain Velocities

Floodplain velocities were measured using an ADV two-dimensional probe and by dye tracing. Dye tracing was found to give more instructive results and hence this method was adopted.

Main Channel Velocities

The velocities in the main channel were measured using a laboratory acoustic Doppler velocimeter (ADV). The ADV uses acoustic sensing techniques to measure flow velocity in a remote sampling volume. Data were collected at 25Hz in three dimensions. The acoustic sensor consists of one central transmit transducer and the receive transducers mounted on short arms around it at 120 azimuth intervals. The measurement sample is approximately 50 mm below the transmitter. The measured flow is relatively undisturbed by the presence of the probe.

Velocities are recorded in verticals spaced 100 mm apart. The readings on each vertical were at 10 mm intervals for the 50 mm closest to the channel bed and at 20 mm intervals for the remainder of the section.

Problems were experienced due to interference from the returning boundary pulse when the probe was at certain distances from the bed. As the signal recorded by the receive transducers is reflected by ambient particles in the flow, low sediment concentration in the water also caused difficulties. For each cross section the probe produced a continuous file of velocity data at 25 Hz. The sections of data pertaining to individual points in the cross section were abstracted by collating the digital file from the probe with the time file produced by the computer operating the traverser.

3.7.5. Core Sampling

In order to observe the process of river formation, core samples were taken from the channel bed using sections of plastic pipe, filed at one end to obtain a sharp edge and split down the center for easy sample recovery.

3.7.6. Surface Sampling

Bed surface samples were obtained using 60mm diameter metal cylinders placed on the bed. These were filled with molten wax. The temperature of the wax was relatively critical: if the wax is too hot it will run into the sample picking up more than the surface layer. This was particularly problematic in the areas in which an armour layer had formed and the large grains had winnowed out leaving a passage for the molten wax. In general the method obtained rather small samples which were hard to grade and should be regarded as giving a general picture only.

3.8. Conclusions

In this chapter it is argued that the model examined in this thesis may be considered an acceptable scale model of an upland meandering river in terms of slope and planform.

Bed sediment has been chosen in which all fractions are mobile at the highest flows. Small scale laboratory tests show that the mixed grain nature of the sediments suppresses ripples and that long flat dunes are formed in their place.

A sediment recirculation system is to be used on the flood channel

Floodplain roughness, formed from folded strips of expanded aluminum has been designed and tested in a small flume to accurately simulate the levels of roughness found heavily roughened floodplains. This represents a degree of roughness unexplored in previous tests.

Instrumentation and methodology have been designed to measure the variation in:

Water levels, bed forms, flow velocities, total and local rates of sediment transport, surface roughness and bed morphology.

These tests will examine the variation in sediment transport rate and sediment transport with changes in floodplain roughness and flow depth.

4. FCF series C, mixed grain tests: Experimental Results

4.1. Introduction

The aim of this chapter is to present the results necessary for the comparison between inbank flow in a meandering mobile bed channel with overbank flow in the same channel at varying flow depths and floodplain roughness.

Explanation of test names

Each test has been given four-letter name. The first two letters refer to the water level i.e. BF = bankfull, HO = High overbank and LO = low overbank. In the inbank tests the second two letters refer to the condition of the inbank channel i.e. MB = mobile bed. The third and fourth letters in the overbank tests refer to the condition of the floodplain. The third letter refers to the floodplain roughness, S = smooth, R = rough and the fourth letter, the extent of the floodplain, W = wide. Hence the test name "HORW" refers to high overbank flow conditions with rough and wide floodplains.

Table 4.1 gives summary data for these tests. Tests examining the effect of changes in floodplain shape and the removal of riffles are presented elsewhere. The limitations of the data in terms of experimental technique and processing are addressed here however the relevance of the results to current theory and engineering practice is explored in Chapters 5 and 6

Test name	Main channel bed condition	Q_{TOT} (l/s)	h_f (mm)	Q_s g/s
BFMB	mobile	97	0	8.74
LOSW*	mobile / frozen♣	163	36	0.45
HOSW	mobile	450	78	11.13
LORW	mobile	120	51	1.02
HORW	mobile	163	85	2.32

** The velocity, profile and water level data in this test was collected by Dr Rameshwaran from Loughborough university using the methods devised by the team of investigators.*

♣The stage discharge data was collected for a mobile bed whilst the velocities were recorded over a frozen bed.

Table 4.1: Summary of main test program

4.2. Results presented

The following sets of data are presented for each test in the table:

Bedforms

The macro bedforms are illustrated in a contour map of the bed for each test. These are constructed from point elevations measured using the bed profiler described in Chapter 3 and mapped using Surfer software, (see Appendix 1 the method being similar to that for processing velocities). On the same page a photograph

showing grain sorting around the following meander bend is shown. This illustrates the grain sorting. The diagrams should be read together as it is hard to judge flow depth and channel wall angles from the photograph. The channel labelling and geometry is given in Appendix 5.

Discharge

The discharge down the main channel, above and below floodplain level for the overbank flows only is shown in Figure 4.5 and Figure 4.6. This information was obtained by summation of the point velocities collected in the channel. The method is expounded in Appendix 1

Flow structure

For each test isovels show the distribution of main stream velocities at the crossover, the apex and the cross section 1/8th of a meander wavelength before and after the apex. Secondary currents are shown at the same sections.

Due to the movement of the bed and the idiosyncrasies of the ADV probe, the data for some sections was relatively incomplete. In tests where equivalent sections were duplicated the most complete sections have been used. In order for easy comparison, however, the sections have in some cases been reversed. As the results showed strong repeatability around apices, this should not seriously effect any conclusions.

The results are presented in a similar format for each test.

The results from the bankfull test are presented first as a special case and the overbank tests are presented as a group. Detailed discussion of the velocity processing techniques may be found in Appendix 1

Sediment transport

The collection of bed load data is widely acknowledged to be an extremely difficult activity. The movement of material in dunes tends to mean that grain size and transport rate vary along the length of the dune. Ideally for comparison, transport data should be collected from one position on the dune, for example the crest. However given the time pressure on the experiments, this was not possible. In some circumstances where no sediment was observed to be moving, no sediment collection was attempted. It should also be noted that when the sediment sampler was placed on the bed a small amount of sediment tended to enter the sampler. This has most effect on the smallest samples and these results should be treated with caution. Zhou and Zou (1996) have published a method for collection of data across a stream based on statistical theory. The method used in these tests disregarded both dune position and variation in sediment transport rate. It was considered to be simple and appropriate to the time scales under which we were operating and given the long flat nature of the bedforms. If in future tests the investigator would be advised to consider carefully the work in the aforementioned paper.

4.3. The Bankfull test

The conditions found in the river channel at bankfull are of great importance for a number of reasons.

Formative Discharge

The induced geometry when the river is flowing at bankfull is that which is found in most rivers even when the flow is below bankfull. This is because in a normal flooding system, when overbank flows are relatively shallow, the bankfull flow has the ability to move most sediment and forms armour layers which are undisturbed at lower less powerful flows. For this reason the bankfull discharge is frequently referred to as the formative discharge. In the current test series steady state bankfull conditions were obtained at the beginning of each of the overbank tests and hence deviation from the bankfull condition must be considered when analysing the resultant bed features and flow structure.

Validation of Data

The issues of scale modelling and data validation have been addressed in chapter 3. It should be reported here however that the inbank bedform and the flow structure are very similar to those observed in the field. This has been confirmed by experience field scientists. From the theory expounded in Chapter 3 we should be reasonably confident of the results for overbank flow.

Comparison with series B data

The most complete set of comparable data for overbank flows is the natural planform 60° meander series B test series. The tests were conducted in a river channel with a generic bankfull bedform and thus the results indicate the initial conditions for overbank flow. Whereas the current series of tests were examined when the channel had reached near equilibrium conditions. A detailed comparison of the two data sets is performed in Chapter 5.

Sediment transport through a meander bend during bankfull flow: A general description

The results in this section present the primary and secondary velocities in the channel at several cross-sections, the variation of flow depth over the channel and the variation in grain size. An understanding of the way in which sediment travels through a river with a meandering plan form may be obtained from studying these figures.

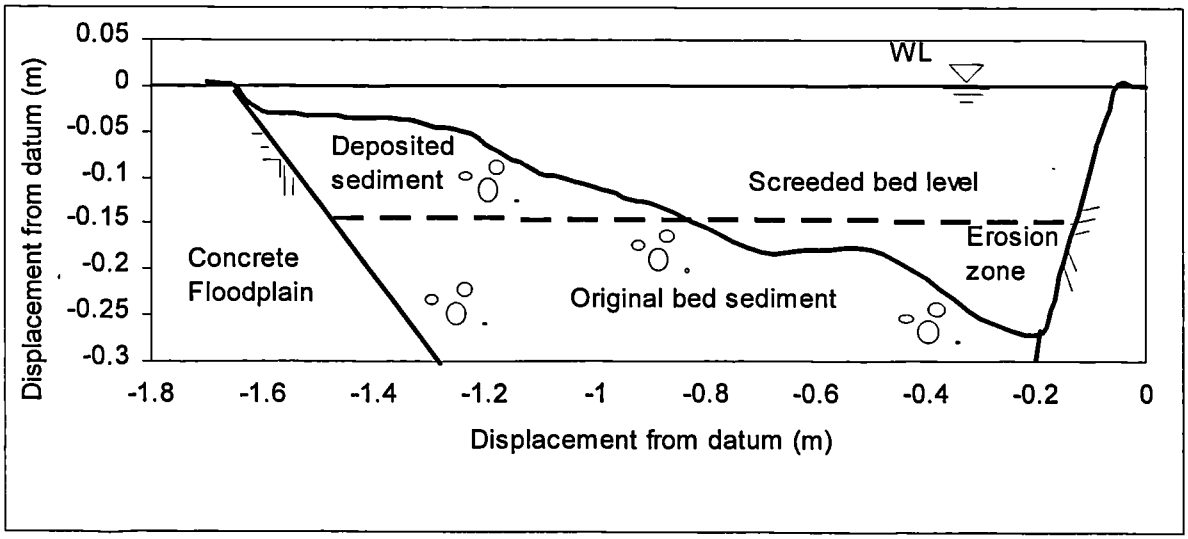

Figure 4.1 Bed profile at section J, bankfull flow. Showing erosion and deposition. The dashed line shows the original screeded level

Figure 4.1 shows the bed profile at section J during the bankfull test. The screeded bed level is shown at 0.15m below the floodplain level. The sediment above this level has been scoured from regions of the channel upstream where the shear stress is high and deposited in the current region of low shear stress where the bed is sheltered by the point bar. The sediment in this region is observed to be finer than the majority of the sediment in the channel. The fine material forms ripples in the shallow flow - see Figure 4.2 and the flow velocity and sediment transport rate is very low.

Material below the 0.15m line in general retains the well-mixed matrix of the original screeded bed. However, there is an active transport layer at the interface between the flow and the sediment. In the regions of scour the finer grains are preferentially transported, winnowed out, leaving an armour layer several grains thick of larger material. This is a region of low sediment transport because whilst the flow is fast and deep the large grains form a rough boundary and, as they are large, do not easily move. The strong secondary currents prevent smaller, more transportable, grains from falling into this high velocity zone.

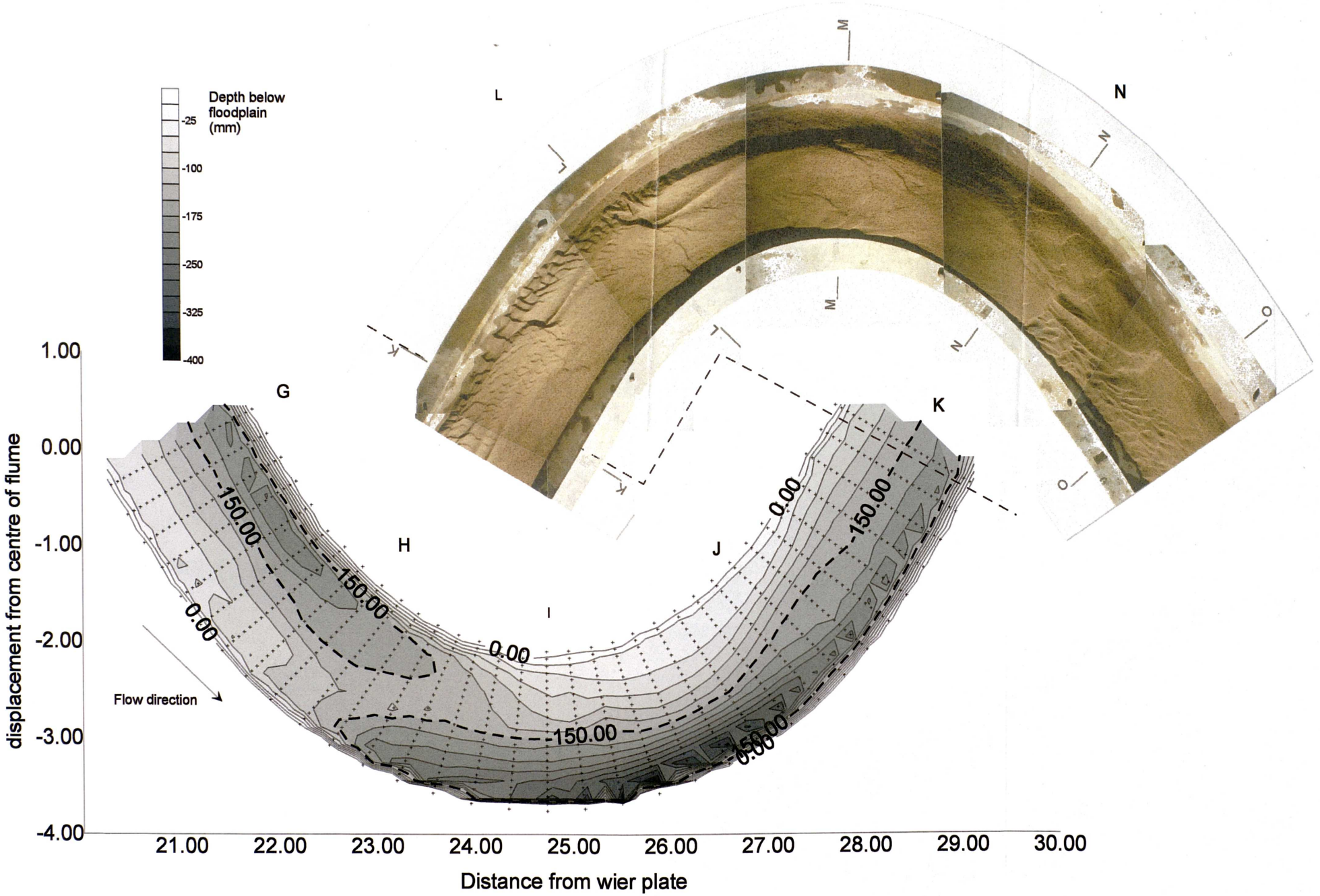

Figure 4.2 Bankful mobile test Contour map of channel bend (sections G-K). Dashed line at depth of 150 mm shows original screeded bed level. The photograph shows grain sorting around the subsequent bend (sections K - 0)

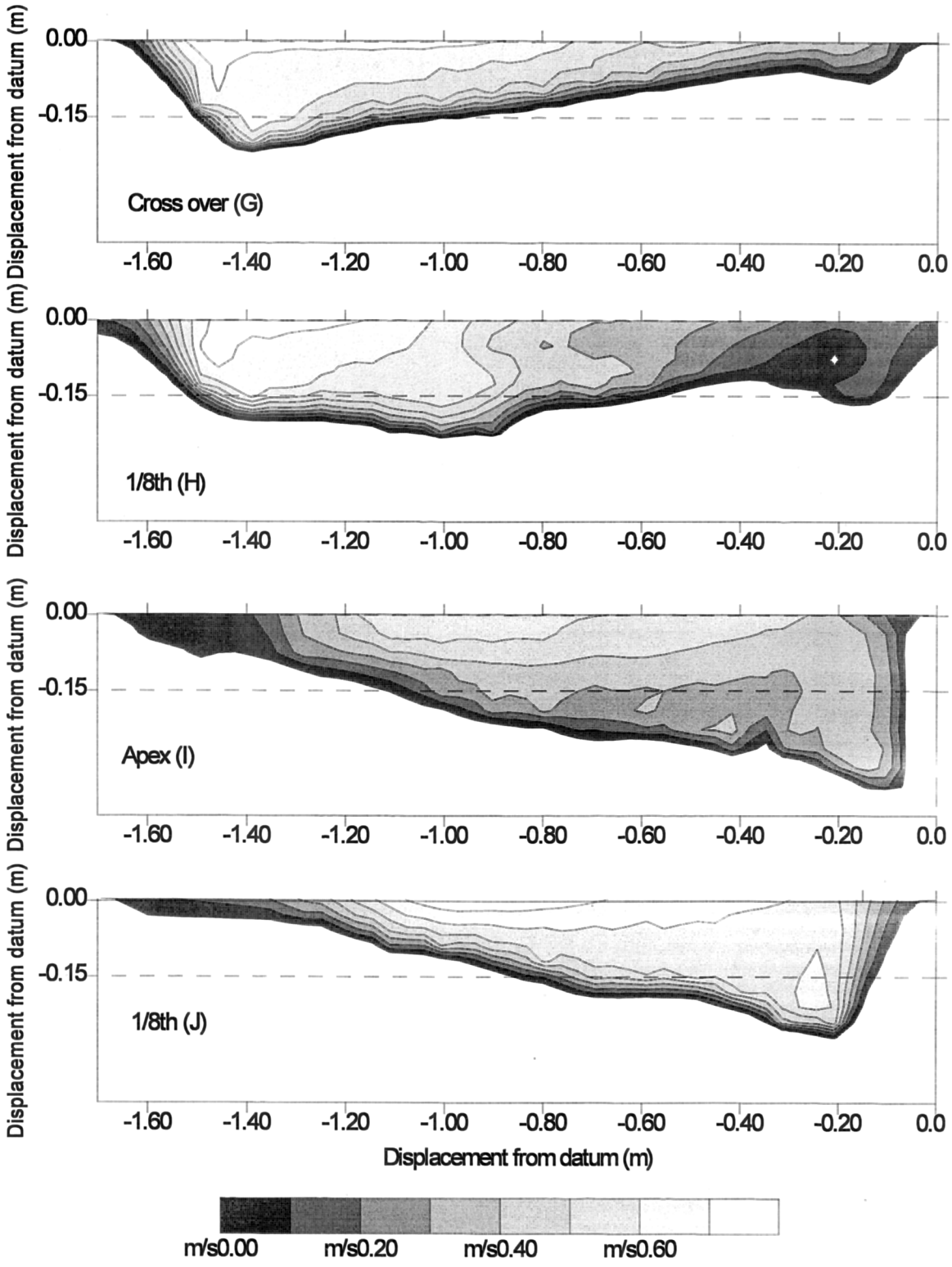

Figure 4.3 Primary velocities from the bankfull test. The dashed line in each diagram shows the original screed bed level.

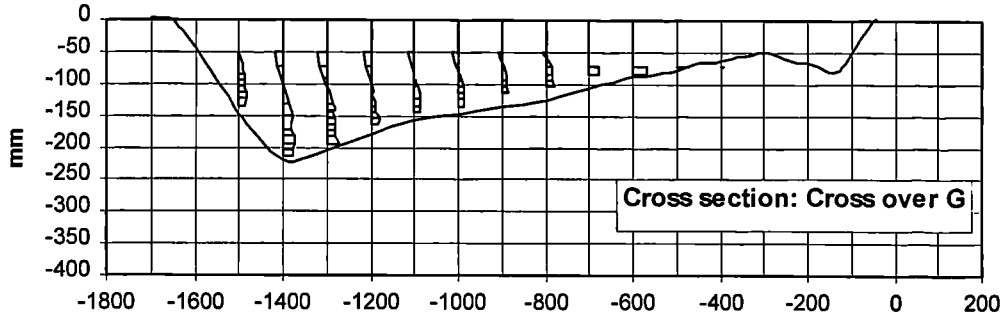
mm
0
-50
-100
-150
-200
-250
-300
-350
-400
-1800 -1600 -1400 -1200 -1000 -800 -600 -400 -200 0 200
Cross section: Cross over G

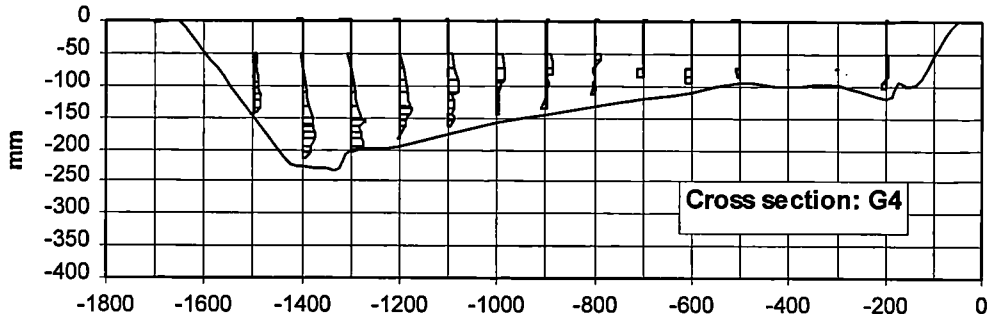
mm
0
-50
-100
-150
-200
-250
-300
-350
-400
-1800 -1600 -1400 -1200 -1000 -800 -600 -400 -200 0
Cross section: G4

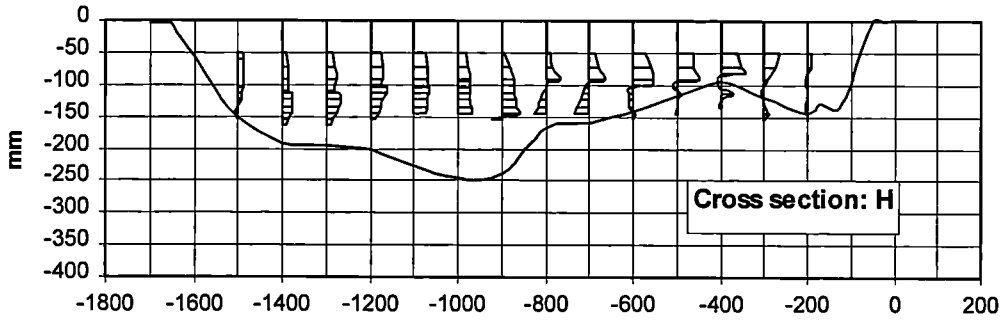
mm
0
-50
-100
-150
-200
-250
-300
-350
-400
-1800 -1600 -1400 -1200 -1000 -800 -600 -400 -200 0 200
Cross section: H

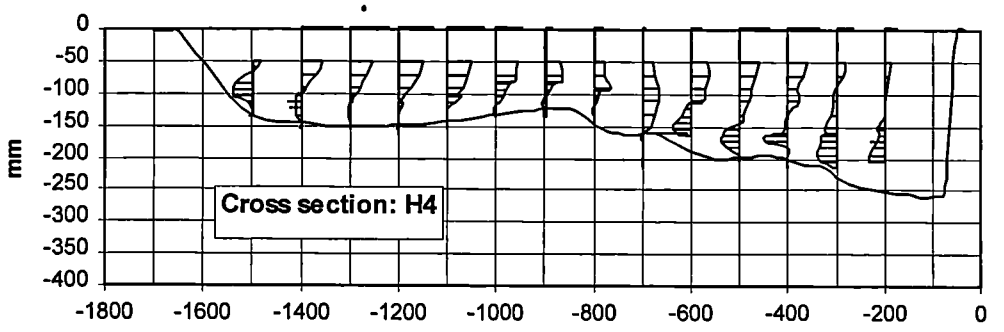
mm
0
-50
-100
-150
-200
-250
-300
-350
-400
-1800 -1600 -1400 -1200 -1000 -800 -600 -400 -200 0
Cross section: H4

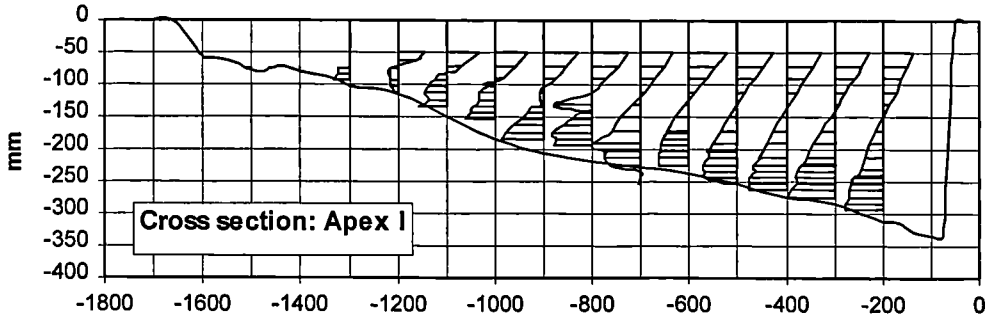
mm
0
-50
-100
-150
-200
-250
-300
-350
-400
-1800 -1600 -1400 -1200 -1000 -800 -600 -400 -200 0
Cross section: Apex I

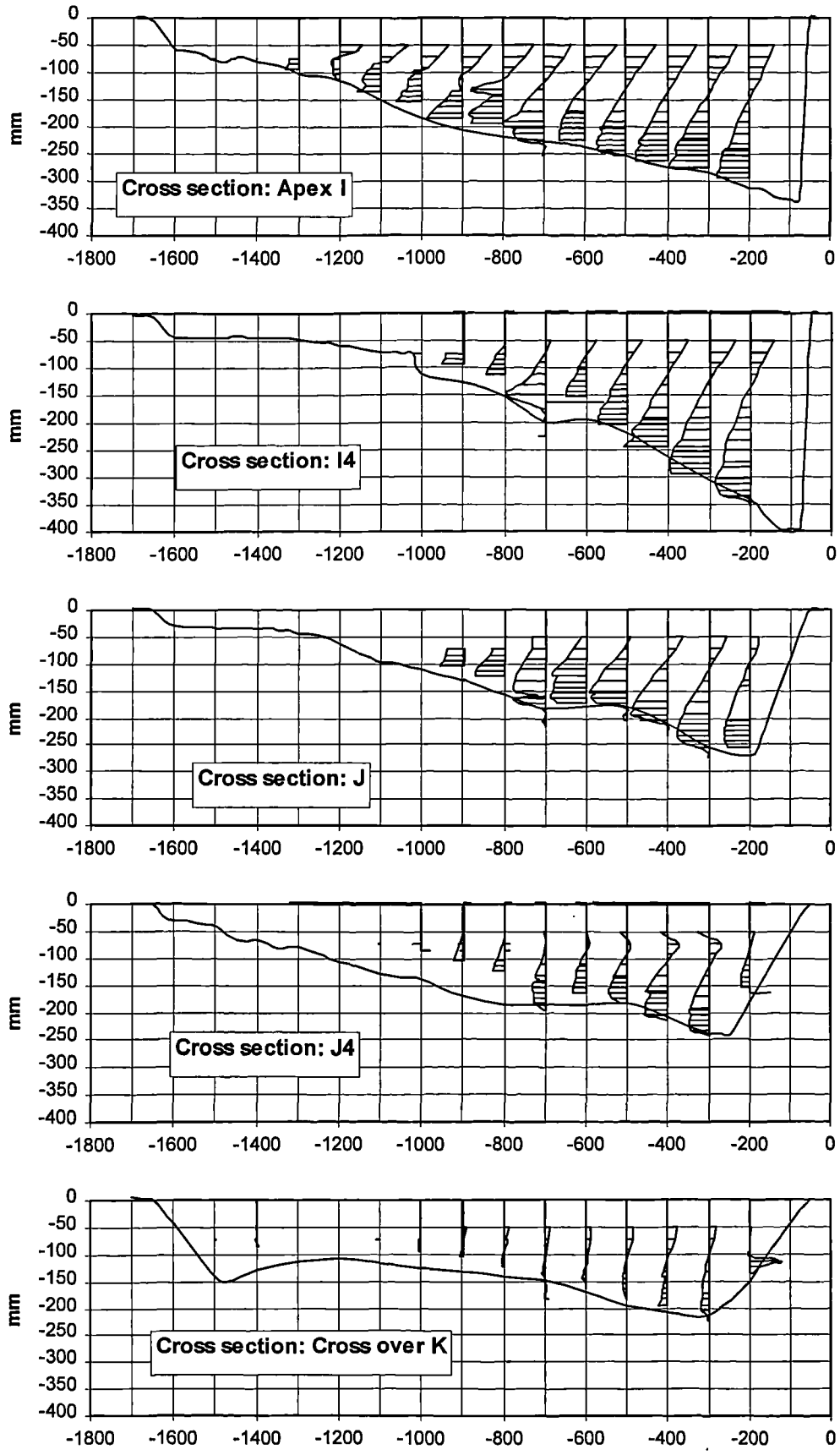

Figure 4.4 Secondary circulation: Bankfull test

4.4. Overbank Tests

Summary data appropriate to the overbank flow tests is presented on this page, namely the variation in flow between tests and between individual sections. The information has been presented in two forms in order to make these differences as clear as possible. The remainder of the information is presented giving bed information first followed by primary and then secondary velocities. It should be noted at this point that no detailed information regarding bed form or grain sorting in the low overbank smooth case was collected and hence this information is absent from the data set.

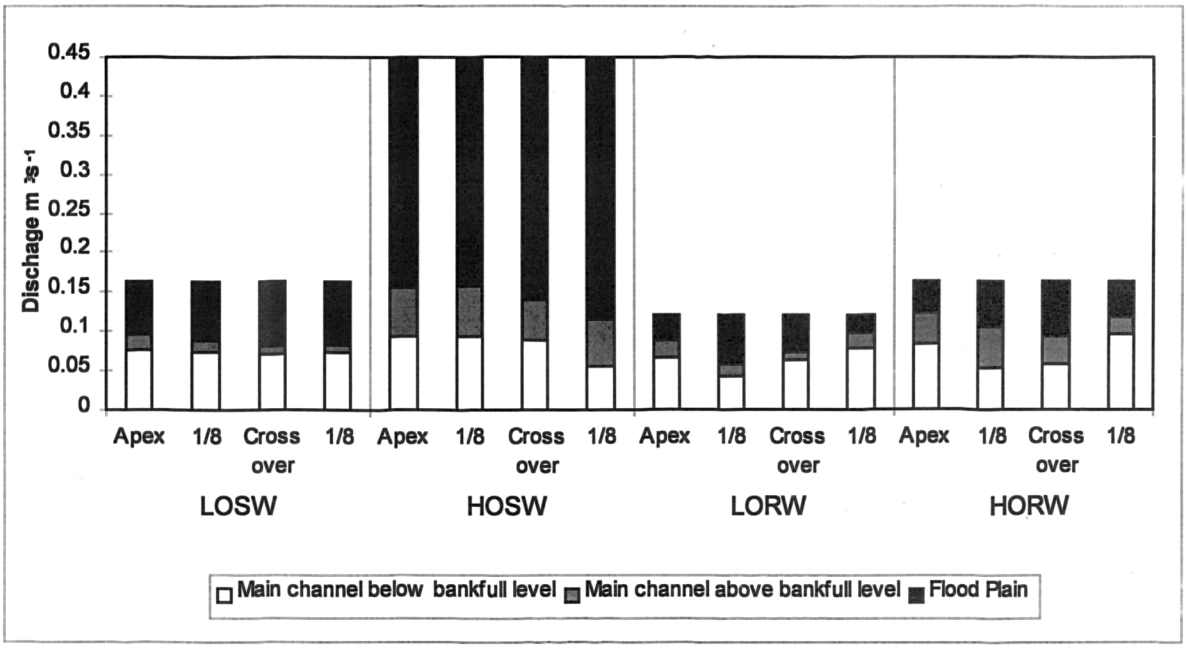

Figure 4.5 Distribution of discharge for overbank flow tests

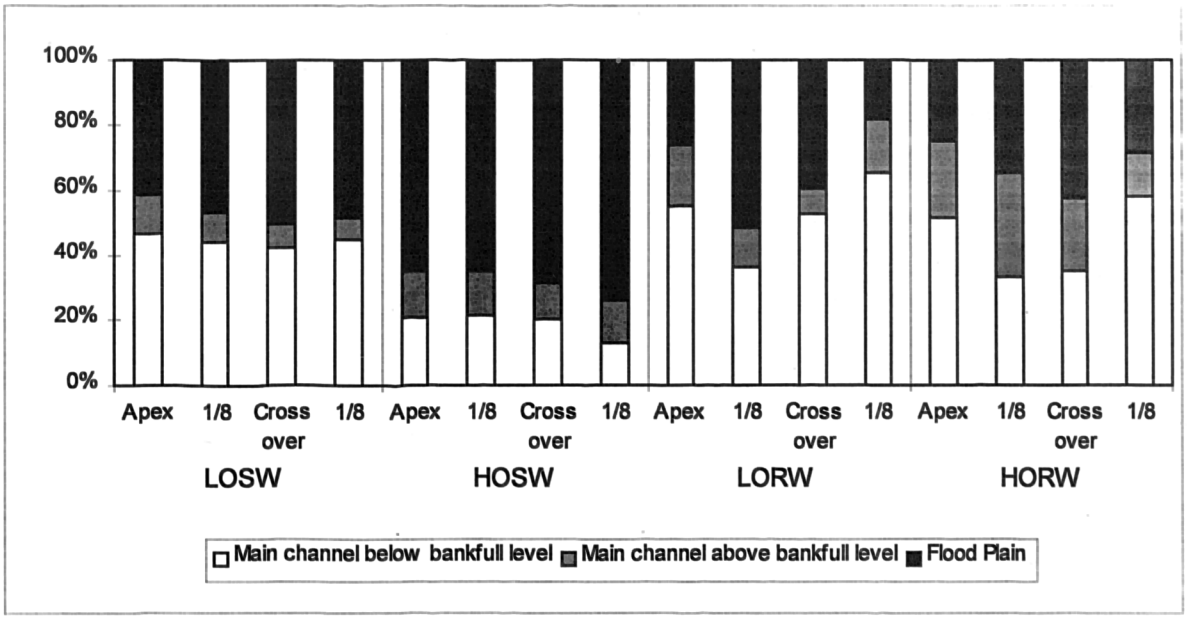

Figure 4.6 Distribution of discharge between main channel and floodplains

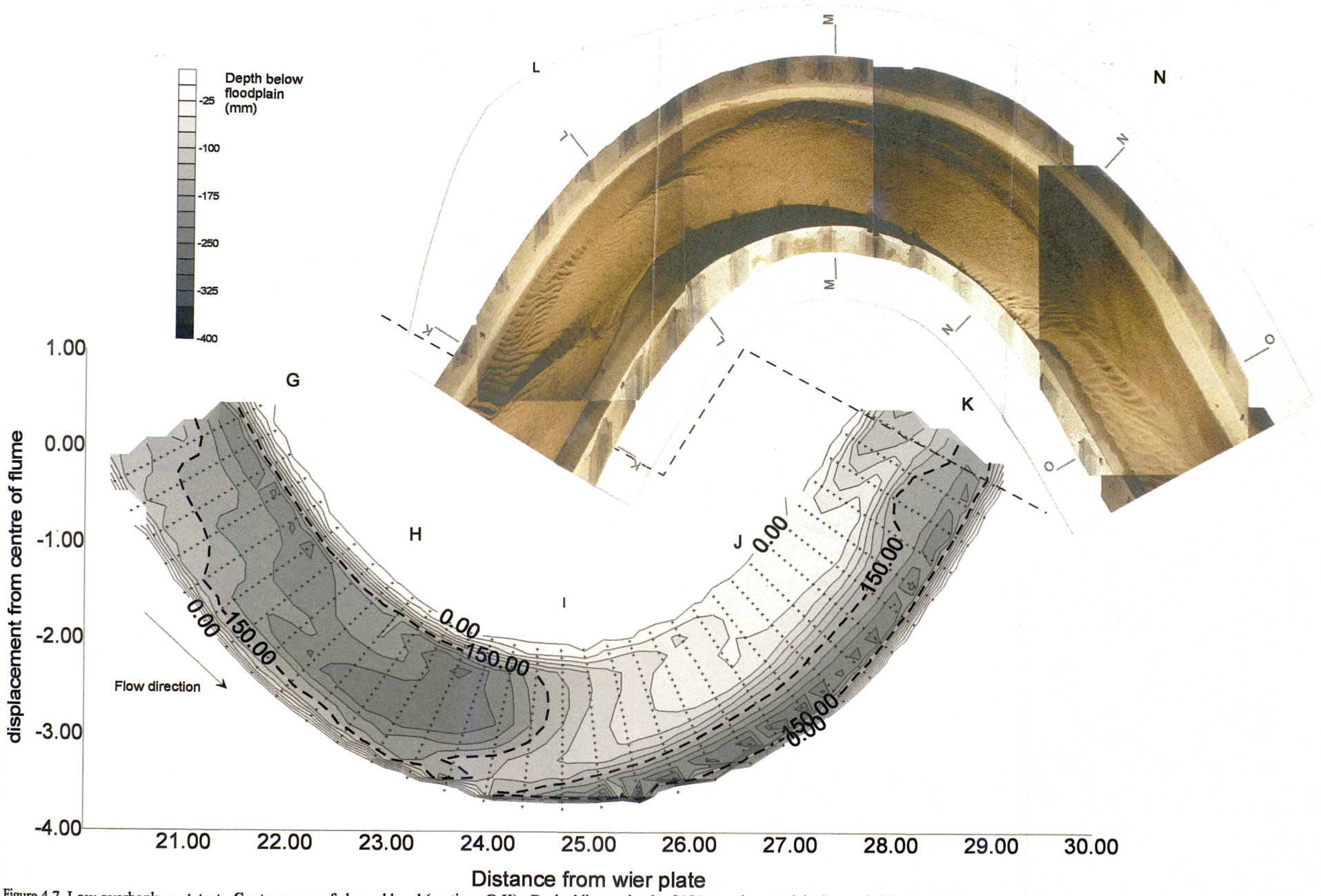

Figure 4.7 Low overbank rough test. Contour map of channel bend (sections G-K). Dashed line at depth of 150 mm shows original screeded bed level. The photograph shows grain sorting around the subsequent bend (sections K - 0)

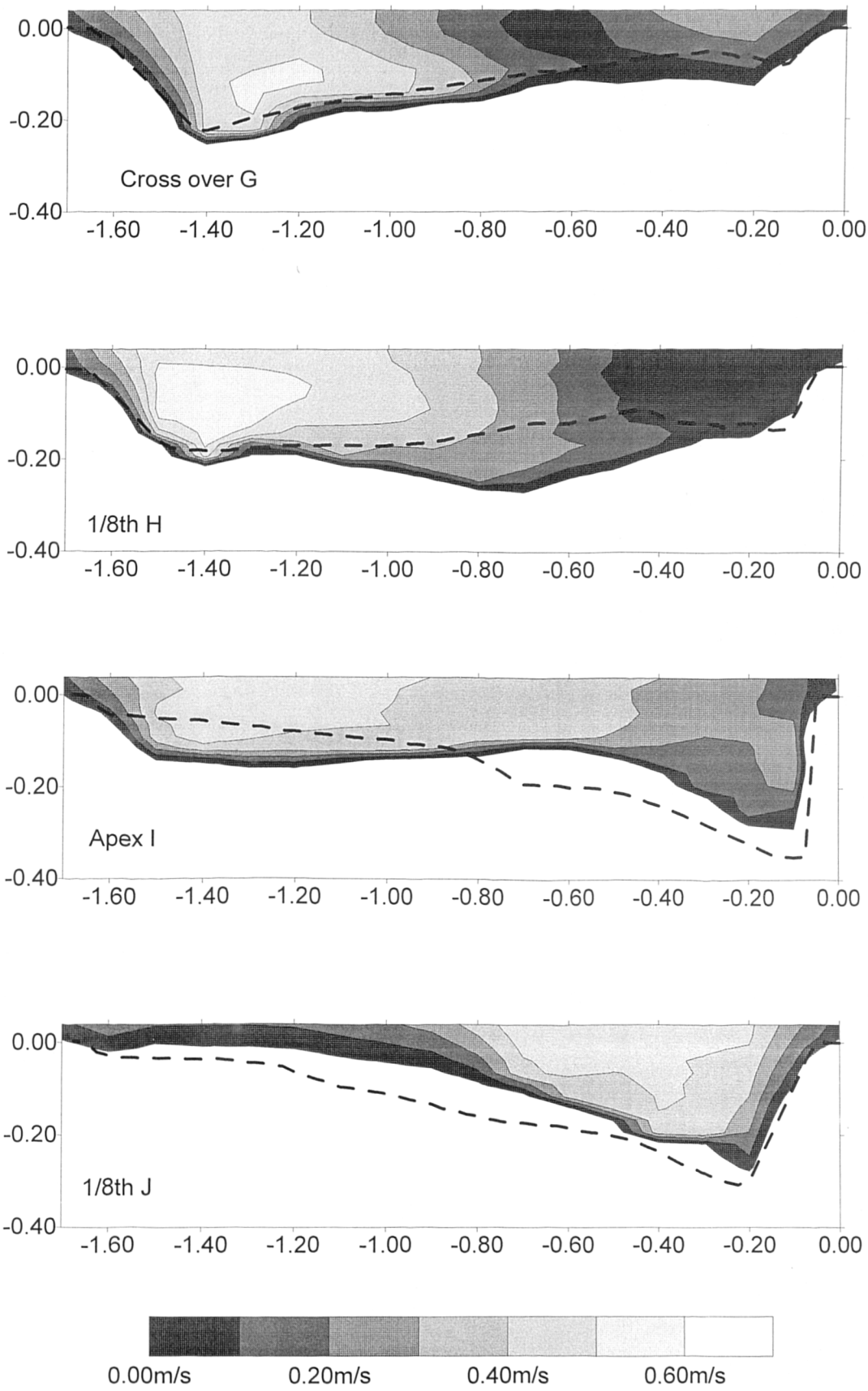

Figure 4.8 Primary velocities from the low overbank rough test The initial conditions (bankfull profile) are given by the dotted line in each case.

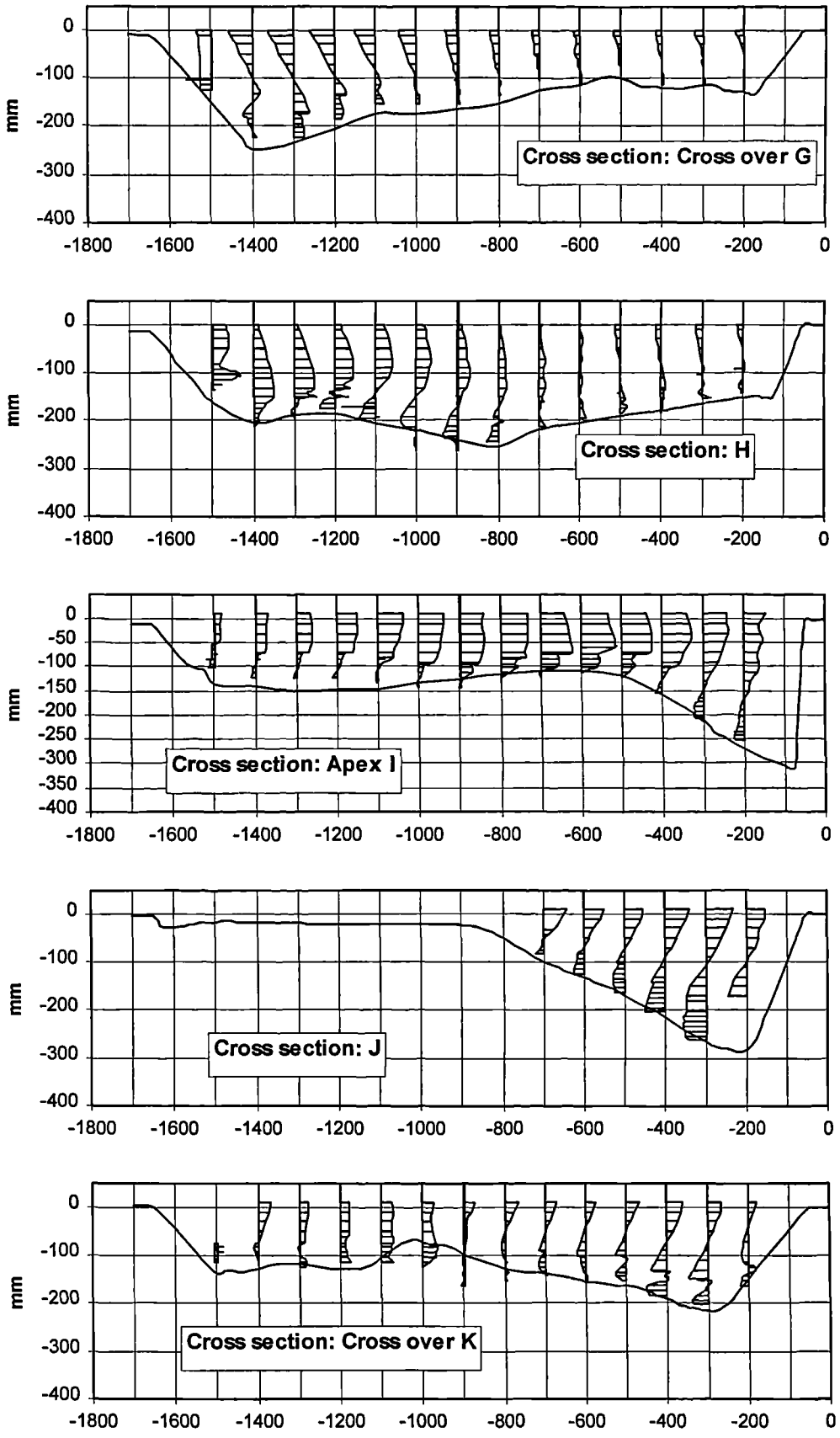

Figure 4.9 Secondary circulation in the low overbank rough test

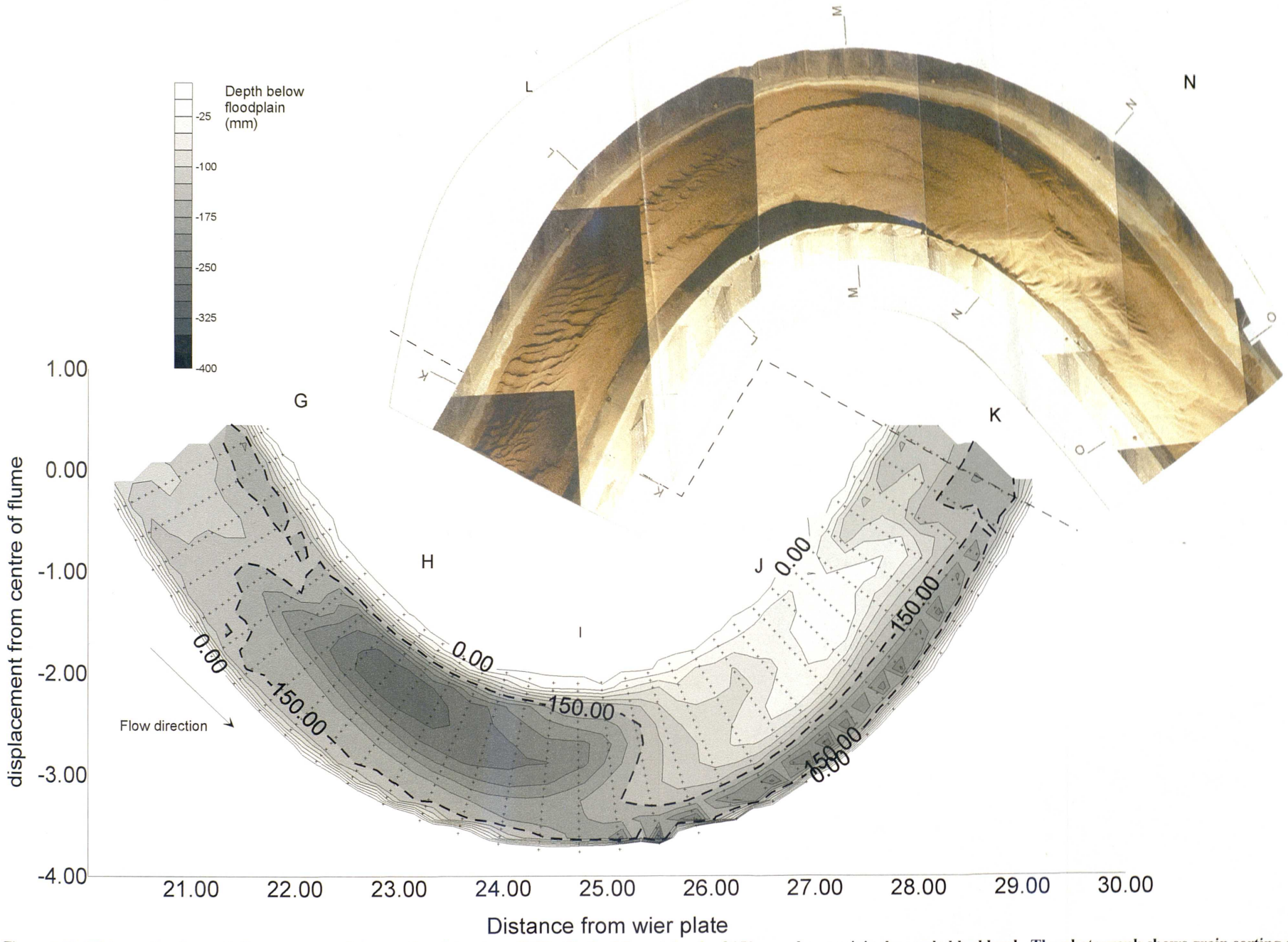

Figure 4.10 High overbank rough Contour map of channel bend (sections G-K). Dashed line at depth of 150 mm shows original screeded bed level. The photograph shows grain sorting around the subsequent bend (sections K - 0)

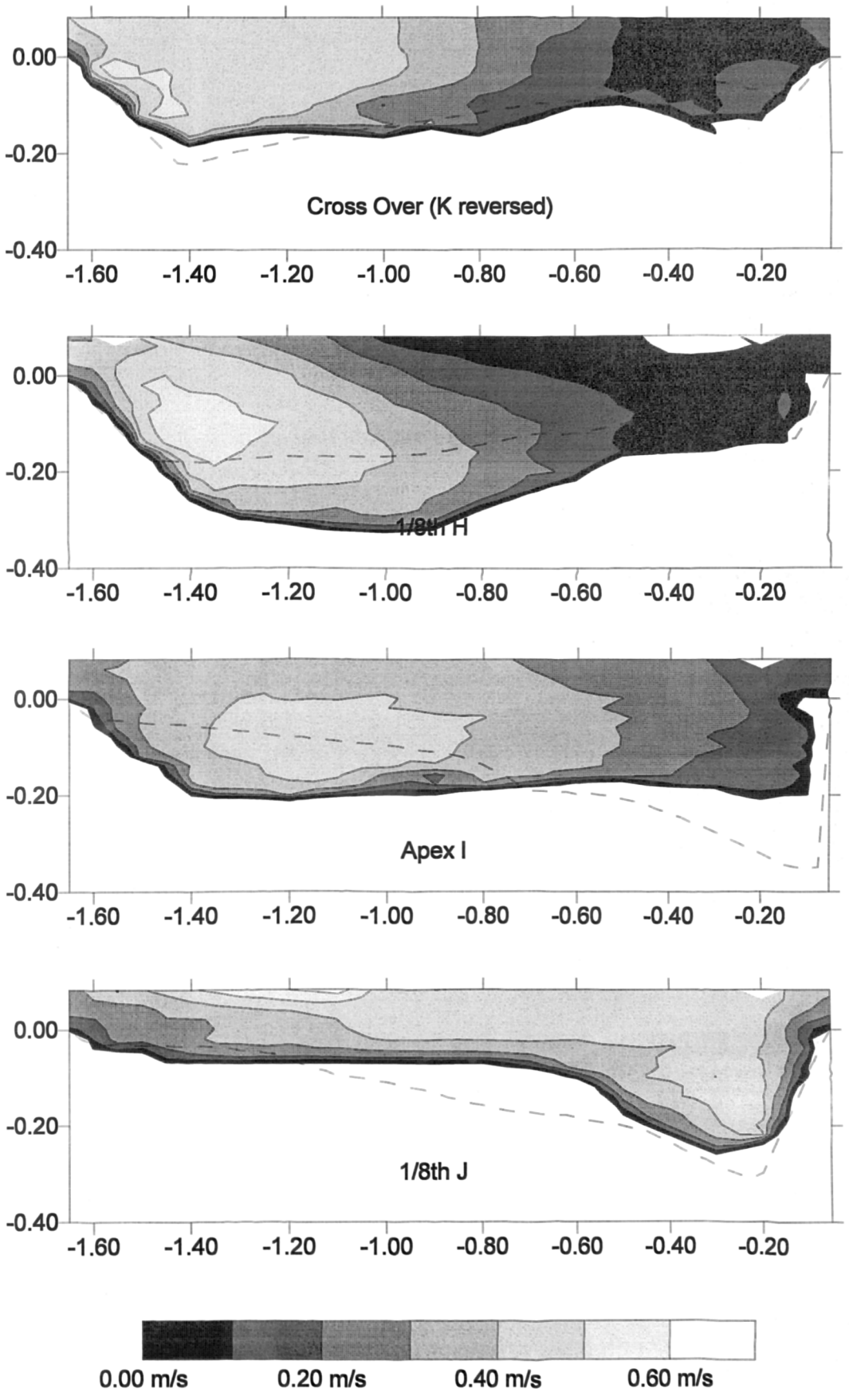

Figure 4.11 Primary velocities from the high overbank rough test. The initial conditions (bankfull profile) are given by the dotted line in each case.

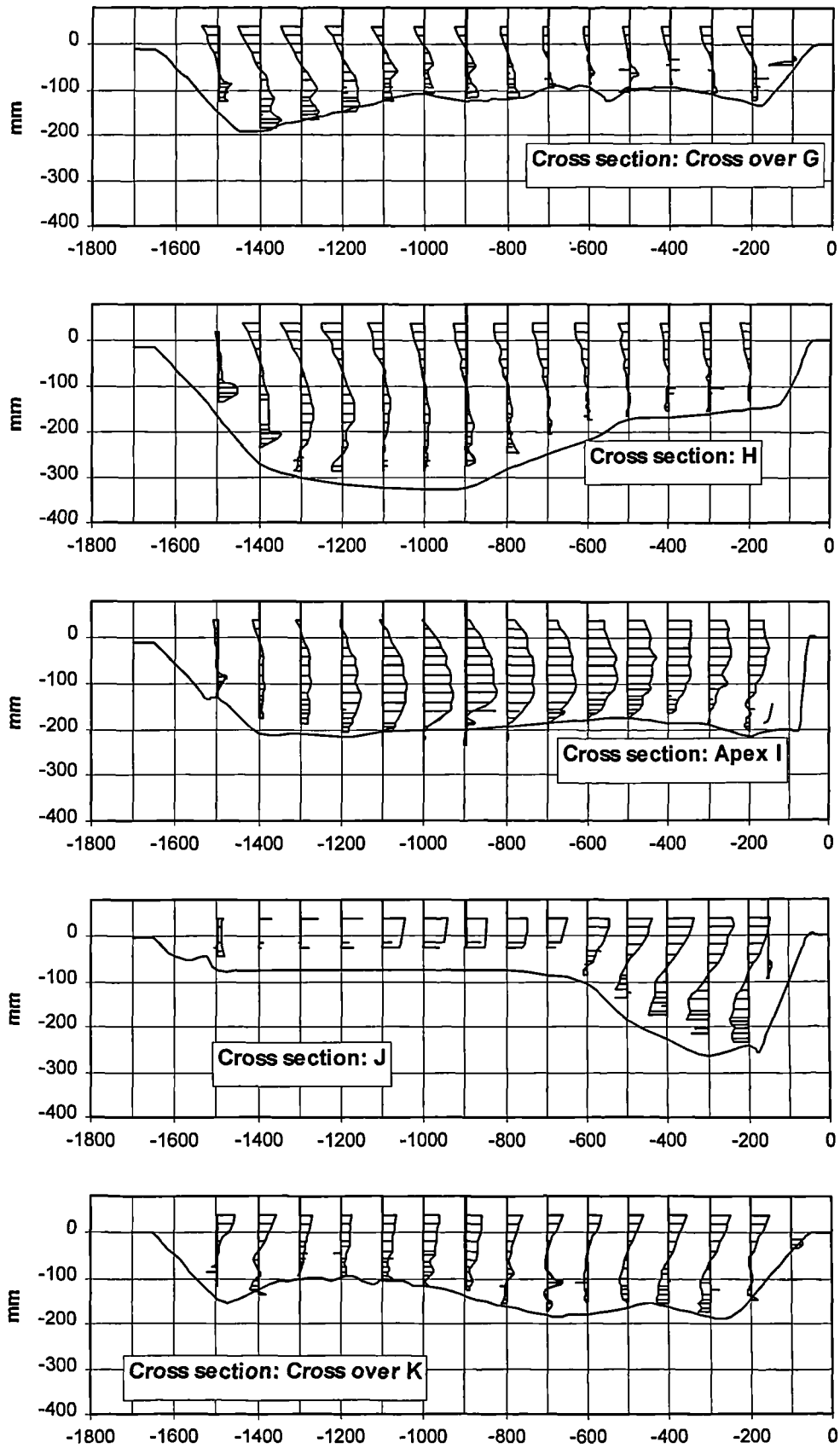

Figure 4.12 Secondary Velocities: High overbank rough test

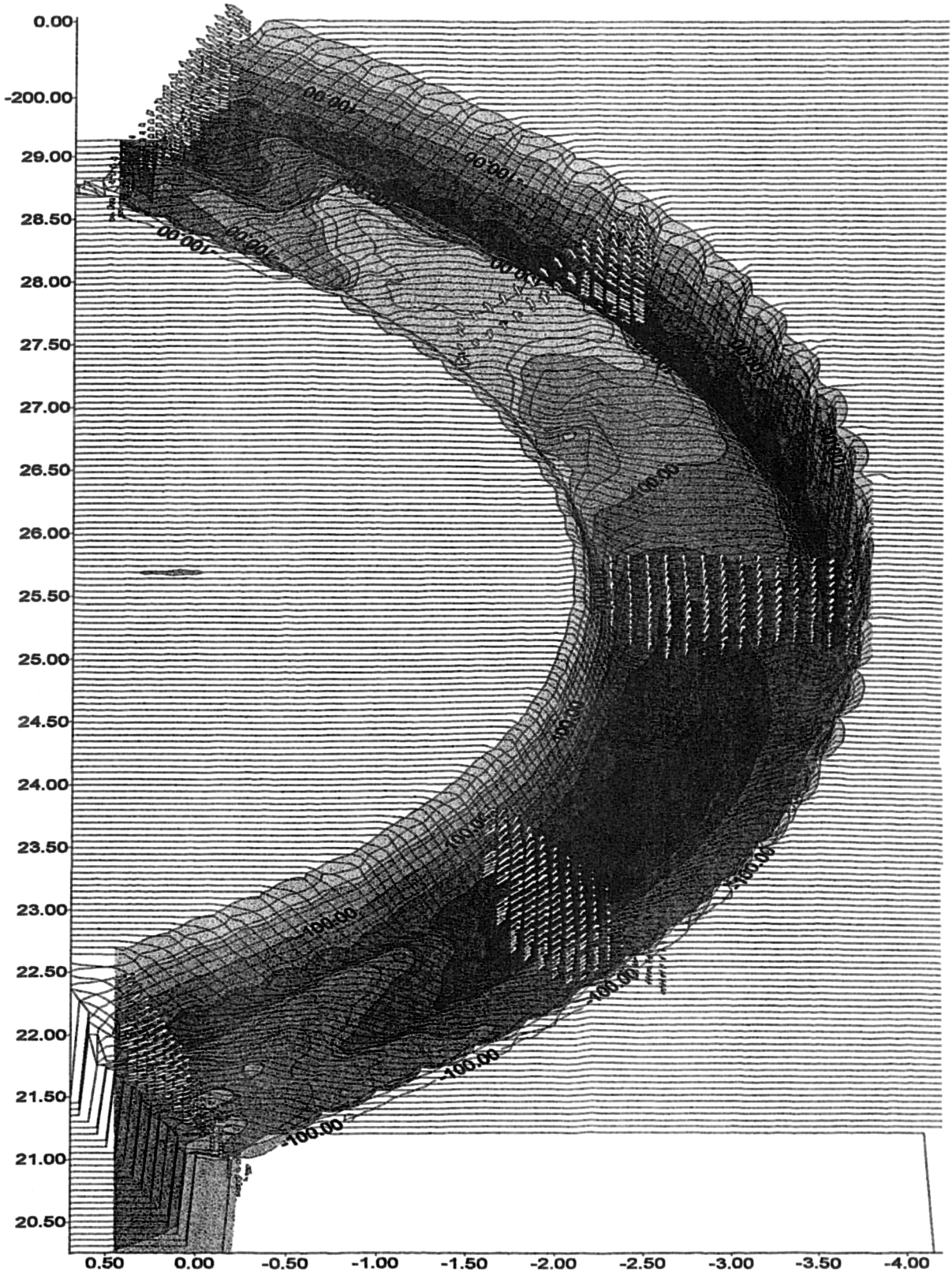

Figure 4.13 Three dimensional representation of the channel bed (HORW) showing horizontal velocity vectors

4.7. Low overbank test with smooth flood plains

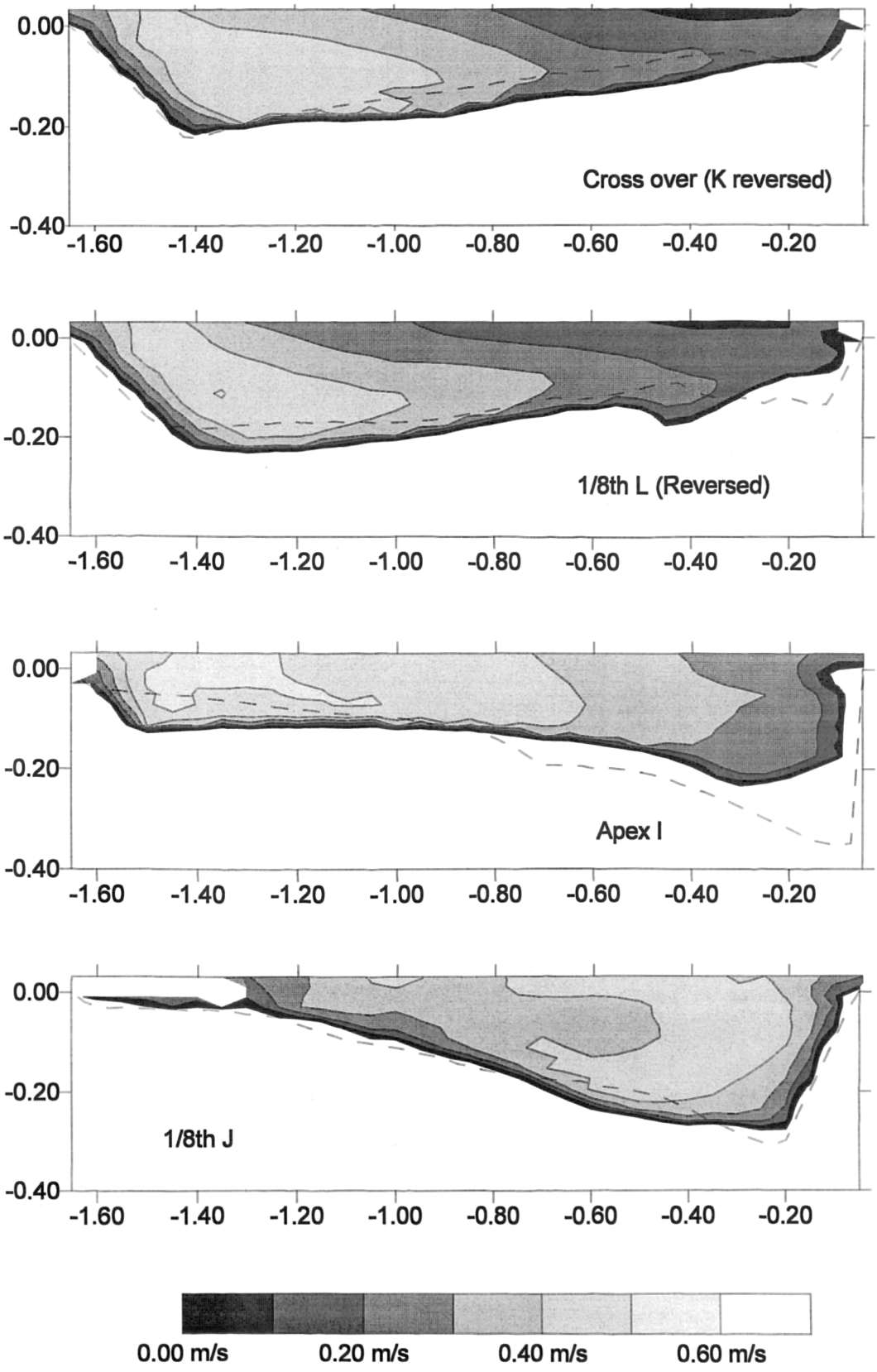

Figure 4.14 Primary velocities : Low overbank smooth test (fixed bed). The initial conditions (bankfull profile) are given by the dotted line in each case.

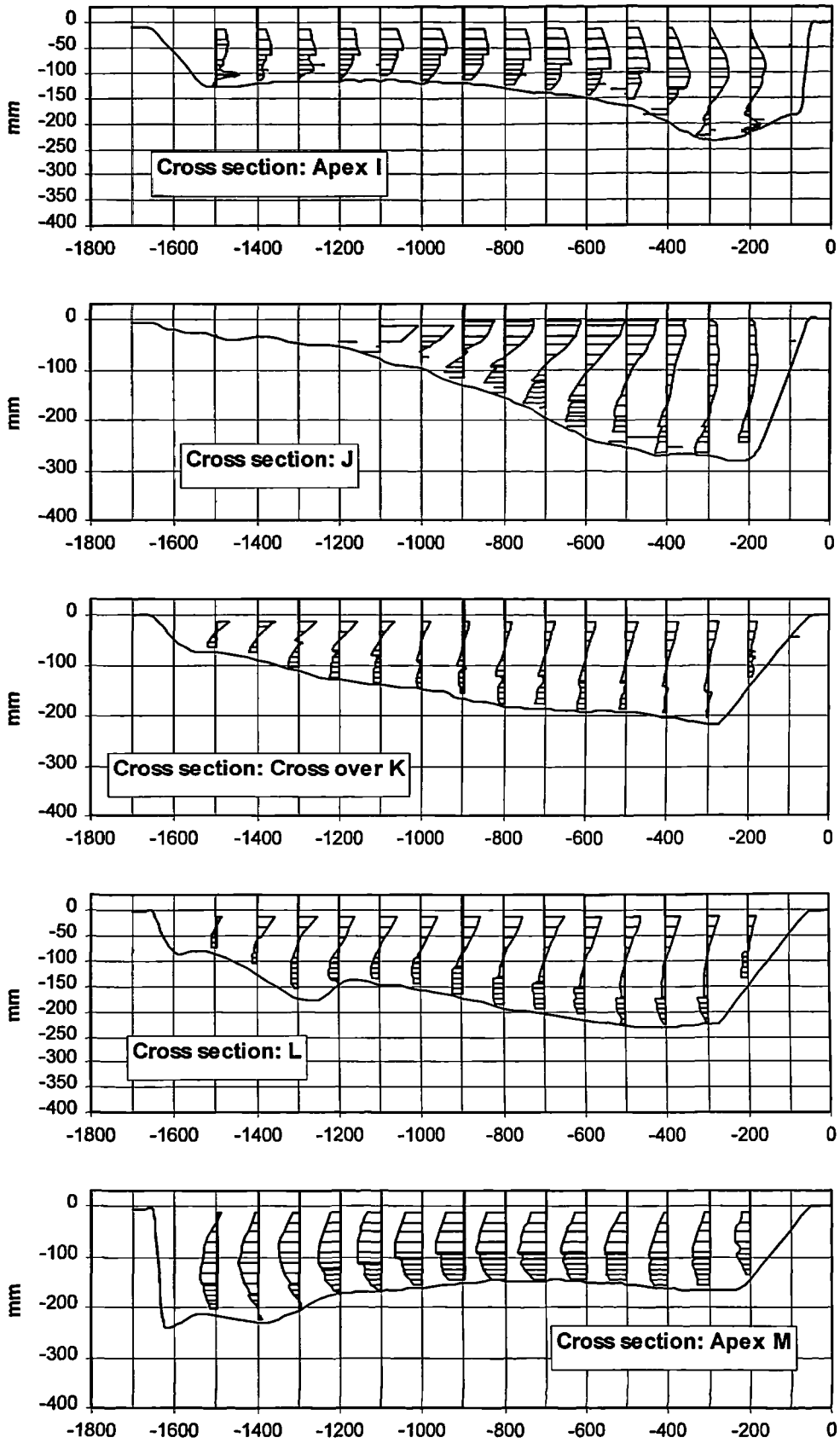

Figure 4.15 Secondary flow: low overbank smooth test (fixed bed).

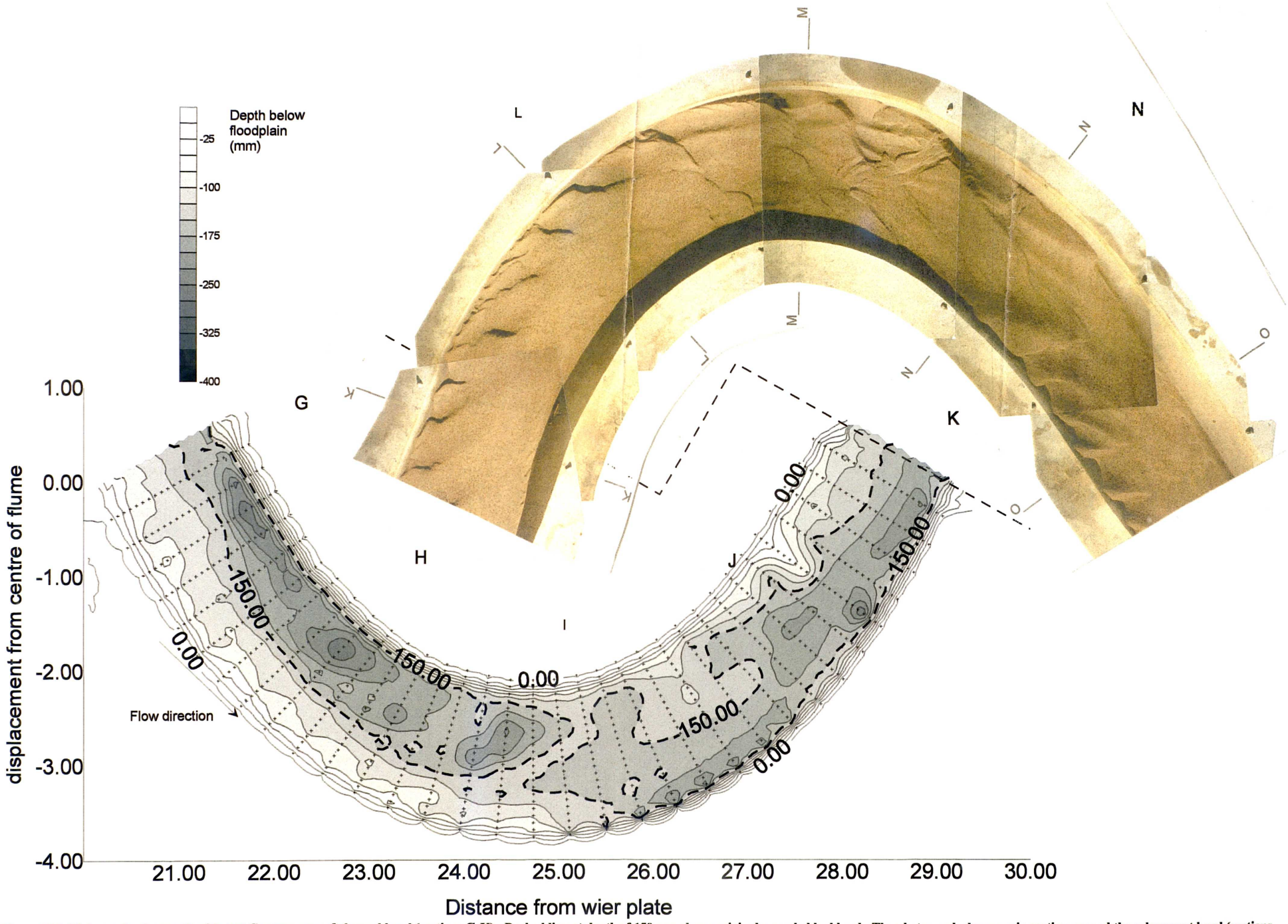

Figure 4.16 High overbank smooth wide test Contour map of channel bend (sections G-K). Dashed line at depth of 150 mm shows original screeded bed level. The photograph shows grain sorting around the subsequent bend (sections

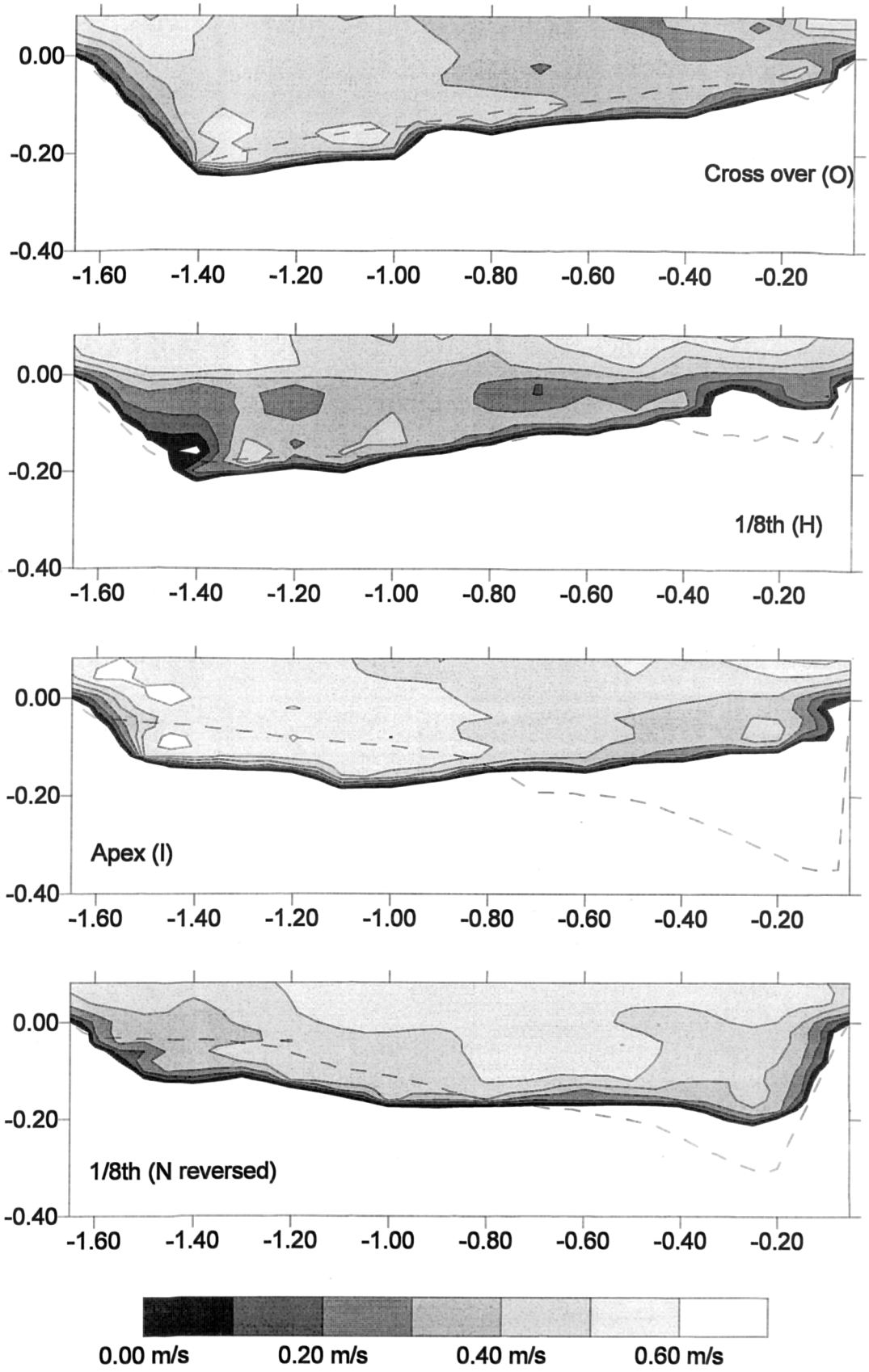

Figure 4.17 Primary velocities: High overbank smooth test. The initial conditions (bankfull profile) are given by the dotted line in each case.

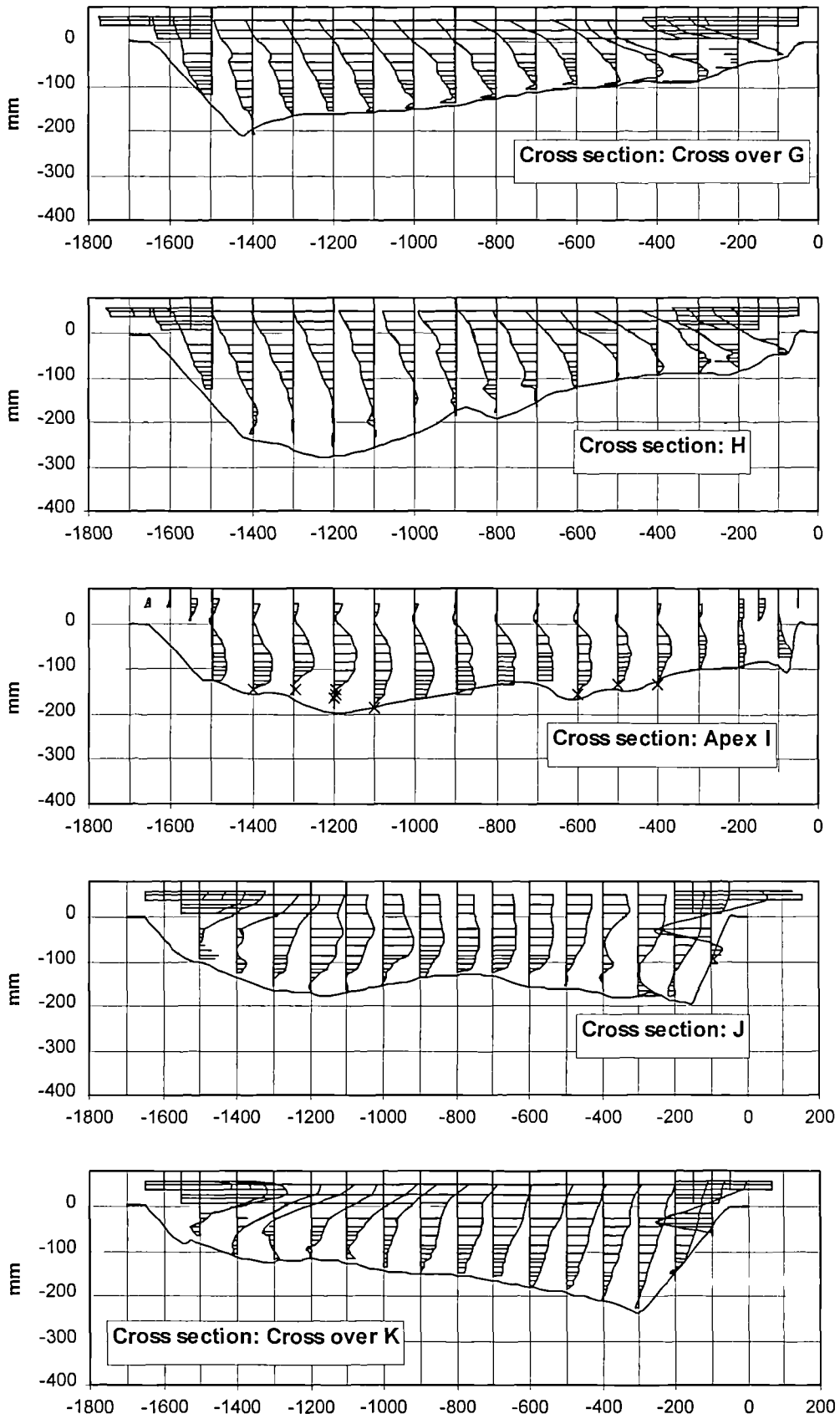

Figure 4.18 Secondary velocities: High overbank smooth test

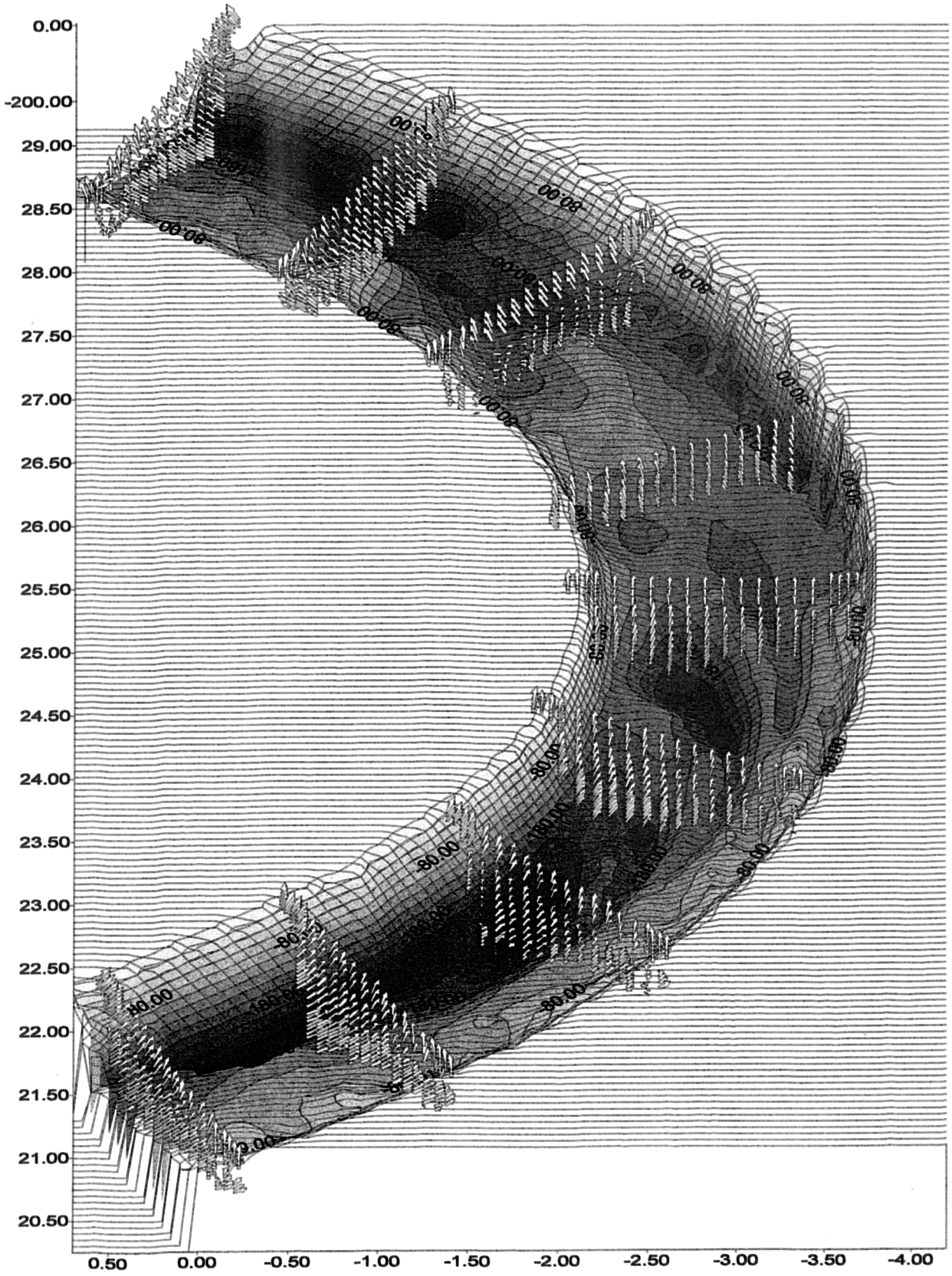

Figure 4.19 Three dimensional representation of channel bed (HOSW), showing horizontal velocity vectors

4.9. Conclusions

The data from the five tests examined in this thesis are presented in this chapter. For each test the following data is presented:-

- The discharge down the main channel, above and below floodplain level (overbank flows only).
- A contour map of the bed for each relevant section, a photograph showing grain sorting around the meander bend.
- Main stream velocity isovels.
- Secondary circulation diagrams.

The data is displayed in a largely uninterpereted form, to encourage the reader to make an unbiased judgement. The shortcomings of the data are explained with respect to the personal experience of the author whilst performing the experiments.

5. Comparison with results from previous tests and results from theoretical models

5.1. Introduction

The tests described in this thesis are unique in combining overbank flow with a mixed grain mobile bed and floodplains in the state of high roughness frequently found in the field. This chapter contains description and discussion of the observations of flow structure presented in Chapter 4. These results are subsequently compared with those obtained by previous investigators. Of particular interest is the Flood Channel Facility Series B group of tests. This is because the Series B results are generally accepted as the most reliable description of flow behaviour in a meandering overbank channel to date.

Two methods designed to predict conveyance in a meandering compound channel are applied to the channel. The James and Wark (1992) method based on the physics of the flow mechanisms observed in the Series B channel and the empirical, F* method, presented by Ervine, Willetts, Sellin and Lorena (1994). The results of the application of these methods to the current channel are presented and the discrepancies discussed. The James and Wark method is of particular interest as it gives a method for predicting the conveyance in that part of the stream contained below the bankfull water level (zone1), of the stream. This is required in the calculation of sediment transport.

Because of the discrepancies between measured flow rates and those predicted by the James and Wark method, the author has proposed a new method based on the momentum transfer between floodplain and main channel.

There are five tests examined in this chapter. The inbank test and four tests with overbank flow and wide floodplains. These flows are described in Table 4.1 by their flood plain roughness and discharge. The smooth floodplain tests were carried out with a plain screeded mortar finish on the floodplain. This represents an extreme condition unlikely to occur in nature but is included in order to provide comparison with similar tests in the Series B programme. The rough floodplain tests, which used the folded strips of expanded aluminium, described in Chapter 3 to simulate floodplain resistance. The roughness ratio between floodplain and main channel in the roughened case is close to that in natural river systems.

5.2. Discussion of variables in flow structure

Variables affecting conveyance in compound channel flows are suggested by Ervine, Willetts, Sellin and Lorena (1993). They are:

1. The sinuosity of the main channel.
2. The relative roughness of the floodplain surface compared with the main channel.
3. The aspect ratio of the main channel.
4. The meander belt width relative to the total floodway width.

5. The relative depth of flow on the floodplain compared with the main channel.
6. The main channel cross-section shape, including the side slope of the banks of the main channel.
7. The floodplain topography, in particular any lateral slope (crossfall) of the floodplains toward the main channel.

The primary aim of the Series C experiments was to investigate the effects of overbank flow on sediment transport. The increased complexity introduced by the mobile bed to the main channel meant that some of these variables could not be explored. For example, all tests were carried out at the same channel sinuosity and aspect ratio (parameters 1 and 3). The meander belt width and form (parameter 4) were investigated in this set of tests but are not considered here. All tests were conducted with zero crossfall and hence it is not possible to comment on the effect of parameter 7.

Tests were, however, performed with two forms of floodplain roughness, a smooth mortar finish floodplain, similar to that used in previous test series, and a roughened floodplain which is considerably rougher than any previously investigated. The mobile bed also creates conditions suitable for examining the variation between the trapezoidal cross-section, and natural bed forms. Tests were conducted on smooth and rough floodplains at two relative floodplain depths. Thus the dependence of the flow behaviour and conveyance on parameters 2, 5 and 6 is investigated.

Three diagrams are shown on the following pages to aid in the investigation of the variables discussed above. In Figure 5.1 the variation of water slope at points down the channel is shown. This has been constructed using the method of cubic splines from water surface elevation data obtained at each measurement point (see Appendix 5 for measurement positions). The slope at each point is a good indicator of the energy processes in the channel and the effect of the major bedform at that point. Figure 5.2 shows the variation of sediment transport across the channel at representative sections down the channel and Figure 5.3 shows the equivalent plan photographs. In this Chapter, these figures are useful in the consideration of channel roughness and in Chapter 6 they aid in the discussion of sediment transport rate.

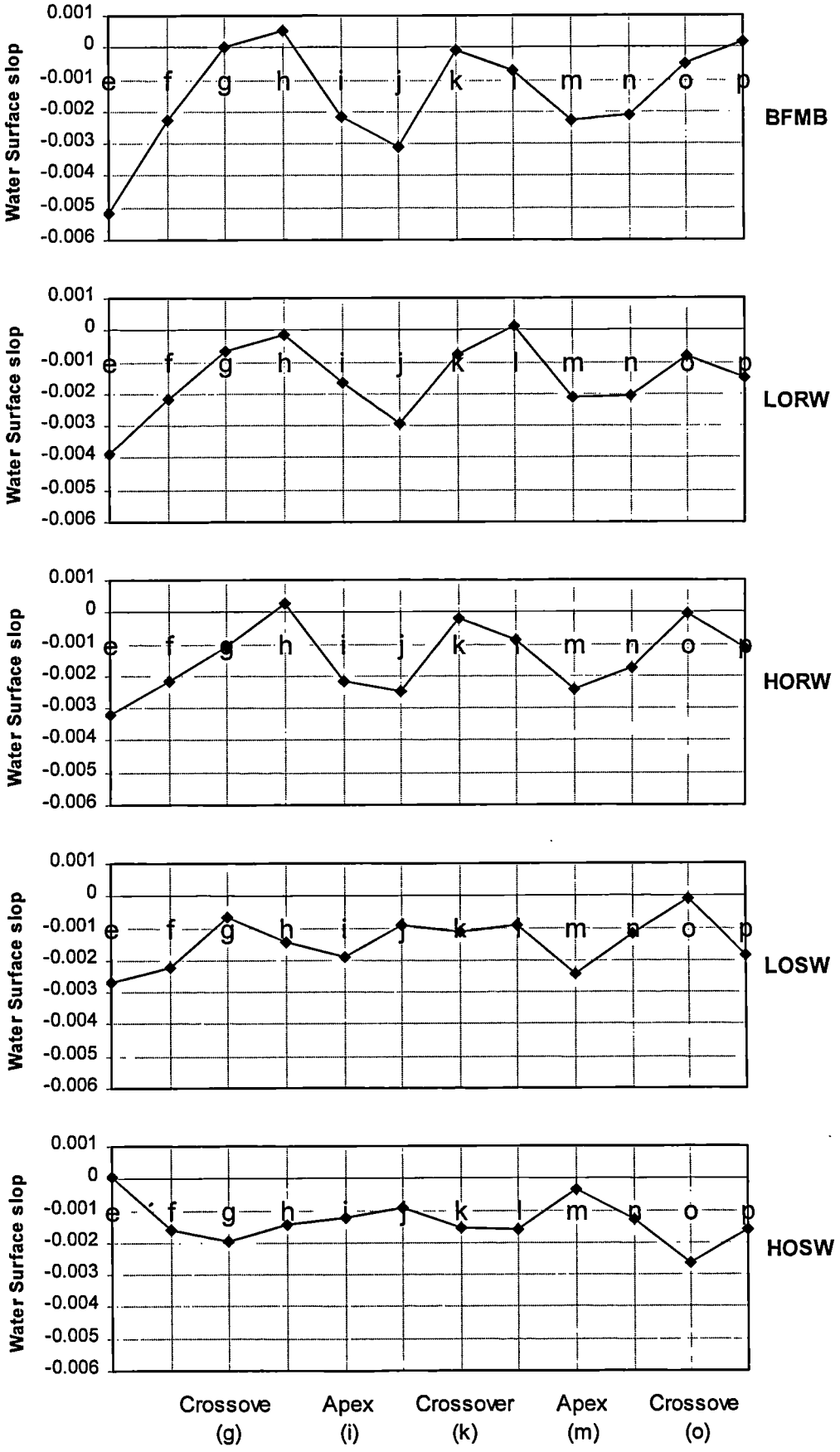

Figure 5.1 The variation of water surface slope down the main channel. Each point represents the water surface slope at the measuring positions using splines.

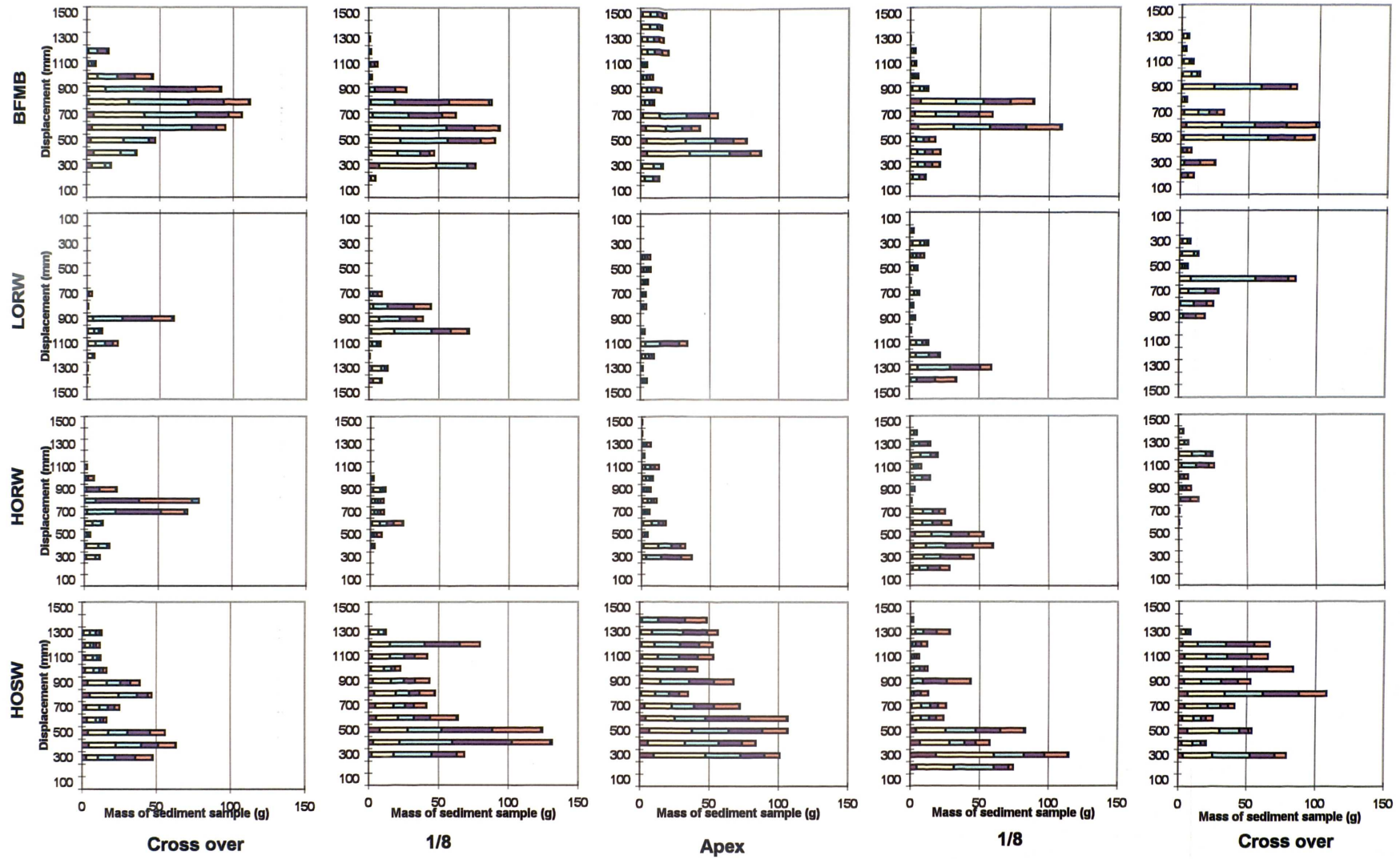

Figure 5. 2 Lateral variation of mass and size distribution of bed load transport samples for the tests BFMB, LORW, HORW and HOSW. The charts show the dry mass of sediment samples collected at 100 mm intervals across the channel and divided into size fractions by sieving. Each sample was collected over a five minute duration. The y axis gives distance across the channel from the right hand datum pin in mm and the x axis sediment mass in grams. The size distribution of the original sediment is shown to the right, the legend applies to all the data. The test data was all collected at the positions shown other than LORW which was collected at GHIJK. In this test the y axis is plotted in reverse for direct comparison.

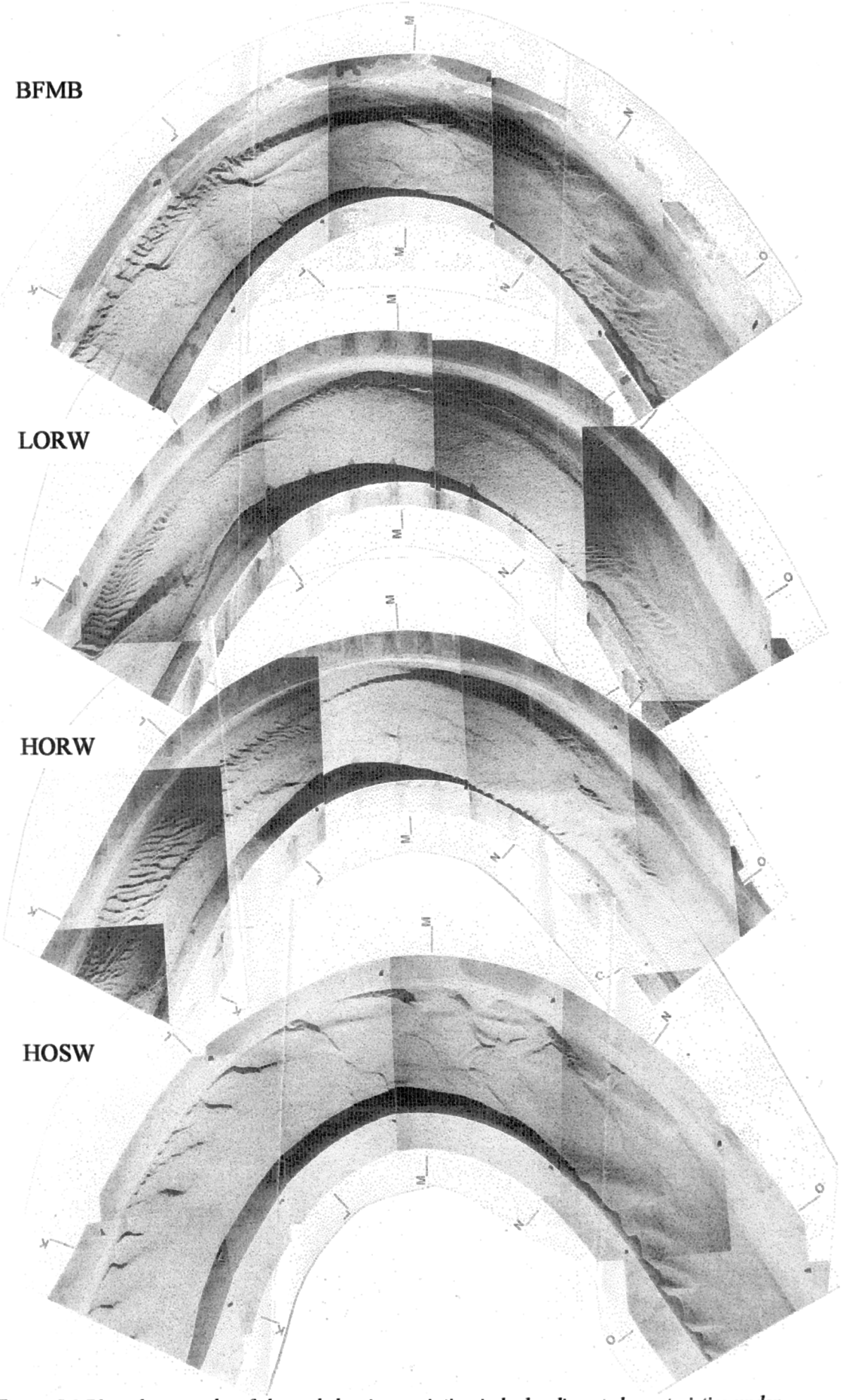

Figure 5.3 Plan photographs of channel showing variation in bed sediment characteristics under various flow conditions

5.3. Flow behaviour in the bankfull test

5.3.1. Channel form

Comparing the bankfull planform in Figure 4.2 with the schematic illustration of river meandering in Figure 2.10 we can see that the model is a good representation of observed natural behaviour. The bedform shape is formed by scour and deposition of the screeded bed. This is illustrated in Figure 4.1, which shows the bed profile at section J during the bankfull test. The dashed line at 0.15m below the floodplain level shows the screeded bed level. The sediment above this level has been scoured from regions of the channel upstream where the shear stress is high and deposited in the current region of low shear stress where the bed is sheltered by the point bar. The sediment in this region is finer than the majority of the sediment in the channel see Figure 5.2 and Figure 5.3. This fine material forms ripples in the shallow flow, which can be observed in the photograph (see Figure 5.2) and can be seen to fall into the ripple area of the Simons and Richardson diagram in Figure 5.4. Due to the very low velocities, the measured sediment transport rate in this region is very low. Material below the 0.15m line will in general retain the well-mixed matrix of the original screeded bed. However there is a layer of sediment at the interface between the flow and the original bed sediment, which has characteristics, determined by the effects of sediment transport. In the regions of scour the finer grains are preferentially transported. An armour layer remains which was several grains thick of larger material beyond the sediment size range of Figure 5.4 and contained very few fines. This is also a region of low sediment transport as whilst the flow is fast and deep the large grains form a rough boundary and as they are large they do not easily move. The secondary currents prevent smaller more transportable grains from settling into this high velocity zone.

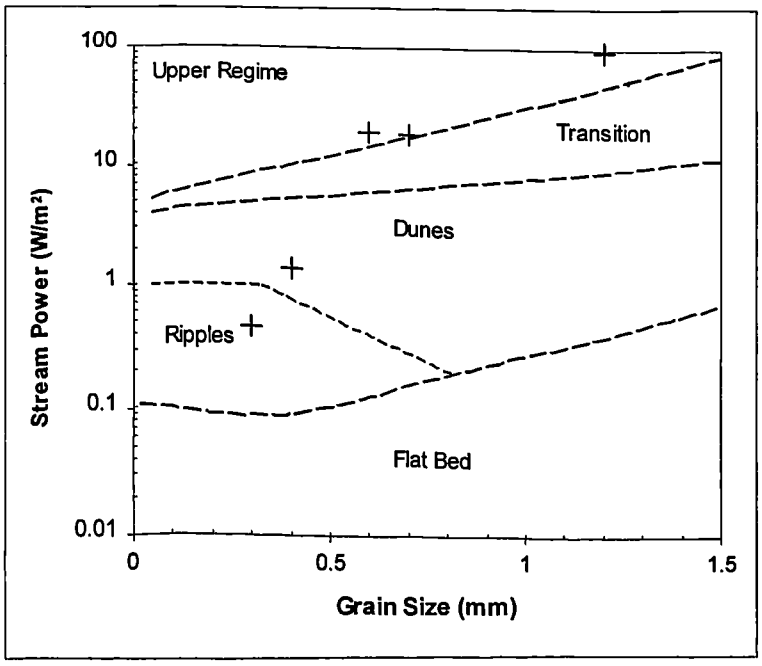

Figure 5.4 Data for bankfull test arranged on the Simons and Richardson (1965) bedform prediction diagram.

5.3.2. Observations of primary and secondary flow.

Flow behaviour in an inbank channel has been studied extensively. The following description is intended to confirm the authenticity of the inbank flow and to highlight the differences with the subsequent descriptions of overbank flow. Figure 4.5 shows the primary flow patterns in an inbank channel and Figure 4.6 the secondary velocities. These diagrams have been combined to obtain Figure 5.5 below.

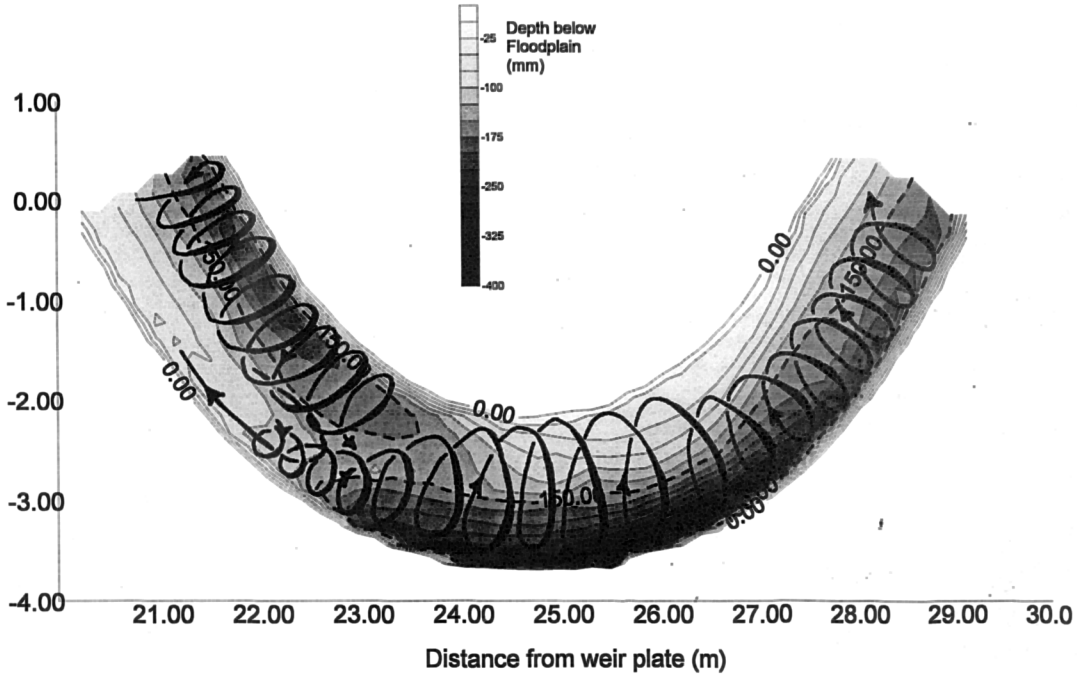

Figure 5.5 Inferred helical flow mechanisms in the bankfull test.

At the inflection point in the channel, the maximum velocity is at the downstream wall of the channel. There is weak secondary circulation in the channel remaining from that set-up at the previous apex. The point bar formed at the previous bend dominates the transverse slope of the bed here. At section G4 the flow is beginning to cross the channel as the next bend is approached. At section H although the main velocity filament is still at the downstream side of the channel the deepest section has moved to the centre of the channel and the net secondary flow is toward the outside of the channel. At the upstream side, there is an area of stagnant flow protected by the point bar and a small element of reverse flow. The thalweg has moved to the outside of the bend in section H4 and a clear secondary circulation caused by the flow curvature in the new bend is evident. There is still however a net transfer of flow to the outside of the bend. The isovel diagram at the apex section (I) shows a region of fast flow, below the surface, at the outside of the bend. However, the data suggests that there is also a region of fast flow, at the surface, in the centre of the channel. This area proved inaccessible to the velocity probe and thus the high velocities are only inferred from data collected below it. The secondary currents and bed profile maintain the same form to the next inflection point decaying in strength with distance from the apex.

The diagram of water surface slope shown in Figure 5.1 shows the pattern of energy loss due to secondary flow currents. The inbank flow displays a strong "signature" form. The steepest slope is between apex and the following 1/8th of a wavelength. This is due to the super elevation at the apex section.

5.4. Flow behaviour in the overbank smooth tests

5.4.1. Location of results

The discharge and floodplain flow depth for the overbank smooth tests can be found in Table 4.1 and water surface slope Figure 5.1. Over bank zonal discharge distribution is given in Figure 4.5 and Figure 4.6. Primary velocity distribution, secondary circulation, 3D flow image and bed details are displayed in Figure 4.14 to Figure 4.19. The local sediment transport rates and composition are given in Figure 5.2

5.4.2. Observation of flow in main channel

The overbank smooth floodplain tests represent overbank flow over perhaps a car park or a sports field which are not uncommon floodplain features. They are useful for comparison with previous tests of similar floodplain roughness and the high overbank test is likely to give the case in which the flow interaction is dominant as the energy loss process.

In the low, overbank test, described by Figure 5.6 clear similarities with the inbank flow structures can be seen. The most significant change is visible at the apex where the floodplain flow induced secondary circulation continues at the upper surface where the flow is not carried around the apex by the channel wall. In the lower section of the stream at this point the conventional secondary circulation still occurs. The importance of the bankfull type structure as an energy loss mechanism is shown by the similarity between low overbank smooth and bankfull tests in Figure 5.1.

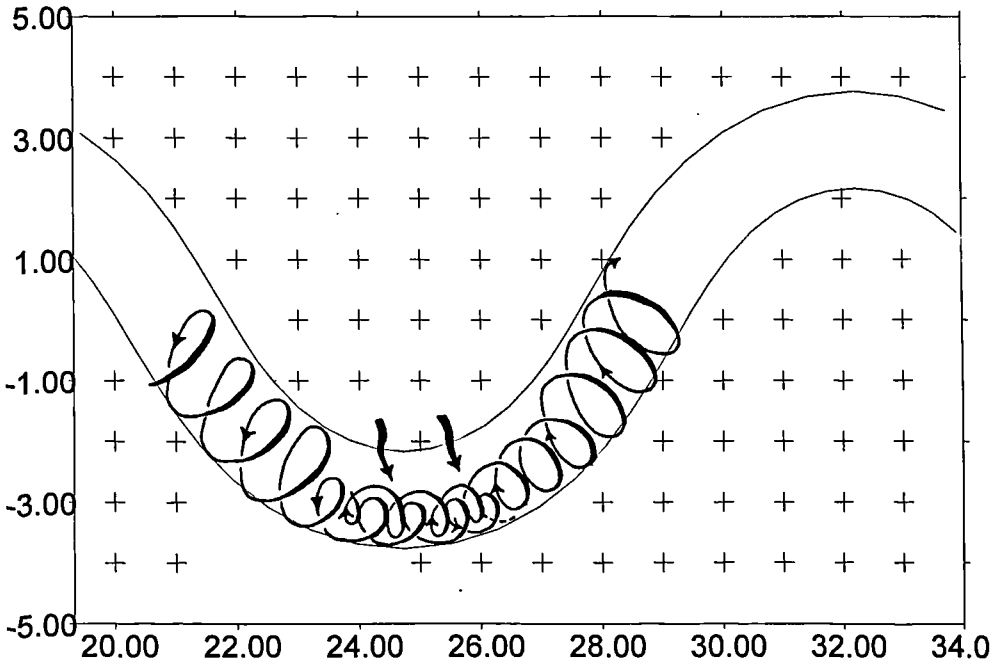

Figure 5.6 Representation of flow mechanisms within flooded meandering channels LOSW

The flow patterns in the high overbank smooth case are summarised in Figure 5.7 below.

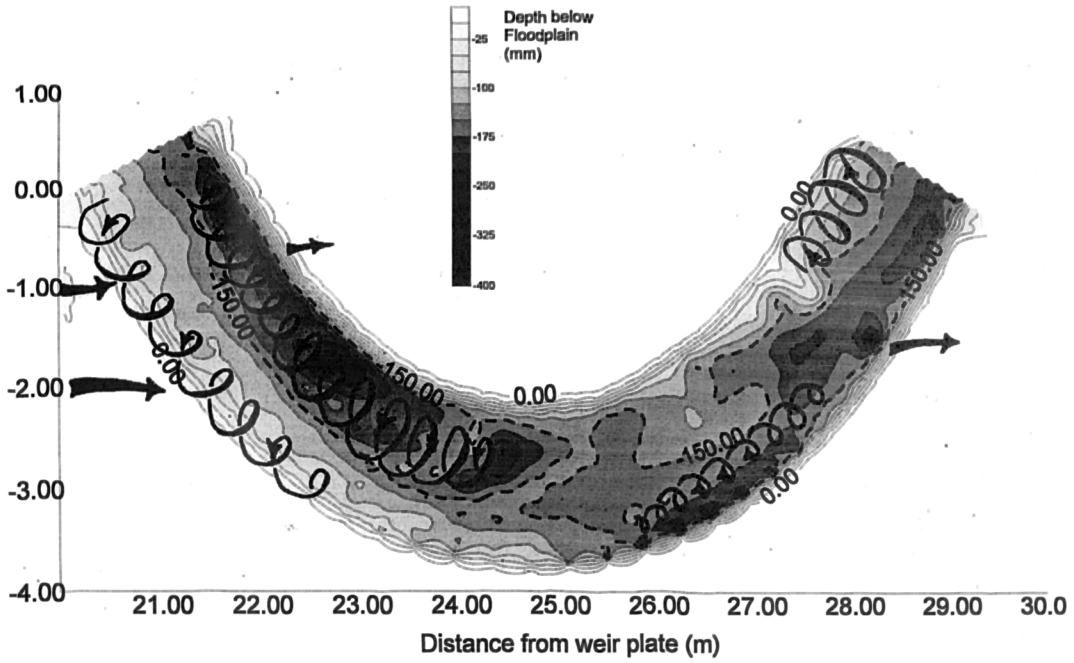

Figure 5.7 Inferred flow mechanisms within flooded meandering channels HOSW

In the high overbank smooth test a major change has occurred in the flow structures in the stream, due to the increased dominance of the overbank flow. Consider Figure 5.1, the comparison of water surface slopes. In the bankfull test the slope from the apex to next 1/8λ down stream is characteristically steep. In the high overbank smooth case we see that this rise in slope now occurs over the section, between the 1/8thλ after the apex and the cross over. It can also be seen that there is significantly less variation in slope. These variations in slope are indications of the energy expended in the maintenance of secondary currents. Considering the secondary currents in Figure 4.20 we can see that the pattern present during bankfull flow has substantially changed.

The strongest currents occur in the crossover section where fast flow on the floodplain causes strong drift across the channel. A small circulation cell is formed under the fixed upstream bank but otherwise the cross-stream flow reduces to zero at the bed with no reverse circulation. This indicates a significant transfer of fluid between the upper floodplain, main channel and lower floodplain. The maximum velocity filament is on the downstream side of the channel and the macro bed form is largely unchanged.

This pattern is maintained in section H, the 1/8thλ before the apex. The secondary flow at this section is in the opposite direction to that observed in the bankfull case where the flow starts to cross the channel to the outside bank of the impending turn.

At the apex, the upper main channel flow is in line with the overbank flow and, below the bankfull level there is some movement toward the outside bank caused by the flow curvature. This is reflected in the shape of the channel bed; The typical formation has changed, the inside bank scouring and scour area on the outside bank filling in with sediment. The main velocity filament is found at the inside bank crossing over the main channel to the downstream bank over the next 1/8thλ. This change is illustrated well in Figure 5.3 where the photograph of the overbank smooth channel shows the relatively uniform distribution of grain roughness at the apex and a flattened profile compared with the bankfull form.

Secondary currents in a bankfull river are driven by the curvature of the flow and the pressure difference between the inside and outside at the apex. In the current situation, the flow in the apex only experiences the constraining effect of the bank at some distance below bankfull level. A large proportion of the flow moves out onto the floodplain rather than around the corner into the crossover. This has the effect of significantly increasing the radius of curvature and thus much reducing the secondary acceleration. As it becomes less easy for the flow to leave the river and exit straight out onto the floodplain, due either to lower relative floodplain depth or greater floodplain roughness, the energy loss due to the flow curvature, and the resultant secondary circulation will increase.

At section J, 1/8thλ after the apex, the floodplain flow is again crossing the main channel at an angle to the main channel flow. A small secondary cell has formed at the lower floodplain edge that persists to the next apex. This feature effectively prevents the movement of bed sediment onto the floodplain.

In the low overbank smooth test many of the features noted above still apply. Examination of the secondary velocities however shows that the bankfull behaviour still dominates the flow structure. This is reflected in the less drastic changes in bed form and water surface slope.

5.4.3. Observation of flow on floodplains

The magnitude and direction of depth averaged floodplain flow in the high overbank smooth floodplain test is illustrated in Figure 5.8. It is noticeable that the floodplain slope dominates the flow direction. The velocities are greatest just beyond the apex and the lower floodplain and reach a steady state by the middle of the floodplain section.

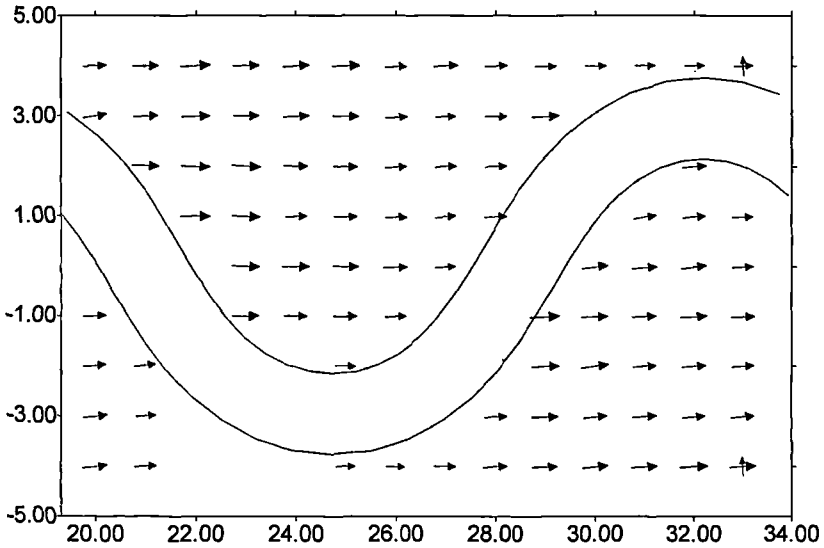

Figure 5.8 Depth averaged floodplain velocity vectors, High Overbank Test with Smooth and wide floodplains (HOSW)

5.5. Flow behaviour in the overbank rough tests

5.5.1. Location of results

The discharge and floodplain flow depth for the overbank rough tests can be found in Table 4.1 and water surface slopes in Figure 5.1. Over bank zonal discharge distribution is given in Figures 4.5 and 4.6.

Primary velocity distribution, secondary circulation, 3D flow image and bed details are displayed in Figure 4.7 to Figure 4.13. Figures 5.9 and 5.10 show the schematic illustration of these flows. The local sediment transport rates and composition are given in Figure 5.2

5.5.2. Observation of flow in main channel

The overbank rough tests represent perhaps the closest approximation to a meandering river in flood modelled to date; in particular the low overbank case. Comparing the rough floodplain slope profiles with those obtained for the bankfull flow in Figure 5.1 we observe a very similar profile suggesting that the energy losses in the channel are similar to those observed at bankfull flow.

In Figure 5.9 derived from Figure 4.10 we see that at the crossover the main velocity filament is situated at the downstream side of the channel as seen in the bankfull flow. The secondary velocities are much the same as for bankfull. The small quantity of flow leaving the floodplain and entering the channel at the upstream side slows the flow and the region of back circulation observed under bankfull conditions is extended. This phenomena is more pronounced at section H. The main velocity filament remains near the downstream bank. The bankfull discharge bedform has scoured significantly at this section.

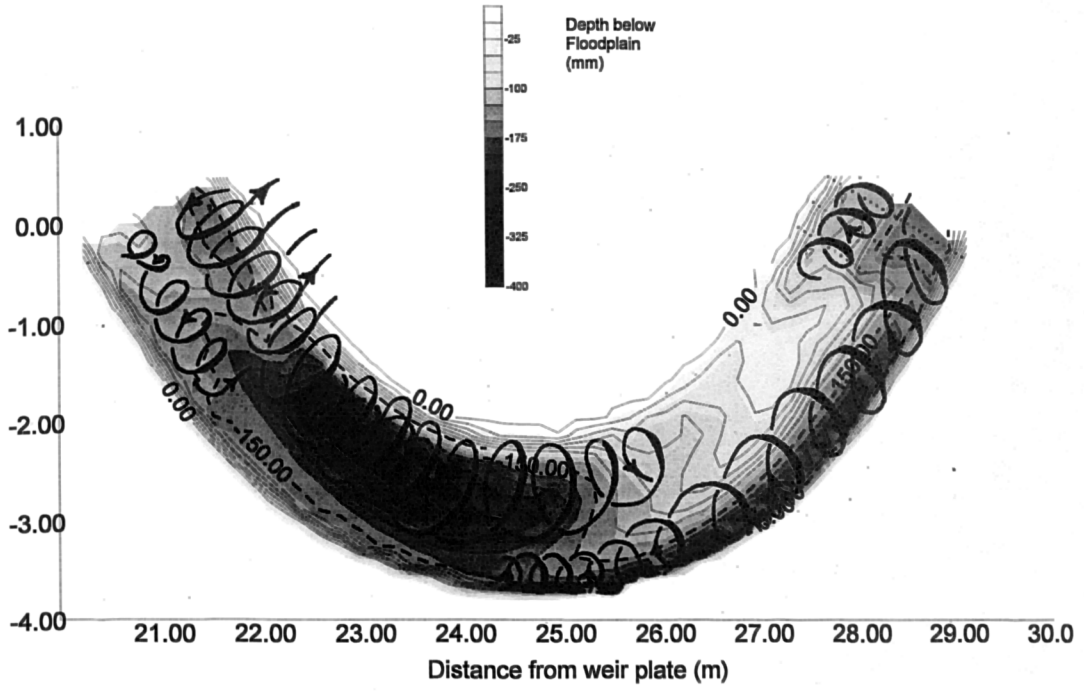

Figure 5.9 Representation of flow mechanisms within flooded meandering channels HORW

At the apex the phenomenon of reverse secondary flow is noticeable on the inside of the bend where the high velocity filament occurs. The development of the expected helical flow is delayed until the next section.

In section J, the flow leaves the channel and moves onto the floodplain and the bed has aggraded forming a large point bar beyond the apex.

In the low overbank rough case, which of the four tests performed is probably most representative of a natural river, the flow structure is very similar to that observed at bankfull. The scouring of the section

upstream of the apex and the flattening of the apex section are present to a lesser degree than that observed in the high overbank rough case. In this test a small circulation cell moving in the inbank sense is present at the outside of the apex (see Figure 5.10).

For all overbank flows the secondary circulation at the apex is changed to outward flow through the majority of the velocity profile. This is reflected by a flattening in the apex cross section and a pronounced rise in the bed level at the inside of the bend before the apex section. These effects on the bed shape increase with increasing relative floodplain flow depth and decreasing relative roughness. The maxima of the secondary velocity at the apex moves closer to the bed as the overbank flow becomes more dominant.

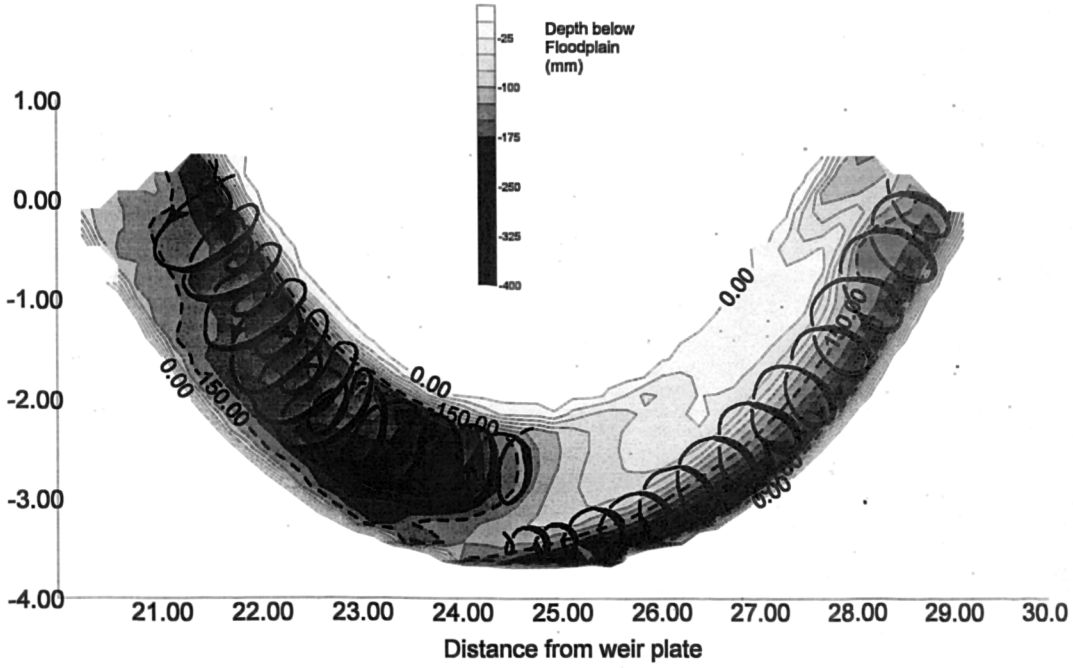

Figure 5.10 Representation of flow mechanisms within flooded meandering channels LORW

Observation of flow on roughened floodplains

The floodplain flow in the rough main channel tests is shown in Figure 5.11. The diagram was constructed from observations of dye traces recorded on video. Several structures are of interest. On the large floodplain next to the apex the flow can be seen to be relatively constant across the floodplain where the velocity is controlled by the floodplain slope and the roughness ratio. On the adjacent bank, there is a reverse circulation. This is due to the large volume of flow ejected onto the floodplain just below the apex. As the floodplain is rough, this flow creates a head to drive flow upstream. The effect of this blockage is that flow is ejected laterally into the main channel between sections H2 and the apex I. Between apex E and H2 the floodplain flow enters the main channel flow in line with the valley slope.

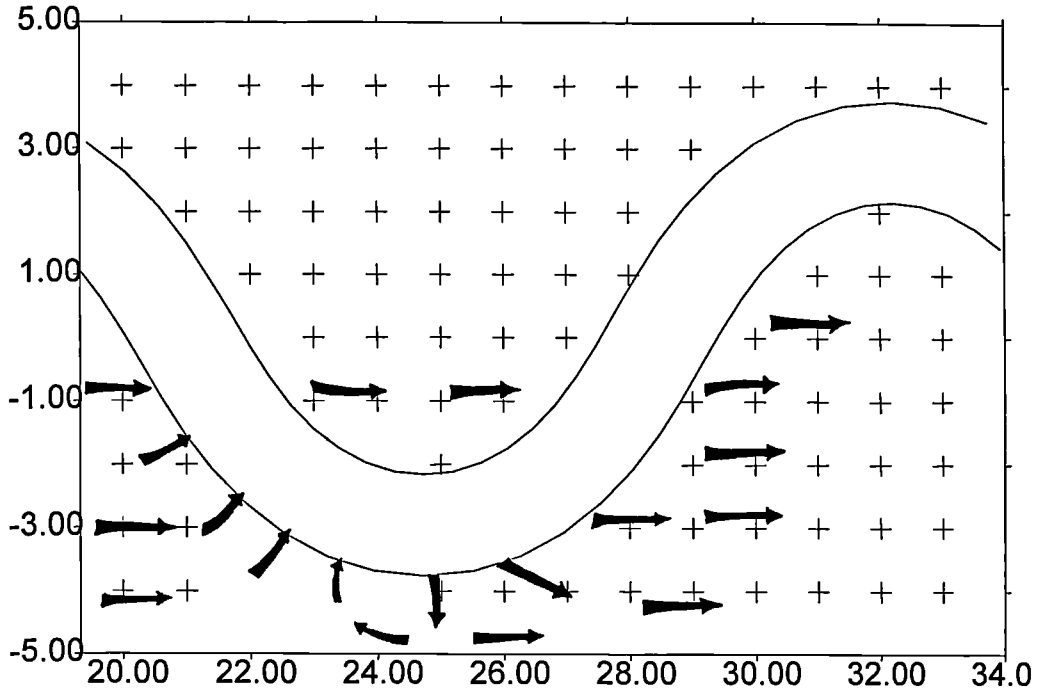

Figure 5.11 Schematic diagram of floodplain flow on rough floodplain constructed from video of dye tracing

5.6. Comparison with Series B

5.6.1. Comparison of geometry

In the following section a comparison is made between the current tests and the 60° "natural" bed form meander bend investigated in the Series B test program. The Series B channel was slightly smaller and had a 45° outside wall at all points. A detailed visual comparison of bed form is provided below.

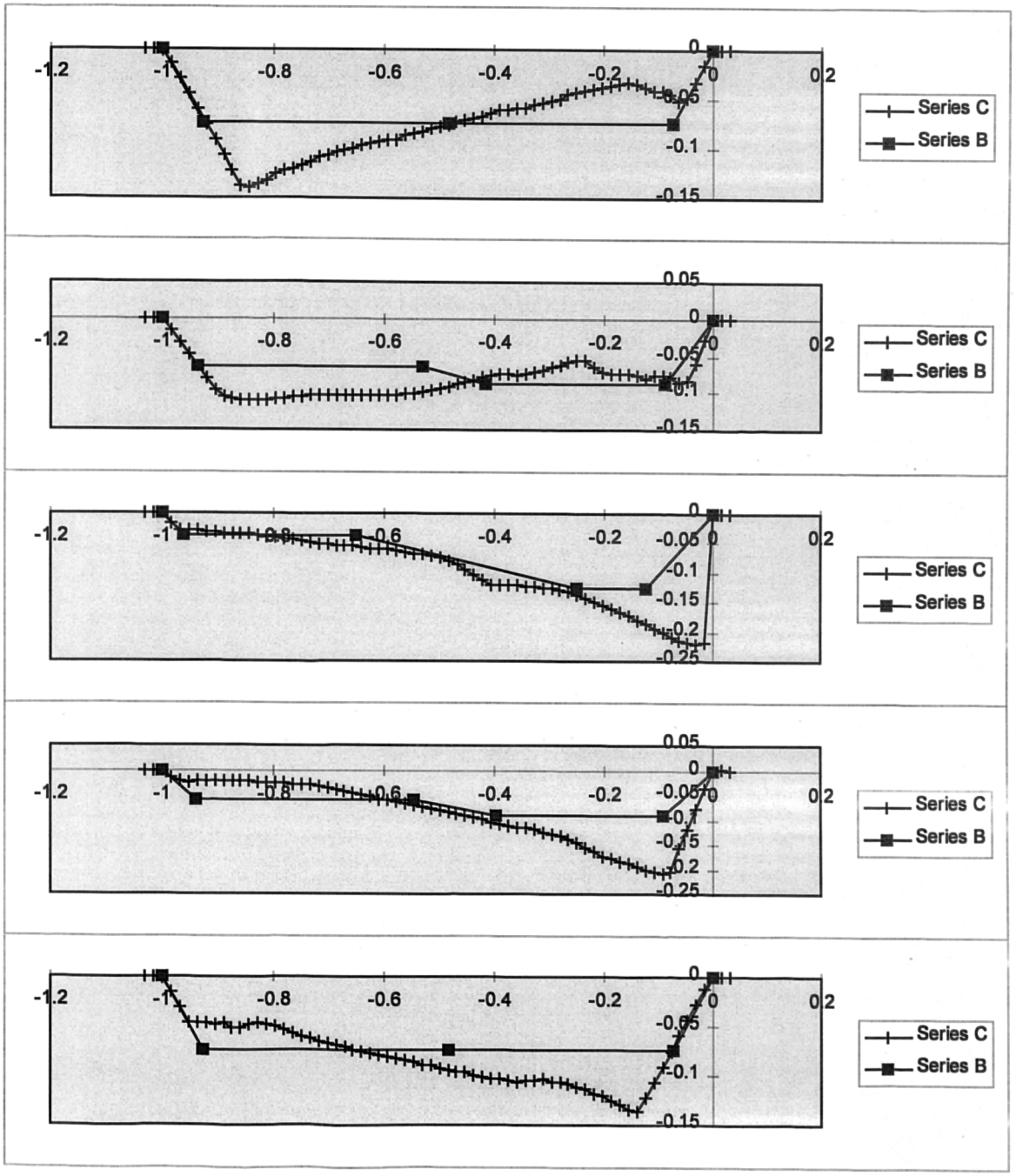

Figure 5.12: Crossover, 1/8th, Apex, 1/8th, Crossover sequence. A comparison between Series B and Series C bed geometry's normalised by the top width

Test Series	Top Width (m)	λ/2 (m)	floodplain Slope S	Sinuosity R	Bankfull depth (m)
C	1.6	10.06	1/550	1.37	0.15*
B	1.2	8.24	~1/1000	1.34	0.15♣

♣ At outside of apex; *Screeded depth.

Table 5.1 Dimensions of the Series B and C channels.

The profile in the Series C case is that obtained by running at bankfull flow, the formative discharge, until a stable bedform was obtained. The Series B channel was designed by Lorena (1993). The channel was designed from information about apex forms from 17 rivers world wide. He designed a channel where the apex form was reversed at consecutive apices and that the bed varied linearly in-between. It is clear from diagrams such as Figure 2.11 that a riverbed is not symmetrical about the apex. However, this form was chosen for ease of construction.

In Series C the fixed channel walls are vertical at the outside of each bend apex and 45° at the crossovers, appropriate for a channel with cohesive banks. At the inside of the apex the 45° slope is maintained. In the Series B channel the main channel walls were set at 45° throughout. Apart from this difference, the apex sections from both tests are very similar. Downstream from the apex, the point bar in the mobile bed case is more pronounced and continues to the 1/8thλ before the next bend apex with the main velocity filament crossing the channel just before the apex. In the fixed bed tests (Series B) the point bar is lost before the inflection point and an artificial point bar is moulded and arranged symmetrically about each apex; the crossover is flat. These variations should be considered when comparing the results of the tests.

5.6.2. Comparison of flow structures

Figures 5.13 - 5.22 present a set of flow diagrams from the 1.37 sinuosity "natural" form channel (Series B). They include those illustrated by Sellin and Willetts (1996) for the smooth floodplain tests and additional diagrams constructed by the author from Series B data for the rod-roughened floodplains. These show isovel and secondary circulation plots around half a meander wavelength for depths above the floodplain of 15mm and 50mm. The diagrams are presented together for easy reference. For each test isovel and secondary circulation diagrams are presented side by side. A schematic diagram of the Series B channel is given in Figure 2.14. The five tests shown are considered to be the closest equivalent to the Series C mixed grain tests. A bankfull test (140mm) a low and high smooth floodplain test (165 and 200 mm respectively) and two similar rough floodplain tests.

The following differences between the Series B and Series C results are noted.

5.6.3. Variations in flow structure between Series B and C smooth floodplain tests

Crossover

In both low and high overbank Series B tests (See Figure 5.16 and Figure 5.18), secondary circulation occurs near the bed at the upstream side of the crossover. This behaviour is seen in the high overbank

smooth Series C test (Figure 4.9) however in the low overbank test secondary circulation occurs throughout the crossover cross section. Flow velocities are highest at the downstream side of the channel in both C and B tests.

Apex

In the low overbank flow Series C test, Figure 4.15, there is a strong current toward the outer bank with a maximum at around 100mm below the bankfull level reducing towards the surface and bed. At the bed there is a small conventionally orientated secondary circulation cell. At the surface flow toward the inside of the bend may be inferred from the data. This is very similar to the pattern seen in the Series B low overbank test, Figure 5.16. The high overbank Series C data shows a strong current toward to outside of the bend reducing in magnitude toward the surface, Figure 4.18. The reverse cell, observed in the Series B test (Figure 5.18), is less clear.

The flow is fastest at the inside of the bend in both test series.

5.6.4. Variations in flow structure between Series B and C roughened floodplain tests

The roughened floodplains used in the Series B tests had significantly lower roughness than those found in the Series C. However, trends are observable.

Crossover

The low overbank rough test exhibits a single secondary cell in the Series B test, Figure 5.19, however, in the Series C test Figure 4.9, a double cell is observed with a reverse cell below the conventional cell. Figure 5.22, the high overbank rough Series B test, shows a single cell at the upstream side of the channel with some signs of another weak secondary cell forming at the downstream side.

In the Series C test, Figure 4.12, this double cell system is clear with the prominent cell at the downstream side. A similar reverse flow cell at the bed to that seen in the low overbank Series C test is present. These variations are again likely to result from the variation in bed shape and the variation in roughness between the two test series.

The velocity maximum is on the downstream side of the channel in both test series.

Apex

At the apex the low overbank flow in the Series B test, Figure 5.19 demonstrates a bankfull type cell at the outside of the bend near the bed whilst showing a reverse cell in the upper flow. This feature is also seen in the Series C tests. In the Series B test however this circulation dies out and does not develop into the continued secondary flow pattern seen in the Series C test. In the high overbank flow tests the Series B test shows reverse circulation to the full depth of the apex section. The high overbank Series C test is similar to that for low overbank flow but shows a reverse cell at inside of the bend.

The velocity maximum is at the centre of the channel in the Series B tests and toward the inside in the Series C test. Significant erosion can be observed in the high overbank rough Series C test due to the erosive capacity of this velocity filament, Figure 4.10.

All the tests share similar features in the disruption of the secondary circulation cell at the apex and the high velocity at the inside of the bend. The bed erosion in the Series C test shows the geomorphic changes resulting from this feature of overbank flow.

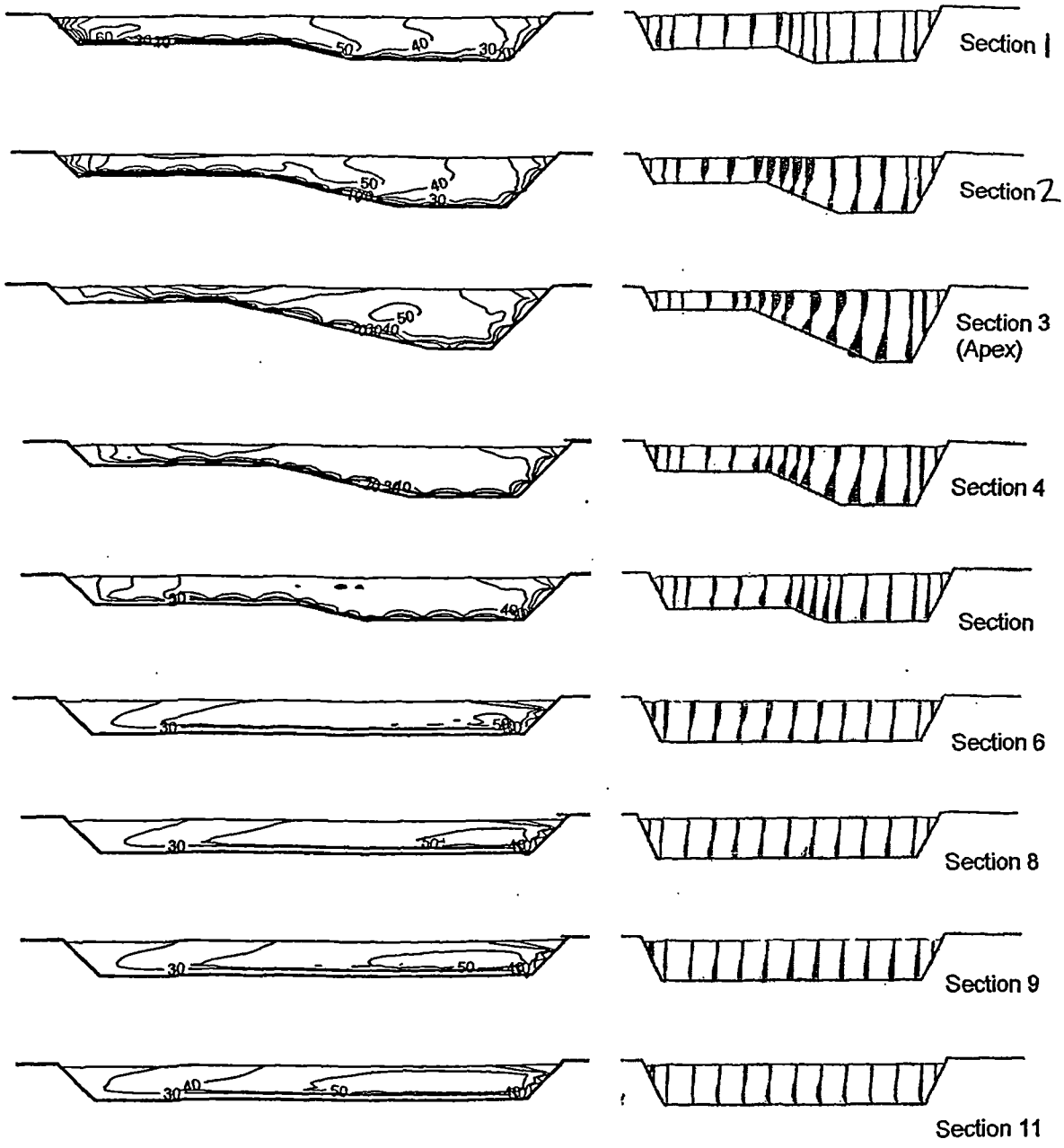

Flow depth 140 mm
Bankfull Depth 150 mm
Bankfull width 1200 mm
Viewed looking down stream

Figure 5.13 Primary and Secondary velocities: Series B, inbank flow

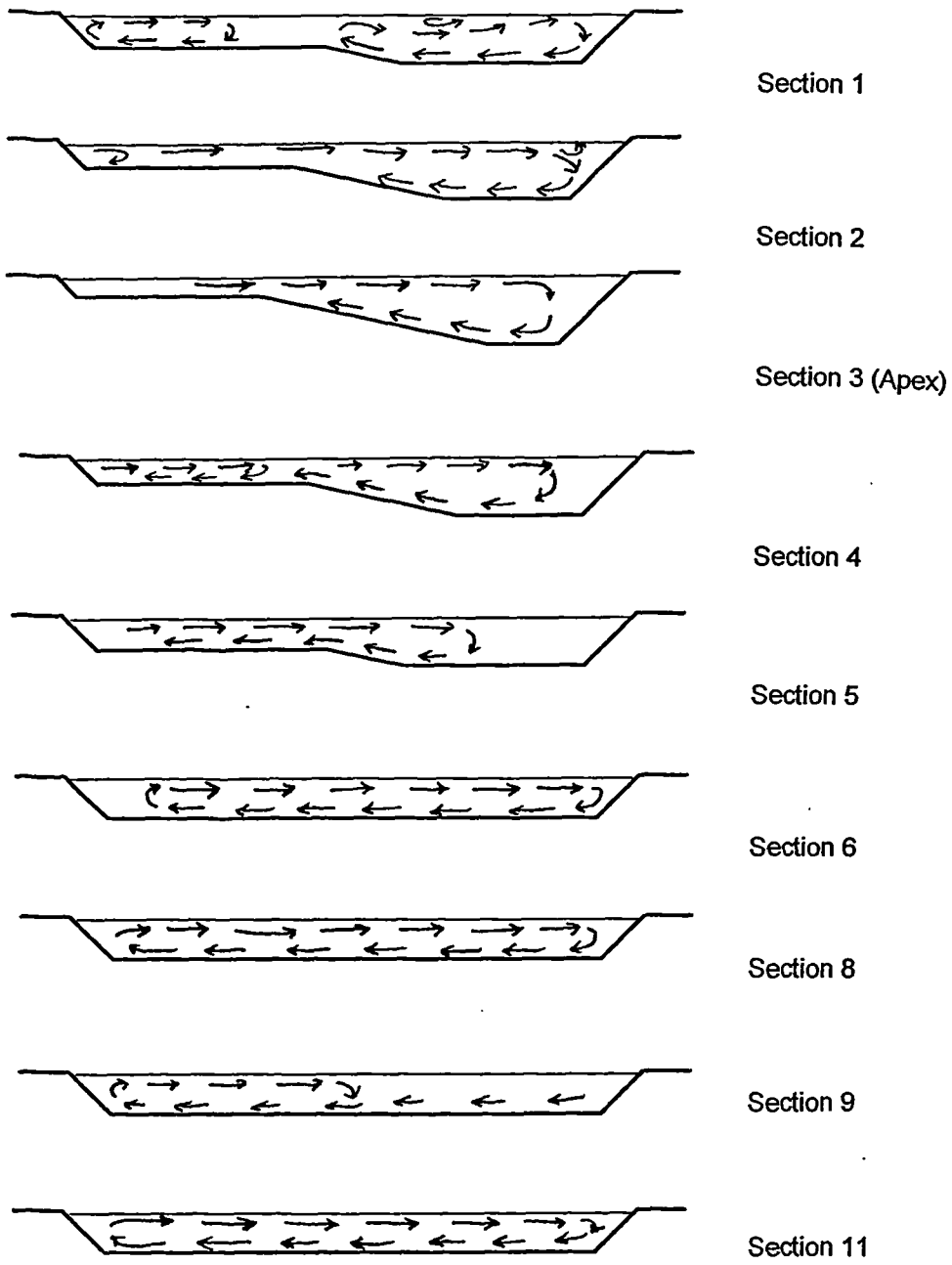

Figure 5.14 Secondary circulation cells: Series B, Inbank flow

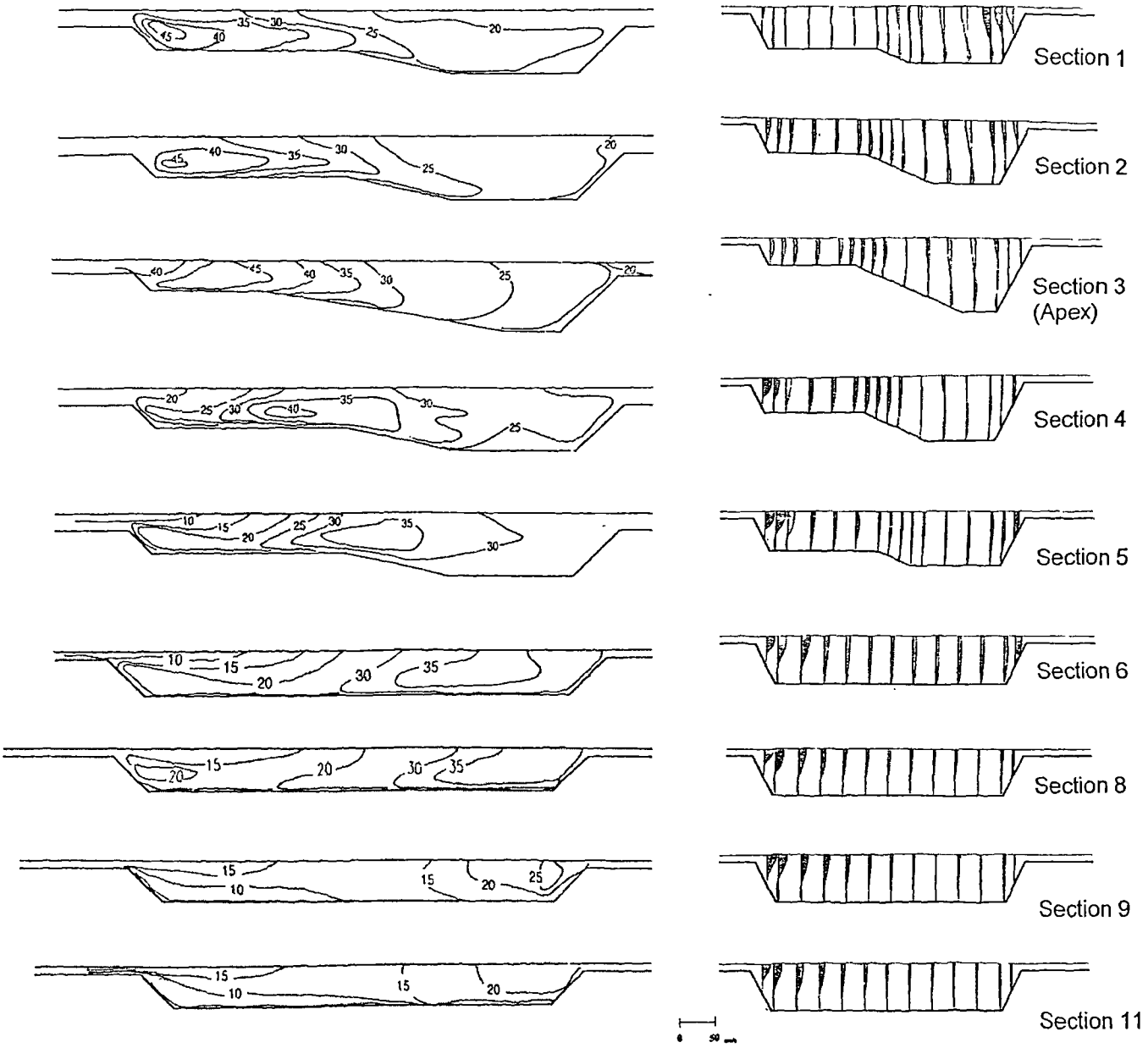

Figure 5.15 Primary and Secondary velocities: Series B, low overbank flow, smooth floodplain

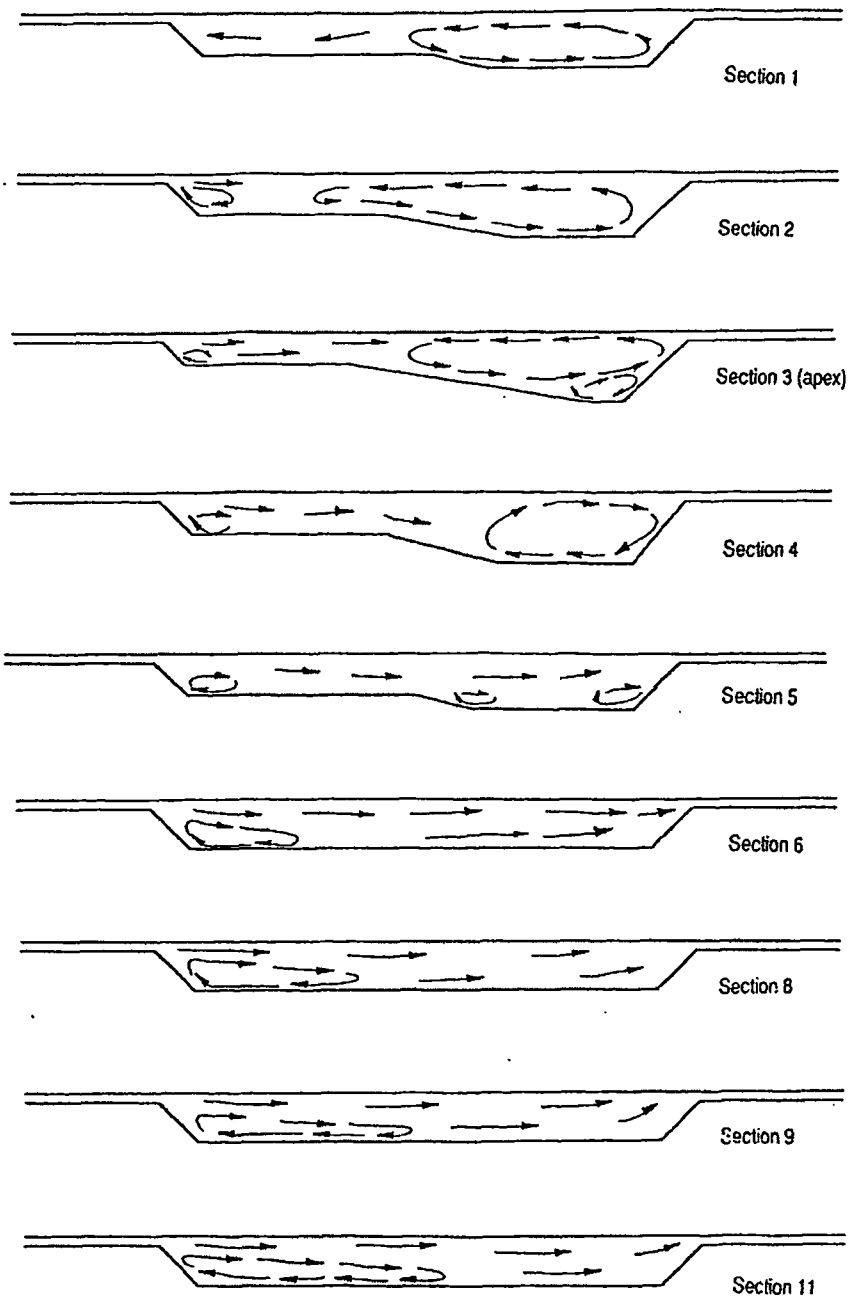

Flow depth 165 mm
Bankfull Depth 150 mm
Bankfull width 1200 mm
Smooth floodplain
Viewed looking down stream

Figure 5.16 Secondary circulation cells: Series B, low overbank flow, smooth floodplains

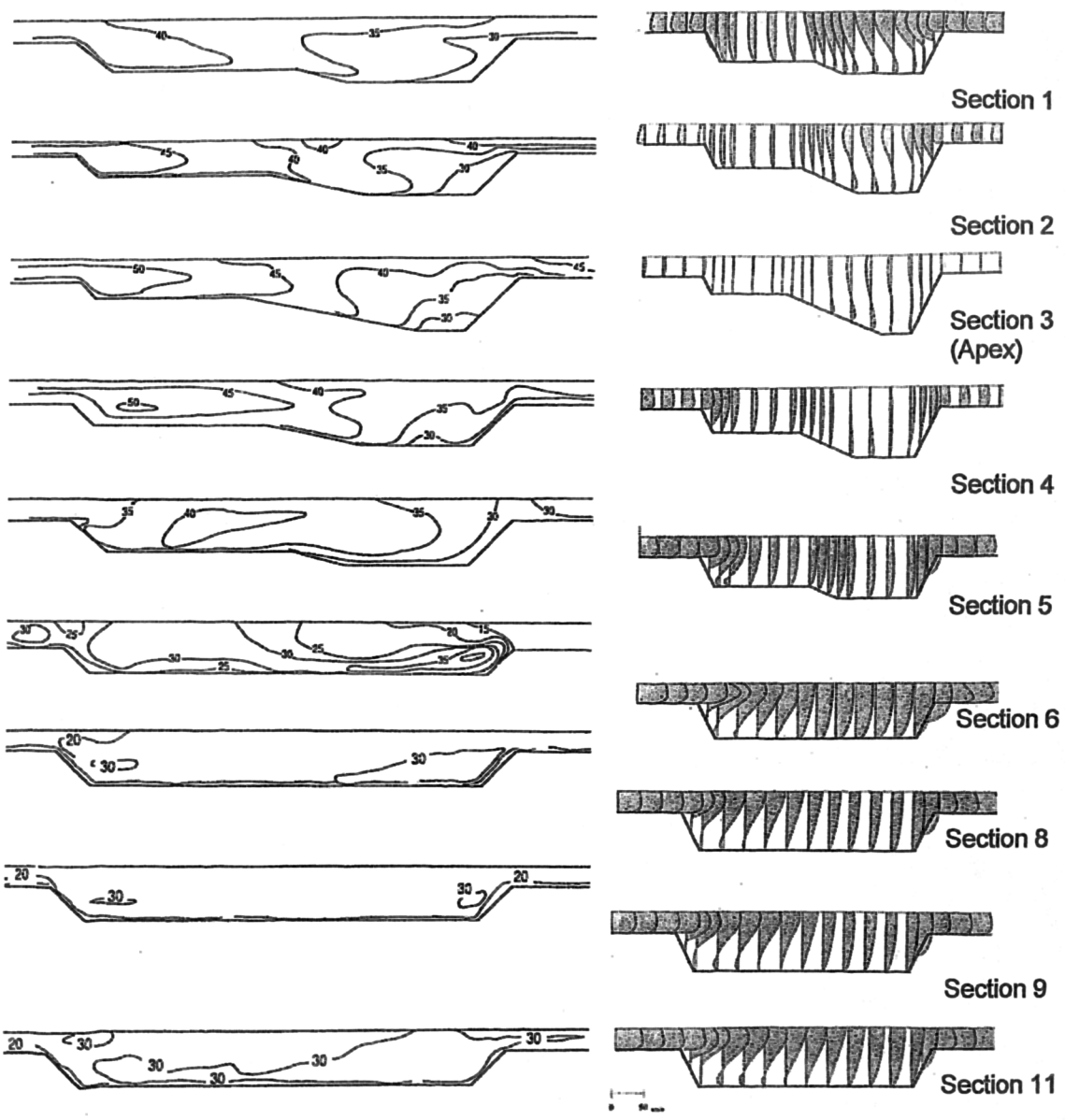

Figure 5.17 Primary and Secondary velocities: Series B, high overbank flow, smooth floodplain

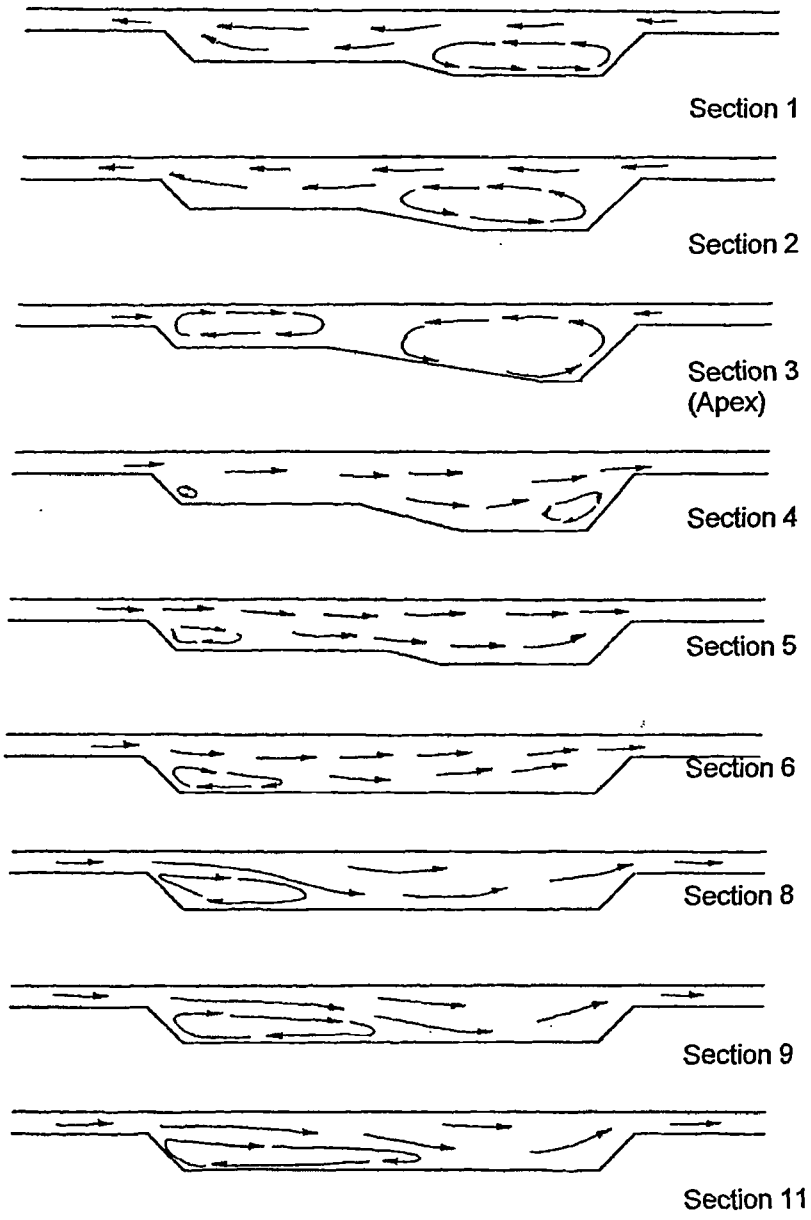

Figure 5.18 Secondary circulation cells: Series B, high overbank flow, smooth floodplains

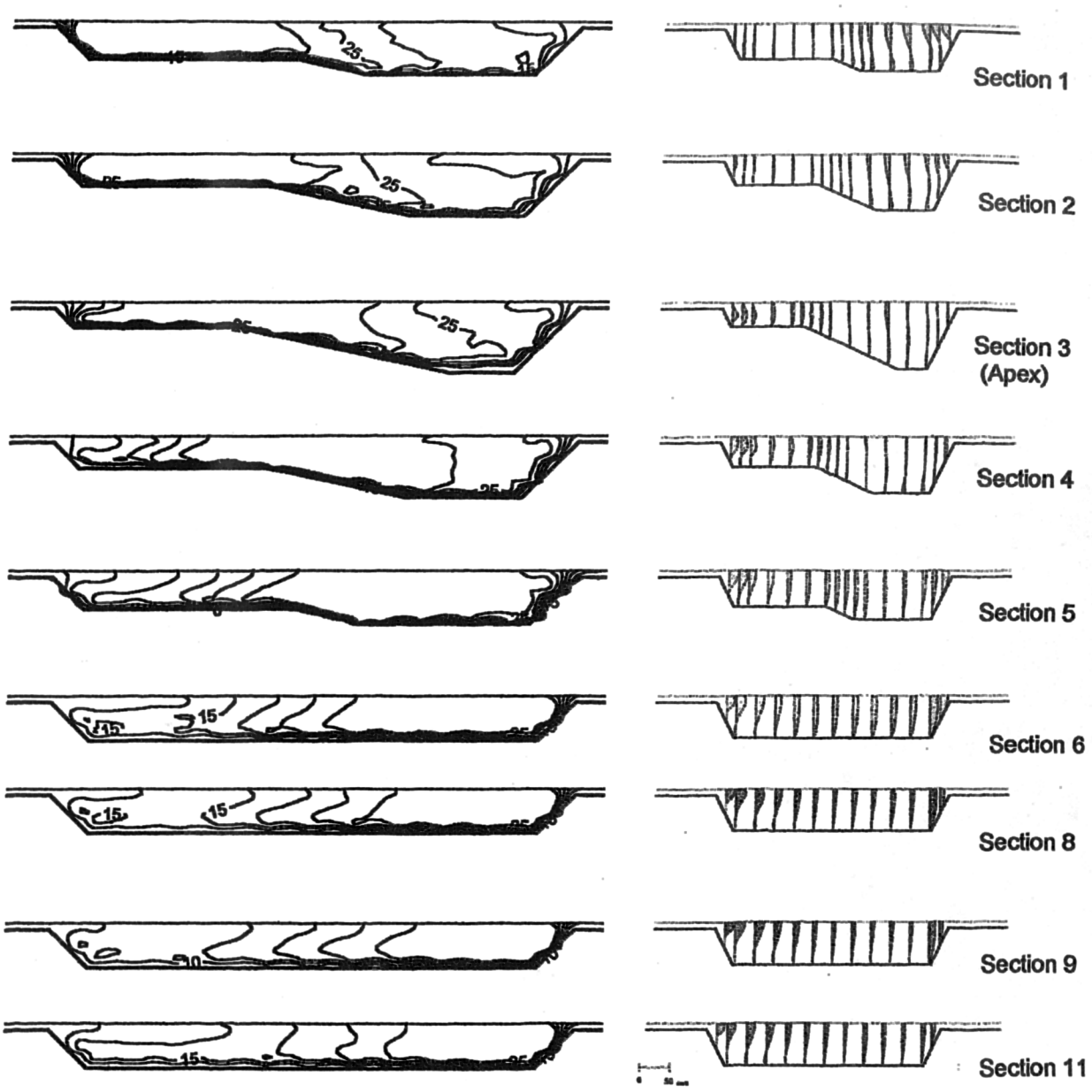

Figure 5.19 Primary and Secondary velocities: Series B, low overbank flow, rough floodplain

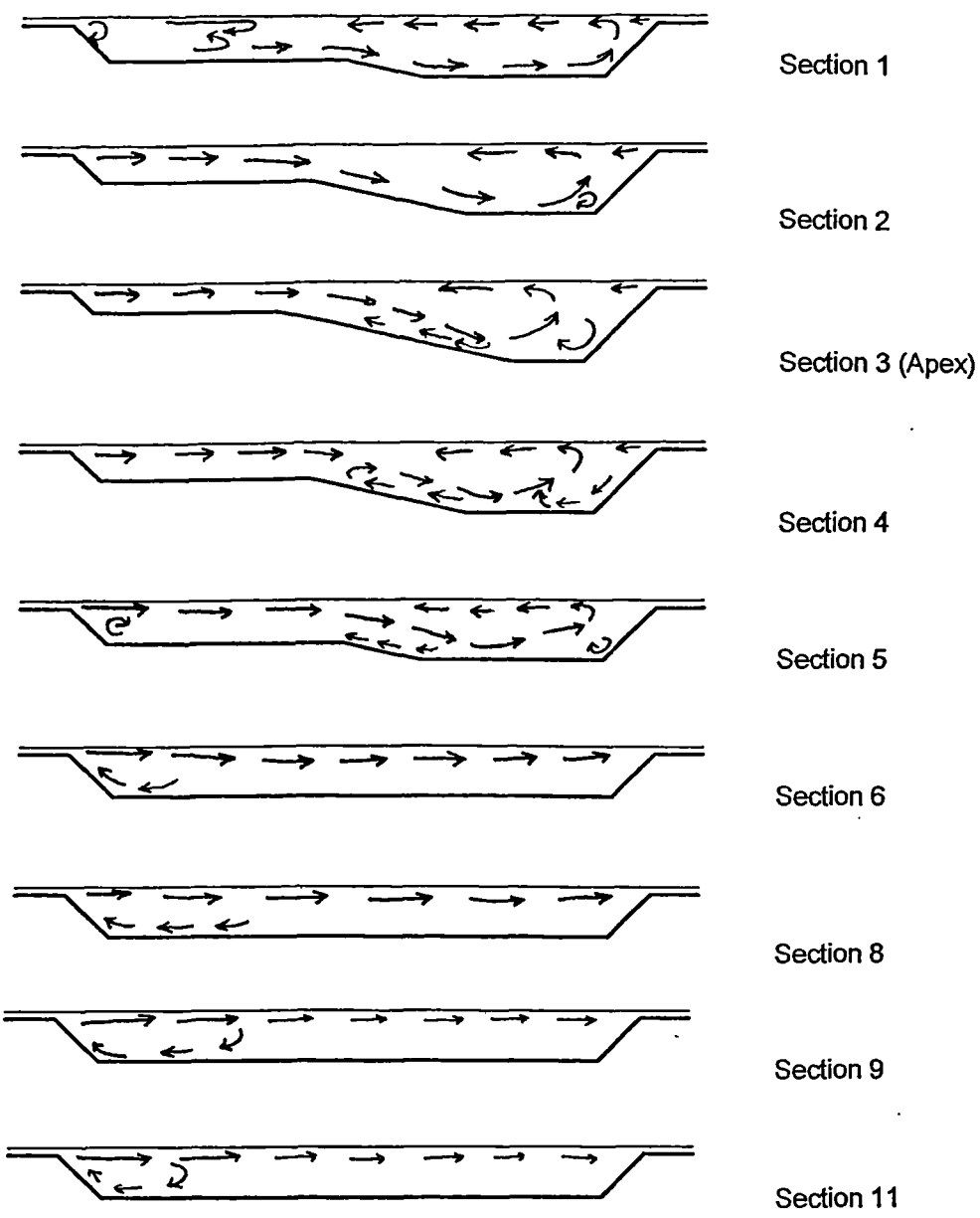

Figure 5.20 Secondary circulation cells: Series B, low overbank flow, rough floodplains

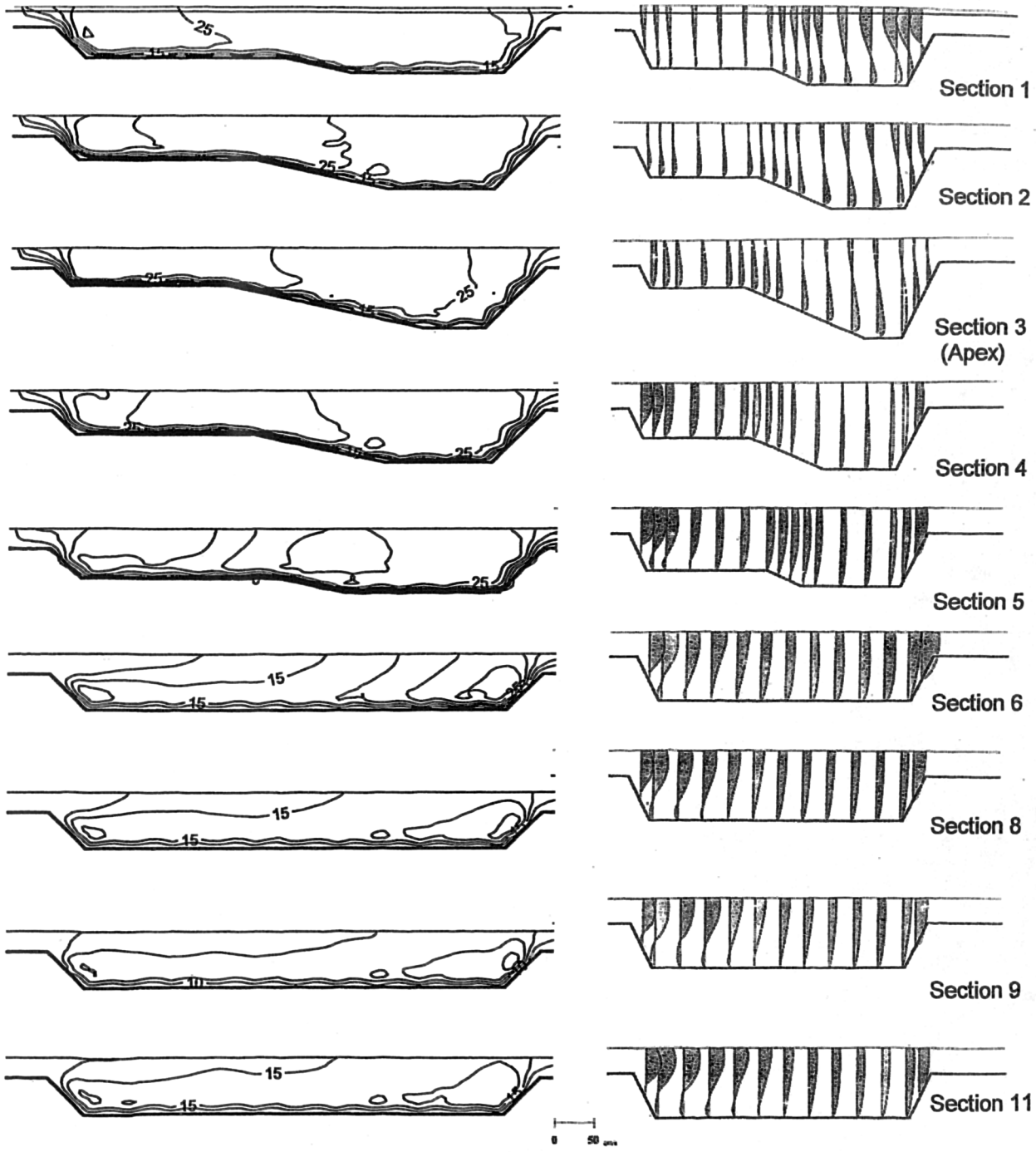

Flow depth 200 mm
Bankfull Depth 150 mm
Bankfull width 1200 mm
Viewed looking down stream
Roughened Floodplains

Figure 5.21 Primary and secondary velocities: Series B, high overbank flow, rough floodplains

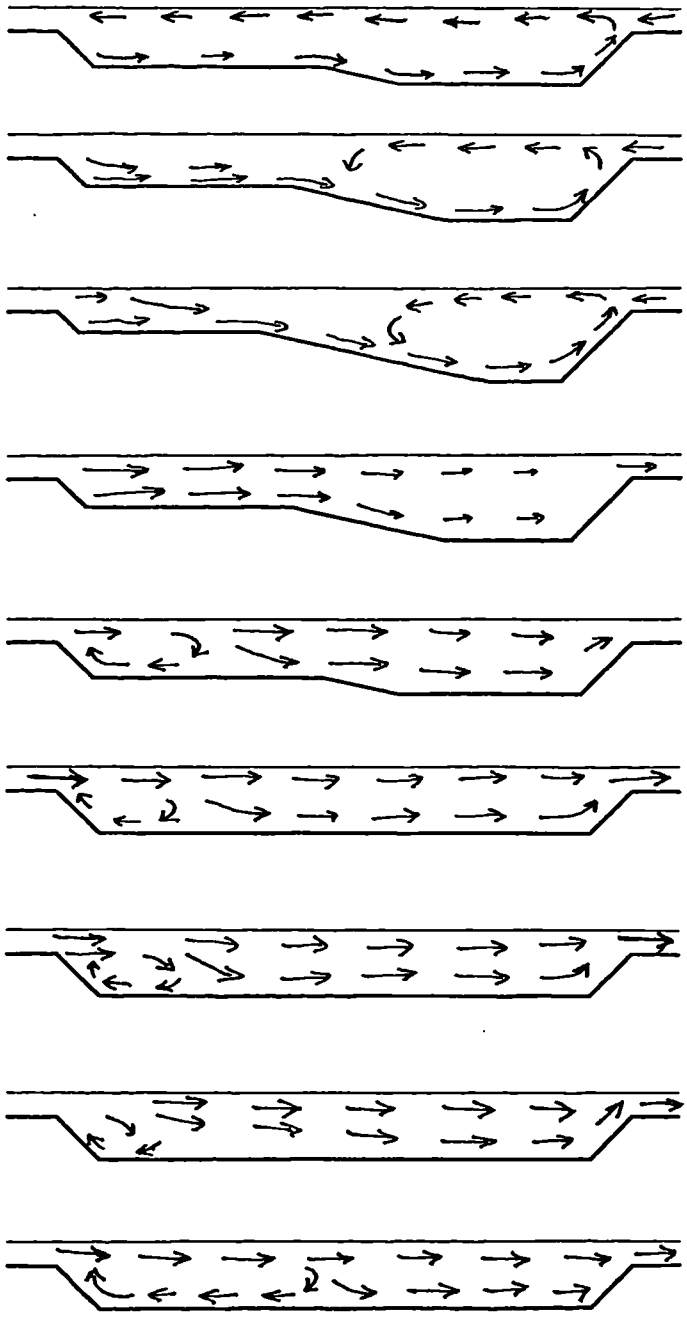

Flow depth	200 mm
Bankfull Depth	150 mm
Bankfull width	1200 mm

Viewed looking down stream

Figure 5.22 Secondary circulation cells: Series B high overbank flow rough floodplains

5.7. Comparison of the Series C values of F* with those obtained in the Series B.

The concept of F* is introduced in the literature review section 2.9.4. Essentially, it is a method of identifying the degree of floodplain interaction by comparing the theoretical discharge at a section with the actual discharge. The resulting ratio can be applied to correct flood estimation using such methods. The method was originally derived for straight channels and hence it is only appropriate for the apex section where main channel and floodplain flow in the same direction. In a meandering stream, the degree of meandering is contained within the factor.

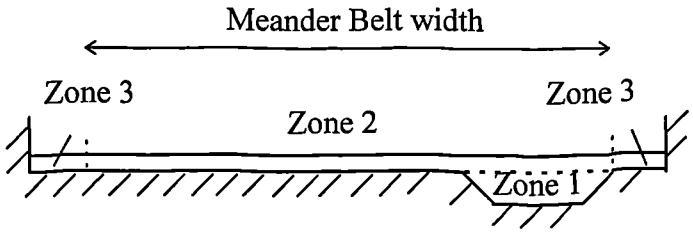

Figure 5.23 Channel division method (After Ervine et al. 1993)

F* is defined as

$$F^* = \frac{\text{actual measured discharge}}{\text{theoretical discharge based on skin friction only } (Q_1 + Q_2 + Q_3)} \qquad (5.1)$$

Ervine, Willetts, Sellin and Lorena propose the calculation of Q_1, Q_2 and Q_3, identified in Figure 5.23, in the following way. Q_1 is calculated from Manning's equation using the meandering channel bed slope and the bed friction characteristics of the main channel. Q_2 is calculated for the areas shown using the floodplain slope and roughness and the floodplain wetted perimeter excluding the main channel width. This is equivalent to deepening the section of flow over the floodplain to include the section of flow above the main channel. Q_3 is computed from Manning's equation using floodplain depth, slope and roughness. The zonal discharges are summed to obtain the total discharge.

The calculations implicitly assume that the main channel does not change form at over bank flow. It is clear from the preceding work that this is not the case, however as a practitioner is likely to obtain a measurement from the bankfull bedform, Q1 has been taken to be the bankfull flow in the following calculations.

Floodplain roughness

F* describes the influence of floodplain interaction on the flow in the main channel. If the water on the floodplain is stagnant due to vegetation or other cause then Manning's n will be very high and Q_2 will be underestimated as the section of Q_2 which is immediately above the main channel, Q_{2mc}, will move at a similar speed to that in zone 1 rather than at the velocity of the floodplain flow. Under these conditions the

horizontal division lines becomes inappropriate and vertical divisions at the top of the banks should be used. As the value of Manning's n on the floodplain decreases, the velocity and influence of the floodplain flow increases. The chart of Manning's n plotted against flow depth for the roughness elements presented in Figure 3.10 shows that Manning's n for the roughness on the floodplains in the Series C tests varies between 0.1 and 0.14 at the depths tested. This is equivalent to a heavily vegetated floodplain where the vegetation remains erect during inundation.

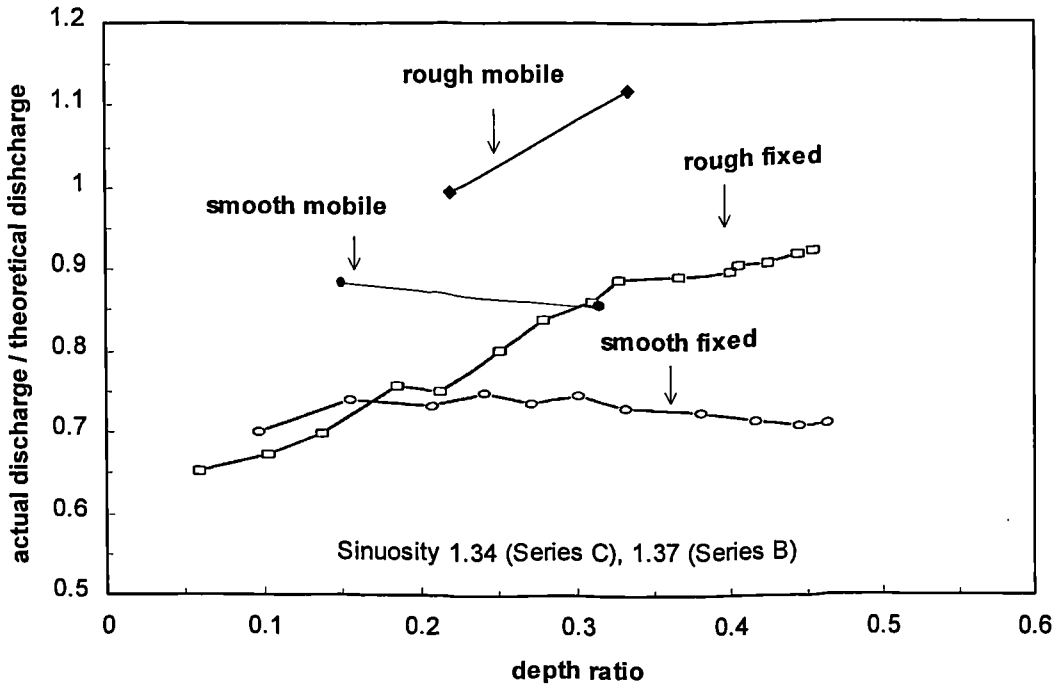

Figure 5.24 Variation of F with Relative flow depth for Smooth and Rough Floodplain Boundaries in Series B and Series C channels*

Plotting depth ratio against F* for rough and smooth cases from B and C we see that the higher relative roughness in the Series B case actually exceeds unity in F*. This suggests that the flow resistance artificially introduced in the calculation of Q_{2mc} is too high to account for the non friction losses in the system. The limited amount of data collected is clearly insufficient to significantly improve the predictive method but it does show the effect of significantly increasing the roughness.

The effect of bed shape.

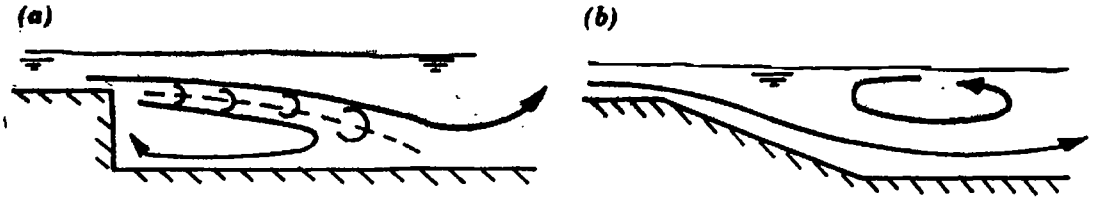

Figure 5.25 Different Regimes of Mixing between Floodplain and Main channel Flow: (a) Floodplain flow causes Separation, Recirculation and Shear; (b) Floodplain flow Dives into main channel with rollers near surface

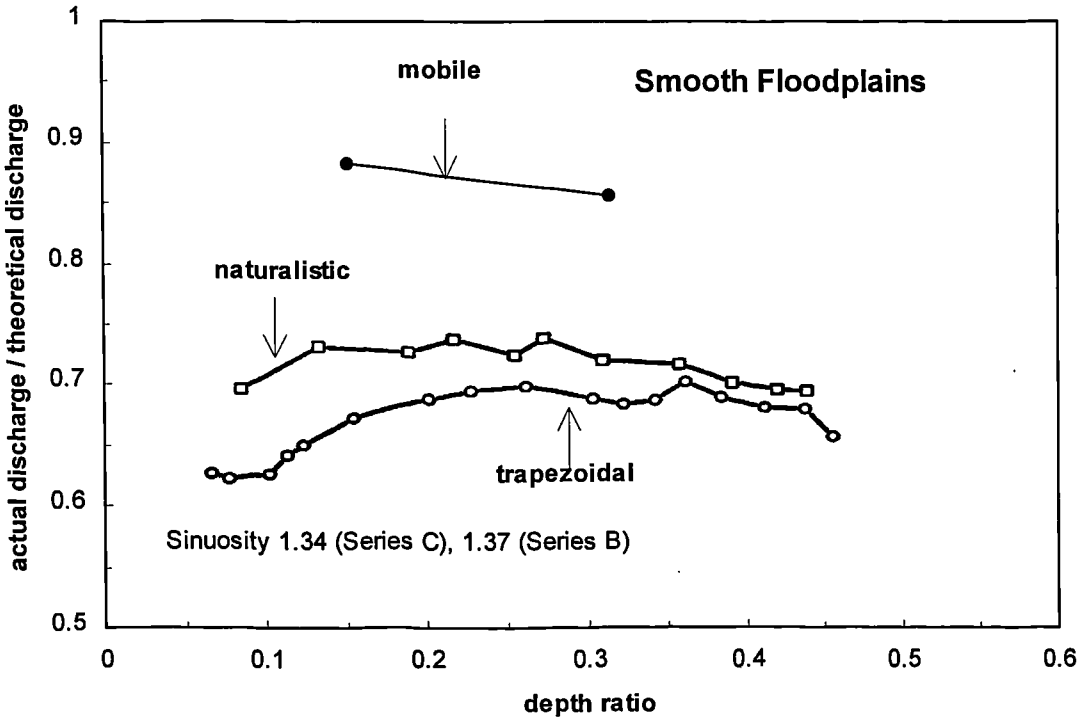

Figure 5.26 Variation of F with Relative Flow Depth for the Series B naturalistic and trapezoidal channel shapes and the Series C Mobile Bed channel*

Figure 5.26 shows a comparison between trapezoidal, natural form and mobile bed flood plain flows with a smooth boundary. Ervine et al. note the increased conveyance in the natural channel as opposed to the trapezoidal channel. The data points available support this observation with respect to a mobile bed meandering channel. At the lower depth ratio the F* value is very similar to that obtained in the artificial natural channel. As the depth ratio increases the mobile bed channel is shown to have a higher F*. This is probably due to changes in the bed form due to the alteration in flow mechanisms, improving the conveyance of the channel.

5.7.1. Comparison of the measured results with those obtained via the James and Wark Model

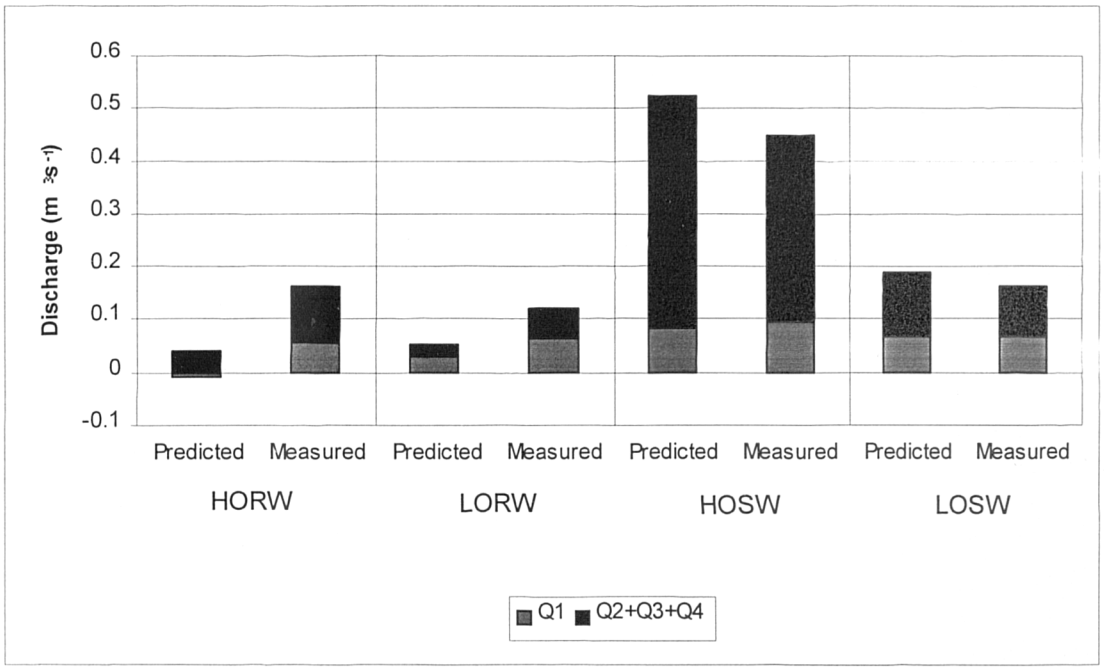

Figure 5.27 Comparison with predicted and measured results for the James and Wark flow prediction method

The James and Wark method was based on the observation of flow mechanisms observed in the Series B tests. It has a semi-physical basis rather than being purely empirical however, the range of data collected in the Series B tests limits its applicability. The method is examined in more detail in Chapter 2.

The flow rate in sections 1 and 2 is dependant on the ratio of floodplain roughnesses, f', the relative depth between floodplain and main channel, the aspect ratio and the sinuosity of the main channel. The roughness ratio n_{fp}/n_{mc} varies between 0.72 and 7.4. In the Series B tests this variation is 1-3.0 Ervine et al (1993). Thus for both the smooth and the rough test the results are outside those on which the method was verified.

Reasons for non-compliance

The results illustrate well the problems with the James and Wark method when applied to rough flood plains. The calculation of the flow in zone 1 is described in section 2.9.5. The method suggests that at high floodplain roughness the discharge in the main channel decreases linearly with relative depth. This presumption drastically underestimates the flow in the main channel in the rough floodplain cases. Further study is required to correct this function.

For the roughened floodplains the method also under predicts the floodplain flow in zone 2. At high roughness levels where the flow leaves the floodplain slowly and is mixed into the main channel flow rather than crossing the main channel, the theory of flow over slots is no longer an appropriate assumption. As shown in Figure 5.24, a method applied to zone 2 which does not take account of the difference in flow rate between flow over rough floodplains and flow in the main channel will result in error.

The method over predicts the conveyance of the floodplain flow in the smooth floodplain cases. As the floodplains are smoother than the channel in this case, which is an unlikely natural scenario this normally is of less concern.

5.7.2. Momentum exchange method

A major problem with the James and Wark method and the F* approach is that they do not behave well in situations where the floodplain is very rough. Where this occurs, velocities on the floodplain are considerably lower than those in the main channel. To divide the channel into areas of similar flow, vertical division lines over the channel banks would be more appropriate than a horizontal division in the main channel at bankfull level. From observation of dye traces, the flow from the floodplain appears to be fully integrated into the main channel by secondary circulation rather than travelling over the main channel to the downstream floodplain. The observations in this chapter have prompted the author to propose a simple model attributing flow resistance to the exchange of momentum, in the main channel direction, between main channel and floodplain. A momentum approach has the advantage of being less sensitive to velocity fluctuations than an energy approach.

The following analysis is loosely based on the calculations for momentum transfer resulting from flow into a side channel spillway presented by Yen and Wenzel (1970).

We shall assume that vertical division lines above each bank divide the channel.

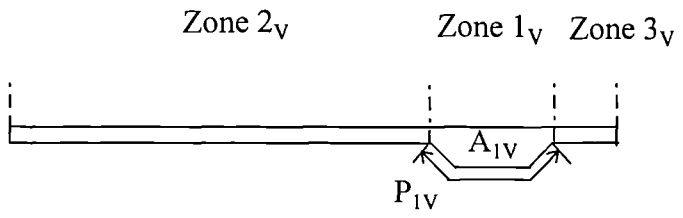

Figure 5.28 Alternative channel division method employing vertical division lines at the channel banks

The control volume under consideration, consists of the flow in zone 1_V (Figure 5.28) between sections A and B (Figure 5.29). The subscript V indicates the vertical division lines.

Over this reach any change in discharge in the main channel is given by

$$\frac{dQ_{mc}}{dx} = U\frac{dA}{dx} + A\frac{dU}{dx} = q_{uf} - q_{lf} \qquad (5.2)$$

For half a wavelength this may be rewritten

$$\frac{\Delta Q_{mc}}{\Delta x} = Q_{uf} - Q_{lf} \qquad (5.3)$$

where

$\Delta x = r\lambda/2$, the distance along the channel centre line between A and B

Q_{uf} = the flow entering the channel from the upper flood plain

Q_{lf} = the flow leaving the main channel for the lower floodplain

The change in momentum between sections A and B is given by

$$\Delta M = M_A - M_B + (M_{uf} - M_{lf}) \qquad (5.4)$$

where M_A and M_B are the main channel momentum at sections A and B respectively and M_{uf} and M_{lf} are the momentum exchanges from upper and lower floodplain. From basic hydrodynamics,

$$M_A - M_B = \iint_A \rho u_x^2 dA \qquad (5.5)$$

In order to obtain expressions for M_{uf} and M_{lf} we must consider the floodplain flow patterns.

5.7.3. Momentum transferred from upper floodplain, M_{uf}

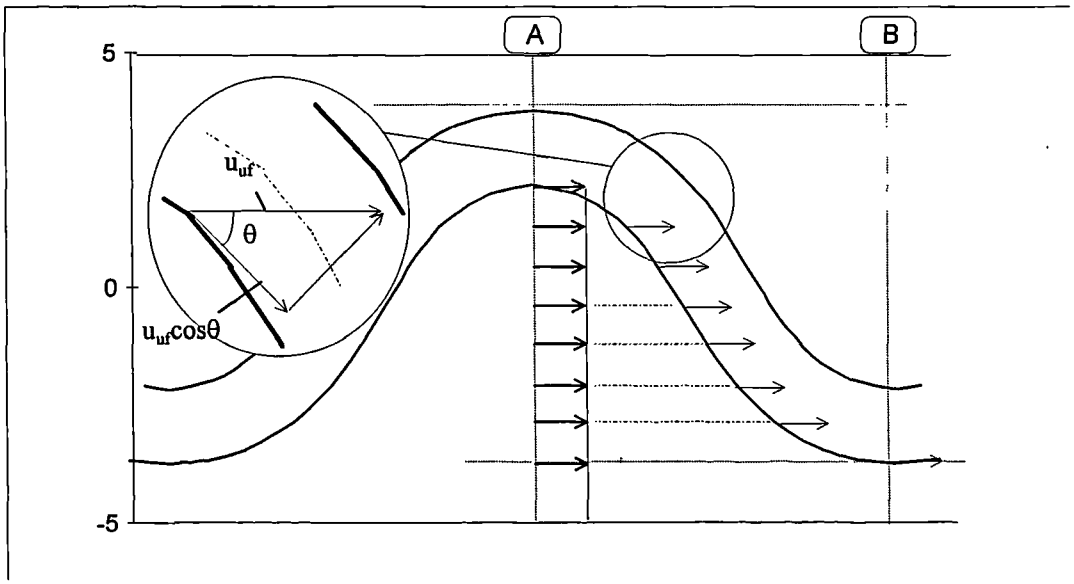

Figure 5.29 Schematic diagram showing the floodplain flow entering the main channel

The momentum of the flow entering the main channel between sections A and B is given by the product of the mass of flow entering the main channel per second, Q_u, and the velocity of that flow in the main channel direction, $u_{uf\text{-}mc}$.

$$M_{uf} = \rho Q_{uf} u_{uf\text{-}mc} \qquad (5.6)$$

In order to evaluate these quantities consider the reach of the channel between the two apices shown in Figure 5.29. It can be observed in Figure 5.8 and Figure 5.11 that the flow on the floodplain beside the apex is travelling at a uniform velocity across the floodplain and is directed in the main valley slope. Therefore, a suitable first assumption would be that the flow entering the main channel from the upstream floodplain is travelling coincident with the floodplain slope at a velocity determined by the floodplain slope and

roughness. From Figure 5.11 we can see that this is an over simplification in the roughened floodplain case, however we shall retain this assumption for the time being.

From the above it seems reasonable to evaluate the volume of flow entering the main channel per second as the discharge of the floodplain adjacent to apex A

$$Q_{uf} = u_{uf} z_{uf} (Y_{mb} - B) \qquad (5.7)$$

Where Y_{mb} is the width of the meander belt and

$$u_{uf} = 1/n_{uf} \cdot z_{uf}^{2/3} S_0^{1/2}, \qquad (5.8)$$

where n_{uf} is a function of z_{uf} and the hydraulic properties of the floodplain roughness.

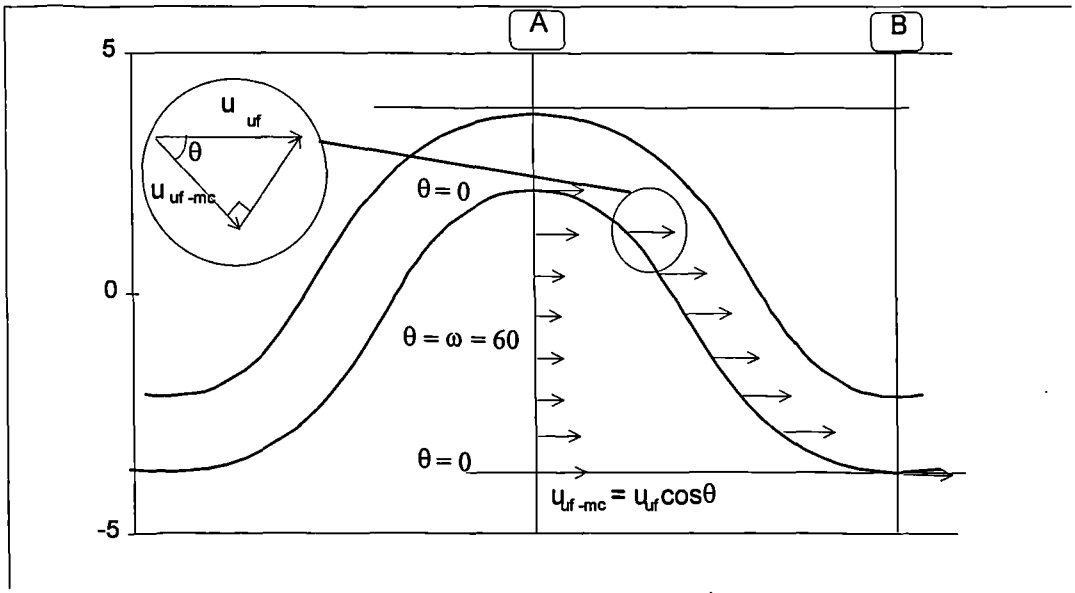

Figure 5.30 Diagram showing the magnitude of velocity entering the main channel resolved in the main channel direction. This is drawn at section 1 for simplicity.

The magnitude of floodplain flow velocity in the main channel direction, entering the main channel at a point, is given by $u_{uf\text{-}mc} = u_{uf}\cos\theta$. As the channel is of sinusoidal form, the average velocity over the channel bank between A and B may be approximated by

$$\bar{U}_{uf\text{-}mc} = u_{uf}(\cos 0 + \cos\omega)/2 = u_{uf}(1 + \cos\omega)/2 \qquad (5.9)$$

where ω is the maximum angle to the floodplain slope.

Substituting Equation 5.7 - 5.9 into Equation 5.6.we obtain

$$M_{uf} = \rho Q_{uf} u_{uf\text{-}mc} = \rho u_{uf}^2 z_{uf} (y_{mb} - B)\,(1+\cos\omega) \qquad (5.10)$$

5.7.4. Momentum transferred to the lower floodplain, M_l

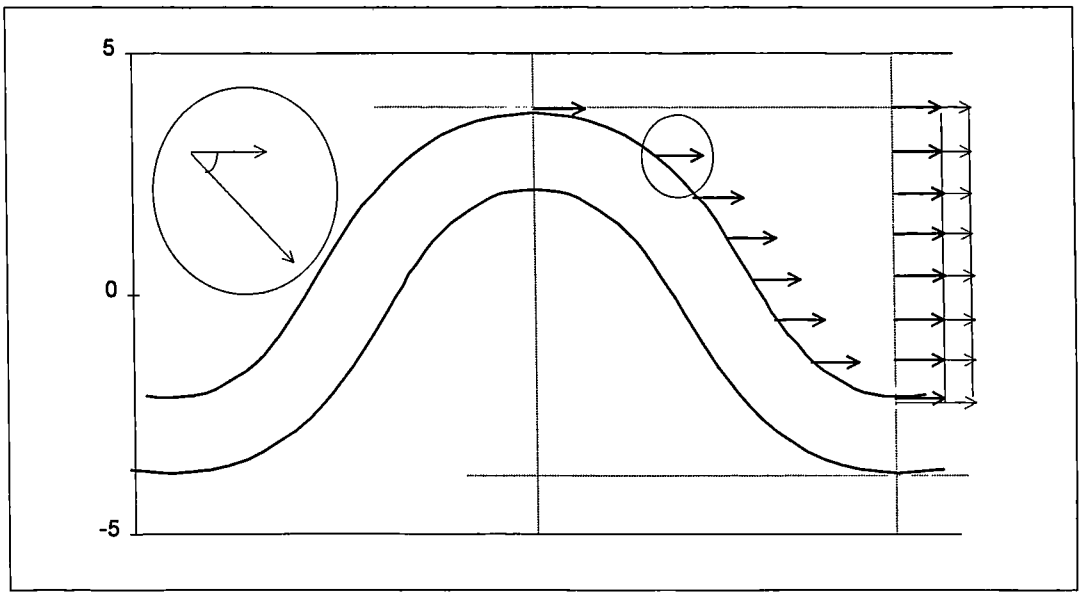

Figure 5.31 Diagram showing and approximation of flow leaving the channel and moving onto the lower floodplain.

The momentum flux over the lower channel boundary, M_{lf}, is the product of the velocity component of the flow leaving the main channel, in the main channel direction and it's mass flow rate.

$$M_{lf} = \rho Q_{lf} u_{mc\text{-}lf} \qquad (5.11)$$

Although the main channel flow velocity, at the lower floodplain boundary, varies down the channel it may be taken as the average flow rate multiplied by a correction factor to account for the slightly higher velocities usually found in that region. Therefore

$$u_{mc\text{-}lf} = u_{mc}\varepsilon \qquad (5.12)$$

where ε is an empirical adjustment to account for variation in velocity leaving the channel from that of the section average,

Using a similar definition for the discharge onto the lower floodplain, Q_{lf}, as that employed for the upper floodplain and substituting equation 5.12 into equation 5.11. We obtain

$$M_l = \rho u_{lf} u_{mc} \varepsilon z_{lf}(Y_{mb} - B) \qquad (5.13)$$

Neglecting the effects due to turbulence and surface tension, the forces acting on an element of fluid in a river flowing at bankfull, consist of the component of weight of the element in the x direction, the boundary shear resistance, and the pressure forces acting at the upstream and downstream faces of the control section. These forces are given as follows.

The component of the fluid weight is

$$\int_0^{\Delta x} \int_A \rho g S_0 A dx \qquad (5.14)$$

The total boundary stress is

$$\int_0^{\Delta x} \tau_{bx} P dx \qquad (5.15)$$

In which τ_{bx} is the average boundary shear stress in the x direction over the boundary of a cross section. The difference of the total pressure forces acting on sections 1 and 2 is

$$\int_2^1 \int_A p dA \qquad (5.16)$$

in which p is the pressure intensity.

In the two stage channel we shall introduce a further conceptual force to account for the transfer of momentum between floodplain and main channel, F_{mt}.

$$\int_0^{\Delta x} F_{mt} dx \qquad (5.17)$$

Equating the total change of momentum flux ΔM to the sum of the forces and then dividing the result by dx the following momentum equation is obtained.

$$\frac{d}{dx}\int \rho u_x^2 dA + \frac{\rho Q_u u_u (1+\cos\omega) - \rho Q_l u_{mc} \varepsilon}{\lambda/2} = \rho g S_0 A - \tau_{bx} P - \frac{d}{dx}\int p dA + F_{mt} \qquad (5.18)$$

Introducing a momentum flux correction factor β to the expression for change in momentum between A and B we obtain

$$\int_A \rho u_x^2 dA = \rho \beta A V^2 \qquad (5.19)$$

and a pressure correction factor K can be introduced such that

$$\int p dA = K \gamma A h \cos\phi \qquad (5.20)$$

By substituting Equations 5.19 and 5.20 into Equation 5.18 and introducing the hydraulic radius we obtain

$$\frac{d}{dx}\left(\rho\beta A V^2 + K\rho g A h \cos\phi\right) + \frac{\rho Q_u u_u (1+\cos\omega) - \rho Q_l u_{mc} \varepsilon}{r\lambda/2}$$

$$= \rho g S_0 A - \frac{\tau_{bx} A}{R} + F_{mt}$$

(5.21)

Introducing the hydraulic mean depth, D = A/B where B is the free surface width,

$$\frac{dA}{dx} = \frac{dA}{dh}\frac{dh}{dx} = \frac{A}{B}\frac{dh}{dx} \qquad (5.22)$$

$$\frac{dh}{dx}=\frac{S_o-\frac{\tau_{bx}}{\rho gR}+\frac{1}{gA}\left(\frac{Q_u u_u(1+\cos\omega)-Q_l U_{mc}\varepsilon}{r\lambda/2}-2\beta U_{mc}(Q_u-Q_l)\right)+\frac{U_{mc}^2}{g}\frac{d\beta}{dx}-h\frac{d(K\cos\phi)}{dx}+\frac{F_{mt}}{\rho gA}}{K\cos\theta\left(1+\frac{h}{D}\right)-\frac{\beta U_{mc}^2}{gD}} \quad (5.23)$$

If ϕ is constant Equation 5.23 can be rewritten

$$\frac{dh}{dx}=\frac{S_o-\frac{\tau_{bx}}{\rho gR}+\frac{1}{gA}\left(\frac{Q_u u_u(1+\cos\omega)-Q_l U_{mc}\varepsilon}{\lambda/2}-2\beta U_{mc}(Q_u-Q_l)\right)+\frac{U_{mc}^2}{g}\frac{d\beta}{dx}+\frac{F_{mt}}{\rho gA}}{\cos\phi\left[K\left(1+\frac{h}{D}\right)+h\frac{dK}{dh}\right]-\frac{\beta U_{mc}^2}{gD}} \quad (5.24)$$

It has been shown that the term[K(1+h/D)+hdK/dh] is equal to unity for any channel shape, Yen and Wenzel (1970). Assuming cosϕ = 1 and β = 1, Equation 5.24 becomes

$$\frac{dh}{dx}=\frac{S_o-\frac{\tau_{bx}}{\rho gR}+\frac{1}{gA}\left(\frac{Q_u u_u(1+\cos\omega)-Q_l U_{mc}\varepsilon}{r\lambda/2}-2U_{mc}(Q_u-Q_l)\right)+\frac{F_{mt}}{\rho gA}}{1-\frac{U_{mc}^2}{gD}} \quad (5.25)$$

This equation is only strictly applicable over whole numbers of half wavelengths and the values of the floodplain specific properties evaluated at each section.

5.7.5. Application to uniform flow

For the special case of uniform flow, the depth is constant and hence dh/dx = 0 and $S_f = S_0$. Therefore the resistance force due to floodplain interaction, may be taken as

$$F_{mt}=\rho Q_{fp}\left(\frac{u_U(1+\cos\omega)-U_{mc}\varepsilon}{r\lambda/2}\right) \quad (5.26)$$

The Chezy equation introduced in Chapter 2 was based on a consideration of the forces on an element of fluid.

The force causing motion is given by

$$F_m = W\sin\theta = \gamma ALS_0 \quad (5.27)$$

where θ is small

The force resisting motion is considered proportional to the square of the average velocity or

$$F_R = Lpku^2 \quad (5.28)$$

Were k is the constant of proportionality

We can now add the force due to momentum transfer between main channel and floodplain to this equation

$$F_R = LPku^2 - F_{mt} \quad (5.29)$$

Balancing the resisting and motivating forces we obtain

$$\gamma ALS_0 = LPku^2 - F_{mt} \quad (5.30)$$

Which rearranged and substituting the hydraulic radius gives us

$$\bar{u}_{mc} = \sqrt{\frac{\gamma}{k}}\sqrt{R}\left(S + \frac{F_{mt}}{A\gamma}\right)^{1/2} \qquad (5.31)$$

Replacing (g/k)0.5 with Chezy's coefficient C we obtain

$$\bar{u}_{mc} = C\sqrt{R}\left(S + \frac{F_{mt}}{A\gamma}\right)^{1/2} \qquad (5.32)$$

and similarly for Manning's equation

$$\bar{u}_{mc} = \frac{1}{n'}R^{2/3}\left(S + \frac{F_{mt}}{A\gamma}\right)^{1/2} \qquad (5.33)$$

Where n' is Mannings's n corrected using the LSCS method.

5.7.6. Methodology for applying the momentum transfer equation

1. Calculate the floodplain velocity from Equation 5.8
2. Calculate the floodplain discharge Qu from Equation 5.7
3. Calculate a first approximation to the main channel velocity using Manning's Equation corrected using the LSCS method (See Chapter 2).
4. Iterate to find a solution for U_{mc}

Results of application of method employing original assumptions and taking velocity adjustment factor ε equal to unity.

In the rough channel tests LORW and HORW the total channel discharge is underpredicted by 1% and 10% at a β value of 1.5 but the main channel flow over predicted by 25% and 35% in the low and high overbank cases respectively. At a β value of 2.7, the main channel discharge is overpredicted by 12% in the high overbank case and 9% in the low overbank case. The total discharge is underpredicted by 4% and 10% respectively. These values are an improvement and suggest that problems are caused by an underprediction of the rate of floodplain flow.

In the smooth cases however the low overbank case shows an underprediction of total channel flow of 1% with a β value of 1.5. The main channel flow is underpredicted by 30%. In the high overbank case the mechanism gives a negative velocity for the flow in the main channel and the flow mechanism must be considered inappropriate.

The predictions for total flow are a significant improvement on those made by the James and Wark method applied to rough floodplains. However whilst they are better, the division between main channel and floodplain flow is still incorrect, appearing to vary with channel roughness. Further terms are required to model this interaction. Calibration against a large data set is likely to further improve the predictive capacity. These developments are regrettably beyond the scope of the thesis.

This method when appropriately adjusted will present engineers with a viable alternative to the James and Wark method for the prediction of floodplain and main channel flows. These predictions will be useful for design of flood prevention schemes and to provide a main channel discharge to be used in the calculation of sediment transport in two stage channels. In addition to improvements in modelling of main channel flow in rivers with rough floodplains it has advantages over James and Wark in being relatively easy to understand and apply.

The results given by the model give significantly less detail than would be obtained by a fully three-dimensional model however in many design scenarios this level of information is sufficient. To obtain noticeably more accurate results from a three-dimensional model a vast amount of input data is required. Where this level of accuracy is required, the momentum exchange model should provide a useful check for reasonableness.

5.8. Conclusions

The following conclusions may be derived from this chapter.
The flow mechanisms observed in the Series B tests are consistent with those in the Series C high overbank smooth case. In the other cases however the effects of secondary circulation at the crossover, probably cause greater mixing with the overbank flow than suggested by the previous tests.
The mechanisms of upstream flow seen in the bankfull and overbank rough cases are also not observed in the Series B channel.

1. F* continues to increase as relative floodplain roughness is increased. At high floodplain roughness Zone 2 should be further subdivided to account for the difference in velocity between the floodplain and upper main channel flow velocities.
2. A mobile boundary has little effect on conveyance at low floodplain depths but may increase conveyance at higher depths.
3. The James and Wark method severely under estimates the flow in zones 1 and 2 at high floodplain roughness. This is largely due to inadequacies in formula for the prediction of flow below the bankfull level in rivers with high flood plain roughness and the significant variation in velocity between flow on the floodplain and in zone 2 above the main channel.
4. A new method is proposed for rough floodplains, based on momentum gained and lost by the main channel due to floodplain exchange over half a wavelength. It relies on estimation of the Manning's n value of the bankfull channel and the floodplain and the dimensions of the channel. A factor is introduced to account for the ratio of velocity of flow entering the floodplain in comparison to average flow in the main channel. The total discharge is predicted within 10% of the actual value however the main channel discharges are significantly too high (25% - 35%) for a rough floodplain and too low (30%) for a smooth

floodplain. The method may be worth pursuing due to the simplicity of application and the absence of many empirical constants. Further testing is required for confirmation.

6. Mixed grain sediment transport in meandering river channels with overbank flow.

6.1. Introduction

The rate of bedload sediment transport is an important factor in the design of river engineering schemes and their environmental impact. Prediction of the rate of sediment transport however is notoriously difficult. An examination of Brownlie's investigation of a selection of sediment transport Figure 2.8, shows that the best sediment transport formula cannot reliably predict transport rates within a factor of 2. We can also see that there is a significant discrepancy between results from formulae applied to natural rivers and those applied to flumes. Typically, the formulae underpredict river discharge compared to flume discharge.

The problem of predicting sediment transport in a stream has traditionally been approached by trying to find a single equation to apply to the average channel properties, such as slope, depth, velocity etc. This method has the advantage of relative simplicity, however it does not account for cross channel variability.
An alternative approach is to divide the problem into two stages. The first stage is the two-dimensional problem of predicting sediment movement given distribution of grain size, flow depth, shear velocity, main stream velocity and channel roughness. The second stage is the three-dimensional problem of applying this formula to natural streams with variation in depth, velocity and sediment size distribution across the section and over the meander wavelength. This approach may be extended to a fully three-dimensional CFD model. Improvements in the estimation of sediment transport in river channels will either lie in a better two dimensional model, one for instance that accounts for changes in bed form, flow temperature and mixed grain sizes or a three-dimensional model which operates on a minimum of data.

Significant work has yet to be done to find a solution to the problem of predicting sediment transport in two dimensional flow situations, such as laboratory flumes. This important work is regrettably beyond the scope of the current project. Further investigation into the transport and behaviour of mixed grain sediments would be particularly valuable. The purpose of this chapter therefore is to explore the scope for improving the application of 2D sediment transport formulae to meandering river channels at inbank and overbank flow conditions.

6.2. The variables that affect sediment transport.

Following the approach favoured in the introduction, two systems of variables are considered. Firstly, the variables that would affect sediment transport locally and then the variables that would affect these variables. Thus, whether variables in the stream are dependent or independent depends on the scale under consideration.

System 1 - Local Sediment Transport

In the literature review it was made clear that flow resistance and bed load transport are interrelated phenomena in sand bed channels. In a two dimensional system the sediment transport rate q_s is a function of: Water surface slope, S, flow rate, q and the sediment properties (bed and transported) size, size distribution, density and shape.

Fall velocity included in many sediment transport formulae is a function of the above sediment properties as well as temperature of flow. From these parameters, it is possible to use a stage discharge predictor such as Brownlie 1981 to calculated depth h and a sediment transport formula such as Ackers White to obtain sediment transport rate q_s.

Algorithms designed to find the equilibrium values have been formulated for example by Bennet (1995) and require iteration to obtain a solution.

System 2 - Flow and bed conditions in a vertical in a river cross section

A vertical section in a river system is a function of slope, gravity, water temperature and flow resistance local to the section and the shear from neighbouring sections. The calculation of flow resistance is highly complex involving factors such as: flow regime, - sediment properties, sediment transport, bed geometry, porosity of bank, in channel / out of channel vegetation - time of year, floodplain width and topography, water table height and others.

6.3. The calculation of local bedload sediment transport

The rest of this chapter assumes an accurate (10%) method of calculating the main channel discharge in a two-stage channel with rough floodplains. Given this information, methods for accounting for cross channel changes in the variables of sediment transport are investigated.

Bedload sediment transport is strongly related to shear velocity. In order to focus our investigation we will now consider a selection of methods involved in the calculation of shear velocity.

6.3.1. Calculation of u and u^*_c by the velocity profile method*

Clearly, in the majority of design cases it is not possible, in terms of cost, time and technical difficulty, to obtain accurate values of near bed velocities and roughness values. Therefore, it is not practical to design a method, which requires direct measurement of these values to obtain a value of bed shear velocity. However, an investigator can obtain these measurements at the required river stages under laboratory conditions. The interpretation of these results however is not straightforward.

It is accepted that in the bottom 10-15% of the flow depth the velocity distribution is described by a logarithmic profile. The slope of the profile is given by u*/k, where k is the von Karman constant for turbulent flow, normally evaluated at 0.41. There has been discussion as to the universal application of this value, particularly in relation to suspended sediment flows. Colebrook (1939) argues that the value is consistent; This position is adopted by the current text (further discussion may be found in standard texts).

Deviation from the logarithmic profile often occurs in higher regions of flow due to form roughness and secondary currents.

Having accepted that we can obtain the grain shear velocity, U*', in this fashion reference to Figure 6.1, showing the velocity profiles obtained over a bed form (Raudkivi 1963), reveals a serious problem. Whilst we may have obtained the correct value of U*' over the bed at a certain time the value is strongly dependant on the position along the dune at which the measurements were taken. The average value of U*' is considered to be most appropriate for calculation of sediment transport. Therefore, this data will only give us an appropriate value over a short range of positions.

A related problem is that the dunes move slowly down the channel. Each point velocity reading takes a finite length of time (60s in our case) and thus the readings in a vertical will be over slightly different areas of the dune. As the dunes are long and flat and move comparatively slowly, this is likely to be a problem only if readings take place over an avalanche face.

Assuming that the inner law applies in all circumstances, this should not affect the use of the profile to obtain the correct bed level. The bed level may be obtained by plotting the values of u and z within the logarithmic zone arithmetically and adjusting z so that a logarithmic path fits through u = 0. In cases where the bed is significantly lower than that predicted there may be no appropriate data points for analysis and errors may arise due to deviations from the logarithmic profile.

If a correct bed level has been found and a single velocity is in the logarithmic zone, additional velocity points may be added using the logarithmic velocity profile assumption. If no points are present in the defined region, it may be reasonable to extend the region higher into the flow. This is justified in regions of shallow flow, as the grain roughness is likely to dominate the flow behaviour. In such regions, this method can be used to obtain a value of the average velocity for use in such formulae that require it.

6.3.2. Calculation of u* and u^*_c using methods based on depth averaged values

The shear velocity, U*, is given by the expression below: it is a convenient way of describing the shear resistance to river flow.

$$u* = \left(\frac{\tau}{\rho}\right)^{1/2} \qquad (6.1)$$

The total shear resistance is given by $\tau=\rho gRS$ and thus $u* = (gRS)^{0.5}$ or $u* = (gDS)^{0.5}$ for a wide channel. In alluvial rivers there are a number of processes contributing to the resistance, including grain resistance, bedform resistance and secondary flow effects. As the value of u* accounted for by grain roughness, u*' is considered to be the fraction of u* relevant to sediment transport rate, finding the correct allocation of resistance to the various processes is clearly important. This problem has been approached in several ways

using as variables: bed roughness k_s, velocity u, slope S, and depth D. Examples of each method are given below including those used in the sediment transport formulae used in this study.

Obtaining values for the grain shear velocity u*' in a stable channel

In wide channels with flat beds in which there are no secondary currents u*' = u*. Substituting a resistance equation such as Manning's equation for the slope gives $U^* = Ung^{1/2} R^{1/6}$ where n is the main channel resistance. n may be related to the grain roughness by a formula relating Manning's n to grain size, such as Strickler's (1923) formula, $n = d^{1/6}/21.1$, to give, in this case, the Manning Strickler formula

$$\frac{U}{U*} = 6.74\left(\frac{R}{d}\right)^{1/6} \qquad (6.2)$$

Other similar expressions may be derived using alternative resistance formulae.

Einstein u*' = f(k_s, u, s)

The forms of flow resistance equation given by Chezy and Manning for fixed bed flumes will clearly require modification or replacement for use in alluvial rivers in which bed forms and secondary currents occur and u*'<u*. An early example of modification of the Manning Strickler equation was proposed by Einstein and Barbarossa (1952) for the lower regime. They introduced the concept of dividing resistance into grain resistance and form resistance as two additive quantities. Thus S= S'+S'' or R= R' +R'' or τ= τ'+τ''. Writing the Manning Strickler equation in terms of R' and U'* they obtained

$$\frac{U}{U*'} = 7.66\left(\frac{R'}{d_{65}}\right)^{1/6} \qquad (6.3)$$

where $U*' = (gR'S)^{1/2}$.

Similar formulations were proposed for cases which were not fully rough using appropriate formulae. Thus it is assumed that the value of U'* appropriate to grains is a function of the grain size, the average velocity, and the slope. It may be written in the same form as the relationship for a fixed bed channel.

Ackers White and van Rijn, u*' = f(k_s, u, D)

An alternative approach is found in turbulent flow theory. The shear stress between turbulent flow layers is given by equation (2.22) substituting equation (2.21) and integrating gives

$$\frac{u}{u*'} = \frac{1}{\kappa}\ln z + C \qquad (6.4)$$

Einstein (1950) integrated this equation over the flow depth to obtain

$$\frac{\bar{u}}{u*'} = 5.75\log\left(\frac{12.3D}{\Delta}\right) \qquad (6.5)$$

Where $\overline{U}$ = average velocity and $\Delta = k_s = d_{65}$ for a flat bed.

The Ackers White formula uses an equation for u*' of similar form to that of Einstein's 1950 formula. The authors assume that the relationship between effective shear velocity and depth averaged velocity is independent of the bedform stage. Hence, flow over a bed with high form roughness would have an equivalent velocity profile to slower flow over a plain granular surface at rest, if the grain roughness and depth averaged velocity were the same in each case. The term $12.3d/\Delta$ is replaced by the expression $\alpha d/D$ in the Ackers White formula. $d = d_{35}$ is adopted for graded sediments and a value of $\alpha = 10$ despite appreciable scatter, on the grounds of limited effect on the sediment transport relationship. Thus in the Ackers White formula

$$\frac{\overline{u}}{u*'} = 5.66\log\left(\frac{10D}{d_{35}}\right) \qquad (6.6)$$

van Rijn gives his value of U*' as

$$u*' = \frac{g^{0.5}\overline{u}}{C'} \qquad (6.7)$$

Where C', the Chezy coefficient related to grains is given by

$$C' = 18\log\left(\frac{12D}{k_s}\right) \qquad (6.8)$$

Substituting $k_s = 3d_{90}$ in equation 6.8 and rearranging gives

$$\frac{u}{u'*} = 5.75\log\left(\frac{12D}{3d_{90}}\right), \qquad (6.9)$$

which is very similar to the Ackers White relationship. From empirical data, van Rijn gives k_s as $3d_{90}$. In order to justify this relationship in the presence of bed forms, van Rijn makes reference an experiment performed by Raudkivi (see Figure 6.1). Raudkivi replaced bedforms in a channel with an identical form in galvanised metal sheet and measured the form and surface shear stress along the dune structure. Normal pressures were measured using taps and surface stresses using Pitot tubes.

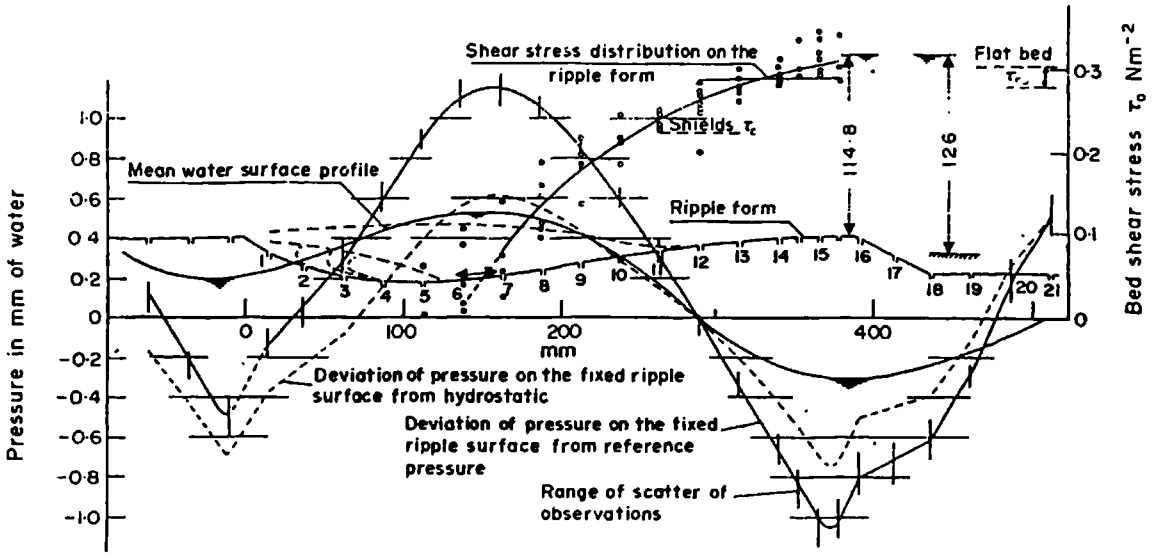

Figure 6.1 Distribution of flow characteristics along a bed form (after Raudkivi 1963)

Application of van Rijn's expression for the surface Chezy coefficient gives a similar value to that derived during this experiment and is thus considered satisfactory.

Engelund and Hansen, $u^{*'} = f(k_s, D, S)$

Engelund defined the dimensionless total shear stress on the bed as

$$\tau^* = \frac{\gamma DS}{(\gamma_s - \gamma)d} \qquad (6.10)$$

and the dimensionless grain shear as

$$\tau'^* = \frac{\gamma D'S}{(\gamma_s - \gamma)d} \qquad (6.11)$$

Plotting τ^* against $\tau^{*'}$ he obtained a relationship for the lower regime ($\tau^{*'}<0.55$) given by

$$\tau^{*'}=0.06+0.4\tau^{*2} \qquad (6.12)$$

taking $u^* = (gDS)^{0.5}$ and $u^{*'} = (gD'S)^{0.5}$ this can be rearranged to give

$$u'^{*2} = 0.06Dg\frac{(\gamma_s - \gamma)}{\gamma} + 0.4u^{*4} \qquad (6.13)$$

where $u^{*'}$ is a function of the water depth, the bed roughness and the slope.

Summary of methods

Author	Variables	Main assumptions
Einstein	k_s, U, S	Divided hydraulic radius, Manning's equation, Strickler's relationship
Ackers White	k_s,U,D	Log law velocity profile, Similarity in relationship between u and u* for same u over rough and smooth beds
van Rijn	k_s,U,D	Log law velocity profile, The obtained grain shear velocity is an acceptable time average
Engelund and Hansen	k_s, D, S	Engelund's "universal" relationship between dimensionless grain shear stress and total shear stress

Table 6.1 Summary of u' calculation methods*

Several methods have been presented each employing different variables and assumptions in the calculation. As all current sediment transport formulas are empirical, assumptions made in the particular form of u*' chosen by the authors are likely to have some effect on the calibration coefficient. Consequently changes in the way in which u*' is calculated for a particular equation are likely to affect its performance. A systematic error and less scatter could however would point to an improved approximation to u*'.

The advantage of using depth rather than slope is that the slope is very hard to measure in the field and laboratory whereas velocity and depth are more accessible. The use of the actual depth has been criticised by Bennet (1995) on the grounds of being difficult to measure and a function of the sediment transport rate and bed forms. However, empirical adjustments still seem to make this approach the most satisfactory.

6.4. Advanced approaches to applying sediment transport formulae in natural rivers

The traditional method of calculating sediment transport in a stream is to apply the averaged channel properties to a relevant formula.

Seed (1996) performed an investigation into the calculation of sediment transport, on a section by section basis, for inbank channels. This work has been subsequently extended by Bettess, Bona, Morris and Seed (1997) to overbank flow. Due to problems obtaining suitable field measurements, both of these investigations are essentially theoretical. Seed (1996) uses the lateral distribution method, derived by Knight and Shiono (1991) for straight compound channels, to predict the velocity at vertical sections across a channel. He compares the rates of sediment transport calculated using two different methods. In the first method the sediment transport rate Q'_{sBULK} is obtained by calculation from the bulk variables in the traditional manner. In the second the sediment transport rate Q'_{sLDM} is obtained by summing the transport rates in sections across the flume. The rate for each section is calculated from the section depth and the velocity predicted by the LDM. These values may be related by the following formulae

$Q_{sBULK} = Q_{sLDM}\ Q_s'$

Where Q_s' is termed the flux ratio. In his numerical experiments Seed found the flux ratio to be dependent on two dimensionless quantities, the relative shear velocity

$\beta = U^*/U^*_c$ and the shape factor defined by the equation.

$$S_f = \frac{1\sum h^2 dy}{wD^2} \qquad (6.14)$$

where D = hydraulic mean depth, W = water surface width and h = local flow depth.

The shape factor is effectively a measure of how far the channel deviates from a rectangular channel in which bulk and LDM methods give the same result.

Using the Ackers White formulae, he obtained the chart shown in Figure 6.2 relating flux ratio to bed shape factor for a range of values of relative shear velocity.

The use of section averaged values was found to underpredict sediment transport at low flow and over predict at high flow levels. The affect was found to increase with bed shape irregularity.

Seed acknowledges the need for further testing of the method and the need for investigation of the effect of cross channel variation in grain size and bed roughness.

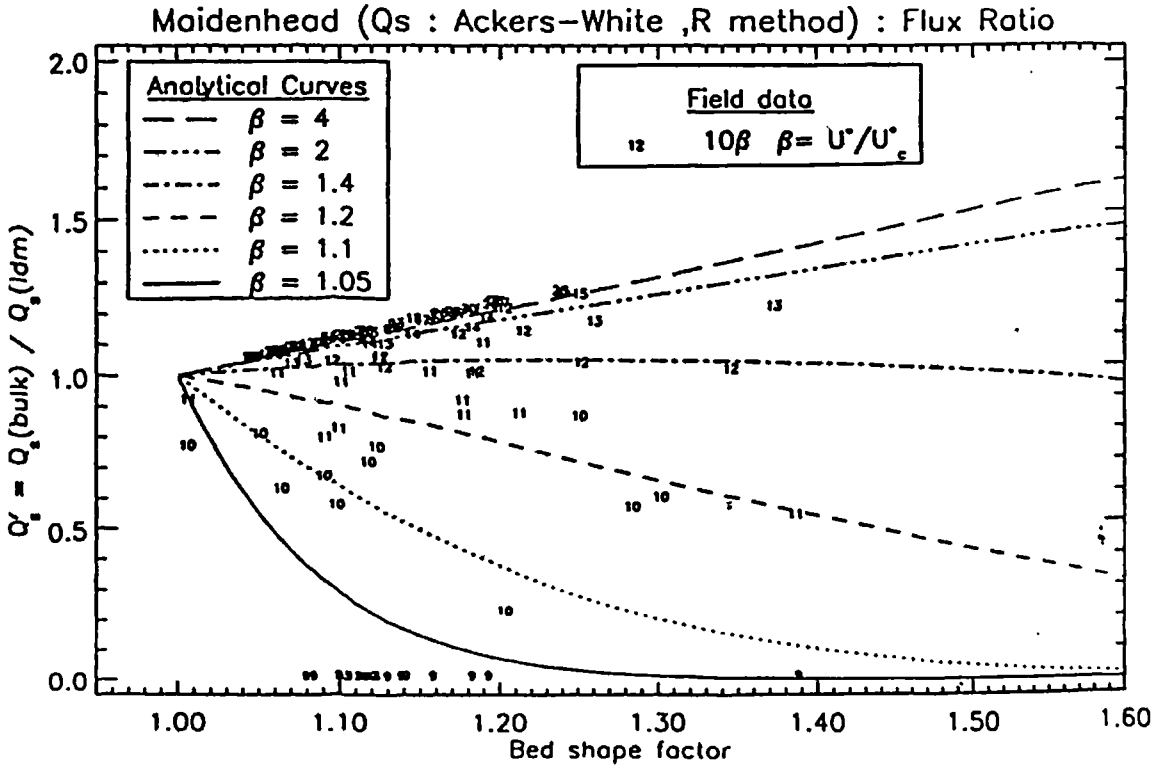

Figure 6.2 Variation in sediment transport rate with shape factor

Bettess, Bona, Morris and Seed (1997) attempted to extend Seed (1996) to rivers with floodplains. They state the problem previously expounded in the literature review of the discontinuity in channel properties above the floodplain level. Four methods are mentioned for use in calculating the conveyance of a two stage channel: Firstly the application of a flow resistance formula, such as Manning. This is rejected on the basis of the discontinuity in depth. Secondly the use of divided channel methods; these have been found

unsatisfactory, as they do not account for interaction mechanisms between different flow areas. Thirdly the use of Ackers coherence method which is good for obtaining the total discharge of a channel but unable to give zonal prediction and fourth the LDM method used in Seed (1996). The LDM method is chosen as the only suitable method for application to zonal areas. The Ackers coherence method and the LDM method are both designed for straight compound channel and are therefore likely to be of limited use in estimating the behaviour of meandering compound channels.

Bettess *et al.* (1997) note that in Ackers theoretical work on sediment transport during flooding he proposed a significant reduction in the sediment transport concentration in the main channel during overbank flows. This was due to the interaction of floodplain flows. Their application of the lateral distribution method suggests that the sediment transport is not overly affected by the transition from inbank to overbank flows. Rather than decrease, the sediment transport rate is approximately proportional to the channel discharge. This is explained by the theory that floodplain interaction is only important at the higher flow levels near the channel banks and that flow in the centre and bed of the main channel is largely unaffected. Despite several attempts Bettess et al. were unable to develop a similar simple relationship to that found by Seed for inbank channel.

It is important to note that in both the studies above, the relationships observed were between two numerical models. The observed results are therefore only as good as the lateral distribution method. Fundamentally, the LDM is only applicable to straight channels and requires fixing of coefficients in order to work.

6.5. Empirical data relating to two stage meandering channels

Knight (1992) obtained bed shear stress data from the natural 1.37 and 2.04 sinuosity meandering two stage channels in the series B test program. His results illustrated in Figure 2.16 show that the average bed shear stress is highest at the apex and lowest at the cross over section. The bed shear at the apex is concentrated at the inner bank for inbank and overbank flows. This seems surprising as the bed agrades in this region. If sediment transport formulae were applied to the channel the sediment transport at the apex would be higher than that at the crossover. This cannot be the case in a stable channel and thus an explanation is required. It does however suggest that the section at which the rate of sediment transport down the stream is controlled, is the crossover section.

Knight also gives the lateral variation in shear stress for cross sections 0 to 6. The reader is reminded that the sections show the upstream section at the bottom of the page and the down stream section at the top, contrary to the majority of diagrams in this thesis.

The author concludes that firstly a method for applying sediment transport formulae to the complex scenario of compound meandering flow has yet to be found, and secondly, the effects of lateral variation in channel properties require further investigation. For a method to be useful in design it should be sufficiently simple for practitioners to be confident of its behaviour and range of accuracy. It should also require as small an amount of data collection as possible. It must also be possible to collect the required data during normal flow conditions.

6.6. Observations of sediment transport in the Series C channel

The following sections present the sediment transport data collected in the flume.

6.6.1. Comparison of the relative overall rates of transport

The overall rates of transport in the four tests considered in this Chapter are given in Table 4.1. The rates in both smooth and rough low over bank tests are significantly lower than those at bankfull. This reflects the lower main channel discharge resulting from floodplain interference.

As floodplain depth increases the smooth floodplain test at the high, overbank level shows rates of sediment transport exceeding those at bankfull. The high overbank rough test however shows a relatively small increase in transport rate compared to the low overbank rough test.

6.6.2. Observations of variation in sediment transport properties across the width at apex and inflection point

The purpose of this section is to present the primary observations in the tests in the light of previous thought. In the set of diagrams the isovel plots from apex and crossover for the tests of interest and the relevant sets of lateral sediment transport rates are placed next to each other for easy comparison. The method of collecting local sediment samples is described in Chapter 3. It is repeated here that all methods investigated have certain problems, a common one being that a small quantity of sediment is often collected when the sampler is placed on the bed. For this reason samples below 20g should not be considered to give an accurate reading of the sample rate but simply to suggest that it was very low.

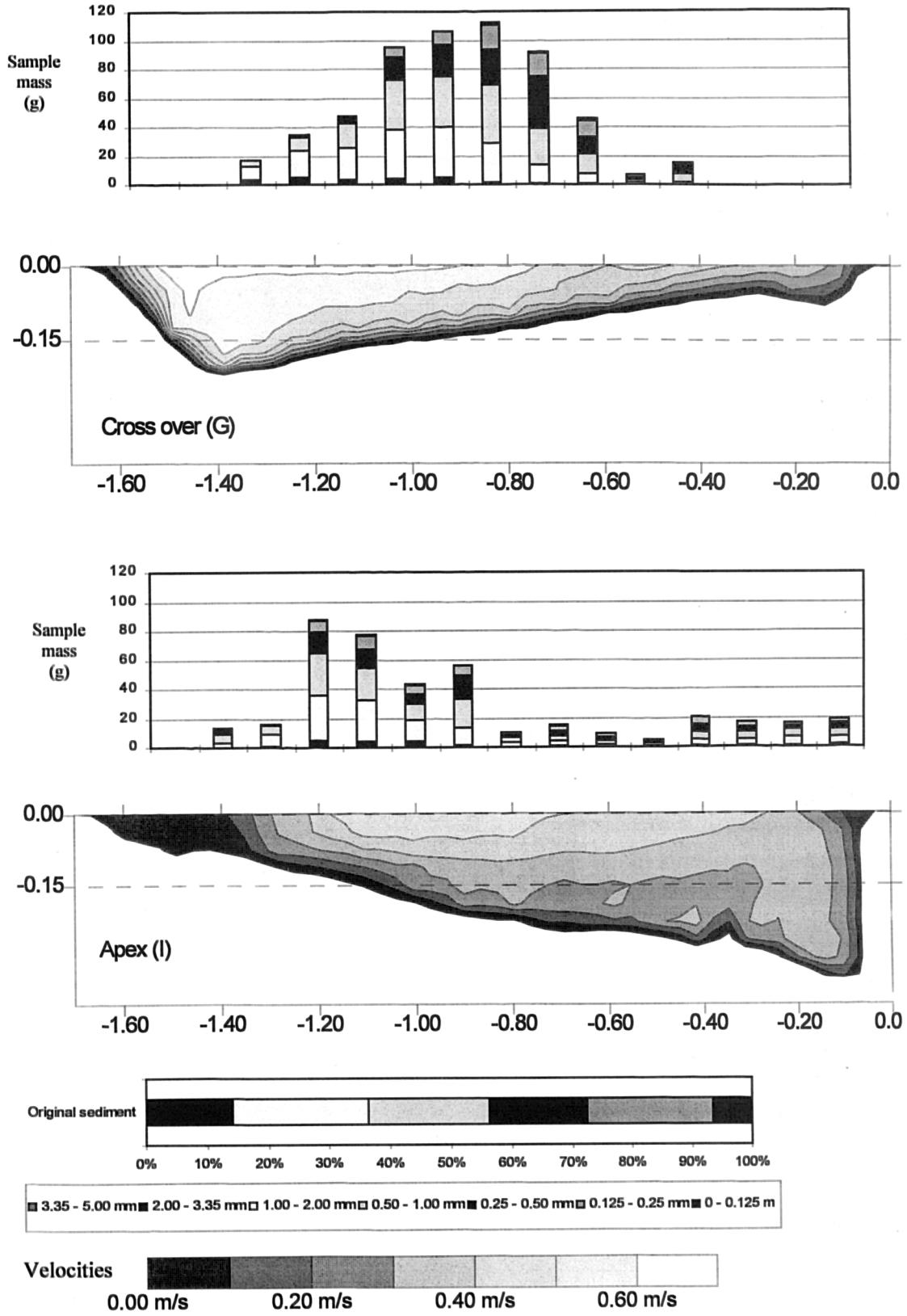

Figure 6.3 Bankfull mobile: Variation in local sediment transport rates across a section in comparison with the variation in *depth and* velocity

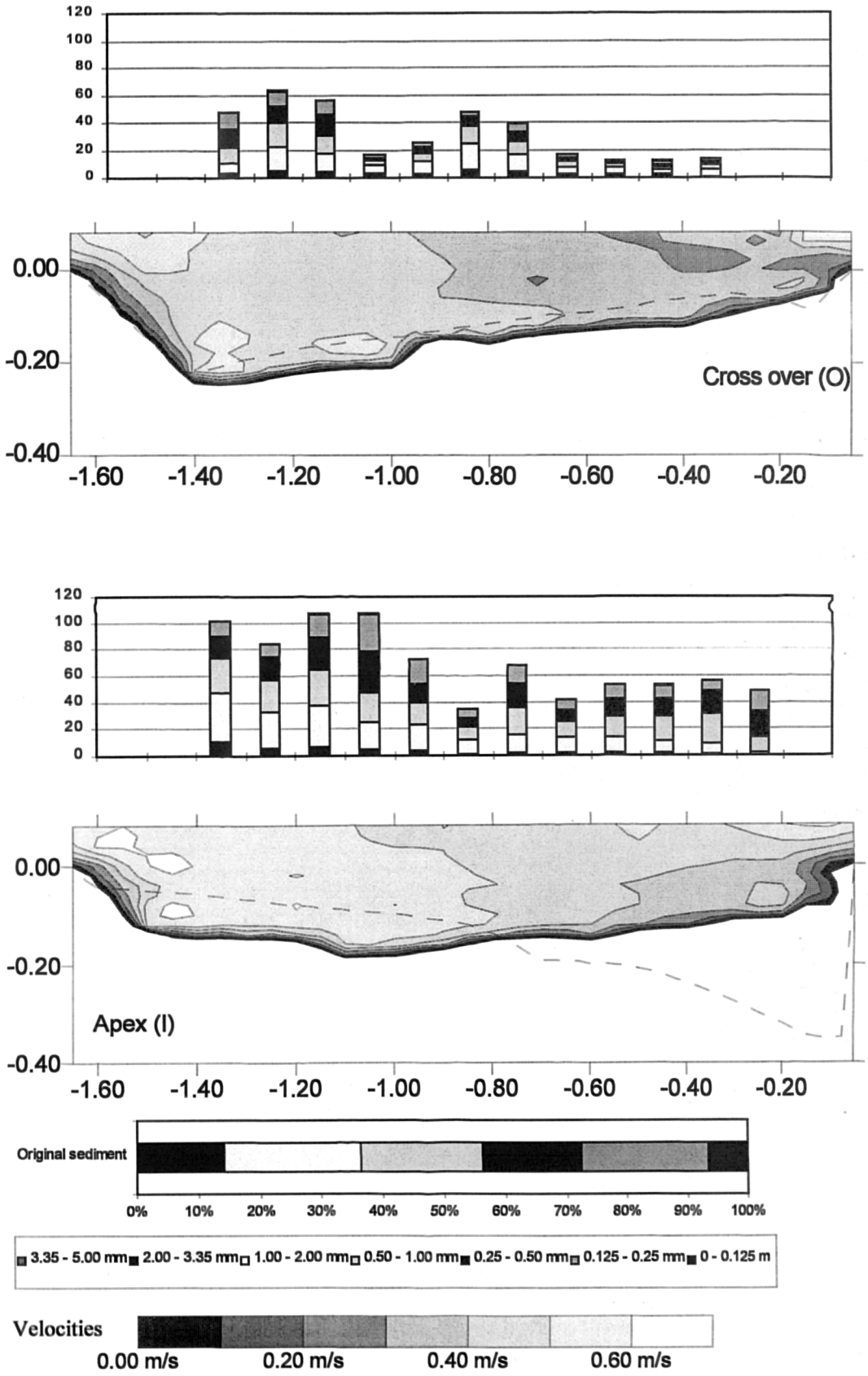

Figure 6.4 Low overbank rough floodplain: Variation in local sediment transport rates across a section in comparison with the variation in velocity

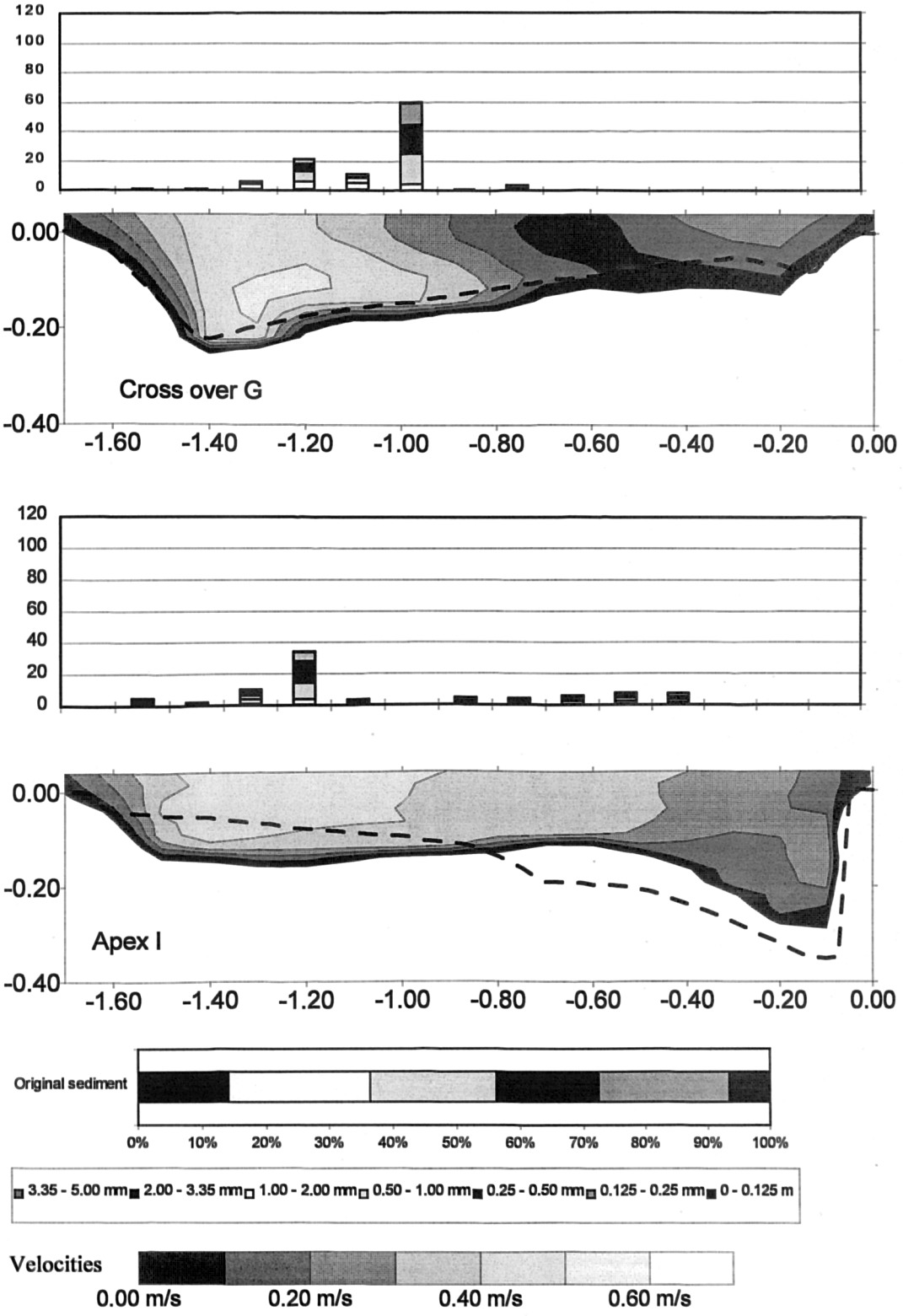

Figure 6.5 High overbank rough floodplain: Variation in local sediment transport rates across a section in comparison with the variation in velocity

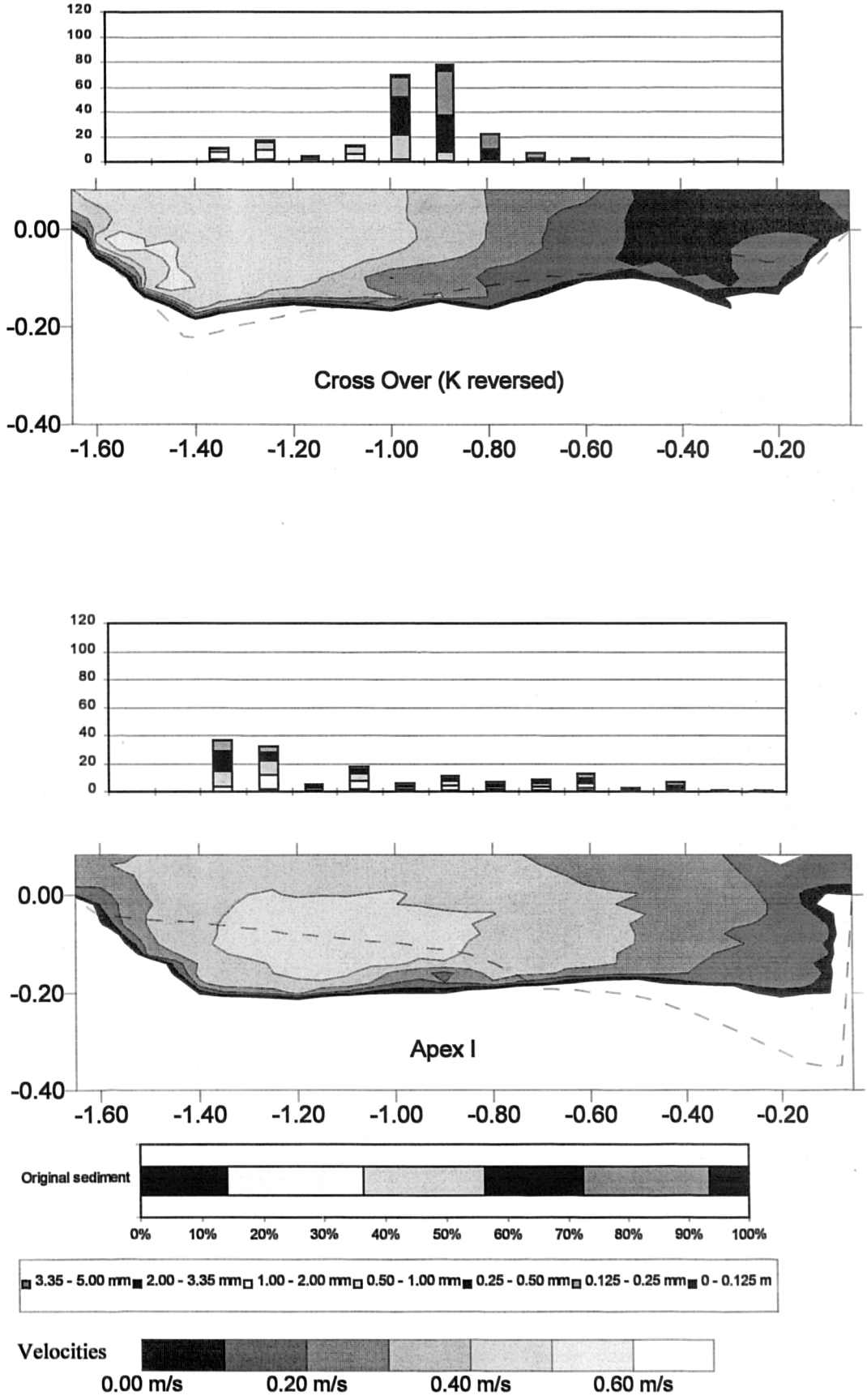

Figure 6.6 High overbank smooth floodplain: Variation in local sediment transport rates across a section in comparison with the variation in velocity

6.7. Variation of channel properties across a channel section

In a meandering stream, depth, velocity and grain size distributions are observed to vary significantly across the channel width and along the wavelength. The results obtained in the Series C experiments confirm this. The following section examines the distribution of these variables associated with bankfull flow and the changes that occur at overbank flows. As depth, grain size and velocity are closely interrelated none may be taken as an independent variable. However, in a smooth channel with a plane bed, such as the screeded main channel used as a starting point for the Series C experiments, velocity variation due to the meandering form is responsible for initial changes in channel form and hence velocity is approached first.

Variation in velocity

A mass of fluid continues along a straight path under inertia until a force is applied to change its direction. In a meandering channel, this is the riverbank. The fastest flow region in a meandering channel is observed at the downstream bank of a river until it crosses the channel at a bend to meet the outside bank. It is carried around the outside of the bend and remains at the lower bank until the next bend where this process occurs again. This is illustrated in Figure 2.10. The effect of overbank flow on this velocity pattern is explored in Chapter 5. Two important features are noted. Firstly the reduction in main channel flow, most marked at low floodplain flows due to interaction losses, and secondly the movement of the main velocity filament to the downstream side of the channel.

Variation in depth

Where the grain shear stress due to channel roughness, flow depth and local velocity are above the critical shear stress required for sediment movement the channel will scour. Similarly if the grain shear is less than the critical shear then aggradation will occur. These processes change the cross-section shape. At bankfull flow conditions the bedform is defined by the effects of flow around a bend described above. The faster flow is concentrated on the outside of the bend causing a scour section. The cross sectional slope observed in the apex gradually degrades in the section of river between one apex and the next. The formation of secondary currents at the apex also carries sediment towards the inner bank. This has often been regarded as the primary cause of channel formation. However, researchers such as Yalin (1982) or Hooke (1987) have suggested the theoretical role of secondary currents is exaggerated due to the increased strength of secondary currents in model rivers with small aspect ratios.

The most striking effect of overbank flow on the inbank bed structure is the scour at the inside of the apex section and in some cases deposition at the outside.

The crossover is largely unaffected by the transition from inbank to overbank flow. The most noticeable feature being the erosion of a small proportion of the fines collected at the upstream side of the bed during overbank flow.

At overbank flow the interaction slows the flow and the sediment transported through the apex section is reduced. As the supply to the high shear zone at the apex is cut, the apex erodes until the shear stress on the apex bed is reduced below the critical level.

Grain Sorting - Bedform roughness and material available for transport

The effect of mixed grain sediment on sediment transport and bed morphology is explored in section 0 of the literature review. Under the bankfull conditions that formed the basis for each subsequent test, the bed is preferentially scoured. The finer grains on regions of the bed experiencing fast flow are carried from the original bed matrix and eventually deposited in the slow flow regions in the lee of the apex, forming the point bar. As the scour becomes deeper, the material available for transportation becomes coarser. As shear stress decreases with depth, an equilibrium position is finally reached.

In regions where the bed is below the screeded level the surface is armoured with large grains. In regions where the bed is above the screeded level the bed consists of smaller grains. This system is evident in the bankfull crossover. The roughness increases with increasing velocity and depth.

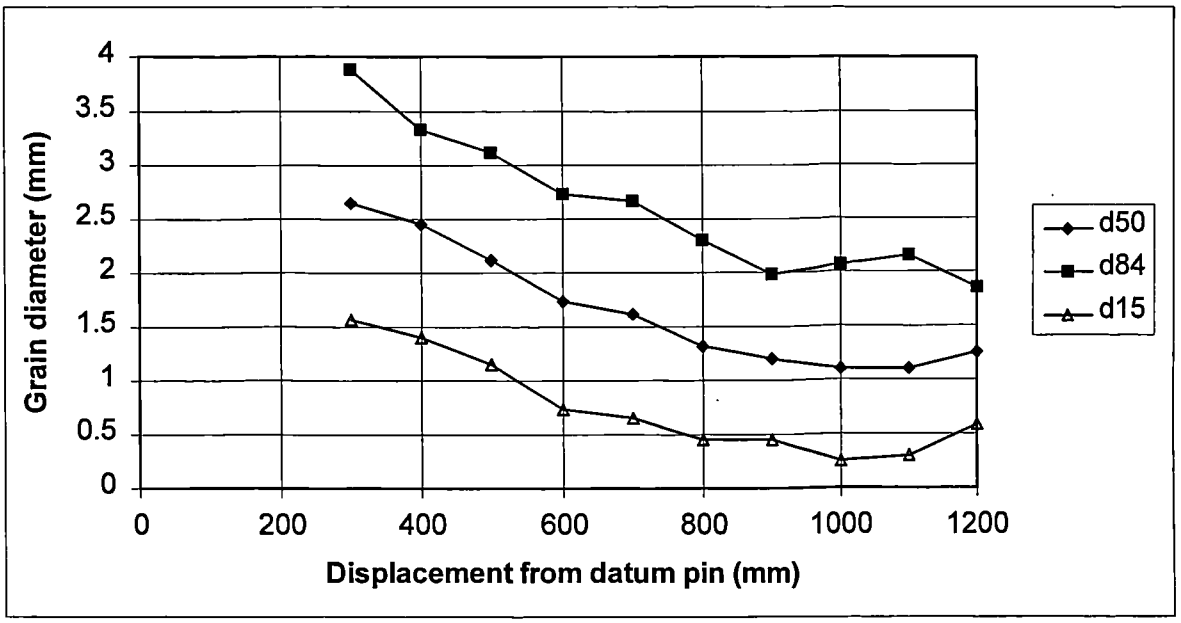

Figure 6.7 Lateral variation in grain size at crossover section (Datum pin at 0 on downstream bank)

An important issue in the variation of sediment across a section is the variation in bedform size, as bedforms are integral in the calculation of the rate of sediment transport Bennet (1995), van Rijn (1984). Figures 2.7 and 2.8 in the literature review show prediction of bedform dimensions given grain size, depth and velocity. In the Series C channel the sediment was observed to move in dunes of mixed grain size down the channel centre line. The fastest flow regions at the downstream side of the channel were populated by coarse grains forming a stationary flat bed on the upper side of the channel fine grains formed an immobile rippled bed. It is documented by Chien (1995), that mixed grain sediment suppresses the formation of bedforms. The bedforms observed on the channel were significantly smaller than those observed in single size sediment of a similar grain size.

Dashed lines show the screeded level and the bankfull level on figures 6.3 to 6.6. The effect of overbank flow on the bed depth is evident from these diagrams. The channel armouring in the deep section is seen to

prevent further degradation in all tests other than the overbank smooth test in which very fast flows were recorded. Erosion does take place however in the areas of fine sediment possibly due to flow entering from the floodplain.

Variation in slope

The variations in channel slope along a meandering channel have been explored in Chapter 5. It is inappropriate to use the water surface slope at a section where due to changes in macro bedform and hence flow velocity, the water surface slope is negative and thus the energy slope should be used. This requirement requires significantly more work from the modeller and thus formulae which require slope calculations are significantly more arduous. The charts in Figure 4.1 show that the slope characteristics in flow with roughened floodplains remain very similar to the inbank flows.

6.7.1. Comparison between observed sediment transport in the Series C channel and the Series B shear stress results.

Figure 6.3 shows that the bulk of sediment movement in the apex section occurred at the inside of the bend, which is what would be expected from Knights measurements of bed shear. The area of highest bed shear crosses the channel in sections 4 and 5 residing at the downstream side of the channel in section 6. In the mobile bed channel the main band of sediment transport was observed to move toward the centre of the channel at the cross over section where the sediment is observed to move in a fairly narrow band down the centre of the channel. Considering the channel overhead photograph given in Figure 4.4 we can see that after the apex the sediment on the inside of the bend is very fine and forms ripples. This region gets wider with progression downstream. The collection of fine sediment is an indication of the very low flows observed in this region and the consequent negligible rates of sediment transport. Knights data shows that the shear stress decreases at the inside of the bend as the flow moves downstream and the maximum moves toward the downstream bank (sections 4, 5 and 6). This is akin to the observations made in the Series C. The sediment transport however is concentrated in the centre of the channel. Observation of the channel at this point shows that where the channel has eroded on the outside of the stream, the bed has armoured and is made up of the largest grain fraction. This is reflected in the composition of the sediment in motion. Visual observation showed very occasional movement of large grains rolling a short distance down the channel.

An interesting morphological question, arising from Knight's data, is why the point bar forms at the inside of the apex bend when the shear stress is so high. The following explanation is proposed. At the apex section, the vast majority of sediment moving down the channel is observed to move as a sheet over the point bar at the inside of the bend, encouraged toward the inside by the secondary currents. This is illustrated by the local measurements of sediment transport. See Figure 6.3. The deep outer section contains a collection of large grains and very little transport is observed.

The crossover shear stress is considerably lower than that recorded at the apex. The maintenance of the apex form may be explained not by low shear stress but because the high shear stress at the inside of the apex is used to transport sediment rather than to erode the bed.
Thus from a sedimentological point of view the apex relies on a constant supply of sediment from the cross over region to maintain its shape.

6.7.2. Overbank flow

The observations presented by Knight for overbank flow were all recorded with smooth floodplains. Given previous observations on the differences between rough and smooth floodplains it is likely that the rough floodplain tests will display a shear stress distribution closest to that observed at bankfull.
It is noticeable from Knights observations average channel shear stress during overbank flow on smooth floodplains (Figure 2.16) that at low overbank depths, the average channel shear stress initially falls significantly due to the reduction in flow velocity caused by floodplain interaction. The basic form remains similar however with a high spot at the apex. As the flow depth increases above bankfull the shear stress rises from the initial low. The sediment transport rate in the overbank series C test support this observation in both the rough and smooth tests.
The flattening of the apex section may now be explained. The reduction in secondary current toward the inside of the bend at the channel bottom reduces the flow of sediment toward the inside of the bend. Significant scour will also occur due to the reduction of sediment transport rate at the crossover section.

6.7.3. Summary of observations

The observations above suggest that in order to calculate the rate of sediment transport travelling down the channel we should concentrate on the crossover section at both inbank and overbank flows. This is the critical section and is also shown to exhibit minor variations in shape during overbank flows.
Confirming field observations such as those from tests performed by Zhou and Zou (1996) the bulk of sediment (70%) is found to move in a narrow band of taking up approximately 30% of the bed width in the bankfull case. This band of flow is characterised by containing a mixture of sediment sizes and lies between a deep fast flowing region of flow over a coarse bed and a shallow slow flowing region over a fine grained bed. All grains are seen to move and the bed is relatively smooth. The bedform type is long flat dunes.
In the overbank rough cases this band narrows significantly to approximately 7% in the case of the low overbank rough test and 15 % in the case of the high overbank rough. The transport rate within the band is also reduced significantly, however this appears to be a secondary feature. Due to the absence of local transport data on the low overbank smooth case it is not possible to comment on the active width. However in the high overbank smooth case there is significant transport over the entire width of the flow. This is probably due to the high velocities being sufficiently strong to disturb the armour layer and the lack of protection from the point bar when there is a significant proportion of high energy overbank flow.

6.8. Comparison of calculated and measured total rates of bed load transport by direct application of averaged channel properties

The following section examines the application of current sediment transport theory to the case of sediment transport in meandering rivers with overbank flow and mixed grain sediment. Sediment transport is calculated using the average channel properties at the crossover firstly using a single nominal diameter derived from the original substrate and secondly dividing the substrate into fractions, each represented by a nominal diameter. The fraction-based calculation is subsequently enhanced using a hiding function developed by Pender (1995). Improvement in predictive ability with increasing complexity is considered at each stage. In each case the effects of a 10% error in the calculation of main channel discharge is shown.

6.8.1. Total transport rate based on a single nominal diameter

The Engelund and Hansen, Ackers White, van Rijn and Yang transport theories were applied to the average cross section data. Yang presents separate equations for sand and gravel transport. As the sediment used was spread over the dividing mark, the gravel transport formula should be used however this proved unsuitable for application to mixed grain sediment. As a result the formula was considered unsuitable and has not been used.

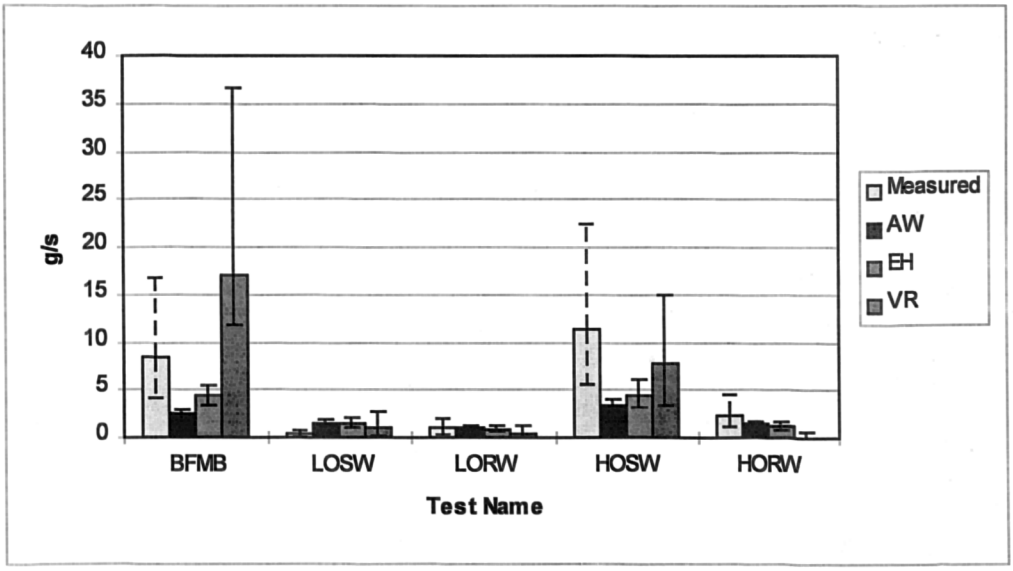

*The error bars on the measured transport rate give a discrepancy ratio of 1/2 to 2. The error bars on the three calculated transport rates show the error resulting from a ±10% error in the discharge calculation.

Figure 6.8 Comparison of calculated and measured rates of total sediment transport calculated using a single nominal diameter.

Figure 6.8 shows the calculated transport rates for the wide floodplain tests calculated using a single nominal grain diameter. The discharge in each case was calculated by summation of the recorded velocities in the main channel. The wetted perimeter was that measured using the profiler and the hydraulic radius taken as the total flow area (surface to bed) divided by the wetted perimeter. The wetted perimeter and flow area used are shown in Figure 5.28. The slope used was the average water surface slope as secondary velocities can largely account for the variations in slope around a wavelength. The d_0 was used for the Engelund and

Hansen and van Rijn formulae and the d_{35} for the Ackers White. The Ackers White gives the closest result in the bankfull case where even with a 10% error in the discharge calculation it falls within the range of 1/2 to 2 times the measured rate of transport. In the low overbank tests the transport rates are very low as the shear stress is close to the critical value for grain movement. In this region sediment transport rates are difficult to predict accurately. All transport rates are too low in the high overbank flow cases.

The use of a single grain size in to represent a mixed sediment makes the formula very sensitive to the size of sediment chosen as the nominal diameter. For widely graded sediment, the rates of transport may be recalculated as shown below.

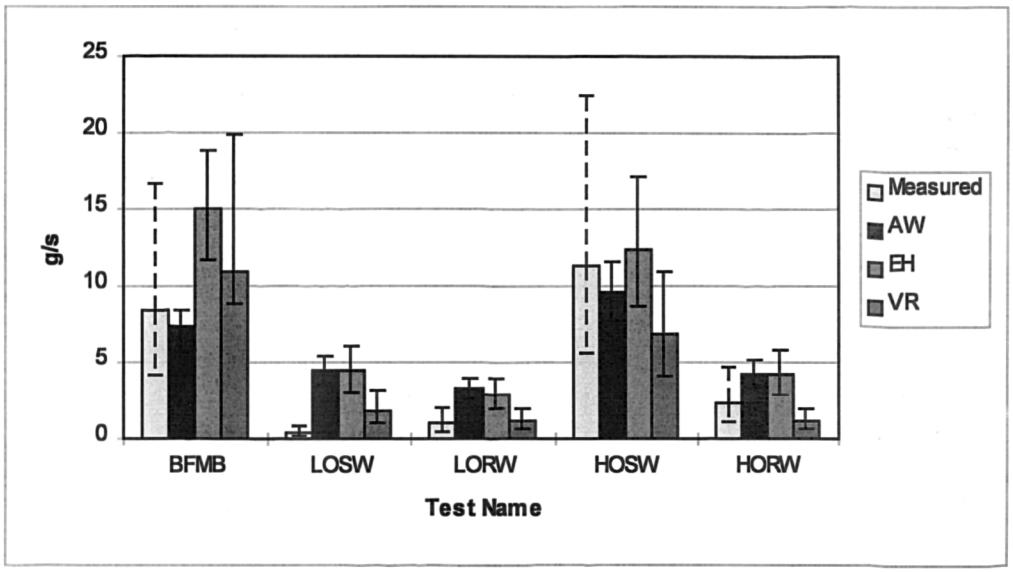

Figure 6.9 Comparison of calculated and measured rates of total sediment transport calculated using a range of sediment sizes. The error bars on the measured transport rate give a discrepancy ratio of 1/2 to 2. The error bars on the three calculated transport rates show the error resulting from a ±10% error in the discharge calculation.

Figure 6.9 shows the calculated total sediment transport using Ackers White, van Rijn and Engelund Hansen equations against the measured total load. The values of discharge area and wetted perimeter were the same as those used in the single grain size analysis.

The treatment of mixed grain sediment in a sediment transport formula is addressed in the literature review. Due to delays in the data processing system the average surface sediment could not be used in calculation. Therefore, calculations presented here were performed by dividing the original sediment mixture into five portions of equal mass and calculating the rate of sediment transport using the d50 of each portion. The total sediment transport rate was obtained by multiplying each rate by the proportion of the fraction by mass and summing the results. In the Ackers White calculation, the roughness value was taken as the d_{35} of the original sediment mixture.

The results from the calculations are shown in Figure 6.5. Both formulae under predict the rate of sediment transport in the bankfull and overbank smooth cases and over predict in the low overbank rough cases. It should be remembered that the calculations are based on discharge calculated from point velocities rather

than a discharge prediction method. Consequently, this is not a result that can be attributed to errors in the calculation of discharge due to flow interaction.

6.8.2. Sediment size distribution.

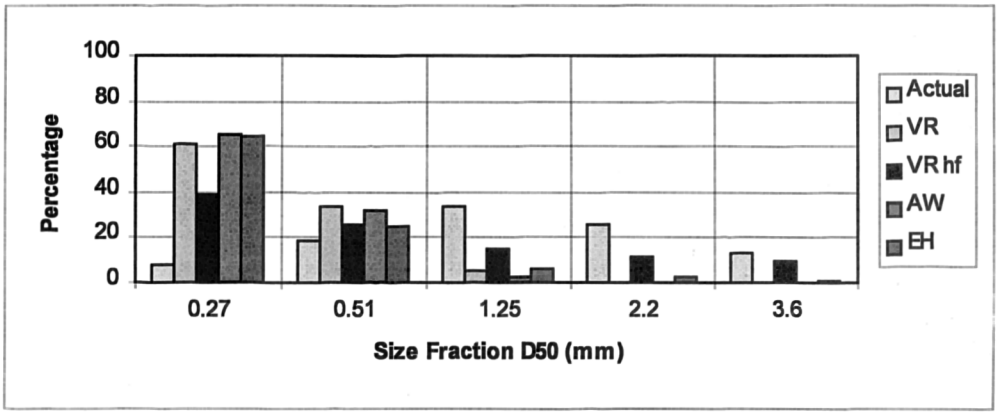

Figure 6.10 Comparison of mobility of individual grain size fractions in a sediment sample (Bankfull mobile test)

Whilst the prediction of bulk sediment transport appears to be adequate the prediction of the movement of small grains is over predicted and the movement of larger grains significantly under predicted.

One reason for this is that the sampler only recorded sediment movement close (19mm) to the bed. In the bankfull and high overbank smooth cases the flow was sufficiently powerful to suspend some sediment and hence some of the sediment may have passed over the sampler artificially coarsening the results. Similarly the sediment in the recirculating flume was collected at the flume exit by a sediment trap which drew the bed sediment back around the system. It was evident from examination of the sediment that collected in the stilling pool at the bottom of the flume that some sediment was passing over the trap and settling out below. This is clearly a feature of the experimental design rather than a fundamental property of sediment behaviour.

It was observed by sight however that particles in the transport belt in the flume appeared to have relatively equal mobility regardless of size. This supports Parker's(1990) concept of equal mobility. Pender (1995) developed this concept into a hiding function for application to the van Rijn equations. The results are illustrated below.

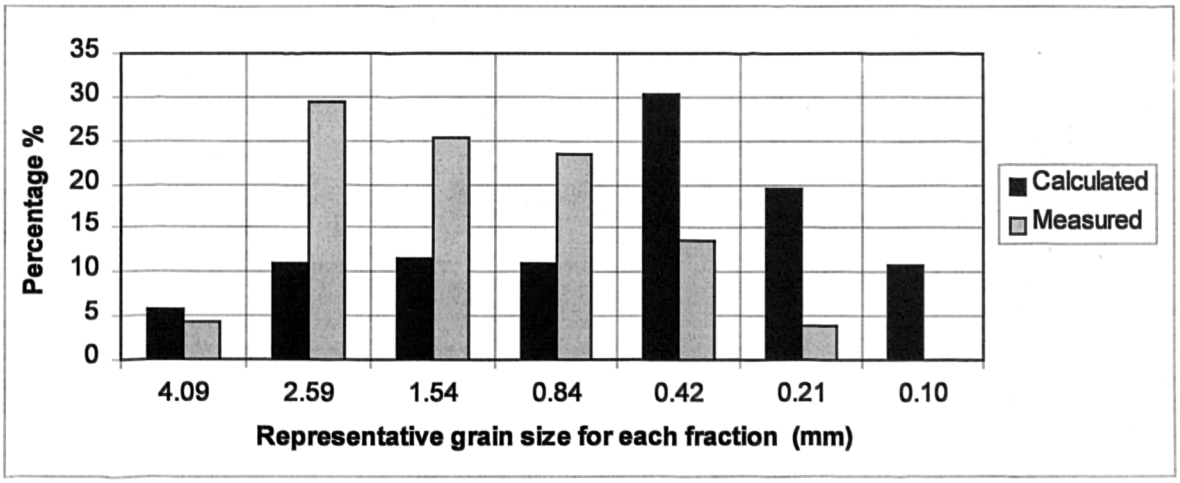

Figure 6.11 Suspended and bedload transport with application of hiding function (bankfull test)

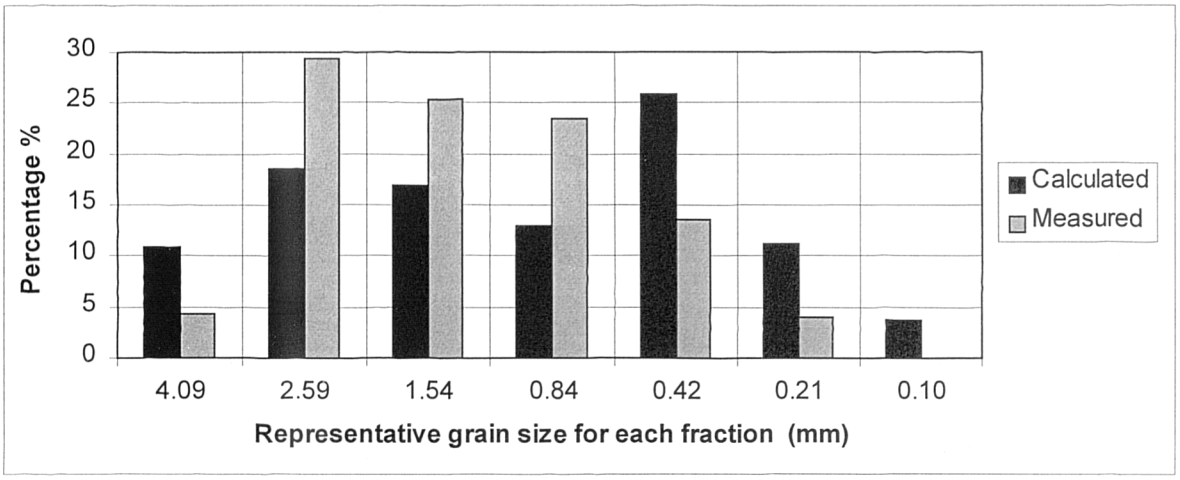

Figure 6.12 Bedload transport only (Bankfull Test)

Pender's hiding function significantly improves the prediction of fractional movement and it appears that the bedload comparison is the most applicable. However there are still significant discrepancies. This may be due to three factors, the experimental issues described earlier, the bimodal nature of the bed sediment, and the effects of lateral distribution.

The work shows that sediment transport may be predicted to traditional levels of accuracy despite overbank flow provided an accurate estimation of discharge at the crossover can be achieved.

The calculation of discharge is shown to be notably better when the sample is slit into smaller gradations however the rates of transport are generally heavily weighted in terms of the smaller fractions.

Pender's (1995) hiding function based on Parker theory of equal mobility has been shown to considerably improve the calculation of individual grain size movement.

The calculations were based on the original sediment mixture - reasons for error. No consideration of armouring, no consideration of cross channel sorting. Hard to distinguish between bed load and suspended load - some suspended load is missed by sampler.

6.9. Consideration of laterally varying parameters

The calculations presented above show that sediment transport may be predicted to an accuracy of ± 50% given the correct discharge. Increased confidence in transport formulae may require increasing complexity in calculation and data collection. Critically the consideration of the lateral variation of depth and grain size. In the following section the effect of laterally varying parameters will be considered

6.9.1. Seed (1996) and Bettess et al. (1997)

Seed (1996) developed a method, described earlier for inbank flow in straight channels, to account for changes in channel depth based on a shape factor. Application of this method to the results obtained showed the method to be highly sensitive to grain size distribution which varies laterally over the channel cross

section and is thus difficult to apply. Consequently it has not been adopted for further development in this thesis.

6.10. Comparison of section averaged and transport belt variables

The observations above suggest that the lateral variations of depth grain size and velocity over the cross over section in a meandering stream create a limited zone of transport in which the depth, velocity and grain size are relatively similar. The width of the zone may considered as that region of the flow in which the critical shear velocity is exceeded by the applied shear velocity.

It was stated in the introduction that sediment transport formulae applied to river cross sections generally under predict transport. This is initially surprising when the observations show a narrow band of transport and transport is generally assumed to occur over the whole width, which would suggest that the value should be higher. However a closer look supports the under prediction of sediment transport formulae. As the rate of sediment transport varies so dramatically over the channel for a transport formula to accurately predict sediment transport rates in a channel it must predict transport slightly below the peak value to account for width of the flow. It is unlikely that these conditions would correspond to the averaged values. The averaged values may be biased towards either fast but very rough flow, or more probably finer sediment but very slow flows.

If the characteristics of the transport zone can be determined using similar information to that used for current prediction then a traditional one dimensional sediment transport formula may be applied to the channel reducing the need for extensive calculation or computational procedures. It is also worth noting at this point that many sediment transport formulae use river data in their calibration factors. If averaged values were then used in fitting these data to the formula (which is the case in most sediment transport formulea) then an error is built in to the formulae so that even if the formula is correctly applied to the transport belt under the correct conditions then the results may still be incorrect.

	Measured		Section Averaged
BFMB	y = -0.9	y = -1.0	
D (m)	0.136	0.148	0.108
V (ms^{-1})	0.51	0.53	0.45
HORW	y = -0.9	y = -1.0	
D (m)	0.336	0.363	0.180
V (ms^{-1})	0.23	0.25	0.27
LORW	y = -0.9	y = -1.0	
D (m)		0.227	0.152
V (ms^{-1})		0.33	0.26

Table 6.2 Variation in section averaged values and velocity and depth values at the transport belt

The variation in averaged values with the measured values at the position at which transport occurs are shown in Table 6.2. The depth is underestimated by averaging the values in all cases. The velocity is underestimated by 10% in the bankfull and low overbank rough cases. As the velocity is highly significant in the calculation of sediment transport this suggests that sediment transport will be largely under predicted.

6.11. Recommendations for application of sediment transport formulae to natural streams

The current results are not sufficiently extensive to support a general theory however the results do suggest that it may be possible to improve the calculation of sediment transport in meandering streams by identifying and using the transport belt properties rather than those from the average stream properties. Confirmation of this thesis would require a wide study of natural streams, which is significantly beyond the scope of this current project.

6.12. Chapter conclusions

Local bedload transport is shown to be affected by a number of variables, slope, velocity flow depth and bed roughness, which is a function of the above and the local sediment properties. These variables are related and one may be considered redundant. Choice of which variable to discard may be based on the ease of collecting data and the theoretical suitability of a transport formula for the required purpose.

The variables may be observed to vary significantly around a wavelength and over a channel width within a small meandering river containing mixed grain sediment. Therefore one-dimensional modelling of the system requires a consideration of the three dimensional nature of the problem.

From the Series B data it was observed that the highest average channel shear stress occurs at the apex and the lowest at the crossover. Observations of the distribution of sediment transport at the apex show that the

majority of sediment transport occurs at the inside of the bend where the local shear stress is observed to be highest.

The low bed shear at the crossover suggests that this region has the lowest transport capacity and therefore should be used in transport calculations as a control section.
This concept can be verified by observing that when the channel flow exceeds bankfull capacity the velocity is reduced and the bed shear drops. The interruption in sediment supply to the apex results in the erosion of the point bar in the area of high shear stress. Therefore the transport rate at the crossover affects the apex form.

Bed load samples collected across the main channel confirm field investigations showing that the sediment transport is concentrated in a narrow band , or active width occupying 30% of the top channel width in the inbank channel reducing to 5 - 15% in the overbank channels with rough floodplains. It is likely that the transport is constrained on the side with deep flow and fast velocities, by the collection of large grains, which have accumulated there due to erosion, and is constrained on the other side by the slow velocities observed in the wake of the point bar. In the high overbank smooth case the narrow band of transport is not observed, with active transport occurring over at least half of the flume.

The points made above suggest that the transport rate down the stream may be characterised by a single set of parameters and an active width over which these parameters apply. It is hypothesised that further research may obtain an expression for the active width and the relevant parameters based on the channel geometry.

7. Summary of conclusions

The purpose of this section is to summarise the main findings of the work and to bring out the original contribution to current knowledge. It is divided into sections reflecting the chapters of the thesis.

7.1. The design of the experiment

The model examined in this thesis is an acceptable model of an upland meandering river in terms of slope and planform at prototype scale. As the sediment is of the same density of natural bed sediment the model cannot be scaled under strict scaling rules. However, It is argued that the relaxation of some scaling conditions is justified given the high Reynolds number in the flume and therefore the flume results may be scaled to larger sizes.

A bed sediment is selected in which all fractions are mobile at the highest flows. Small-scale laboratory tests show that the mixed grain nature of the sediments suppresses ripples and that long flat dunes are formed in their place.

Floodplain roughness, modelled from folded strips of expanded aluminium, has been designed and tested in a small flume to accurately simulate the levels of roughness found of heavily roughened floodplains. This represents a degree of roughness unexplored in previous tests and of great interest to practitioners.

Instrumentation and methodology have been designed the measure the variation in: water levels, bed forms, flow velocities, total and local rates of sediment transport, surface roughness and bed morphology.

The water velocities were measured using an ADV mounted on an automated traverser. The bed was mobile whilst readings were taken. The author was instrumental in the innovative design of this system.

These tests examine the variation in flow structures and sediment transport rate with changes in flow depth floodplain roughness and bedform at a scale and level of control previously unavailable.

7.2. Presentation of results

Experimental data from the five tests performed by the author are presented in Chapter 4. For each test the following data is presented:-

- The discharge down the main channel, above and below floodplain level (overbank flows only).
- A contour map of the bed for each relevant section, a photograph showing grain sorting around the meander bend.
- Main stream velocity isovels.
- Secondary circulation diagrams.

7.3. Flow mechanisms and conveyance

The subject of compound channels has been studied extensively for 35 years the primary focus being the resistance due to flow interaction between the floodplain and main channel flows.

7.3.1. Floodplain flow

The literature review exposes the need for more detailed consideration of roughness on floodplains. The following points are considered particularly important:

- Inbank channels are attributed a roughness parameter, either Manning's n or Chezy's C that has dimensions and is not constant with depth. They also strictly only apply to uniform flow, which rarely occurs in practice. Any formulae in which these parameters are used are subject to the resultant inaccuracy.
- For vegetated floodplains the use of n or an equivalent as a roughness parameter is less appropriate as n varies strongly with depth as well as plant density and stiffness, the time of year and the length of inundation. The attribution of a single value of roughness can lead to errors in Manning's n of up to a factor of 4 or greater.
- Research has been conducted into improved formulae for the calculation of vegetative roughness, for dense vegetation and for incremental roughness such as hedges. Application of these formulae however requires the collection of significant quantities of field data.

Improved calculation of floodplain flow is a prerequisite to improved calculation of flow interaction between main channel and floodplain.

7.3.2. Main channel and floodplain flow interaction

The following points are noted from the literature.

- The F* approach to categorising interaction losses in meandering channels has shown that interaction losses decrease as the floodplain side walls become of shallower slope and with increased floodplain roughness.
- Of the methods available for prediction of flow rates in meandering two stage channels the James and Wark method has been found to predict flow rates most accurately. However, the semi-empirical model is fitted to a limited set of data and incorporates a single value for Manning's n for the floodplain roughness.
- The division method suggested incorporating a horizontal division line at the bankfull level, used in both the F* and James and Wark Methods, may not be the most appropriate for rough floodplains. Because the floodplain flow velocity is much lower than that of the main channel.

The following conclusions were obtained from an analysis of the results

- The flow mechanisms observed in the Series B tests are consistent with those in the Series C high overbank smooth case. In the other cases however the effects of secondary circulation at the crossover, appear to show greater mixing with the overbank flow than suggested by the previous tests. This is confirmed by dye and velocity measurements.

- The phenomena of reverse flow seen in the bankfull and overbank rough cases are also not observed in the Series B channel.
- F* continues to increase as relative floodplain roughness is increased. At high floodplain roughness, Zone 2 should be split with vertical division lines at the edges of the floodplain to account for the difference in velocity between the floodplain and upper main channel flow velocities.
- A mobile boundary has little effect on conveyance at low floodplain depths but increases conveyance at higher depths.
- The James and Wark method severely under estimates the flow in zones 1 and 2 at high floodplain roughness. This is due to inadequacies in the formula for predicting discharge below the bankfull level (Zone 1), in rivers with high flood plain roughness.
- A new method is proposed for rough floodplains, based on momentum gained and lost by the main channel due to floodplain exchange over half a wavelength. The parameters are, an estimation of the Manning's n value of the bankfull channel and the floodplain and the dimensions of the channel. A factor is introduced to account for the ratio of velocity of flow entering the floodplain in comparison to average flow in the main channel. The total discharge is predicted within 10% of the actual value however the main channel discharges are significantly too high (25% - 35%) for a rough floodplain and too low (30%) for a smooth floodplain.
- The advantages of the method are the simplicity of application and the absence of a large number of empirical constants. Testing on a large data set is required for confirmation of its value.

7.4. Sediment Transport

The theory of sediment transport is reviewed in Chapter 2. The following points are noted.

- The best sediment transport formulae are shown to be incapable of reliably predicting sediment transport rate to better than a factor of 2 of the actual value. This is in part due to assumptions in the formula, which fail to accurately describe the processes occurring at the bed and partly due to the variation in flow properties across channels. These issues are considered in more detail in Chapter 6.

- Study of flow over bedforms shows that the vertical velocity profile above a bedform changes considerably between crest and trough. It is unclear at which point along the form, the shear velocity is most closely related to the sediment transport rate.

- Local bedload transport is shown to be affected by a number of variables, slope, velocity flow depth and bed roughness, which is a function of the above and the local sediment properties. These variables are related and one may be considered redundant. The choice of which variable to discard may be based on the ease of collecting data and the theoretical suitability of a transport formula for the required purpose.

The study of mixed grain sediment transport in a meandering two-stage channel has not previously been investigated by physical model, to the knowledge of the author.

- Total bedload transport rate in the stream is shown to drop dramatically when the flow first goes overbank and then to increase at with floodplain depth.
- When predicting local transport, the variables listed above may be observed to vary significantly around a wavelength and over a channel width within a small meandering river containing mixed grain sediment. Therefore one-dimensional modelling of the system requires a consideration of the three dimensional nature of the problem.
- From the Series B data it was observed that the highest average channel shear stress occurs at the apex and the lowest at the crossover. Observations of the distribution of sediment transport at the apex show that the majority of sediment transport occurs at the inside of the bend where the local shear stress is observed to be highest.
- The low bed shear at the crossover suggests that this region has the lowest transport capacity and therefore should be used in transport calculations as a control section.
- This concept can be verified by observing that when the channel flow exceeds bankfull capacity the velocity slows and the bed shear drops. The interruption in sediment to the apex results in the erosion of the point bar in the area of high shear stress.
- During overbank flow the apex profile tends to flatten due to erosion of the point bar (see point above) and deposition at the outside of the bed due to the reduction in strength of secondary currents. The crossover profile is relatively unaffected.
- Bed load samples collected across the main channel confirm field investigations showing that the sediment transport is concentrated in a narrow band, or active width occupying 30% of the top channel width in the inbank channel. This reduces to 5 - 15% in the overbank channels with rough floodplains. It is likely that the transport is constrained on the side of the transport belt with deep flow and fast velocities, by the collection of large grains that have accumulated there due to erosion. It does not occur on the other side of the belt because the velocities observed in the wake of the point bar are too slow to initiate transport. In the high overbank smooth case the narrow band of transport is not observed, with active transport occurring over at least half of the flume.
- The points made above suggest that the transport rate down the stream may be characterised by a single set of parameters and an active width over which these parameters apply. The best cross-section at which to apply the formula is the crossover, due to the minimal change in bed shape and the low point in the bed shear. It is hypothesised that further research may obtain an expression for the active width and the relevant parameters based on the channel geometry. This would in turn improve calculation of transport rates.

7.5. Further Work

Common to many projects further work suggested by this thesis falls into two areas. One consisting of filling in the gaps in the current work and confirming or refuting the assumptions and theories contained and another using the work as a basis for more complex study.

In the first category there is a need to: -

- Perform straight flume analysis of various grain sizes to establish further the behaviour of mixed grain sediments.
- Collect sediment transport data taking into account the important time factors involved in dune movement and develop an acceptable method for measuring shear velocity over a mobile bed.
- Extend and re-examine the proposed momentum theory taking into account the change of momentum within the body of the flow and establishing bounds within which the formula may be useful.

The work that is recorded here also creates a significant springboard for future work including:

- Examination of the morphological effects of the return from overbank to inbank
- "Chemical Freezing" of the bed at the inbank condition and conduct test at low and high overbank to establish the initial overbank conditions for each of these tests.
- Examination of existing fieldwork and performance of further tests to establish general applicability of the ideas of transport bands.
- Establishing the sensitivity of flood prediction packages to estimation of floodplain roughness.

In the long term a database of applicable characteristics of a range of floodplain vegetation may be assembled in order to improve prediction. In the short term an awareness of the problems of vegetative resistance should help with defining safety margins when designing channels for overbank flow.

Further investigations of the behaviour of metal strip roughness may also be performed in order to inform the design of new physical model tests. In particular the variation in coefficient with mesh size, strip height and flow velocity.

References and Bibliography

Ackers, P. And White, W.R., Sediment Transport: A new approach and Analysis, *Journal of Hydraulic Engineering, ASCE*, Vol 99, No 11, pp 2041-2060, November 1973

Ackers, P.(1989). Appendix 2, Resistance functions for the SERC-FCF at Wallingford.

Ackers, P., Resistance functions for the Wallingford Facility, *SERC Flood Channel Research Design Manual Technical Report No 1*, August 1989

Ackers, P., Hydraulic Design of Two-Stage Channels, *Proceedings of the ICE - Water, Maritime & Energy*, Vol 96, pp247-257, December 1992

Ackers, P., Sediment Transport in Open Channels: Ackers and White update, *Proceedings of the ICE - Water, Maritime & Energy*, Vol 101 (4), pp 247-249, December 1993

Ackers, P., Flow Formulae for Straight Two Stage Channels, Journal of Hydraulic Research, IAHR, Vol 31, No 4, pp509-531, 1993

Acrement and Schneider (1989). "Guide for selecting Manning's roughness coefficients for natural channels and flood plains." Water supply paper/ US Geological survey; 2339

Aldridge, B.N. and Garret,J.M., (1973)., Roughness coefficients for stream channels in Arizona: *U.S.Geological Survey Open-File report,* 87p

Anonymous, (1963b). Guide for selecting roughness coefficient 'n' values for channels, U.S.Department of Agriculture, Soil conservation service, Washington, December

Bagnold, R.A., An Approach to the Sediment Transport Problem from General Physics, USGS Professional Paper 422-J, 1966.

Bagnold, R. A. and Barndorff- Nielsen, O. 1980. The pattern of natural size distributions. *Sedimentology* , 27,199-207

Barnes (1967)., H.H., "Roughness Characteristics of Natural Channels," Journal of the Hydraulics Division, ASCE, Vol. 96, No. HY12, Proc. Paper 7773, Dec., 1970, pp. 2581-2610.

Bennet J.P. Algorithm for resistance to Flow and Sediment Transport in Sand-Bed channels, *Journal of Hydraulic Engineering, ASCE*, Vol 121, No 8, pp 578-590, August 1995

Bettess and White 1979, "A One Dimensional Morphological River Model," Report No. IT194, Hydraulics Research Station, Wallingford, England, 1979

Bettess R., Bona P., Morris M. and Seed D., Sediment transport in natural rivers HR Report SR 515, October 1997

Borah et al 1982, "Routing Graded Sediments in Streams: Formations," *Journal of Hydraulic Engineering, ASCE*, Vol 102, No 12, pp 1486-1503, December 1982

Brownlie, W.R., "Prediction of Flow Depth and Sediment Discharge in Open Channels," Rept No. KH-R-43A, W.M.Keck Laboratory of Hydraulics and Water Resources, California Institute of Technology, Pasenda, California, November 1981

Brownlie, W.R., Flow Depth in Sand Bed Channels, *Journal of Hydraulic Engineering, ASCE*, Vol 109, No 7, pp 959-990, December 1983

Chadwick, A. & Morfett, J., Hydraulics in Civil and Environmental Engineering, Harper Collins, 1993

Chang, H. H., Energy Expenditure in Curved Open Channels, *Journal of Hydraulic Engineering, ASCE*, Vol 109, No 7, pp1012-1022, July 1983

Chang, H.H., Fluvial Processes in River Engineering, John Wiley and Sons, 1988

Chiew, Y. M., Bed Features in Nonuniform Sediments, *Journal of Hydraulic Engineering, ASCE*, Vol 117, No 1, pp 116-120, January 1991

Chow, V. T., Open Channel Hydraulics, McGraw Hill, 1959

Colebrook, C. F., Turbulent Flows in Pipes, with Particular Reference to the Transition Region Between the Smooth and Rough Pipe Laws, Journal of the ICE, Vol 11, pp133-156, 1939

Cowan, W. L., Estimating Hydraulic Roughness Coefficients, *Agricultural Engineering*, Vol 37, No 7, pp473-475, July 1956

Day T.J., A study of the transport of graded sediment. HR Wallingford Report No.

Dietrich, W. E., Smith, J. D. & Dunne, T., Boundary Shear Stress, Sediment Transport and Bed Morphology in a Sand-bedded River Meander During High and Low Flow, *Proceedings of the River Meandering Conference 1983*, ASCE New Orleans, Louisiana, Ed. C. M. Elliott, pp632-639, 24-26 October 1983

Dyer, K.R. 1986. Coastal and estuarine sediment dynamics,Wiley

Egiazorov, I.V., Calculation of non-uniform sediment concentrations. *Journal of Hydraulic Engineering, ASCE*, Vol 91, No 4, pp 225-247, April 1965

Engelund and Hansen A Monograph on Sediment Transport in Alluvial Streams. Teknisk Forlag, Copenhagen, Denmark, 1967

Einstein H.A., The Bed Load Function for Sediment Tranportation in Open Channels, Technical Bulletin 1026, U.S. Department of Agriculature, 1950.

Einstein, H.A. and Barbarossa, N., River Channel Roughness, *Journal of Hydraulic Engineering* ASCE 117, pp. 1121-1146, 1952

Ervine, D. A. & Jasem, H. K., Flood Mechanisms in Meandering Channels with Floodplain Flow, *Proceedings of 23rd IAHR Congress*, Ottawa, Canada, ppB449-B456, 1989

Ervine, D. A., Sellin, R. H. J. & Willetts, B. B., Large Flow Structures in Meandering Compound Channels, *Proceedings of the 2nd International Conference on River Flood Hydraulics*, York, Ed. W. R. White & J. Watts, pp459-469, 22-25 March 1994

Ervine, D. A., Willetts, B. B., Sellin, R. H. J. & Lorena, M., Factors Affecting Conveyance in Meandering Compound Flows, *Journal of Hydraulic Engineering, ASCE*, Vol 119, No 12, pp1383-1399, December 1993

Fathi- Maghadam, M. and Kouwen,N. (1997). Nonrigid, nonsubmerged, vegetative roughness on floodplains, Proceedings, ASCE, Journal of the hydraulics division, vol. 123, HY1, pp 51-57
French, R.H., (1985). *Open channel hydraulics*, McGraw Hill

French, R.H. Open Channel Hydraulics. McGraw-Hill 1986

Greenhill, R. K., An Investigation into the Mechanisms of Compound Meandering Channel Flow, PhD thesis, February 1992

Greenhill, R. K. & Sellin, R. H. J., Development of a Simple Method to Predict Discharges in Compound Meandering Channels, *Proceedings of the ICE - Water, Maritime & Energy*, Vol 101, pp37-44, March 1993

Henderson, F. M., Open Channel Flow, Macmillan Press Ltd, 1966

Hey, R., Plan Geometry of River Meanders, *Proceedings of the River Meandering Conference 1983*, ASCE New Orleans, Louisiana, Ed. C.M. Elliott, pp30-43, 24-26 October 1983

Hey, R. D., Environmental River Engineering, *Journal of the IWEM*, No 4 pp335-340, August 1990

Holden, A. P. & James, C. S., Boundary Shear Distribution on Flood Plains, *Journal of Hydraulic Research, IAHR*, Vol 27, No 1, pp78-89, 1989

IAHR 50 years Hydraulic Engineering

James, C. S. & Wark, J. B., Hydraulics Manual for Meandering Compound Channels, HR Report EX2606, June 1992

Keulegan, G. H., Laws of Turbulent Flow in Open Channels, *Journal of Research of the National Bureau of Standards*, Paper RP1151, Vol 21, No 6, December 1938

Klaassen, G.J. and Zwaard, J.J. van der (1974). Roughness coefficients of vegetated floodplains, Journal of Hydraulics Research, Vol.12 no.1

Klaassen, G. J. & van Urk, A., Resistance to Flow of Floodplains with Grasses and Hedges, *Proceedings of 21st IAHR Congress*, Melbourne, Australia, pp469-473, August 1985

Knight, D. W. & Demetriou, D., Flood Plain and Main Channel Flow Interaction, *Journal of Hydraulic Engineering, ASCE*, Vol 109, No 8, pp1073-1092, August 1983

Knight, D. W. & Sellin, R.H.J., The SERC Flood Channel Facility, *Journal of the IWEM*, Vol 1, No 2, pp198-204, October 1987

Knight, D. W., Shiono, K. & Pirt, J., Prediction of Depth Mean Velocity and Discharge in Natural Rivers with Overbank Flow, *Proceedings of International Conference on Hydraulic and Environment Modelling of Coastal, Esturine and River Waters*, University of Bradford, 19-21 September 1989

Knight, D. W. & Shiono, K., Turbulence Measurements in a Shear Layer of a Compound Channel, *Journal of Hydraulic Research, IAHR*, Vol 28, No 2, pp175-196, 1990

Krumbein, W.C. 1934. Size frequency distributions of sediments. J. Sediment. Petrol., **4**, 65-77

Laursen, E.M., The Total Sediment Load of Streams, *Journal of Hydraulics Division, ASCE*, Vol 54, No 1, pp1-36, February 1958

Leopold, L. B. & Emmett, W. W., Bedload Movement and its Relation to Scour, *Proceedings of the River Meandering Conference 1983*, ASCE New Orleans, Louisiana, Ed. C. M. Elliott, pp640-649, 24-26 October 1983

Lyness, J. F., Myers, W. R. C. & Wark, J. B., A Comparative Study of the Use of the Lateral Distribution Method in Modelling Flood Hydrographs in a Compound Channel, *Proceedings of the 26th IAHR Congress, HYDRA 2000*, London, UK, Vol 1, pp302-307, 11-15 September 1995

Martin, L. A. & Myers, W. R. C., Measurement of Overbank Flow in a Compound River Channel, *Proceedings of the ICE*, Part 2, Vol 91, pp645-657, December 1991

Massey, B. S., Mechanics of Fluids, van Nostrand Reinhold, 1989

McKeogh, E. J. & Kiely, G. K., Experimental Study of the Mechanisms of Flood Flow in Meandering Channels, *Proceedings of 23rd IAHR Congress*, Ottawa, Canada, pp491-498, 1989

Myers, W. R. C., Momentum Transfer in a Compound Channel, *Journal of Hydraulic Research, IAHR*, Vol 16, No 2, pp139-150, 1978

Myers, W. R. C., Velocity and Discharge in Compound Channels, *Journal of Hydraulic Engineering, ASCE*, Vol 113, No 6, June 1987

Myers, W. R. C., & Brennan, E. K., Flow Resistance in Compound Channels, *Journal of Hydraulic Research, IAHR*, Vol 28, No 2, pp141-155, 1990

Naish, C. & Sellin, R.H.J., Scale Effects in the Hydraulic Modelling of Compound River Channels, *Proceedings of the 2nd International Conference on Hydraulic Modelling*, Stratford-upon-Avon, UK, pp361-377, 14-16 June 1994

Naish, C. & Sellin, R.H.J., Scaling of Hydraulic Roughness for Small and Large Scale River Models, *Proceedings of the 26th IAHR Congress, HYDRA 2000*, London, UK, Vol 1, pp111-116, 11-15 September 1995

Nezu, I. & Rodi, W., Open Channel Flow Measurements with a Laser Doppler Anemometer, *Journal of Hydraulic Engineering, ASCE*, Vol 112, No 5, pp335-355, May 1986

Odgaard, A. J., Transverse Bed Slope in Alluvial Channel Beds, *Journal of Hydraulic Engineering, ASCE*, Vol 107, No 12, pp1677-1694, December 1981

Onishi, Y., Jain, S. C., and Kennedy J.F., (1976) Effects of meandering in alluvial streams, *Journal of Hydraulic Engineering, ASCE*, Vol 102, HY7

Parker, G.(1978), Self formed Rivers with Equilibrium Banks and Mobile Bed: Part II the Gravel river," *J.Fluid Mech.*, 89(1), pp.127-148

Parker and Sutherland (1990), Fluvial Armour, *J.Hyd.Res*, Vol. 28(4), 417-436

Parker, G. Surface Based bedload transport relations for gravel rivers. J. Hydraul Res., 28, No. 4, pp 417 - 436, 1991

Pender, G., Comparison of two hiding function formulations for sediment transport calculations, *Proceedings of the ICE - Water, Maritime & Energy*, Vol 112, pp 127 - 135, June 1995

Petryk, S. and Bosmajian, G., (1975). Analysis of flow through vegetation: Proceedings, ASCE, Journal of the hydraulics division, v. 101, no. HY7, pp. 871-884

Ramser (1929), C.E., " Flow of water in drainage channels," Technical Bulletin No. 129, U.S. Department of Agriculture, Nov.,1929, p. 101.

Raudkivi (1963). Study of sediment ripple formation. Proc. ASCE, Vol. 89(HY6), 15-33

Raudkivi, A.J.(1998), Loose Boundary Hydraulics, 4th Ed. A.A.Balkema/Rotterdam/Brookfield

Ree, W.O., (1958), "Retardation Coefficients for row crops in diversion terraces," Transactions of the American Society of Agricultural Engineers, Vol. 1, 1958, pp.78-80

Ree, W.O. and Crow, F.R., (1977), Friction factors for vegetated waterways of small slope: Agricultural Research Service, U.S. Department of Agriculture, ARS-S-151, 56 p.

Samuels, P. G., The Hydraulics of Two Stage Channels - Review of Current Knowledge, *Presented at Conference of River Engineers*, University of Loughborough, July 1989

Schlichting, H., (1960) Boundary Layer Theory, McGraw Hill

Searle, D. J., A Laboratory and Field Investigation into the Discharge Characteristics of an Experimental Flood Alleviation Scheme on the River Roding in Essex, PhD thesis, September 1986

Seed D.J., Lateral variation of sediment transport in rivers, HR Report SR 454, March 1996.

Sellin, R.H.J., A Laboratory Investigation into the Interaction Between the Flow in the Channel of a River and that over its Flood Plain, *La Houille Blanche, Grenoble, France*, No 7, pp793-802, 1964

Sellin, R.H.J., Towards the identification of flow mechanisms in channels of complex geometry, *Proceedings of 24th IAHR Congress*, Madrid, ppA534-A530, 1991

Sellin, R.H.J., Turbulent Flow Structures and Velocity Distribution in a Two-Stage Channel Bend, *Proceedings of the 26th IAHR Congress, HYDRA 2000*, London, UK, Vol 1, pp27-32, 11-15 September 1995b

Sellin, R.H.J., Ervine, D. A. & Willetts, B. B., Behaviour of Meandering Two-Stage Channels, *Proceedings of the ICE - Water, Maritime & Energy*, Vol 101, pp99-111, June 1993

Sellin, R.H.J., and Willets B.,Three dimensional structures, memory and energy dissipation in meandering compound channel flow. Floodplain Processes, John Wiley and Sons 1996.

Shiono, K. & Knight, D. W., Two Dimensional Analytical Solution for a Compound Channel, *Proceedings of 3rd Symposium on Refined Flow Modelling and Turbulence Measurements*, Tokyo, Japan, pp503-510, July 1988

Shiono, K. & Knight, D. W., Mathematical Models of Flow in Two or Multi-Stage Straight Channels, *Proceedings of International Conference on River Flood Hydraulics*, Wallingford, Ed. W. R. White, pp229-238, September 1990

Shiono, K. & Knight, D. W., Turbulent open channel flows with variable depth across the channel, *Journal of Fluid Mechanics*, Vol 222, pp617-646, 1991

Simons, D.B., and Richardson, E.V., Forms of Bed Roughness in Alluvial channels, *Journal of Hydraulics Division, ASCE*, Vol 87, No 3, pp87-105, 1961

Simons, D.B., and Richardson, E.V., Resistance to flow in Alluvial channels, *USGS Professional Paper 422-J*, 1966

Simons, D.B., Richardson, E.V., and Nordin, C.F., Sedimentary structures generated by flow in Alluvial channels, *Am. Assoc. Petrol. Geologists, Special Publication No. 12*, 1965

Smith, J.D. and McLean, S.R. (1977). Spatially averaged flow over a wavy surface, J. Geophysical Research, 84(12), pp 1735-1746

Song, T., Chiew, Y.M. and Chim, C.O., Effect of Bed-Load Movement on Friction Factor, *Journal of Hydraulics Division, ASCE*, Vol 124, No 2, pp165-175, February 1998

Thorne, C. R. & Hey, R. D., Direct Measurements of Secondary Currents at a River Inflexion Point, *Nature*, Vol 280, pp226-228, 19 July 1979

Thorne, C. R. & Rais, S., Secondary Current Measurements in a Meandering River, *Proceedings of the River Meandering Conference 1983*, ASCE New Orleans, Louisiana, Ed. C. M. Elliott, pp675-686, 24-26 October 1983

Thorne, C. R., Zevenbergen, L. W., Pitlick, J. C., Rais, S., Bradley, J. B. & Julien, P. Y., Direct Measurements of Secondary Currents in a Meandering Sand-Bed River, *Nature*, Vol 315, pp746-747, 27 June 1985

van Rijn L.C. Equivalent Roughness of an Alluvial Bed. *Journal of Hydraulic Engineering, ASCE*, Vol 108, No10 pp 1215-1218, 1982

van Rijn L.C. Sediment transport, Part 1: bed-load transport. *Journal of Hydraulic Engineering, ASCE*, Vol 110, No10 pp1431-1456, 1984a

van Rijn L.C. Sediment transport, Part 2: suspended-load transport. *Journal of Hydraulic Engineering, ASCE*, Vol 110, No10 pp1431-1456, 1984b

van Rijn L.C. Sediment transport, Part 3: Bedforms and Alluvial roughness. *Journal of Hydraulic Engineering, ASCE*, Vol 110, No12 pp 1733-1754, 1984c

Wark, J.B. James, C.S. and Ackers P. Design of straight and Meandering compound channels, Interim guidelines on hand calculation methodology. R&D Report 13, HRWallingford, 1994

Willetts, B. B. & Hardwick, R. I., Model Studies of Overbank Flow from a Meandering Channel, *Proceedings of International Conference on River Flood Hydraulics, Wallingford*, Ed. W. R. White, pp197-205, September 1990

Willetts, B. B. & Hardwick, R. I., Stage Dependency for Overbank Flow in Meandering Channels, *Proceedings of the ICE - Water, Maritime & Energy*, Vol 101, pp45-54, March 1993

Yang, C.T., Incipient Motion and Sediment Transport, *J.Hydraulics Division* ASCE 99 (HY10), pp 1679-1704, October 1973.

Yang, C.T., Unit Stream Power Equation for Gravel, *J.Hydraulics Division* ASCE 99 (HY10), pp 1783-1798, December 1984.

Yang, C.T., (1996) Sediment transport, McGrawHill

Yalin, M. S., Theory of Hydraulic Models, Macmillan Press Ltd, 1971

Yalin, M.S., River Mechanics, Pergamon Press 1992

Zhou, G. & Zou, J (1997). Advances in measuring techniques of bed load. Int. J. Sed. Research

Appendix 1: Processing of velocities -technical comments

The following section describes the process of obtaining reliable visual representations and volume calculations from the Series C mixed grain data.

Recording Method

Velocities were recorded using a Nortek "Acoustic Doppler Velocimeter" (ADV). The velocity collection routine is described in detail in Chapter 3 including descriptions of probe orientation and a discussion of the issues of data quality. The data was processed to give 60s averages of velocity, signal to noise ratio and correlation values used with correlation > 50 and signal to noise ratio > 5.

Determining the position of the bed.

In the majority of tests, velocities were recorded over a mobile bed. Around 100 point velocities were measured in each cross section and two probes were used. As each point was measured for 60 s and there was a period of time during which the probes were exchanged. Thus the recording time for each cross section was approximately two hours. Due to this time interval the position of the bed may have a changed slightly and it is certainly likely to have moved since the previous bed profile at that section was recorded on a dry bed. It was on these profiles that the probe measurements were based. A method is thus required to find the position of the bed relevant to when the velocities were recorded.

Three sets of data are useful in determining the bed position: The velocity, the correlation and the signal to noise ratio. In most cases the logarithmic zone is extremely small as the flow is dominated by secondary currently, consequently it is very hard to use the velocity profile shape to find the position of the bed. In regions where the bed has risen however the velocity falls to zero once the sample volume is within the bed. It can also be seen that the signal to noise ratio rises significantly in the saltation zone immediately above the bed

The correlation may be used when the bed has scoured in the following way. When the sampling volume is a certain distance from the bed, determined by the velocity range, the correlation drops due to interference from the boundary. If this distance is know then the distance to the bed can bed determined from the position at which the correlation drops. By observing the pattern of correlation in verticals where the bed can be determined by the velocity profile and signal to noise ration, the interface zone can be used to find the bed in places where this is not possible.

Using these indicators the position of the bed can be determined to +/- 2.5mm.

Determining the velocity at the surface.

Velocities in the top 40mm of the flow could not be obtained due to the geometry of the probes. In order to estimate the surface velocities the velocity gradient between the top two points has been extrapolated to the surface. The results were subsequently checked visually to make sure that they were reasonable. Results such as discharge measurements obtained from this section must clearly be treated with caution.

Visual presentation of flow structure

Gridding.

As the point velocity data collected was not spaced at regular intervals in the vertical direction, a gridding routine was used to calculate the value of mainstream velocity at regularly distributed grid nodes. The interpolation method chosen was the Kriging method, recommended by the software package developers, because it gave results most consistent with the underlying data. This consistency can be checked using the "residuals" feature which gives the difference between the gridded data and the original data points.

The grid was set at a spacing of 50mm in the y direction and 20 mm in the z direction.

There are two major difficulties in obtaining a realistic grid file over the surface. Firstly the gridding methods give weight to the influence of data points within the search ellipse on the basis of their distance from the grid node under consideration, this is known as weighted averaging. This is entirely appropriate for randomly distributed data. However, the spacing between the data points under consideration was much larger in the y direction than the z direction.

The second problem and the reason for this uneven distribution of grid points, is the logarithmic nature of the boundary layer. The values of velocity vary non-linearly in the z direction reducing rapidly as they reach the bed.

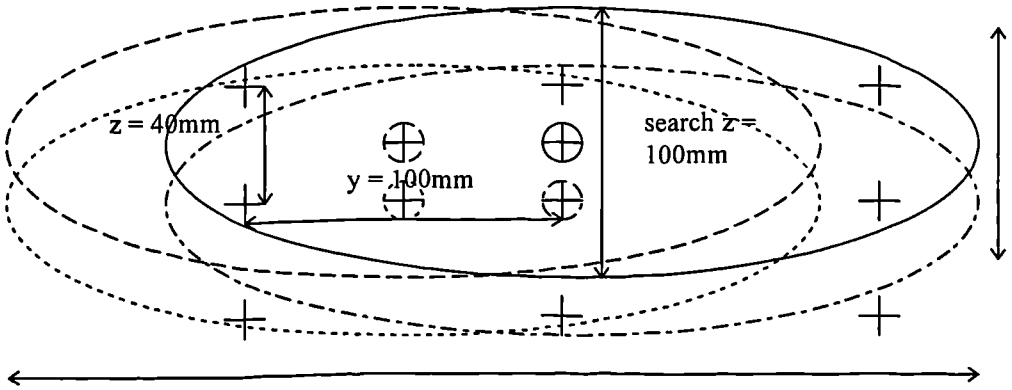

The problem of unequally spaced data points is acknowledged in the software. In order to avoid a bulls eye pattern developing around the data points due to their anisotropy, a flattened search ellipse and an equivalent anisotropy factor may be specified. The figure above shows data points spaced at 40mm separation in the z axis and 100 in the y axis. Our data was spaced at 100mm in the y direction and 10 mm separation for the bottom 60mm and 20 mm above this however as some data is missing due to poor quality or difficulties in taking readings due to probe geometry a 40mm spacing gives a worst case scenario. The shape of the search ellipse is mirrored by the anisotrophy factor of 2.5 which adds weight to points in the y direction - see diagram

The grids all tend to reduce the gradient at the boundary. A more realistic grid may be achieved by placing velocity values below zero outside the boundary.

The search ellipse can be divided into quadrants of which a specified number must be filled. This means that the grid node will obtain data from all around it rather than from just one direction. To achieve this there should be at least 3 quadrants represented for each node The maximum number of data points in the ellipse is 15, for a node in the boundary layer. Thus we may specify 4 points per sector, a minimum total data of 3 and the maximum number of empty sectors as 1. (Further investigation of this method has shown that in order to grid successfully the layer closest to the water surface a minimum number of two data points and a maximum number of empty sectors of two is appropriate.)
As a full investigation of the variograms on which the Kriging method is based proved too time consuming, the default linear variograms were used.

Contouring

The grid resulting from the process described above may then be contoured to divide the cross section into velocity regions. The dividing lines of constant velocity will be referred to as isovels. The velocity regions have been shaded consistently throughout so that different cross sections may be directly compared. The lines have been slightly smoothed to remove sharp edges. Corragated effects at the bed and in the flow are due to the imbalance on the grid spacing not wholly avoided by the anisotropy factor. Data point positions have been pasted over the maps to avoid spurious conclusions obtained from regions of absent or synthesised data (I have not done this yet).

Secondary circulation - surfer/excel

The secondary circulation is presented in two formats, the traditional method in which only the velocities in the cross stream direction are shown and also presenting each velocity as a vector arrow, giving size and direction.
In some tests only the former is given due to the unavailability of vertical velocity data in the majority of each section.

3D view - excel

This chart is intended to help visualise the behaviour of the flow around an apex bend and should be useful for tying in the other presentations. The program written by the author to construct this plot is found in module fplot of vels.xls

Discharge calculation

In calculating flow discharge we are interested in the flow down the main channel in total and the flow below the bankfull level. This will allow us to compare with the predictions of the James and Wark method and give some scope for the development of a simple sediment transport formula.

The discharge may be calculated from the grid. Surfer uses the available data to produce a grid of velocity readings. (It is possible to check the accuracy of this grid by comparing the actual values and the equivalent grid values). Using this grid we obtain a number of cells each of which has a velocity value at each corner. The program calculates the volume of the column up to the lowest velocity reading and then adds an approximation for the volume of the prism above the column.

The total volume is then calculated using the incremental volumes by applying numerical approximations such as Simpson's rule, Simpson's 1/3rd rule and the trapezoidal rule. These methods can be compared - the closer they are together the more confidence may be placed in the results.

Sources of error lie in the data values, areas in which data could not be obtained, particularly large shallow areas, and in the numerical procedure of gridding and calculation. Clearly the subject of the main stream direction has not been breached and this may account for the discrepancies.

Appendix 2: Simulating vegetative roughness in physical models

A number of methods of roughening have been used in scale river models. Two roughness methods are described below. The first, rod roughness has been widely used in two stage channel tests. The second, expanded aluminium strips, was designed for use for the mixed grain series C tests on the flood channel facility. In the following analysis a friction factor, Darcy f, rather than Manning's n is used as the flow is smooth turbulent on the floodplain and thus not independent of Reynolds number. The strengths and weaknesses of each method are considered.

Rod Roughness

A full analysis of rod roughening is given by Ackers (1989). The main points are summarised below: Seven tests were performed in a straight 50m x 1.5m flume at a bed slope of 1/1000 to provide data for calibration of an expression for rod roughness. The tests were performed at flow depths between 44mm and 119mm. The rods were distributed in a triangular pattern based on an angle of 60°. The frames tested had a density of 12 rods per m^2, $\Delta_1/d = (310/25)$, $\Delta_2/d = (268.5/25)$

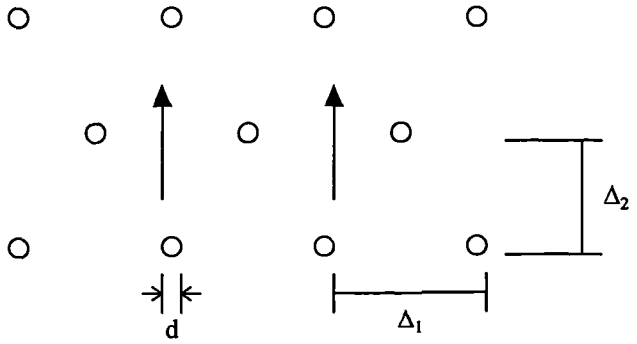

Figure A2. 1. Layout of rods used on the Flood Channel Facility

Bed resistance was derived by experiment and may be expressed, in the form derived by Keulegan (1938), as

$$1/\sqrt{f_s} = 2.02\log\left(\mathrm{Re}\sqrt{f_s}\right) - 1.38 \qquad (A2.1)$$

Flow resistance due to the rods can be attributed to a number of physical processes, but predominantly form drag. The resistance force due to form drag is given by

$$F_{ROD} = C_D \rho g d z \alpha \frac{\bar{u}^2}{2g} N_L \qquad (A2.2)$$

(adjust all to unit bed area)
where
F_{ROD} = the form drag of the rods per unit bed area
C_D = the drag coefficient
N_L = number of rods per unit channel length

d = diameter of rods
z = flow depth
α = velocity distribution coefficient
$\overline{u}$ = the mean velocity over the flow depth

The velocity distribution coefficient allows for the variation of velocity over the length of the rod, i.e. the depth of flow. The depth mean velocity per unit width $\overline{u}$ is calculated allowing for the blockage of the transverse rows of rods:

$$\overline{u} = \frac{q}{z - rzd} \qquad (A2.3)$$

Where q = discharge per unit width, r = number of rods in each row.

On this basis, a blockage coefficient, β, may be defined

$$\beta = \left(\overline{u}/\overline{v}\right)^2 = \left(1 - rd\right)^{-2} \qquad (A2.4)$$

where $\overline{v}$ = approach velocity.
The total drag per unit length of channel is given by assuming that bed and rod roughness are additive, thus substituting Equations A2.3 and A2.4 into Equation A2.2 and using the roughness obtained for the smooth bed f_s we can write:

$$F_t = \beta\rho\,\overline{v}^2\left(\alpha dz\frac{C_D}{2}N_L + f_s P/8\right) \qquad (A2.5)$$

where P = wetted perimeter of channel = 1 for unit area.
The drag equation can be converted into a conventional form of resistance equation using the force balance equation

$$F_t = \rho gAS = \rho gRSP \qquad (A2.6)$$

Where,
S = channel gradient
R = hydraulic mean depth, A/P

$$f_t = 8gRS/\overline{v} = \beta\left[4\left(N_L dz\right)\alpha C_D + f_s\right] \qquad (A2.7)$$

Where f_t = overall friction factor per unit area of bed.

C_D is the only unknown and hence may be found by experiment. When using Equation A2.7 in the reverse direction with f_t or $\overline{v}$ unknown then iteration is required as f_t depends on the overall Reynolds number.

Expanded metal strip roughness

A new method of roughening the floodplain was used on the FCF series C mixed grain tests. Expanded aluminium sheet was folded to form "tent" shaped roughness elements 100mm high. These were placed at regular intervals perpendicular to the floodplain slope.

In order to establish the basic resistance function for the frames a series of calibration tests were conducted in a 300 mm wide flume over a range of depths from 20 mm to 120 mm. This includes the range of flow depths used during the main tests on the flood channel facility.

The tests also examine the effect of varying the spacing of roughness elements with spacing ranging from 50 mm to 200 mm; the 50mm spacing was used on the FCF.

The channel bed, walls and the roughness elements caused resistance to the flow in these tests. It is assumed in the analysis that the presence of the frames does not affect the roughness of the flume boundaries. In a similar way to the rods, variation in the vertical velocity field is adjusted using a suitable distribution coefficient.

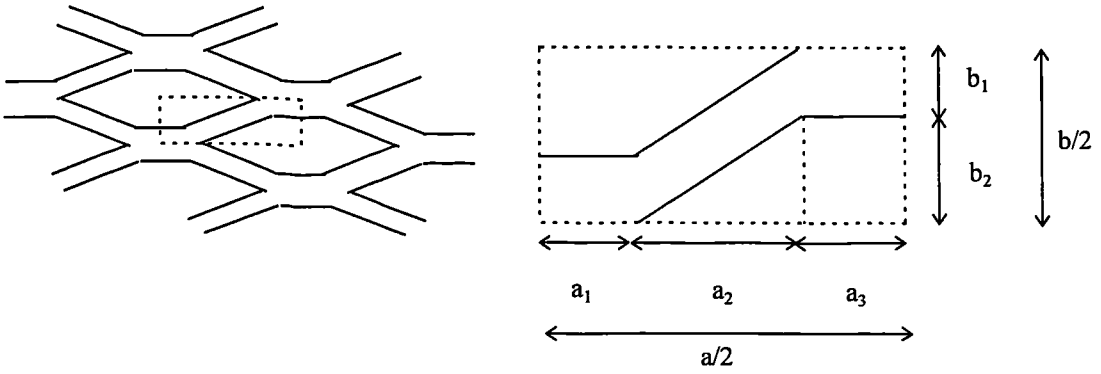

Figure A2. 2. Geometry of the expanded aluminium

The aluminium mesh is structured as shown. A_0, the orifice area is given by

$$A_0 = 4(a_3 b_2) + 2(a_2 b_2) \qquad (A2.8)$$

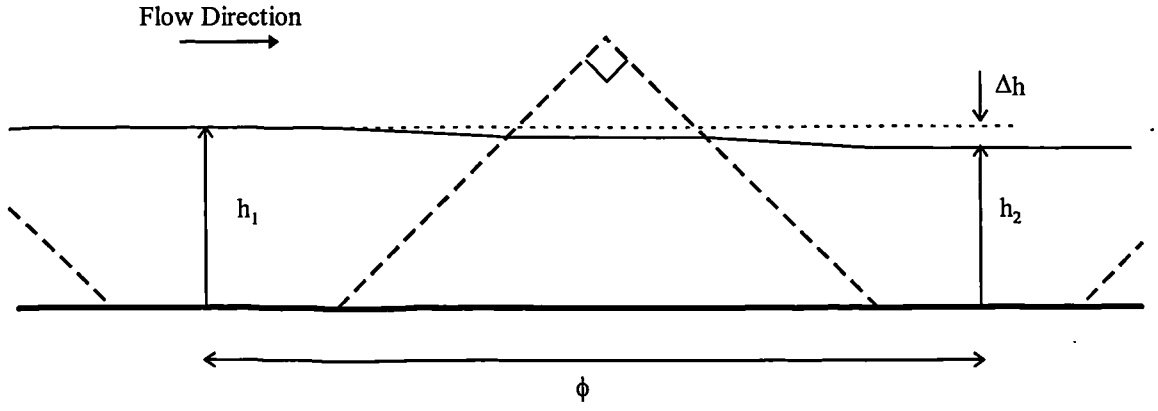

Figure A2. 3. Schematic diagram for flow through roughness frames

Where Φ denotes the spacing between frames.

The analysis of the roughness frames is based on the Klassen and Zwaard (1974,1985) analysis of hedgerows. Consider the inclined face of a roughness frame facing into the flow. The frame may be considered a grid of orifices. As they are staggered, the head is lost gradually, reducing afflux interference. Taking one orifice,

$$h_1 + \frac{V_1^2}{2g} = h_c + \left(\frac{aV_c^2}{2g}\right) \qquad (A2.9)$$

Where subscript c indicates values at the *vena contracta.*

Rearranging, this gives

$$V_c = C_O\sqrt{\left(\Delta h + \frac{V^2}{2g}\right)} \qquad (A2.10)$$

Where C_0 accounts for jet contraction as the flow passes through the orifices, including angle of attack effects.

Considering total flow through a frame per metre width

$$q = AV = \text{reduced flow area} * V_c = \frac{z}{b}\frac{1}{a}A_0C_O\sqrt{2g\left(\Delta h + \frac{V^2}{2g}\right)} \qquad (A2.11)$$

as the number of orifices increases with increasing flow depth it would seem likely that

$$C_O = f(z/b) \qquad (A2.12)$$

where b is the depth of one orifice. Writing $pA=(z/ba)A_0$ and rearranging Equation A2.11 gives

$$C_Op = \sqrt{\frac{1}{1+\left(\frac{2g\Delta h}{V^2}\right)}} \qquad (A2.13)$$

where Δh is the head drop due to the frames

In order to isolate the effects of the frames, the resistance due to the bed and walls of the flume must be accounted for. The effect of the walls is removed using the Vanoni and Brookes method (1959). The bed roughness has been accounted for using experimental and theoretical techniques

The value of C_0 appears to increase regularly up to a relative flow depth of 0.75. From observation it appears that this is due to interference between the two frames; the separation decreases as the flow depth increases.

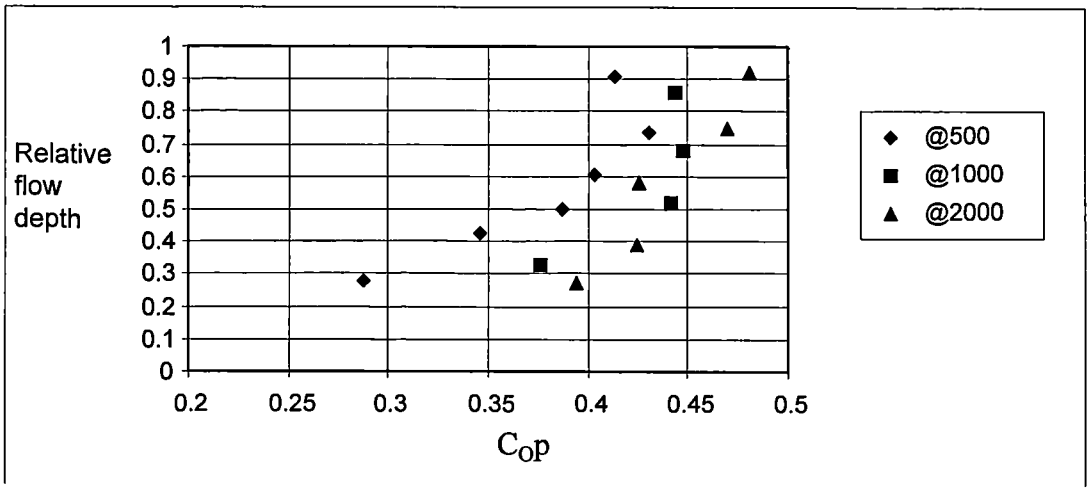

Figure A2. 4. Variation of Discharge coefficient with relative flow rate

For relative flow depths below 0.75, writing R= z for a wide floodplain, $S_e = \Delta h/\phi$ and substituting Equation A2.10 into the Darcy Weisbach Friction formula gives

$$f_e = \frac{8gRS_e}{V} = \frac{4Vz}{\phi}\left(\frac{1-p^2C_O{}^2}{p^2C_O{}^2}\right) \qquad (A2.\ 14)$$

Where $C_O p$ is given by 0.43y/z +0.44 or can be read off Figure A2.4

and

$$f_t = \frac{4Vz}{\phi}\left(\frac{1-p^2C_O{}^2}{p^2C_O{}^2}\right) + f_s \qquad (A2.\ 15)$$

where f_s is the bed surface roughness.

For the FCF, the equation for the smooth mortar channel wall roughness determined during the Series A tests and recommended for future analysis is given by

$$1/\sqrt{f_s} = 2.02\log\left(\mathrm{Re}\sqrt{f_s}\right) - 1.38 \qquad (A2.\ 16)$$

where,

f_s = the friction factor arising form the drag on the channel perimeter

Re = the Reynolds number of the flow as a whole

Example

To model non submerged densely planted floodplain vegetation:

Obtain values for roughness in terms of Darcy f and average velocity at a range of stages. Use Froudian scaling laws to obtain these values at the desired scale. Enter these values into Equation A2.14 to obtain the appropriate strip spacing. If the spacing is above or below the acceptable range, defined by accessibility at the bottom end and model geometry at the top end, then use a larger or smaller mesh size.

The chart shows the stage roughness curve derived by experiment by Ree (1958) for flow through sorghum, Redlan Kafir. For one point on the stage roughness curve,

	Prototype	1:5 Model
z	= 0.28m	0.056m
n	= 0.056	
f	$= 8gn^2/R^{1/3} = 0.376$	= 0.376
V	$= R^{2/3} S^{1/2}/n = 0.33$ ms-1	= sqrt(Lr)Vp = 0.150 ms-1
R	= UL/v = 64166	= 5833
fs	not applicable	by equation = 0.043
Φ	not applicable	by equation = 0.52m

Table A2. 1. Scaling vegetative roughness

This analysis may be extended to modelling hedges on the floodplain.

Summary of physical modelling methods

Factor	**Strips**	**Rods**
Similarity to real vegetation	Discrete lines (hedges, crops, vineyards etc.)	Distributed roughness (Forests)
Cost	c.£4 / m2	c.£20 / m2
Time to Build	low	high
Access to model	Can step between frames	Can walk on frames if built on a grid
Ease of varying roughness	Decreasing or increasing spacing changes roughness - very flexible	Selective removal of rods can decrease roughness - low flexibility

Table A2. 2. Summary of factors involved in choosing a method of physically modelling vegetation roughness

Conclusions

Manning's n for a floodplain is a complex function of flow depth and velocity, vegetation type, density, dimensions and flexibility that in turn are functions of age and season. A single value of Manning's n is hence inappropriate if accurate results are desired.

Improvements in evaluation require more time and money for data collection and analysis than resistance prediction based on tables and photographs.

Theoretical methods exist and, if general rules can be substantiated, may be useful in the future. However, further empirical tests are required before they can be used with confidence. Until this is done however estimations may be incorrect by more that 10%. This figure must be reduced if other improvements in estimation of flood flows resulting from the work on two stage channels are to come to fruition.

In order to represent correctly floodplain vegetation in a physical model, the roughening materials used must give a correctly scaled stage roughness curve and operate under the same flow regime.

The new form of roughness may be used to achieve the above whilst improving on previous methods in terms of: cost, accessibility, adjustably and ease of placement.

Appendix 3: Methods of calculating channel discharge

The calculation of F*

The calculation of zonal discharges using boundary roughness

	Tot. Dis.	Zonal Discharges m^3/s				Zone 1										
	QT	Q1	Q2	Q3r	Q3l	A	P	B	s	So	S	Ss	n1	n'	R	V
Units	m^3/s	m^3/s	m^3/s	m^3/s	m^3/s	m^2	m	m								m/s
Trapezoid	0.64	0.097	0.433	0.056	0.056	0.218	1.724	1.6	1.344	0.00182	0.001353	1	0.018	0.021	0.1262	0.440569
HORW	0.15	0.097	0.040	0.005	0.005	0.208	1.896	1.6	1.344	0.00182	0.001353	1	0.018	0.021	0.1096	0.401136
LORW	0.12	0.097	0.019	0.002	0.002	0.214	1.874	1.6	1.344	0.00182	0.001353	1	0.018	0.021	0.1141	0.411914
HOSW	0.52	0.097	0.339	0.044	0.044	0.236	1.901	1.6	1.344	0.00182	0.001353	1	0.018	0.021	0.1243	0.436162
LOSW	0.19	0.097	0.070	0.009	0.009	0.220	1.824	1.6	1.344	0.00182	0.001353	1	0.018	0.021	0.1207	0.427835

	Zone 2						Zone 3 [Right (r) and Left (l) floodplains]							
	W2	y2	A2	P2	n2	R2	A3r	P3r	R3r	n3r	A3l	P3l	R3l	n3l
Units	m	m	m^2	m			m^2	m			m^2	m		
Trapezoid	7.6	0.08	0.61	6	0.013	0.101	0.096	1.28	0.075	0.013	0.096	1.28	0.075	0.013
HORW	7.6	0.07574	0.58	6	0.13	0.096	0.091	1.2757	0.071	0.13	0.090888	1.276	0.071	0.13
LORW	7.6	0.04248	0.32	6	0.105	0.054	0.051	1.2425	0.041	0.105	0.050976	1.242	0.041	0.105
HOSW	7.6	0.06903	0.52	6	0.013	0.087	0.083	1.269	0.065	0.013	0.082836	1.269	0.065	0.013
LOSW	7.6	0.02684	0.20	6	0.013	0.034	0.032	1.2268	0.026	0.013	0.032208	1.227	0.026	0.013

2.09

The calculation of F*

	QT Predicted	QT Measured	F*	Floodplain Depth	Depth Ratio
Units	m^3/s	m^3/s		m	
HORW	0.15	0.164	1.12	0.076	0.34
LORW	0.12	0.12	0.99	0.042	0.22
HOSW	0.52	0.449	0.86	0.069	0.32
LOSW	0.19	0.164	0.88	0.027	0.15

Data
Calculation

Application of the James and Wark Method

	Main Channel												Inner Floodplain						Outer Floodplain					
Units	A m^2	P m	B m	s	So	S	Ss	n1	n'	R	V m/s	Qbf m^3/s	W2 m	y2 m	A2 m^2	P2 m	n2	R2	A3 m^2	P3 m	R3	n3	A4 m^2	P4 m	R4	n4
example	5.07	6.4	6.1	1.37	0.001	0.001	1.54	0.025	0.029	0.79219	0.943607	4.784	49.4	1.2	47.77	37.94	0.045	1.259	16.28	18.9	0.861376	0.045	8	21	0.381	0.045
Trapezoid	0.2175	1.724	1.6	1.344	0.002	0.001	1	0.018	0.021	0.12616	0.440569	0.096	7.6	0.08	0.608	7.88	0.013	0.077	0.096	1.28	0.075	0.013	0.096	1.28	0.075	0.013
HORW	0.20786	1.896	1.6	1.344	0.002	0.001	1	0.018	0.021	0.10961	0.401136	0.083	7.6	0.076	0.5756	7.88	0.13	0.073	0.091	1.276	0.071243	0.13	0.091	1.276	0.071	0.13
LORW	0.21377	1.874	1.6	1.344	0.002	0.001	1	0.018	0.021	0.11405	0.411914	0.088	7.6	0.042	0.3228	7.88	0.105	0.041	0.051	1.242	0.041028	0.105	0.051	1.242	0.041	0.105
HOSW	0.23629	1.901	1.6	1.344	0.002	0.001	1	0.018	0.021	0.12427	0.436162	0.103	7.6	0.069	0.5246	7.88	0.013	0.067	0.083	1.269	0.065275	0.013	0.083	1.269	0.065	0.013
LOSW	0.220	1.824	1.6	1.344	0.002	0.001	1	0.018	0.021	0.12073	0.427835	0.094	7.6	0.027	0.204	7.88	0.013	0.026	0.032	1.227	0.026253	0.013	0.032	1.227	0.026	0.013

	Calculation of zone 1 discharge										Calculation of zone 2 Discharge													
Units	Q1' (4.3)	Q1' (4.	B^2/A	y'	m	f'	K	c	Q1'	Q1	V2	L (m)	f2	F1	F2	Csl	Cwd	Csse	Cssc	h	y2/(y2+h)	Kc	Ke	Q2 m^3/s
*example	-1.44	0.935	7.34	1.444	0.366	2.776	0.762	0.534	0.935	4.47443	0.93	91.67	0.147	0.73	0.978571	1.753	0.837	0.7298	0.384	0.831	0.590799	0.217	0.302	44.55
Trapezoid	0.00543	0.848	11.77	0.589	0.361	0.595	1.059	0.6	0.848	0.0813	0.57	91.67	0.031	1.00	0.96	1.5789	0.925	0.8246	0.6	0.136	0.370478	0.375	0.806	0.347
HORW	0.0147	-2.802	12.32	0.583	2.2	57.81	-6.72	0.608	0.015	0.00123	0.06	91.67	3.173	1.00	0.96	1.5789	0.936	0.8246	0.6	0.13	0.368295	0.41	0.85	0.033
LORW	0.46267	-2.533	11.98	0.318	1.828	46.34	-5.16	0.603	0.463	0.04074	0.05	91.67	2.51	1.00	0.96	1.5789	0.93	0.8246	0.6	0.134	0.241243	0.419	1.065	0.016
HOSW	0.21004	0.783	10.83	0.467	0.348	0.622	1.055	0.588	0.783	0.08074	0.52	91.67	0.033	1.00	0.96	1.5789	0.907	0.8246	0.6	0.148	0.318537	0.387	0.881	0.273
LOSW	0.67049	0.685	11.62	0.195	0.367	0.844	1.025	0.599	0.685	0.06457	0.28	91.67	0.045	1.00	0.96	1.5789	0.922	0.8246	0.6	0.138	0.163164	0.447	1.232	0.058

	Tot. Dis.	Zonal Discharges m^3/s			
Units	QT m^3/s	Q1 m^3/s	Q2 m^3/s	Q3 m^3/s	Q4 m^3/s
*example	65	4.5	44.5	12.3	3.5
Trapezoid	0.54	0.081	0.347	0.056	0.056
HORW	0.04	0.001	0.033	0.005	0.005
LORW	0.06	0.041	0.016	0.002	0.002
HOSW	0.44	0.081	0.273	0.044	0.044
LOSW	0.14	0.065	0.058	0.009	0.009

data
Contraction coefficient

*The example given is that included in:
"The Design of Straight and Meandering Compound Channels"
J.B. Wark, C.S. James and P. Ackers
HR Wallingford, R&D report 13
In which this method is presented.

Application of the Momentum Method

	Main Channel														Inner Floodplain							
	A bf avg	Aob	A all	lamda	P avg	B	r	So	S	Ss	n1	n'	R		W2	y2	A2	P2	n2	R2	V	Qfp
Units	m^2	m^2	m^2	m	m	m								0.41	m	m	m^2	m			m/s	
example	5.07	7.32	12.39	91.7	6.4	6.1	1.37	0.0014	0.00102	1.54	0.025	0.029	1.9359	0.41	43.3	1.2	40.45	43.3	0.045	0.93418	0.794582	32.14
HORW	0.207857	0.12118	0.329	14.693	1.896	1.6	1.344	0.001818	0.00135	1	0.018	0.021	0.1096	1	5.9	0.076	0.447	5.9	0.134	0.07574	0.056964	0.025
LORW	**0.214**	**0.06797**	**0.2817**	14.693	**1.874**	**1.6**	**1.344**	**0.001818**	**0.00135**	**1**	**0.018**	**0.021**	**0.1141**	1	5.9	**0.042**	**0.251**	5.9	**0.106**	**0.04248**	0.048974	**0.012**
HOSW	0.236287	0.11045	0.3467	14.693	1.901	1.6	1.344	0.001818	0.00135	1	0.018	0.021	0.1243	1	5.9	0.069	0.407	5.9	0.013	0.06903	0.551951	0.225
LOSW	**0.220**	**0.04294**	**0.2632**	14.693	**1.824**	**1.6**	**1.344**	**0.001818**	**0.00135**	**1**	**0.018**	**0.021**	**0.1207**	1	5.9	**0.027**	**0.158**	5.9	**0.013**	**0.02684**	0.294034	**0.047**

	Outer Floodplain								
	A3	P3	R3	n3	Q3	A4	P4	R4	n4
Units	m^2	m				m^2	m		
example	16.28	18.9	0.8614	0.045	12.25	8	21	0.38095	0.045
HORW	0.090888	1.27574	0.0712	0.134	0.005	0.091	1.27574	0.07124	0.134
LORW	**0.050976**	**1.24248**	**0.041**	**0.106**	**0.002**	**0.051**	**1.24248**	**0.04103**	**0.106**
HOSW	0.082836	1.26903	0.0653	0.013	0.044	0.083	1.26903	0.06528	0.013
LOSW	**0.032208**	**1.22684**	**0.0263**	**0.013**	**0.009**	**0.032**	**1.22684**	**0.02625**	**0.013**

		Tot. Dis.	Zonal Discharges m^3/s										
		QT	Q1		Q2	Q3	F	F/Arg		u1			
Units		m^3/s	m^3/s		m^3/s	m^3/s							
example		**67.177**	19.28	-0.886	32.14	12.25	-21.53	-0.00018	0.00	1.56			
HORW	0.164	**0.154**	0.119	0.114	0.025	0.005	-0.82	-0.00025	0.000	0.361	0.119	0.109	9.106
LORW	**0.12**	**0.126**	**0.109**	**0.083**	**0.012**	**0.002**	-0.44	-0.00016	0.000	**0.387**	**0.109**	0.083	31.43
HOSW	0.44	**0.460**	0.147	0.134	0.225	0.044	-0.24	-0.00007	0.000	0.425	0.147	0.138	6.680
LOSW	**0.16**	**0.165**	**0.100**	**0.094**	**0.047**	**0.009**	-0.75	-0.00029	0.000	**0.379**	**0.100**	0.086	16.06

Appendix 4: Sediment transport formulae

Prediction of total bed material load using the Ackers and White (1973) formulae incorporating Acker's 1993 update

The sediment concentration by volume is calculated from:

D depth (m)

S slope

U mean velocity (m/s)

d_i grain size of which i% of grain size is finer (mm)

s specific gravity of particles (can be taken as 2.65 for sand)

and ν, kinematic viscosity (it can be calculated from temperature, Appendix 1)

1. Calculate dgr , the dimensionless particle size

$$d_{gr} = d\left[\frac{g(s-1)}{\upsilon^2}\right]^{1/3} \qquad (A4.\ 1)$$

2. The values of the parameters have been recalculated and appear in Ackers 1993 as

for d_{gr}>60, coarse sediment (d>2mm)

n = 0, A_{gr} = 0.17, m = 1.78 and C = 0.025

for 1<dgr<60 (transitional and fine sediments,0.06<d<2 mm)

$$n = 1.00 - 0.56 \log d_{gr} \qquad (A4.\ 2)$$

$$A = 0.14 + 0.23/\sqrt{d_{gr}} \qquad (A4.\ 3)$$

$$m = 1.67 + 6.83/d_{gr} \qquad (A4.\ 4)$$

$$\log C = -3.46 + 2.79 \log d_{gr} - 0.98(\log d_{gr})^2 \qquad (A4.\ 5)$$

3. $u^* = (gDS)^{0.5}$ (A4. 6)

4. Calculate the grain shear velocity, u.' from the equation

$$\frac{U}{U_*'} = 5.66 Log\left(\frac{10D}{d}\right) \qquad (A4.\ 7)$$

4. Calculate mobility number, Fgr from the equation

$$F_{gr} = \frac{U_*^n U_*'^{n-1}}{\sqrt{[g(s-1)D]}} \qquad (A4.\ 8)$$

5. Calculate Ggr from equation:

$$G_{gr} = C\left[\left(F_{gr} - A_{gr}\right)/A_{gr}\right]^m \qquad (A4.\ 9)$$

(Note: if G gr is negative then there is no sediment movement and X AW 0)

6. And finally calculate Q_s) the sediment concentration, from

$$G_{gr} = \left(\frac{Qs}{Q}\frac{D}{d}\right)\left(\frac{U^*}{U}\right)^n \qquad (A4.\ 10)$$

There was originally no provision for calculation of mixed grain sediments. The equation may be used for mixed grain sediments. However by splitting the bed material into fractions, calculating the transport rate of each fraction and weighting each concentration by the proportion by weight of each fraction in the bed. Thus

$$C_{\text{mix}} = \sum pC_i \qquad (A4.\ 11)$$

Where C is sediment concentration and p is the percentage by weight of the mixture represented by grain size d_i.

Directions for using spread sheet,

1. Split bed sample into five fractions and enter the mean diameter for each fraction and the d35 for the whole sample into the sediment properties box. The values of n, A, m and C are calculated using the formulae noted above.
2. Enter the proportion by weight, β into the sediment properties box
3. Input flow and channel properties into the columns noted in the data box

The spreadsheet will give the sediment concentration for single representative diameter and a mixed grain calculation based on the proportion by weight of each fraction in the bed.

Ackers White Sediment Transport Calculations

Sediment Properties - From Averaged Profile							
Fraction i		1	2	3	4	6	d35
d mm		0.27	0.51	1.25	2.2	3.6	0.61
d (m)	d(mm)/1000	0.00027	0.00051	0.0013	0.0022	0.0036	0.00061
β	From Grading Curve	20	20	20	20	20	20
∞	From Chart (sf = 0.7)	0.025	0.05	0.12	0.2	0.26	0.26
dgr	d35(g(s-1)/v^2)^(1/3)	6.26	11.82	28.98	51.00	83.45	14.14
n	if dgr<60, 1-0.56log (dgr), if dgr>60, 0	0.55	0.40	0.18	0.04	0.00	0.36
A	if dgr<60, 0.14+0.23/dgr^0.5, if dgr>60, 0.17	0.23	0.21	0.18	0.17	0.17	0.20
m	if dgr<60, 1.67+6.83/dgr, if dgr>60, 1.78	2.76	2.25	1.91	1.80	1.78	2.15
log C	if dgr<60, -3.46+3.79 log dgr-0.98(log dgr)^2	-1.860	-1.595	-1.478	-1.553	-1.717	-1.547
C	dgr>60, 0.025	0.014	0.025	0.033	0.028	0.025	0.028

Data	
Qa	From point velocities
Aa	From profile
Ua	Qa/Aa
P	From profile
R	Aa/P
S	Main channel slope

Formulae	
Ua*	gRS
Ua'*	Ua/(32^0.5(Log(10d/D))
ks	1.25 d35
Fi	Ua*^n/(gd(s-1))^0.5 (Ua/(32^0.5 Log (10 R/d)))^(1-n)
Gi	C (Fi/Ai-1)^m
Xi	Gi s d / R (Ua/Ua')^n
Qs	Qa. R. sum i=1 to n, Xiβi

Test: **BFMB**
Depth above bankfull: -7 mm
Discharge measured: 0.097 m³/s
Dischage calculated by summation of velocities

Section	Discharge (m³/s)			Areas (m²)				Velocities (m/s)										Mobility Number						Non-dimensional Transport rate						Sediment Transport = Mass flux of solid / Mass flux of liquid						Mix	Single
	Main channel Qa	Below BF Qbf	Above BF	Main channel Aa	Below BF Abf	Above BF	actual	Main channel Ua	Below BF Ubf	Above BF Ua-bf	P (m)	R	S	Ua* (m/s)	Ua'* (m/s)	d35 (mm)	ks (mm)	F1	F2	F3	F4	F5	F35	G1	G2	G3	G4	G5	G35	X1	X2	X3	X4	X5	X35	Qs (g/s)	Qs (g/s)
g	0.097	0.0878	-			-	-			-	1.84																									
h	0.097	0.0858	-	0.229	0.229	-	-	0.42	0.38	-	1.89	0.12	0.00136	0.04009	0.023	0.61	0.7625	0.426	0.288	0.174	0.131	0.109	0.259	0.008	0.003	0	0	0	0.002	1.65E-04	8.79E-05	0.00E+00	0.00E+00	0.00E+00	5.95E-05	5.30	5.77
i	0.097	0.0953	-	0.293	0.293	-	-	0.33	0.33	-	2.07	0.14	0.00136	0.04336	0.017	0.61	0.7625	0.414	0.269	0.154	0.112	0.092	0.240	0.007	0.002	0	0	0	8E-04	1.11E-04	3.69E-05	0.00E+00	0.00E+00	0.00E+00	1.90E-05	2.87	1.84
j	0.097	0.0900	-	0.207	0.207	-	-	0.47	0.43	-	1.92	0.11	0.00136	0.03789	0.025	0.61	0.7625	0.443	0.310	0.197	0.153	0.128	0.281	0.011	0.005	0.0002	0	0	0.004	2.86E-04	1.80E-04	1.18E-05	0.00E+00	0.00E+00	1.43E-04	9.26	13.89
k	**0.097**	**0.0914**	-	**0.202**	**0.202**	-	-	**0.48**	**0.45**	-	**1.87**	**0.11**	**0.00136**	**0.03796**	**0.026**	**0.61**	**0.7625**	**0.462**	**0.318**	**0.203**	**0.169**	**0.134**	**0.289**	**0.012**	**0.006**	**0.0005**	**0**	**0**	**0.005**	**3.23E-04**	**2.16E-04**	**2.55E-05**	**0.00E+00**	**0.00E+00**	**1.76E-04**	**10.92**	**17.06**
l - o	Data not chosen		-			-	-			-																											
k (Qa+10%)	0.107	0.107	-	0.202	0.202	-	-	0.53	0.53	-	1.87	0.11	0.00136	0.03796	0.029	0.61	0.7625	0.484	0.349	0.231	0.185	0.158	0.319	0.017	0.011	0.0026	2E-04	0	0.009	4.96E-04	3.87E-04	1.29E-04	1.45E-05	0.00E+00	3.44E-04	19.93	36.66
k (Qa-10%)	0.087	0.087	-	0.202	0.202	-	-	0.43	0.43	-	1.87	0.11	0.00136	0.03796	0.024	0.61	0.7625	0.443	0.309	0.196	0.152	0.128	0.281	0.011	0.005	0.0002	0	0	0.004	2.70E-04	1.71E-04	1.05E-05	0.00E+00	0.00E+00	1.36E-04	8.77	11.88

Test: **LOSW**
Depth above bankfull: 26.84 mm
Discharge measured: 0.163 m³/s
Dischage calculated by summation of velocities

Section	Discharge (m³/s)			Areas (m²)				Velocities (m/s)																												Mix	Single
	Main channel Qa	Below BF Qbf	Above BF Qa-bf	Main channel Aa	Below BF Abf	Above BF Aa-bf	actual	Main channel Ua	Below BF Ubf	Above BF Ua-bf	P (m)	R	S	Ua* (m/s)	Ua'* (m/s)	d35 (mm)	ks (mm)	F1	F2	F3	F4	F5	F35	G1	G2	G3	G4	G5	G35	X1	X2	X3	X4	X5	X35	Qs (g/s)	Qs (g/s)
g - h	Data not collected																																				
i	0.0908	0.0762	0.0145	0.263	0.220	0.043	0.043	0.346	0.347	0.337	1.922	0.11	0.00136	0.039	0.019	0.65	0.8125	0.407	0.273	0.163	0.123	0.102	0.245	0.006	0.002	0	0	0	0.001	1.32E-04	5.46E-05	0.00E+00	0.00E+00	0.00E+00	3.26E-05	3.39	2.96
j	0.0844	0.0717	0.0128	0.258	0.209	0.049	0.043	0.327	0.342	0.281	1.911	0.11	0.00136	0.0382	0.018	0.65	0.8125	0.400	0.269	0.162	0.122	0.101	0.242	0.006	0.002	0	0	0	9E-04	1.22E-04	4.92E-05	0.00E+00	0.00E+00	0.00E+00	2.84E-05	2.89	2.40
k	**0.0788**	**0.0692**	**0.0096**	**0.263**	**0.220**	**0.043**	**0.043**	**0.300**	**0.314**	**0.226**	**1.824**	**0.12**	**0.00136**	**0.04009**	**0.016**	**0.65**	**0.8125**	**0.394**	**0.268**	**0.160**	**0.111**	**0.091**	**0.231**	**0.005**	**0.001**	**0**	**0**	**0**	**6E-04**	**9.21E-05**	**2.80E-05**	**0.00E+00**	**0.00E+00**	**0.00E+00**	**1.26E-05**	**1.89**	**0.99**
l	0.0821	0.0735	0.0087	0.291	0.248	0.043	0.043	0.282	0.296	0.204	1.876	0.13	0.00136	0.04196	0.015	0.65	0.8125	0.391	0.252	0.143	0.103	0.084	0.224	0.005	8E-04	0	0	0	3E-04	7.61E-05	1.82E-05	0.00E+00	0.00E+00	0.00E+00	8.28E-06	1.55	0.52
m	0.0886	0.0739	0.0128	0.291	0.248	0.043	0.043	0.297	0.297	0.298	1.991																										
n - o	Data not collected																																				
k (Qa+10%)	0.08670206	0.07611	0.0106	0.263	0.220	0.043	0.043	0.330	0.348	0.247	1.824	0.12	0.00136	0.04009	0.018	0.65	0.8125	0.411	0.274	0.163	0.121	0.100	0.245	0.007	0.002	0	0	0	0.001	1.28E-04	5.20E-05	0.00E+00	0.00E+00	0.00E+00	3.08E-05	3.12	2.67
k (Qa-10%)	0.07093805	0.06228	0.0087	0.263	0.220	0.043	0.043	0.270	0.283	0.202	1.824	0.12	0.00136	0.04009	0.015	0.65	0.8125	0.378	0.243	0.138	0.100	0.082	0.216	0.004	5E-04	0	0	0	1E-04	6.27E-05	1.18E-05	0.00E+00	0.00E+00	0.00E+00	2.59E-06	1.06	0.18

Test: **LORW**
Depth above bankfull: 42.48 mm
Discharge measured: 0.12 m³/s
Dischage calculated by summation of velocities

Section	Discharge (m³/s)			Areas (m²)				Velocities (m/s)																												Mix	Single
	Main channel Qa	Below BF Qbf	Above BF Qa-bf	Main channel Aa	Below BF Abf	Above BF Aa-bf	actual	Main channel Ua	Below BF Ubf	Above BF Ua-bf	P (m)	R	S	Ua* (m/s)	Ua'* (m/s)	d35 (mm)	ks (mm)	F1	F2	F3	F4	F5	F35	G1	G2	G3	G4	G5	G35	X1	X2	X3	X4	X5	X35	Qs (g/s)	Qs (g/s)
g	**0.0706**	**0.0630**	**0.0076**	**0.271**	**0.214**	**0.058**	**0.088**	**0.260**	**0.296**	**0.131**	**1.87**	**0.11**	**0.00136**	**0.03896**	**0.014**	**0.65**	**0.8125**	**0.378**	**0.247**	**0.143**	**0.106**	**0.086**	**0.220**	**0.004**	**6E-04**	**0**	**0**	**0**	**2E-04**	**6.88E-05**	**1.61E-05**	**0.00E+00**	**0.00E+00**	**0.00E+00**	**4.99E-06**	**1.20**	**0.36**
h	0.0963	0.0782	0.0181	0.345	0.280	0.065	0.088	0.279	0.279	0.278	1.88	0.15	0.00136	0.04451	0.015	0.65	0.8125	0.391	0.247	0.136	0.096	0.078	0.218	0.005	6E-04	0	0	0	1E-04	6.50E-05	1.19E-05	0.00E+00	0.00E+00	0.00E+00	2.83E-06	1.48	0.27
i	0.0868	0.0660	0.0208	0.295	0.228	0.067	0.088	0.294	0.290	0.308	2.08	0.11	0.00136	0.03818	0.016	0.65	0.8125	0.372	0.243	0.141	0.104	0.088	0.217	0.003	5E-04	0	0	0	1E-04	6.90E-05	1.44E-05	0.00E+00	0.00E+00	0.00E+00	3.74E-06	1.45	0.32
j	0.0641	0.0420	0.0221	0.203	0.125	0.078	0.088	0.316	0.336	0.283	1.94	0.09	0.00136	0.03461	0.018	0.65	0.8125	0.380	0.260	0.160	0.123	0.103	0.235	0.004	0.001	0	0	0	6E-04	1.08E-04	4.30E-05	0.00E+00	0.00E+00	0.00E+00	2.36E-05	1.94	1.51
k - o	Data not collected										1.88																										
g (Qa+10%)	0.0776	0.0693	0.0083	0.271	0.214	0.058	0.088	0.286	0.324	0.144	1.87	0.11	0.00136	0.03896	0.016	0.65	0.8125	0.394	0.262	0.154	0.115	0.095	0.234	0.005	0.001	0	0	0	6E-04	9.74E-05	3.35E-05	0.00E+00	0.00E+00	0.00E+00	1.68E-05	2.03	1.30
g (Qa-10%)	0.0635	0.0567	0.0068	0.271	0.214	0.058	0.088	0.234	0.265	0.118	1.87	0.11	0.00136	0.03896	0.013	0.65	0.8125	0.360	0.232	0.131	0.095	0.078	0.206	0.003	2E-04	0	0	0	9E-06	4.58E-05	5.31E-06	0.00E+00	0.00E+00	0.00E+00	2.33E-07	0.85	0.01

Test: **HOSW**
Depth above bankfull: 69.03 mm
Discharge measured: 0.449 m³/s
Dischage calculated by summation of velocities

Section	Discharge (m³/s)			Areas (m²)				Velocities (m/s)																												Mix	Single
	Main channel Qa	Below BF Qbf	Above BF Qa-bf	Main channel Aa	Below BF Abf	Above BF Aa-bf	actual	Main channel Ua	Below BF Ubf	Above BF Ua-bf	P (m)	R	S	Ua* (m/s)	Ua'* (m/s)	d35 (mm)	ks (mm)	F1	F2	F3	F4	F5	F35	G1	G2	G3	G4	G5	G35	X1	X2	X3	X4	X5	X35	Qs (g/s)	Qs (g/s)
g	Low quality data										1.82																										
h	0.106	0.056	0.050	0.312	0.202	0.110	0.110	0.341	0.278	0.457	1.85	0.11	0.00136	0.0381	0.019	0.65	0.8125	0.364	0.237	0.136	0.100	0.082	0.211	0.003	3E-04	0	0	0	4E-05	6.46E-05	9.91E-06	0.00E+00	0.00E+00	0.00E+00	1.41E-06	1.58	0.15
i	0.147	0.092	0.055	0.323	0.212	0.110	0.110	0.455	0.433	0.496	1.86	0.11	0.00136	0.03898	0.025	0.65	0.8125	0.449	0.311	0.196	0.152	0.127	0.282	0.011	0.005	0.0002	0	0	0.004	2.60E-04	1.73E-04	1.01E-05	0.00E+00	0.00E+00	1.37E-04	13.59	20.07
j - m	Low quality data										1.88																										
n	0.148	0.094	0.052	0.348	0.236	0.112	0.110	0.419	0.398	0.485	1.90	0.12	0.00136	0.04067	0.023	0.65	0.8125	0.440	0.299	0.182	0.138	0.115	0.289	0.01	0.004	0	0	0	0.003	2.15E-04	1.14E-04	0.00E+00	0.00E+00	0.00E+00	8.26E-05	9.60	12.05
o	**0.130**	**0.089**	**0.041**	**0.346**	**0.236**	**0.110**	**0.110**	**0.376**	**0.379**	**0.368**	**1.86**	**0.13**	**0.00136**	**0.04096**	**0.020**	**0.65**	**0.8125**	**0.432**	**0.291**	**0.178**	**0.132**	**0.109**	**0.262**	**0.009**	**0.003**	**0**	**0**	**0**	**0.002**	**1.75E-04**	**8.71E-06**	**0.00E+00**	**0.00E+00**	**0.00E+00**	**6.00E-06**	**6.89**	**7.77**
o (Qa+10%)	0.143	0.098	0.045	0.345	0.235	0.110	0.110	0.413	0.417	0.405	1.86	0.13	0.00136	0.04096	0.022	0.65	0.8125	0.451	0.308	0.189	0.144	0.120	0.276	0.012	0.005	6E-05	0	0	0.004	2.41E-04	1.37E-04	2.39E-06	0.00E+00	0.00E+00	1.05E-04	10.66	14.91
o (Qa-10%)	0.117	0.080	0.037	0.345	0.235	0.110	0.110	0.338	0.341	0.331	1.86	0.13	0.00136	0.04096	0.018	0.65	0.8125	0.412	0.273	0.161	0.119	0.098	0.244	0.007	0.002	0	0	0	0.001	1.26E-04	4.88E-05	0.00E+00	0.00E+00	0.00E+00	2.81E-05	4.08	3.28

Test: **HORW**
Depth above bankfull: 75.74 mm
Discharge measured: 0.163 m³/s
Dischage calculated by summation of velocities

Section	Discharge (m³/s)			Areas (m²)				Velocities (m/s)																												Mix	Single
	Main channel Qa	Below BF Qbf	Above BF Qa-bf	Main channel Aa	Below BF Abf	Above BF Aa-bf	actual	Main channel Ua	Below BF Ubf	Above BF Ua-bf	P (m)	R	S	Ua* (m/s)	Ua'* (m/s)	d35 (mm)	ks (mm)	F1	F2	F3	F4	F5	F35	G1	G2	G3	G4	G5	G35	X1	X2	X3	X4	X5	X35	Qs (g/s)	Qs (g/s)
g	Low quality data										1.86																										
h	0.115	0.095	0.020	0.452	0.346	0.106	0.121	0.254	0.275	0.186	1.93	0.16	0.00136	0.04889	0.013	0.65	0.8125	0.405	0.250	0.133	0.093	0.075	0.220	0.006	8E-04	0	0	0	2E-04	6.14E-05	1.11E-05	0.00E+00	0.00E+00	0.00E+00	2.73E-06	1.66	0.31
i	0.116	0.084	0.034	0.397	0.280	0.117	0.121	0.298	0.300	0.293	1.96	0.14	0.00136	0.04357	0.016	0.65	0.8125	0.400	0.257	0.144	0.104	0.085	0.228	0.006	0.001	0	0	0	4E-04	8.30E-05	2.10E-05	0.00E+00	0.00E+00	0.00E+00	8.02E-06	2.46	0.95
j	0.101	0.054	0.047	0.291	0.173	0.119	0.121	0.346	0.312	0.395	1.94	0.09	0.00136	0.0344	0.020	0.65	0.8125	0.367	0.248	0.151	0.115	0.096	0.224	0.003	7E-04	0	0	0	3E-04	8.92E-05	2.60E-05	0.00E+00	0.00E+00	0.00E+00	1.04E-05	2.32	1.05
k	**0.090**	**0.057**	**0.033**	**0.327**	**0.208**	**0.119**	**0.121**	**0.274**	**0.274**	**0.274**	**1.90**	**0.11**	**0.00136**	**0.0382**	**0.016**	**0.65**	**0.8125**	**0.363**	**0.235**	**0.135**	**0.098**	**0.081**	**0.210**	**0.003**	**3E-04**	**0**	**0**	**0**	**3E-05**	**5.60E-06**	**8.01E-06**	**0.00E+00**	**0.00E+00**	**0.00E+00**	**9.02E-07**	**1.13**	**0.08**
l - o	Data not collected																																				
k (Qa+10%)	0.099	0.063	0.036	0.327	0.208	0.119	0.121	0.302	0.302	0.301	1.90	0.11	0.00136	0.0382	0.017	0.65	0.8125	0.378	0.249	0.148	0.108	0.089	0.223	0.004	7E-04	0	0	0	2E-04	7.95E-05	2.03E-05	0.00E+00	0.00E+00	0.00E+00	7.19E-06	1.97	0.71
k (Qa-10%)	0.081	0.051	0.029	0.327	0.208	0.119	0.121	0.247	0.247	0.247	1.90	0.11	0.00136	0.0382	0.014	0.65	0.8125	0.346	0.221	0.124	0.089	0.073	0.196	0.002	6E-05	0	0	0	0	3.56E-05	1.57E-06	0.00E+00	0.00E+00	0.00E+00	0.00E+00	0.80	0.00

Prediction of total bed material load using the Engelund and Hansen (1967) formula

The sediment concentration in parts per million by weight is calculated from:

R Hydraulic Radius (m)

S slope

U mean velocity (m/s)

di grain size (mm)

and s, the specific gravity of particles (can be taken as 2.65 for sand)

1. Calculate shear velocity:

$$U^* = (gDS)^{0.5} \qquad (A4.12)$$

2. Compute the sediment concentration:

$$\frac{Q_s}{Q} = 0.05\left(\frac{s}{s-1}\right)\frac{US}{\left[(s-1)gd\right]^{1/2}}\frac{RS}{(s-1)d} \qquad (A4.13)$$

Englund Hansen Sediment Transport Calculations

Sediment Properties - From Averaged Profile

gradation		1	2	3	4	5 d50	
d mm		0.27	0.51	1.25	2.2	3.6	1.2
d (m)	d(mm)/1000	0.00027	0.00051	0.00125	0.0022	0.004	0.0012
β	From Grading Curve	20	20	20	20	20	20

Data

Qa	From point velocities
Aa	From profile
Ua	Qa/Aa
P	From profile
R	Aa/P
S	Average main channel slope

Calculations

CS 0.05(s/(s-1))(US/[(s-1)gd]^0.5)(RS/((s-1)d))

Qs

Test: **BFMB**
Depth above bankfull: -7 mm
Discharge measured: 0.097 m³/s
Dischage calculated by summation of velocities

Section	Discharge (m³/s)			Areas (m²)				Velocities (m/s)							Sediment Concentration by volume						Mix	Single
	Main channel Qa	Below BF Qbf	Above BF	Main channel Aa	Below BF Abf	Above BF	Actual	Main channel Ua	Below BF Ubf	Above BF Ua-bf	P (m)	R	S	CS1	CS2	CS3	CS4	CS5	CS(d50)	Qs (g/s)	Qs (g/s)
g	0.088	0.088									1.838										
h	0.086	0.086	-	0.229	0.229	-	-	0.375	0.375	-	1.894	0.121	0.00136	2.27E-04	8.76E-05	2.28E-05	9.78E-06	4.67E-06	2.43E-05	6.83394	2.35412
i	0.095	0.095	-	0.293	0.293	-	-	0.326	0.326	-	2.072	0.141	0.00136	2.31E-04	8.89E-05	2.32E-05	9.92E-06	4.74E-06	2.46E-05	6.93695	2.3896
j	0.090	0.090	-	0.207	0.207	-	-	0.434	0.434	-	1.924	0.108	0.00136	2.35E-04	9.05E-05	2.36E-05	1.01E-05	4.83E-06	2.51E-05	7.06158	2.43254
k	**0.091**	**0.091**	-	**0.202**	**0.202**	-	-	**0.453**	**0.453**	-	**1.866**	**0.108**	**0.00136**	**2.46E-04**	**9.48E-05**	**2.47E-05**	**1.06E-05**	**5.05E-06**	**2.63E-05**	**7.39443**	**2.54719**
l - o	Data not chosen		-			-	-			-	1.91										
k (Qa+10%	0.101	0.101	-	0.202	0.202	-	-	0.498	0.498	-	1.866	0.108	0.00136	2.71E-04	1.04E-04	2.72E-05	1.16E-05	5.56E-06	2.89E-05	8.43518	2.9057
k (Qa-10%	0.082	0.082	-	0.202	0.202	-	-	0.407	0.407	-	1.866	0.108	0.00136	2.21E-04	8.53E-05	2.22E-05	9.52E-06	4.55E-06	2.36E-05	5.64669	1.94514

Test: **LOSW**
Depth above bankfull: 26.84 mm
Discharge measured: 0.163 m³/s
Dischage calculated by summation of velocities

Section	Discharge (m³/s)			Areas (m²)				Velocities (m/s)							Sediment Concentration by volume						Mix	Single
	Main channel Qa	Below BF Qbf	Above BF Qa-bf	Main channel Aa	Below BF Abf	Above BF Aa-bf	Actual	Main channel Ua	Below BF Ubf	Above BF Ua-bf	P (m)	R	S	CS1	CS2	CS3	CS4	CS5	CS(d50)	Qs (g/s)	Qs (g/s)
g - h	Data not chosen																				
i	0.091	0.076	0.015	0.263	0.220	0.043	0.043	0.346	0.347	0.337	1.922	0.114	0.00136	2.0E-04	7.6E-05	2.0E-05	8.5E-06	4.1E-06	2.1E-05	5.57345	1.91991
j	0.084	0.072	0.013	0.258	0.209	0.049	0.043	0.327	0.342	0.261	1.911	0.11	0.00136	1.8E-04	6.9E-05	1.8E-05	7.7E-06	3.7E-06	1.9E-05	4.7027	1.61996
k	**0.079**	**0.069**	**0.010**	**0.263**	**0.220**	**0.043**	**0.043**	**0.300**	**0.314**	**0.225**	**1.824**	**0.121**	**0.00136**	**1.8E-04**	**7.0E-05**	**1.8E-05**	**7.8E-06**	**3.7E-06**	**1.9E-05**	**4.43431**	**1.52751**
l	0.082	0.073	0.009	0.291	0.248	0.043	0.043	0.282	0.296	0.204	1.876	0.132	0.00136	1.9E-04	7.2E-05	1.9E-05	8.1E-06	3.9E-06	2.0E-05	4.77345	1.84433
m	0.087	0.074	0.013	0.291	0.248	0.043	0.043	0.297	0.297	0.298	1.991										
n - o	Data not chosen																				
k (Qa+10%	0.087	0.076	0.011	0.263	0.220	0.043	0.043	0.330	0.346	0.247	1.824	0.121	0.00136	2.0E-04	7.7E-05	2.0E-05	8.6E-06	4.1E-06	2.1E-05	5.36552	1.84828
k (Qa-10%	0.071	0.062	0.009	0.263	0.220	0.043	0.043	0.270	0.283	0.202	1.824	0.121	0.00136	1.6E-04	6.3E-05	1.6E-05	7.0E-06	3.4E-06	1.7E-05	3.59179	1.23728

Test: **LORW**
Depth above bankfull: 42.48 mm
Discharge measured: 0.12 m³/s
Dischage calculated by summation of velocities

Section	Discharge (m³/s)			Areas (m²)				Velocities (m/s)							Sediment Concentration by volume						Mix	Single
	Main channel Qa	Below BF Qbf	Above BF Qa-bf	Main channel Aa	Below BF Abf	Above BF Aa-bf	Actual	Main channel Ua	Below BF Ubf	Above BF Ua-bf	P (m)	R	S	CS1	CS2	CS3	CS4	CS5	CS(d50)	Qs (g/s)	Qs (g/s)
g	**0.071**	**0.063**	**0.008**	**0.271**	**0.214**	**0.058**	**0.068**	**0.260**	**0.295**	**0.131**	**1.874**	**0.114**	**0.00136**	**1.5E-04**	**5.7E-05**	**1.5E-05**	**6.4E-06**	**3.1E-06**	**1.6E-05**	**3.25372**	**1.12082**
h	0.096	0.078	0.018	0.345	0.280	0.065	0.068	0.279	0.279	0.278	1.884	0.149	0.00136	2.1E-04	8.0E-05	2.1E-05	9.0E-06	4.3E-06	2.2E-05	6.21217	2.13993
i	0.087	0.066	0.021	0.295	0.228	0.067	0.068	0.294	0.290	0.308	2.078	0.11	0.00136	1.6E-04	6.2E-05	1.6E-05	7.0E-06	3.3E-06	1.7E-05	4.3453	1.49684
j	0.064	0.042	0.022	0.203	0.125	0.078	0.068	0.316	0.338	0.283	1.937	0.09	0.00136	1.4E-04	5.5E-05	1.4E-05	6.1E-06	2.9E-06	1.5E-05	2.83476	0.9765
k - o											1.879										
g (Qa+10%	0.078	0.069	0.008	0.271	0.214	0.058	0.068	0.286	0.324	0.144	1.874	0.114	0.00136	1.6E-04	6.3E-05	1.6E-05	7.0E-06	3.4E-06	1.7E-05	3.937	1.3562
g (Qa-10%	0.063	0.057	0.007	0.271	0.214	0.058	0.068	0.234	0.265	0.118	1.874	0.114	0.00136	1.3E-04	5.2E-05	1.3E-05	5.8E-06	2.8E-06	1.4E-05	2.63551	0.90787

Test: **HOSW**
Depth above bankfull: 69.03 mm
Discharge measured: 0.449 m³/s
Dischage calculated by summation of velocities

Section	Discharge (m³/s)			Areas (m²)				Velocities (m/s)							Sediment Concentration by volume						Mix	Single
	Main channel Qa	Below BF Qbf	Above BF Qa-bf	Main channel Aa	Below BF Abf	Above BF Aa-bf	Actual	Main channel Ua	Below BF Ubf	Above BF Ua-bf	P (m)	R	S	CS1	CS2	CS3	CS4	CS5	CS(d50)	Qs (g/s)	Qs (g/s)
g											1.817										
h	0.106	0.056	0.050	0.312	0.202	0.110	0.110	0.341	0.278	0.457	1.851	0.109	0.00136	1.9E-04	7.2E-05	1.9E-05	8.0E-06	3.8E-06	2.0E-05	6.14457	2.11665
i	0.147	0.092	0.055	0.323	0.212	0.110	0.110	0.455	0.433	0.496	1.86	0.114	0.00136	2.6E-04	1.0E-04	2.6E-05	1.1E-05	5.4E-06	2.8E-05	11.852	4.0827
j - m											1.876										
n	0.146	0.094	0.052	0.348	0.236	0.112	0.110	0.419	0.398	0.465	1.901	0.124	0.00136	2.6E-04	1.0E-04	2.6E-05	1.1E-05	5.4E-06	2.8E-05	11.828	4.07446
o	**0.130**	**0.089**	**0.041**	**0.345**	**0.235**	**0.110**	**0.110**	**0.376**	**0.379**	**0.368**	**1.862**	**0.126**	**0.00136**	**2.4E-04**	**9.2E-05**	**2.4E-05**	**1.0E-05**	**4.9E-06**	**2.5E-05**	**9.54633**	**3.28847**
o (Qa+10%	0.143	0.098	0.045	0.345	0.235	0.110	0.110	0.413	0.417	0.405	1.862	0.126	0.00136	2.6E-04	1.0E-04	2.6E-05	1.1E-05	5.4E-06	2.8E-05	11.5511	3.97905
o (Qa-10%	0.117	0.080	0.037	0.345	0.235	0.110	0.110	0.338	0.341	0.331	1.862	0.126	0.00136	2.1E-04	8.2E-05	2.1E-05	9.2E-06	4.4E-06	2.3E-05	7.73253	2.66366

Test: **HORW**
Depth above bankfull: 75.74 mm
Discharge measured: 0.163 m³/s
Dischage calculated by summation of velocities

Section	Discharge (m³/s)			Areas (m²)				Velocities (m/s)							Sediment Concentration by volume						Mix	Single
	Main channel Qa	Below BF Qbf	Above BF Qa-bf	Main channel Aa	Below BF Abf	Above BF Aa-bf	Actual	Main channel Ua	Below BF Ubf	Above BF Ua-bf	P (m)	R	S	CS1	CS2	CS3	CS4	CS5	CS(d50)	Qs (g/s)	Qs (g/s)
g											1.864										
h	0.115	0.095	0.020	0.452	0.348	0.106	0.121	0.254	0.275	0.186	1.927	0.18	0.00136	2.3E-04	8.8E-05	2.3E-05	9.8E-06	4.7E-06	2.4E-05	8.1286	2.8001
i	0.118	0.084	0.034	0.397	0.280	0.117	0.121	0.298	0.300	0.293	1.963	0.143	0.00136	2.1E-04	8.2E-05	2.1E-05	9.2E-06	4.4E-06	2.3E-05	7.80256	2.68778
j	0.101	0.054	0.047	0.291	0.173	0.119	0.121	0.346	0.312	0.395	1.945	0.089	0.00136	1.5E-04	5.9E-05	1.6E-05	6.6E-06	3.2E-06	1.6E-05	4.82555	1.66228
k	**0.090**	**0.057**	**0.033**	**0.327**	**0.208**	**0.119**	**0.121**	**0.274**	**0.274**	**0.274**	**1.896**	**0.11**	**0.00136**	**1.5E-04**	**5.8E-05**	**1.5E-05**	**6.5E-06**	**3.1E-06**	**1.6E-05**	**4.19145**	**1.44385**
l - o																					
k (Qa+10%	0.099	0.063	0.036	0.327	0.208	0.119	0.121	0.302	0.302	0.301	1.896	0.11	0.00136	1.7E-04	6.4E-05	1.7E-05	7.1E-06	3.4E-06	1.8E-05	5.07166	1.74706
k (Qa-10%	0.081	0.051	0.029	0.327	0.208	0.119	0.121	0.247	0.247	0.247	1.896	0.11	0.00136	1.4E-04	5.2E-05	1.4E-05	5.8E-06	2.8E-06	1.4E-05	3.39508	1.16952

Prediction of total bed material load using the van Rijn simplified formula

1. Calculate dgr , the dimensionless particle size

$$d_{gr} = d\left[\frac{g(s-1)}{\upsilon^2}\right]^{1/3} \qquad (A4.\ 14)$$

Calculate the Shields critical bed shear velocity for the following form of the Shields curve

$\theta_{cr} - 0.24(d_{gr})^{-1}$ for $d_{gr}<4$

$\theta_{cr} = 0.14(d_{gr})^{-0.64}$ for $4<d_{gr}<10$

$\theta_{cr} = 0.04(d_{gr})^{-0.10}$ for $10<d_{gr}<20$

$\theta_{cr} = 0.013(d_{gr})^{-0.29}$ for $20<d_{gr}<150$

$\theta_{cr} = 0.055$for $d_{gr}>150$

$u_{*cr} = \{0.001\theta_{cr}(s-1)gd_i\}^{0.5}$

2. Calculate the critical velocity which is related to the critical shear velocity by the equation

$$u_{cr,i} = u*'_{cr,i}\, C/(\sqrt{g}) \qquad (A4.\ 15)$$

3 Calculate the sediment concentration for suspended and bed load for the ith fraction from the following equations respectively

$$\frac{q^*_{s,i}}{uhb} = 0.012\left(\frac{u-u_{cr,i}}{\sqrt{[g(s-1)d]}}\right)^{2.4}\left(\frac{d}{h}\right)d_*^{-0.6} \qquad (A4.\ 16)$$

$$\frac{q^*_{b,i}}{uhb} = 0.005\left(\frac{u-u_{cr,i}}{\sqrt{[g(s-1)d]}}\right)^{2.4}\left(\frac{d}{h}\right)^{1.2} \qquad (A4.\ 17)$$

Calculate total transport for suspended and bed load from the following equations respectively

$$q^*_s = \sum_{i=1}^{n}\beta_i q^*_{s,i} \qquad (A4.\ 18)$$

$$q^*_b = \sum_{i=1}^{n}\beta_i q^*_{b,i} \qquad (A4.\ 19)$$

Where β is the proportion of each fraction.

Van Rijn Sediment Transport Calculations - No hiding function

Sediment Properties - From Averaged Profile

	notes	1	2	3	4	5	d50
gradation		0.27	0.51	1.25	2.2	3.8	1.2
d mm		0.0003	0.0005	0.0013	0.0022	0.0038	0.0012
d (m)	d(mm)/1000	20	20	20	20	20	100
%	From Grading Curve	8.258814	11.8218268	28.97507	50.9961	83.45	27.8160831
d*	d(g(s-1)/v^2)^(1/3)	0.043289	0.03124579	0.034509	0.04066	0.047	0.03410273
θcr	From Shields curve	0.013755	0.01606044	0.026424	0.03805	0.052	0.02573722
u*scr	(θcr(s-1)gd50)^0.5						

Data

Qa	From point velocities
Aa	From profile
Ua	Qa/Aa
P	From profile
R	Aa/P
S	Average main channel slope

Equations

U*	(gdS)^0.5
C	Ua/(RS)^0.5
C' vr	18 Log(12R/3D90)
U**	g^0.5Ua/C'
Usor	C/g^0.5 U*scr
Ucr	Uscr
CSs	0.012((Ua-Ucr)/(g(s-1)d)^0.5)^2.4(d/R)d*^-0.6
CSb	0.005((Ua-Ucr)/(g(s-1)d)^0.5)^2.4(d/R)^1.2
Qs	Q sum i=1 to n, βi(CSbi+CSsi)

Test: BFMB
Depth above bankfull: -7 mm
Discharge measured: 0.097 m³/s
Dischage calculated by summation of velocities

Section	Discharge (m³/s) Main channel Qa	Qbf		Areas (m²) Main channel Aa	Abf			Velocities (m/s) Main channel Ua	Ubf	Ua-bf	P (m)	R	S	Ua*	C	C' vr	Ua*'vr	d90 (mm)	ks (mm)	Critical Velocities Ucr1	Ucr2	Ucr3	Ucr4	Ucr5	Ucr50	Suspended Load Concentration CSs1	CSs2	CSs3	CSs4	CSs5	CSs50	Bed Load Concentration CSb1	CSb2	CSb3	CSb4	CSb5	CSb50	Mix Qs (g/s)	Single Qs (g/s)
g	0.088	0.088	-								1.838																											
h	0.088	0.088	-	0.229	0.229	-	-	0.375	0.375	-	1.894	0.121	0.00136	0.040	29.3	38.3	0.031	3.60	10.800	0.13	0.15	0.25	0.36	0.49	0.24	210.09	101.38	12.77	0.08	0.00	14.84	77.62	62.30	16.08	0.17	0.00	16.08	9.32	3.19
i	0.095	0.095	-	0.293	0.293	-	-	0.326	0.326	-	2.072	0.141	0.00136	0.043	23.5	39.5	0.026	3.60	10.800	0.10	0.12	0.20	0.29	0.39	0.19	140.14	69.36	10.76	0.42	0.00	12.24	50.18	41.30	13.13	0.81	0.00	14.46	9.33	2.59
j	0.090	0.090	-	0.207	0.207	-	-	0.434	0.434	-	1.924	0.108	0.00136	0.038	35.9	37.4	0.036	3.60	10.800	0.16	0.18	0.30	0.44	0.60	0.29	309.90	146.41	15.24	0.00	0.00	16.10	117.11	92.03	19.62	0.00	0.00	22.56	13.69	3.84
k	0.091	0.091	-	0.202	0.202	-	-	0.453	0.453	-	1.888	0.108	0.00136	0.038	37.4	37.4	0.038	3.60	10.800	0.16	0.19	0.32	0.46	0.62	0.31	342.44	161.92	16.97	0.00	0.00	20.16	129.51	101.70	21.54	0.00	0.00	28.09	16.02	4.39
l - o											1.910																												
k	0.101	0.101	-	0.202	0.202	-	-	0.498	0.498	-	1.868	0.108	0.00136	0.038	41.1	37.4	0.042	3.60	10.800	0.18	0.21	0.35	0.50	0.69	0.34	430.46	203.53	21.34	0.00	0.00	25.33	162.56	127.63	27.45	0.00	0.00	31.54	18.66	5.62
k	0.082	0.082	-	0.202	0.202	-	-	0.407	0.407	-	1.868	0.108	0.00136	0.038	33.6	37.4	0.034	3.60	10.800	0.15	0.17	0.28	0.41	0.56	0.28	265.93	125.74	13.18	0.00	0.00	15.65	100.42	78.97	16.96	0.00	0.00	19.49	11.96	3.41

Test: LOSW
Depth above bankfull: 26.84 mm
Discharge measured: 0.163 m³/s
Dischage calculated by summation of velocities

Section	Discharge (m³/s) Main channel Qa	Below BF Qbf	Above BF Qa-bf	Areas (m²) Main channel Aa	Below BF Abf	Above BF Aa-bf	Actual	Velocities (m/s) Main channel Ua	Below BF Ubf	Above BF Ua-bf	P (m)	R	S	Ua*	C	C' vr	Ua*'vr	d90 (mm)	ks (mm)	Ucr1	Ucr2	Ucr3	Ucr4	Ucr5	Ucr50	CSs1	CSs2	CSs3	CSs4	CSs5	CSs50	CSb1	CSb2	CSb3	CSb4	CSb5	CSb50	Mix Qs (g/s)	Single Qs (g/s)
g - h																																							
i	0.0908	0.0762	0.0145	0.262647	0.220	0.043	0.043	0.346	0.347	0.337	1.922	0.11	0.00136	0.039	27.75	37.866	0.0286	3.6	10.800	0.12	0.14	0.23	0.34	0.46	0.23	175.89	84.03	9.99	0.01	0.00	11.36	65.71	52.21	12.34	0.03	0.00	14.02	7.26	2.3046
j	0.0844	0.0717	0.0128	0.258315	0.209	0.049	0.043	0.327	0.342	0.281	1.911	0.11	0.00136	0.0382	26.79	37.542	0.0273	3.6	10.800	0.12	0.14	0.23	0.33	0.45	0.22	155.97	73.93	7.93	0.00	0.00	9.39	58.75	46.32	10.18	0.00	0.00	11.66	5.96	1.7767
k	0.0788	0.0692	0.0096	0.263069	0.220	0.043	0.043	0.300	0.314	0.225	1.824	0.12	0.00136	0.0401	23.41	38.296	0.0245	3.6	10.800	0.10	0.12	0.20	0.28	0.39	0.19	122.45	59.09	7.44	0.06	0.00	8.66	46.24	36.51	9.37	0.10	0.00	10.64	4.41	1.5124
l	0.0821	0.0735	0.0087	0.290828	0.248	0.043	0.043	0.282	0.296	0.204	1.876	0.13	0.00136	0.042	21.08	39.012	0.0227	3.6	10.800	0.09	0.11	0.18	0.26	0.35	0.17	102.50	50.22	7.19	0.17	0.00	8.24	37.19	30.30	8.89	0.32	0.00	9.86	3.89	1.4672
m	0.0868	0.0739	0.0128	0.291408	0.248	0.043	0.043	0.297	0.297	0.298	1.991																													
n - o																																							
k	0.08670206	0.076114	0.0106	0.263069	0.220	0.043	0.043	0.330	0.346	0.247	1.824	0.12	0.00136	0.0401	25.75	38.296	0.027	3.6	10.800	0.11	0.13	0.22	0.31	0.43	0.21	153.921	74.271	9.355	0.062	0.000	#######	56.870	45.643	11.777	0.122	0.000	13.248	6.10	2.0913
k	0.07093805	0.062275	0.0087	0.263069	0.220	0.043	0.043	0.270	0.283	0.202	1.824	0.12	0.00136	0.0401	21.07	38.296	0.0221	3.6	10.800	0.09	0.11	0.18	0.26	0.35	0.17	95.091	45.884	5.779	0.038	0.000	6.717	35.134	28.197	7.276	0.076	0.000	8.184	3.09	1.0571

Test: LORW
Depth above bankfull: 42.48 mm
Discharge measured: 0.12 m³/s
Dischage calculated by summation of velocities

Section	Discharge (m³/s) Main channel Qa	Below BF Qbf	Above BF Qa-bf	Areas (m²) Main channel Aa	Below BF Abf	Above BF Aa-bf	Actual	Velocities (m/s) Main channel Ua	Below BF Ubf	Above BF Ua-bf	P (m)	R	S	Ua*	C	C' vr	Ua*'vr	d90 (mm)	ks (mm)	Ucr1	Ucr2	Ucr3	Ucr4	Ucr5	Ucr50	CSs1	CSs2	CSs3	CSs4	CSs5	CSs50	CSb1	CSb2	CSb3	CSb4	CSb5	CSb50	Mix Qs (g/s)	Single Qs (g/s)
g	0.071	0.063	0.008	0.271	0.214	0.058	0.058	0.260	0.256	0.131	1.874	0.11	0.00136	0.039	20.9	37.862	0.0216	3.6	10.800	0.09	0.11	0.18	0.26	0.36	0.17	88.92	42.47	4.88	0.01	0.00	5.78	33.23	26.40	6.23	0.01	0.00	7.01	2.66	0.9031
h	0.096	0.078	0.018	0.345	0.280	0.065	0.058	0.279	0.279	0.278	1.884	0.15	0.00136	0.0445	19.61	39.933	0.0219	3.6	10.800	0.09	0.10	0.17	0.24	0.33	0.16	94.30	47.02	7.74	0.42	0.00	8.74	33.41	27.71	9.34	0.79	0.00	10.22	4.25	1.6256
i	0.087	0.066	0.021	0.295	0.228	0.067	0.058	0.294	0.290	0.308	2.078	0.11	0.00136	0.0382	24.12	37.535	0.0245	3.6	10.800	0.11	0.12	0.20	0.29	0.40	0.20	121.06	57.36	6.16	0.00	0.00	7.26	45.61	36.96	7.69	0.00	0.00	9.04	4.76	1.4156
j	0.064	0.042	0.022	0.203	0.125	0.078	0.058	0.316	0.336	0.283	1.937	0.09	0.00136	0.0346	28.57	36	0.0275	3.6	10.800	0.13	0.15	0.24	0.35	0.48	0.23	151.44	66.73	4.71	0.00	0.00	5.91	59.34	44.80	9.29	0.00	0.00	7.63	4.30	0.8664
k - o											1.879																													
g	0.078	0.069	0.008	0.271	0.214	0.056	0.068	0.286	0.324	0.144	1.874	0.11	0.00136	0.039	22.99	37.852	0.0237	3.6	10.800	0.10	0.12	0.19	0.28	0.38	0.19	111.77	53.36	6.14	0.01	0.00	7.21	41.77	33.16	7.62	0.01	0.00	8.66	3.94	1.2467
g	0.063	0.057	0.007	0.271	0.214	0.056	0.068	0.234	0.265	0.118	1.874	0.11	0.00136	0.039	18.81	37.852	0.0194	3.6	10.800	0.08	0.10	0.16	0.23	0.31	0.15	69.05	32.96	3.79	0.00	0.00	4.45	25.80	20.50	4.83	0.01	0.00	5.49	1.99	0.6312

Test: HOSW
Depth above bankfull: 69.03 mm
Discharge measured: 0.449 m³/s
Dischage calculated by summation of velocities

Section	Discharge (m³/s) Main channel Qa	Below BF Qbf	Above BF Qa-bf	Areas (m²) Main channel Aa	Below BF Abf	Above BF Aa-bf	Actual	Velocities (m/s) Main channel Ua	Below BF Ubf	Above BF Ua-bf	P (m)	R	S	Ua*	C	C' vr	Ua*'vr	d90 (mm)	ks (mm)	Ucr1	Ucr2	Ucr3	Ucr4	Ucr5	Ucr50	CSs1	CSs2	CSs3	CSs4	CSs5	CSs50	CSb1	CSb2	CSb3	CSb4	CSb5	CSb50	Mix Qs (g/s)	Single Qs (g/s)
g											1.817																												
h	0.106	0.056	0.050	0.312	0.202	0.110	0.110	0.341	0.276	0.457	1.851	0.11	0.00136	0.0381	26.0	37.5	0.0285	3.6	10.800	0.12	0.14	0.24	0.34	0.47	0.23	173.01	81.92	8.70	0.00	0.00	10.31	65.24	51.36	11.16	0.00	0.00	12.62	6.32	2.4567
i	0.147	0.092	0.055	0.323	0.212	0.110	0.110	0.455	0.433	0.496	1.86	0.11	0.00136	0.039	36.5	37.9	0.0376	3.6	10.800	0.16	0.19	0.31	0.44	0.61	0.30	340.33	162.56	18.72	0.02	0.00	21.98	127.16	101.03	23.84	0.05	0.00	27.06	22.71	7.2002
j - m																																							
n	0.146	0.094	0.052	0.348	0.236	0.112	0.110	0.419	0.398	0.466	1.901	0.12	0.00136	0.0407	32.3	38.5	0.0341	3.6	10.800	0.14	0.17	0.27	0.39	0.54	0.27	271.28	131.55	17.29	0.19	0.00	20.00	99.65	80.35	21.65	0.37	0.00	24.24	16.17	6.4574
o	0.130	0.089	0.041	0.348	0.238	0.110	0.110	0.376	0.379	0.368	1.862	0.13	0.00136	0.041	29.7	38.8	0.0304	3.6	10.800	0.13	0.16	0.24	0.35	0.48	0.24	207.10	100.67	13.51	0.15	0.00	15.59	76.86	61.33	16.86	0.26	0.00	18.83	12.34	4.4630
o	0.143	0.098	0.045	0.345	0.235	0.110	0.110	0.413	0.417	0.405	1.862	0.13	0.00136	0.041	31.6	38.6	0.0335	3.6	10.800	0.14	0.16	0.27	0.38	0.53	0.26	260.33	126.55	16.96	0.23	0.00	19.60	95.35	77.10	21.19	0.45	0.00	23.66	17.06	6.1712
o	0.117	0.080	0.037	0.345	0.235	0.110	0.110	0.338	0.341	0.331	1.862	0.13	0.00136	0.041	25.6	38.6	0.0274	3.6	10.800	0.11	0.13	0.22	0.31	0.43	0.21	160.83	78.18	10.49	0.14	0.00	12.11	58.91	47.63	13.09	0.28	0.00	14.63	8.62	3.1193

Test: HORW
Depth above bankfull: 75.74 mm
Discharge measured: 0.163 m³/s
Dischage calculated by summation of velocities

Section	Discharge (m³/s) Main channel Qa	Below BF Qbf	Above BF Qa-bf	Areas (m²) Main channel Aa	Below BF Abf	Above BF Aa-bf	Actual	Velocities (m/s) Main channel Ua	Below BF Ubf	Above BF Ua-bf	P (m)	R	S	Ua*	C	C' vr	Ua*'vr	d90 (mm)	ks (mm)	Ucr1	Ucr2	Ucr3	Ucr4	Ucr5	Ucr50	CSs1	CSs2	CSs3	CSs4	CSs5	CSs50	CSb1	CSb2	CSb3	CSb4	CSb5	CSb50	Mix Qs (g/s)	Single Qs (g/s)
g											1.864																												
h	0.115	0.095	0.020	0.452	0.348	0.106	0.121	0.254	0.275	0.186	1.927	0.18	0.00136	0.049	16.3	41.4	0.019	3.6	10.800	0.07	0.08	0.14	0.20	0.27	0.13	68.57	35.03	5.65	0.76	0.00	7.64	23.40	19.85	5.00	1.39	0.00	5.60	3.76	1.8627
i	0.118	0.084	0.034	0.397	0.280	0.117	0.121	0.298	0.300	0.293	1.963	0.14	0.00136	0.044	21.4	39.6	0.024	3.6	10.800	0.09	0.11	0.18	0.26	0.36	0.18	112.66	55.85	6.77	0.37	0.00	9.95	40.27	33.19	10.66	0.70	0.00	11.73	6.20	2.5609
j	0.101	0.054	0.047	0.291	0.173	0.119	0.121	0.348	0.312	0.395	1.945	0.09	0.00136	0.034	31.5	35.9	0.030	3.6	10.800	0.14	0.16	0.27	0.38	0.53	0.26	189.16	85.59	5.67	0.00	0.00	7.14	74.30	55.92	7.56	0.00	0.00	9.24	5.44	1.6520
k	0.090	0.057	0.033	0.327	0.208	0.119	0.121	0.274	0.274	0.274	1.896	0.11	0.00136	0.038	22.5	37.5	0.023	3.6	10.800	0.10	0.12	0.19	0.27	0.38	0.18	102.32	48.50	5.29	0.00	0.00	6.16	38.54	30.38	8.88	0.00	0.00	7.65	4.16	1.2382
l - o																																							
k	0.099	0.063	0.036	0.327	0.208	0.119	0.121	0.302	0.302	0.301	1.896	0.11	0.00136	0.038	24.7	37.5	0.025	3.6	10.800	0.11	0.13	0.21	0.30	0.41	0.20	128.61	60.96	6.54	0.00	0.00	7.74	48.45	38.19	8.39	0.00	0.00	9.61	5.75	1.7121
k	0.061	0.051	0.029	0.327	0.208	0.119	0.121	0.247	0.247	0.247	1.896	0.11	0.00136	0.038	20.2	37.5	0.021	3.6	10.800	0.09	0.10	0.17	0.25	0.34	0.17	79.46	37.66	4.04	0.00	0.00	4.78	29.93	23.60	5.18	0.00	0.00	5.94	2.90	0.9654

Prediction of bed and suspended load using the van Rijn simplified formula incorporating Pender's hiding function

For each size fraction

1. Calculate the hiding function, e_i from

$$\varepsilon_i = \frac{\left(d_i / d_g\right)^{-0.105}}{\sigma_g^{\alpha}} \qquad (A4.20)$$

Where, by regression analysis from laboratory data.

$$\alpha = 4.198\text{-}2.548\sigma_g + 0.192\sigma_g^2 + 0.275Fr - 7.488Fr^2 + 2.490\sigma_g Fr$$

The Froude number $Fr - U/(gR)^{0.5}$

The standard deviation $\sigma_g = (d_{84}/d_{15})^{0.5}$

2. Calculate the shields critical velocity from

$$\frac{u_{scr}^2}{(s-1)gd_g} = 2.89\left(\frac{h}{d_g}\right)^{0.19} \qquad (A4.21)$$

3. Calculate the adjusted critical velocity, $u_{cr,i}$ from

$$u^2_{cr,i} - u^2_{cr,g}\,\varepsilon_i \qquad (A4.22)$$

4. Now calculate the bed and suspended load transport rates as before using the adjusted value of $u_{cr,i}$

Van Rijn Sediment Transport Calculations - With hiding function

Sediment Properties - From Averaged Profile

	notes	1	2	3	4	5	6	7	d50	
gradation										
d (mm)		4 0926784	2 5884582	1 536229	0 64143	0 4243	0 212132	0 09721		1.2
d m	d(mm)/1000	0 0041	0 0026	0 0015	0 0006	0 0004	0 0002	0 0001	0 0012	
%	From Grading Curve	13.9	21 6	18 0	12.5	22 5	8 9	2 7	21	100 0
d*	d(g(s-1)/v^2)^(1/3)	94 868454	60 0000784	35 80967	19 5043	9 8345	4 91723171	2 25338	27 81606	
theta	From Shields curve	0 0486753	0 0426194	0 036835	0 02972	0 0324	0 05051575	0 10851	0 034103	
u*cr	(tao(s-1)gd50)^0 5	0 0567851	0 04225702	0 036182	0 02012	0 0149	0 01317022	0 01295	0 025737	

Data

Qs	From point velocities
As	From profile
Us	Qs/As
P	From profile
R	As/P
S	Average main channel slope

Equations

U*	(gdS)^0 5
C	Us/(RS)^0 5
C'=r	18 Log(12R/3D90)
U**	g^0 5/Us/C
Ucr	C/g^0 5 U*cr
CSs	0 012(Us-Ucr)^(s-1)d)^0 5)^2 4(d/R)^(-0 8
CSb	0 005/((Us-Ucr)^(s-1)d)^0 5)^2 4(d/R)^1 2
Qs	Q sum(e1 to n (CSb+CSs)

Hiding Function

ai	bcr,i/tcr Critical shields velocity for mean sediment by critical velocity for fraction d50
ai	(d/dg)^-0 105log ^a
a	-log2 d
eqi	(a70-a80-a90-a97-a3-a10-a20-a30)/9 1
Fr	Us/(gR)^0 5
a	4 196-2 548(eqi)+0 182(eqi)-0 275(Fr)-7 486(Fr^2)+2 490(Frog)

Test: BFMB
Depth above bankfull -7 mm
Discharge measured 0 097 m^3/s
Discharge calculated by summation of velocities

Section	Discharge (m^3/s) Main channel Qs	Qbf	-	Areas (m^2) Main channel As	Abf	-	-	Velocities (m/s) Main channel Us	Ubf	Us-bf	P m	R	S	Us*	C	C'=r	Us*/w	d90 mm	Fr	eg	Hiding Functions e1	e2	e3	e4	e5	e6	e7	Critical Velocities Ucr1	Ucr2	Ucr3	Ucr4	Ucr5	Ucr6	Ucr7	Concentration of Suspended Sediment CSs1	CSs2	CSs3	CSs4	CSs5	CSs6	CSs7	Concentration of Bedload Sediment CSb1	CSb2	CSb3	CSb4	CSb5	CSb6	CSb7	0 21	0 10	kg/s
g	0 068	0 097	-	0 228	0 228	-	-	0 375	0 424	-	1 836																																								
h	0 066	0 097	-	0 228	0 228	-	-	0 375	0 424	-	1 894	0 121	0 00136	0 040	29 3	38 3	0 031	3 6	0 345	2 8	1 08	1 13	1 20	1 26	1 37	1 48	1 60	0 23	0 23	0 22	0 21	0 21	0 20	0 19	6 5	10 3	17 2	30 9	59 6	115 0	238 5	21 2	23 2	25 6	28 4	31 6	35 0	38 9	0 0013	0 0007	6 5384
i	0 065	0 097	-	0 293	0 293	-	-	0 326	0 331	-	2 072	0 141	0 00136	0 043	23 5	39 5	0 026	3 6	0 277	2 6	0 96	0 92	0 97	1 04	1 12	1 20	1 30	0 21	0 20	0 20	0 19	0 18	0 18	0 17	3 8	9 7	9 6	17 3	33 7	65 2	136 1	11 3	12 5	13 6	15 4	17 3	19 3	21 5	0 0007	0 0004	3 6317
j	0 060	0 097	-	0 207	0 207	-	-	0 434	0 468	-	1 924	0 108	0 00136	0 038	35 9	37 4	0 036	3 6	0 422	2 8	1 24	1 30	1 37	1 48	1 57	1 69	1 83	0 26	0 26	0 25	0 24	0 24	0 23	0 22	10 8	17 1	28 4	50 9	97 9	188 2	349 6	34 0	39 3	43 2	47 8	53 1	58 7	65 0	0 0021	0 0012	10 6471
k	0 091	0 097	-	0 202	0 202	-	-	0 453	0 480	-	1 986	0 108	0 00136	0 038	37 4	37 4	0 038	3 6	0 438	2 8	1 26	1 32	1 40	1 49	1 60	1 72	1 86	0 27	0 27	0 26	0 25	0 24	0 23	0 22	12 4	19 5	32 4	57 8	111 0	212 9	438 8	41 2	44 8	48 1	54 2	60 1	66 3	73 3	0 001	0 000	5 0789
l - o											1 91																																								
k +10%	0 101	0 107	-	0 202	0 202	-	-	0 496	0 528	-	1 986	0 108	0 00136	0 038	41 1	37 4	0 0417	3 6	0 483	2 8	1 28	1 34	1 42	1 51	1 63	1 75	1 90	0 30	0 29	0 28	0 27	0 26	0 26	0 25	16 1	25 2	41 8	74 8	142 8	273 6	564 2	53 4	58 0	63 5	69 9	77 4	85 2	94 1	0 001	0 000	5 6387
k -10%	0 082	0 087	-	0 202	0 202	-	-	0 407	0 432	-	1 886	0 108	0 00136	0 038	33 6	37 4	0 0341	3 6	0 395	2 8	1 20	1 26	1 33	1 41	1 52	1 63	1 77	0 25	0 25	0 24	0 23	0 22	0 22	0 21	8 7	13 8	23 1	41 5	80 1	154 5	320 9	29 0	31 8	35 0	38 9	43 4	48 1	53 5	0 000	0 000	3 2487

Test: LOSW
Depth above bankfull 28 84 mm
Discharge measured 0 183 m^3/s
Discharge calculated by summation of velocities

Section	Discharge (m^3/s) Main channel Qs	Below BF Qbf	Above BF Qa-bf	Areas (m^2) Main channel As	Below BF Abf	Above BF Aa-bf	Actual	Velocities (m/s) Main channel Us	Below BF Ubf	Above BF Ua-bf	P m	R	S	Us*	C	C'=r	Us*/w	d90 mm	Fr	eg	Hiding Functions e1	e2	e3	e4	e5	e6	e7	Critical Velocities Ucr1	Ucr2	Ucr3	Ucr4	Ucr5	Ucr6	Ucr7	Concentration of Suspended Sediment CSs1	CSs2	CSs3	CSs4	CSs5	CSs6	CSs7	Concentration of Bedload Sediment CSb1	CSb2	CSb3	CSb4	CSb5	CSb6	CSb7	0 21	0 10	kg/s
g - h																																																			
i	0 091	0 078	0 015	0 283	0 220	0 043	0 043	0 348	0 347	0 337	1 922	0 114	0 00136	0 039	27 8	37 9	0 0286	3 6	0 326	3 21	0 76	0 82	0 86	0 92	0 99	1 06	1 15	0 26	0 25	0 25	0 24	0 23	0 22	0 21	2 1	3 5	8 4	12 3	25 4	52 2	114 9	8 9	9 1	9 6	11 4	13 6	16 1	19 0	0 0003	0 0002	0 0035
j	0 084	0 072	0 013	0 258	0 209	0 049	0 043	0 327	0 342	0 261	1 911	0 110	0 00136	0 038	28 8	37 5	0 0273	3 6	0 315	3 21	0 74	0 78	0 83	0 88	0 94	1 02	1 10	0 26	0 25	0 24	0 23	0 23	0 22	0 21	1 4	2 4	4 4	8 7	16 6	30 0	57 8	4 5	5 5	6 7	8 2	10 1	12 1	14 6	0 0002	0 0001	0 0024
k	0 079	0 069	0 010	0 263	0 220	0 043	0 043	0 300	0 314	0 225	1 824	0 121	0 00136	0 040	23 4	36 3	0 0245	3 6	0 275	3 21	0 62	0 65	0 69	0 73	0 78	0 85	0 92	0 24	0 24	0 23	0 22	0 22	0 21	0 20	0 7	1 2	2 4	4 9	10 0	23 2	53 8	2 2	2 8	3 5	4 5	5 7	7 1	8 7	0 0001	0 0001	0 0014
l	0 042	0 073	0 008	0 291	0 248	0 043	0 043	0 292	0 298	0 204	1 676	0 132	0 00136	0 042	21 1	37 1	0 0238	4 8	0 248	3 21	0 54	0 57	0 60	0 64	0 69	0 74	0 80	0 24	0 23	0 22	0 22	0 21	0 20	0 19	0 4	0 8	1 5	3 2	7 3	16 0	37 8	1 3	1 7	2 2	2 9	3 8	4 8	6 0	0 0001	0 0000	0 0010
m	0 087	0 074	0 013	0 291	0 248	0 043	0 043	0 297	0 297	0 298	1 881																																											
n - o																																																						

Test: LORW
Depth above bankfull 42 46 mm
Discharge measured 0 12 m^3/s
Discharge calculated by summation of velocities

Section	Discharge (m^3/s) Main channel Qs	Below BF Qbf	Above BF Qa-bf	Areas (m^2) Main channel As	Below BF Abf	Above BF Aa-bf	Actual	Velocities (m/s) Main channel Us	Below BF Ubf	Above BF Ua-bf	P (m)	R	S	Us*	C	C'=r	Us*/w	d90 (mm)	Fr	eg	Hiding Functions e1	e2	e3	e4	e5	e6	e7	Critical Velocities Ucr1	Ucr2	Ucr3	Ucr4	Ucr5	Ucr6	Ucr7	Concentration of Suspended Sediment CSs1	CSs2	CSs3	CSs4	CSs5	CSs6	CSs7	Concentration of Bedload Sediment CSb1	CSb2	CSb3	CSb4	CSb5	CSb6	CSb7	0 21	0 10	kg/s
g	0 071	0 063	0 008	0 271	0 214	0 058	0 058	0 260	0 295	0 131	1 874	0 114	0 00136	0 038	26 8	40 4	0 0202	2 8	0 246	3 21	0 54	0 56	0 59	0 63	0 68	0 73	0 78	0 23	0 23	0 22	0 22	0 21	0 20	0 19	0 1	0 2	0 6	1 4	3 6	8 7	22 2	0 4	0 5	0 6	1 0	1 3	1 9	2 7	3 7	0 0001	0 0000	0 0005
h	0 096	0 078	0 018	0 345	0 260	0 085	0 058	0 278	0 279	0 278	1 864	0 149	0 00136	0 045	19 6	39 9	0 0219	3 6	0 231	3 21	0 49	0 52	0 55	0 58	0 62	0 67	0 73	0 23	0 22	0 22	0 21	0 20	0 20	0 19	0 4	0 7	1 5	3 1	6 6	14 6	34 4	1 3	1 6	2 1	2 7	3 5	4 3	5 4	0 0001	0 0001	0 0012
i	0 087	0 066	0 021	0 295	0 228	0 067	0 058	0 294	0 290	0 308	2 078	0 110	0 00136	0 038	24 1	37 5	0 0245	3 6	0 264	3 21	0 65	0 68	0 72	0 76	0 82	0 88	0 96	0 25	0 24	0 23	0 23	0 22	0 21	0 20	0 5	1 0	1 9	4 1	8 4	20 7	48 6	1 7	2 2	2 9	3 9	5 1	6 4	8 1	0 0002	0 0001	0 0014
j	0 064	0 042	0 022	0 203	0 125	0 078	0 058	0 316	0 336	0 283	1 937	0 090	0 00136	0 035	28 8	36 0	0 0275	3 6	0 336	3 21	0 81	0 85	0 90	0 95	1 03	1 10	1 20	0 28	0 25	0 25	0 24	0 23	0 22	0 21	0 9	1 8	3 2	6 8	14 8	32 3	75 4	3 0	3 8	5 0	6 5	8 3	10 4	13 0	0 0003	0 0002	0 0018
k - o											1 879																																											

Test: HOSW
Depth above bankfull 89 03 mm
Discharge measured 0 449 m^3/s
Discharge calculated by summation of velocities

Section	Discharge (m^3/s) Main channel Qs	Below BF Qbf	Above BF Qa-bf	Areas (m^2) Main channel As	Below BF Abf	Above BF Aa-bf	Actual	Velocities (m/s) Main channel Us	Below BF Ubf	Above BF Ua-bf	P (m)	R	S	Us*	C	C'=r	Us*/w	d90 (mm)	Fr	eg	Hiding Functions e1	e2	e3	e4	e5	e6	e7	Critical Velocities Ucr1	Ucr2	Ucr3	Ucr4	Ucr5	Ucr6	Ucr7	Concentration of Suspended Sediment CSs1	CSs2	CSs3	CSs4	CSs5	CSs6	CSs7	Concentration of Bedload Sediment CSb1	CSb2	CSb3	CSb4	CSb5	CSb6	CSb7	0 21	0 10	kg/s
g											1 817																																									
h	0 106	0 056	0 050	0 312	0 202	0 110	0 110	0 341	0 278	0 457	1 851	0 109	0 00136	0 038	28 0	40 0	0 0267	2 8	0 33	3 21	0 79	0 83	0 87	0 93	1 00	1 08	1 17	0 26	0 25	0 25	0 24	0 23	0 22	0 21	1 9	3 2	5 8	11 4	23 8	49 2	109 1	8 2	7 4	8 8	10 6	12 9	15 3	18 2	0 0008	0 0004	0 0038
i	0 147	0 092	0 055	0 323	0 212	0 110	0 110	0 455	0 433	0 498	1 860	0 114	0 00136	0 039	36 5	37 9	0 0378	3 6	0 43	3 21	1 07	1 12	1 18	1 26	1 36	1 48	1 56	0 28	0 28	0 26	0 27	0 26	0 25	0 24	9 5	15 2	25 8	46 4	90 3	175 9	367 1	31 4	34 8	36 5	43 1	46 5	54 1	60 8	0 0022	0 0013	0 0162
j - m																																																					
n	0 148	0 094	0 052	0 348	0 236	0 112	0 110	0 419	0 394	0 465	1 901	0 124	0 00136	0 041	32 3	39 1	0 0374	5 6	0 38	3 21	0 94	0 98	1 04	1 11	1 19	1 28	1 39	0 27	0 27	0 26	0 25	0 24	0 23	0 23	6 5	10 5	17 6	32 4	63 5	124 1	261 0	21 1	23 5	26 2	29 8	33 9	37 8	42 3	0 0016	0 0009	0 0120
o	0 130	0 089	0 041	0 345	0 235	0 110	0 110	0 378	0 379	0 369	1 882	0 128	0 00136	0 041	28 7	39 8	0 0347	8 8	0 338	3 21	0 81	0 85	0 90	0 96	1 03	1 11	1 21	0 28	0 26	0 25	0 24	0 23	0 22	0 21	3 8	5 8	10 2	18 1	36 2	78 1	193 1	11 8	13 2	15 0	17 3	20 1	23 0	26 4	0 0010	0 0006	0 0070

Test: HORW
Depth above bankfull 75 74 mm
Discharge measured 0 183 m^3/s
Discharge calculated by summation of velocities

Section	Discharge (m^3/s) Main channel Qs	Below BF Qbf	Above BF Qa-bf	Areas (m^2) Main channel As	Below BF Abf	Above BF Aa-bf	Actual	Velocities (m/s) Main channel Us	Below BF Ubf	Above BF Ua-bf	P (m)	R	S	Us*	C	C'=r	Us*/w	d90 (mm)	Fr	eg	Hiding Functions e1	e2	e3	e4	e5	e6	e7	Critical Velocities Ucr1	Ucr2	Ucr3	Ucr4	Ucr5	Ucr6	Ucr7	Concentration of Suspended Sediment CSs1	CSs2	CSs3	CSs4	CSs5	CSs6	CSs7	Concentration of Bedload Sediment CSb1	CSb2	CSb3	CSb4	CSb5	CSb6	CSb7	0 21	0 10	kg/s
g											1 864																																									
h	0 115	0 095	0 020	0 452	0 348	0 106	0 121	0 254	0 275	0 188	1 927	0 180	0 00136	0 049	16 3	43 9	0 0181	2 8	0 191	3 21	0 39	0 41	0 43	0 46	0 49	0 53	0 58	0 21	0 21	0 20	0 20	0 19	0 18	0 18	0 2	0 4	0 8	1 7	3 8	8 5	20 1	0 8	0 9	1 1	1 4	1 8	2 4	3 0	0 0001	0 0001	0 0008
i	0 118	0 084	0 034	0 387	0 280	0 117	0 121	0 296	0 300	0 293	1 963	0 143	0 00136	0 044	21 4	39 6	0 0238	3 6	0 252	3 21	0 55	0 58	0 61	0 65	0 70	0 75	0 82	0 24	0 23	0 22	0 22	0 21	0 20	0 19	0 7	1 3	2 4	4 8	10 4	22 0	50 0	2 2	2 8	3 4	4 3	5 3	6 5	7 9	0 0003	0 0002	0 0021
j	0 101	0 054	0 047	0 291	0 173	0 119	0 121	0 348	0 312	0 395	1 945	0 089	0 00136	0 034	31 5	35 9	0 0302	3 6	0 371	3 21	0 91	0 96	1 01	1 06	1 13	1 24	1 35	0 27	0 26	0 26	0 25	0 24	0 23	0 22	1 9	3 3	6 1	12 1	25 9	54 4	122 5	6 4	7 9	9 6	11 8	14 6	17 6	21 3	0 0008	0 0005	0 0040
k	0 090	0 057	0 033	0 327	0 208	0 119	0 121	0 274	0 274	0 274	1 896	0 110	0 00136	0 038	22 5	37 5	0 0228	3 6	0 284	3 21	0 58	0 62	0 65	0 70	0 75	0 80	0 87	0 24	0 23	0 23	0 22	0 21	0 21	0 20	0 2	0 5	1 0	2 3	5 5	12 8	31 8	0 7	1 1	1 5	2 2	3 0	4 0	5 3	0 0002	0 0001	0 0009
- o																																																					

Van Rijn Sediment Transport Calculations - With hiding function

Sediment Properties - From Averaged Profile

	notes	1	2	3	4	5	6	7	d50	
gradation										
d (mm		4 0926764	2 58843582	1 536229	0 64143	0 4243	0 21213203	0 09721		1 2
d im	d(mm)/1000	0 0041	0 0026	0 0015	0 0008	0 0004	0 0002	0 0001		0 0012
%	From Grading Curve	13 9	21 6	18.0	12 5	22 5	8 9	2 7	21	100.0
d*	d(g(s-1)/v^2 ^(1/3)	94 868454	60 0000784	35 60987	19 5043	9 8345	4 91723171	2 25338	27 81606	
theta	From Shields curve	0 0486753	0 0426194	0 036635	0 02972	0 0324	0 05051575	0 10851	0 034103	
u*cr	θcr(s-1)gd50)^0 5	0 0567851	0 04225702	0 030182	0 02012	0 0149	0 01317022	0 01295	0 025737	

Data

Qa	From point velocities
Aa	From profile
Ua	Qa/Aa
P	From profile
R	Aa/P
S	Average main channel slope

Equations

U*	(gdS)^0.5
C	Ua/(RS)^0.5
C' vr	18 Log(12R/3D90)
U*'	g^0 5Ua/C'
Ucr	C/g^0.5 U*scr
Ucr.i	(Ucr g^2/ei)^0.5
CSs	0 012((Ua-Ucr)/(g(s-1)d)^0.5)^2.4(d/R)d*^-0.6
CSb	0.005((Ua-Ucr)/(g(s-1)d)^0.5)^2.4(d/R)^1.2
Qs	Q.sum i=1 to n βi(CSbi+CSsi)

Hiding Function

ei	tscr,g/tcr,i Critical shields velocity for mean sediment by critical velocity for fraction d50
ei	(d/dg)^-0.105/σg ^α
ϕ	-log2 d
σg	(ϕ70+ϕ80+ϕ90+ϕ97-ϕ3 ϕ10 ϕ20 ϕ30)/9.1
Fr	Ua/(gR)^0.5
α	4.198-2.548(σg)+0 192(σg)+0.275(Fr)-7.486(Fr^2)+2.490(Fr σg

Test BFMB

Depth above bankfull: -7 mm
Discharge measured 0 097 m /s
Discharge calculated by summation of velocities

Section	Discharge (m /s) Main channel Qa	Qbf		Areas (m²) Main channel Aa	Abf			Velocities (m/s) Main channel Ua	Ubf	Ua-bf	P (m)	R	S	Ua*	C	C' vr	Ua*'vr	d90 (mm)	Fr	σg	Hiding Functions e1	e2	e3	e4	e5	e6	e7	Critical Velocities Ucr1	Ucr2	Ucr3	Ucr4	Ucr5	Ucr6	Ucr7	Concentration of Suspended Sediment CSs1	CSs2	CSs3	CSs4	CSs5	CSs6	CSs7	Concentration of Bedload Sediment CSb1	CSb2	CSb3	CSb4	CSb5	CSb6	CSb7	0 21	0 10	kg/s
g	0 088	0 097	-			-	-			-	1 838																																					
h	0 086	0 097	-	0 229	0 229	-	-	0.375	0 424	-	1 894	0 121	0 00136	0 040	29 3	38.3	0.031	3 6	0.345	2 8	1 08	1.13	1 20	1.28	1 37	1.48	1 60	0.23	0 23	0.22	0.21	0.21	0.20	0.19	6 5	10 3	17.2	30.9	59.6	115.0	238.5	21.2	23.2	25.6	28 4	31 6	35.0	38.9	0.0013	0 0007	6.5384
i	0 095	0 097	-	0 293	0 293	-	-	0 326	0 331	-	2.072	0.141	0 00136	0 043	23.5	39 5	0 026	3 6	0.277	2 8	0 88	0.92	0 97	1.04	1 12	1.20	1 30	0.21	0 20	0.20	0 19	0.18	0.18	0.17	3.6	5 7	9.6	17.3	33.7	65.2	136.1	11.3	12.5	13.8	15 4	17 3	19 3	21.5	0 0007	0.0004	3.6317
j	0 090	0 097	-	0 207	0 207	-	-	0 434	0 468	-	1 924	0 108	0 00136	0 038	35 9	37.4	0 036	3.6	0.422	2 8	1 24	1.30	1 37	1.46	1 57	1.69	1 83	0.26	0 26	0.25	0.24	0.24	0.23	0.22	10 8	17 1	28.4	50.9	97 9	188.2	389.6	36 0	39.3	43.2	47.8	53 1	58.7	65.0	0.0021	0 0012	10.8471
k	0.091	0.097	-	0.202	0.202	-	-	0.453	0.480	-	1.866	0.108	0.00136	0.038	37.4	37.4	0.038	3.6	0.439	2.8	1.26	1.32	1.40	1.49	1.60	1.72	1.86	0.27	0.27	0.26	0.25	0.24	0.23	0.22	12.4	19.5	32.4	57.8	111.0	212.9	439.8	41.2	44.8	49.1	54.2	60.1	66.3	73.3	0.001	0.000	5.0799
l - o											1 91																																						
k +10%	0 101	0 107	-	0 202	0 202	-	-	0 498	0.528	-	1.866	0.108	0 00136	0 038	41 1	37 4	0 0417	3.6	0.483	2 8	1 28	1.34	1 42	1.51	1 63	1.75	1 90	0.30	0 29	0.28	0.27	0.26	0.26	0.25	16 1	25.2	41.8	74.6	142 8	273.6	564.2	53 4	58.0	63.5	69.9	77.4	85.2	94.1	0.001	0 000	5.8387
k -10%	0 082	0 087	-	0 202	0 202	-	-	0 407	0 432	-	1.866	0.108	0 00136	0 038	33 6	37 4	0 0341	3.6	0.395	2 8	1 20	1.26	1 33	1.41	1 52	1 63	1 77	0.25	0 25	0.24	0.23	0.22	0.22	0.21	8 7	13 8	23 1	41.5	80.1	154 5	320.9	29 0	31 8	35.0	38 9	43 4	48.1	53.5	0.000	0 000	3.2487

Test LOSW

Depth above bankfull: 26 84 mm
Discharge measured 0 163 m³/s
Discharge calculated by summation of velocities

Section	Discharge (m /s) Main channel Qa	Below BF Qbf	Above BF Qa-bf	Areas (m²) Main channel Aa	Below BF Abf	Above BF Aa-bf	Actual	Velocities (m/s) Main channel Ua	Below BF Ubf	Above BF Ua-bf	P (m)	R	S	Ua*	C	C vr	Ua*'vr	d90 (mm)	Fr	σg	Hiding Functions e1	e2	e3	e4	e5	e6	e7	Critical Velocities Ucr1	Ucr2	Ucr3	Ucr4	Ucr5	Ucr6	Ucr7	Concentration of Suspended Sediment CSs1	CSs2	CSs3	CSs4	CSs5	CSs6	CSs7	Concentration of Bedload Sediment CSb1	CSb2	CSb3	CSb4	CSb5	CSb6	CSb7	0.21	0.10	kg/s
g - h																																																	
	0 091	0 076	0 015	0 263	0 220	0 043	0 043	0 346	0 347	0 337	1 922	0 114	0 00136	0 039	27 8	37 9	0 0286	3.6	0 328	3 21	0 78	0 82	0 86	0 92	0 99	1 06	1 15	0 26	0 25	0 25	0 24	0.23	0.22	0.21	2.1	3.5	6.4	12 3	25 4	52.2	114.9	6.9	8.1	9 6	11.4	13 6	16 1	19 0	0.0003	0 0002	0.0035
j	0 084	0 072	0 013	0 258	0 209	0 049	0 043	0 327	0 342	0 261	1 911	0 110	0 00136	0 038	26 8	37 5	0 0273	3.6	0 315	3 21	0 74	0 78	0 83	0 88	0 94	1 02	1 10	0 26	0 25	0 24	0 23	0 23	0.22	0.21	1.4	2.4	4.4	8.7	18 6	39.0	87.8	4.5	5.5	6.7	8.2	10 1	12.1	14.6	0.0002	0 0001	0.0024
k	0.079	0.069	0.010	0.263	0.220	0.043	0.043	0.300	0.314	0.225	1.824	0.121	0.00136	0.040	23.4	38.3	0.0245	3.6	0.275	3.21	0.82	0.85	0.89	0.73	0.79	0.85	0.92	0.24	0.24	0.23	0.22	0.22	0.21	0.20	0.7	1.2	2.4	4.9	10.8	23.2	53.6	2.2	2.8	3.5	4.5	5.7	7.1	8.7	0 0001	0 0001	0.0014
	0 082	0 073	0 009	0 291	0 248	0 043	0 043	0 282	0 296	0 204	1 876	0 132	0 00136	0 042	21 1	37 1	0 0238	4 6	0 248	3 21	0 54	0 57	0 60	0 64	0 69	0 74	0 80	0 24	0 23	0 22	0 22	0 21	0 20	0 19	0 4	0 8	1 5	3 2	7 3	16.0	37.6	1 3	1 7	2 2	2 9	3 8	4 8	6 0	0.0001	0 0000	0 0010
m	0 087	0 074	0 013	0 291	0 248	0 043	0 043	0 297	0 297	0 298	1 991																																									
n - o																																																			

Test LORW

Depth above bankfull 42 48 mm
Discharge measured 0 12 m /s
Discharge calculated by summation of velocities

Section	Discharge (m³/s) Main channel Qa	Below BF Qbf	Above BF Qa-bf	Areas (m²) Main channel Aa	Below BF Abf	Above BF Aa-bf	Actual	Velocities (m/s) Main channel Ua	Below BF Ubf	Above BF Ua-bf	P (m)	R	S	Ua*	C	C vr	Ua*'vr	d90 (mm)	Fr	σg	Hiding Functions e1	e2	e3	e4	e5	e6	e7	Critical Velocities Ucr1	Ucr2	Ucr3	Ucr4	Ucr5	Ucr6	Ucr7	Concentration of Suspended Sediment CSs1	CSs2	CSs3	CSs4	CSs5	CSs6	CSs7	Concentration of Bedload Sediment CSb1	CSb2	CSb3	CSb4	CSb5	CSb6	CSb7	0 21	0 10	kg/s
g	0.071	0.063	0 008	0.271	0.214	0.058	0.068	0.260	0.295	0.131	1.874	0.114	0.00136	0.039	20.9	40.4	0.0202	2 6	0.246	3.21	0.54	0.56	0.59	0.63	0.68	0.73	0.79	0.23	0.23	0.22	0.22	0.21	0.20	0.19	0.1	0.2	0.6	1.4	3.6	8.7	22.2	0.4	0.6	0.9	1.3	1.9	2.7	3.7	0 0001	0 0000	0.0005
h	0.096	0 078	0 018	0 345	0.280	0 065	0 068	0 279	0 279	0 278	1 884	0 149	0 00136	0 045	19 6	39 9	0 0219	3 6	0 231	3 21	0 49	0 52	0 55	0 58	0 62	0 67	0 73	0 23	0 22	0 22	0 21	0 20	0 20	0 19	0 4	0 7	1 5	3 1	6 8	14 8	34.4	1 3	1 6	2 1	2 7	3 5	4 3	5 4	0 0001	0 0001	0.0012
i	0.087	0 066	0 021	0 295	0 228	0 067	0 068	0 294	0 290	0 308	2 078	0 110	0 00136	0 038	24 1	37 5	0 0245	3 6	0 284	3 21	0 65	0 68	0 72	0 76	0 82	0 88	0 96	0 25	0 24	0 23	0 23	0 22	0 21	0 20	0 5	1 0	1 9	4 1	9 4	20 7	48.8	1 7	2 2	2 9	3 9	5 1	6 4	8 1	0 0002	0 0001	0 0014
j	0 064	0 042	0 022	0 203	0.125	0.078	0 068	0 316	0.336	0 283	1 937	0 090	0 00136	0 035	26 6	36.0	0 0275	3 6	0 336	3 21	0 81	0 85	0 90	0 95	1 03	1 10	1 20	0 26	0 25	0 25	0 24	0 23	0 22	0 21	0 9	1 6	3 2	6 6	14 8	32 3	75.4	3 0	3 9	5 0	6 5	8 3	10 4	13 0	0.0003	0 0002	0.0016
k - o											1 879																																								

Test HOSW

Depth above bankfull 69 03 mm
Discharge measured 0 449 m /s
Discharge calculated by summation of velocities

Section	Discharge (m³/s) Main channel Qa	Below BF Qbf	Above BF Qa-bf	Areas (m²) Main channel Aa	Below BF Abf	Above BF Aa-bf	Actual	Velocities (m/s) Main channel Ua	Below BF Ubf	Above BF Ua-bf	P (m)	R	S	Ua*	C	C vr	Ua*'vr	d90 (mm)	Fr	σg	Hiding Functions e1	e2	e3	e4	e5	e6	e7	Critical Velocities Ucr1	Ucr2	Ucr3	Ucr4	Ucr5	Ucr6	Ucr7	Concentration of Suspended Sediment CSs1	CSs2	CSs3	CSs4	CSs5	CSs6	CSs7	Concentration of Bedload Sediment CSb1	CSb2	CSb3	CSb4	CSb5	CSb6	CSb7	0 21	0.10	kg/s
g											1 617																																							
h	0 106	0 056	0 050	0 312	0 202	0 110	0 110	0 341	0 278	0 457	1 651	0 109	0 00136	0 038	28 0	40 0	0 0267	2 6	0 33	3 21	0 79	0 83	0 87	0 93	1 00	1 08	1 17	0 26	0 25	0 25	0 24	0 23	0 22	0 21	1 9	3 2	5 8	11.4	23 8	49.2	109.1	8.2	7.4	8.8	10.6	12 9	15.3	18.2	0.0006	0.0004	0.0039
i	0.147	0 092	0 055	0 323	0 212	0 110	0 110	0 455	0 433	0 496	1 660	0 114	0 00136	0 039	36 5	37 9	0 0378	3 6	0 43	3 21	1 07	1 12	1 18	1 28	1 36	1 48	1 58	0 29	0 28	0 28	0 27	0 26	0 25	0 24	9 5	15 2	25.6	46 4	90.3	175 5	367.1	31 4	34.6	38.5	43.1	48 5	54.1	60 6	0.0022	0.0013	0.0162
j - m																																																			
n	0 146	0 094	0 052	0 348	0 236	0 112	0 110	0 419	0 398	0 465	1 901	0 124	0 00136	0 041	32 3	35 1	0 0374	5 6	0 38	3 21	0 94	0 98	1 04	1 11	1 19	1 28	1 39	0 27	0 27	0 26	0 25	0 24	0 23	0 23	6 5	10 5	17.8	32 4	63 5	124 1	261.0	21.1	23.5	26.2	29 6	33 5	37 6	42 3	0.0016	0.0009	0.0120
o	0.130	0.089	0 041	0.345	0.235	0.110	0.110	0.376	0.379	0.368	1.882	0.126	0.00136	0.041	28.7	33.9	0.0347	6.6	0.338	3.21	0.81	0.85	0.90	0.98	1.03	1.11	1.21	0.26	0.26	0.25	0.24	0.23	0.22	0.21	3.6	5.9	10.2	19.1	38.2	76.1	163.1	11.6	13.2	15.0	17.3	20.1	23.0	26.4	0.0010	0.0006	0.0070

Test HORW

Depth above bankfull 75 74 mm
Discharge measured 0 163 m /s
Discharge calculated by summation of velocities

Section	Discharge m /s) Main channel Qa	Below BF Qbf	Above BF Qa-bf	Areas (m²) Main channel Aa	Below BF Abf	Above BF Aa-bf	Actual	Velocities (m/s) Main channel Ua	Below BF Ubf	Above BF Ua-bf	P (m)	R	S	Ua*	C	C' vr	Ua*'vr	d90 (mm)	Fr	σg	Hiding Functions e1	e2	e3	e4	e5	e6	e7	Critical Velocities Ucr1	Ucr2	Ucr3	Ucr4	Ucr5	Ucr6	Ucr7	Concentration of Suspended Sediment CSs1	CSs2	CSs3	CSs4	CSs5	CSs6	CSs7	Concentration of Bedload Sediment CSb1	CSb2	CSb3	CSb4	CSb5	CSb6	CSb7	0 21	0 10	kg/s
g											1 864																																							
h	0 115	0 095	0 020	0 452	0 346	0 108	0 121	0 254	0 275	0 186	1 927	0 180	0 00136	0 049	16 3	43 9	0 0181	2 6	0 191	3 21	0 39	0 41	0 43	0 46	0 49	0 53	0 58	0 21	0 21	0 20	0 20	0 19	0 18	0 18	0 2	0 4	0 8	1 7	3 8	8.5	20 1	0 8	0 8	1 1	1 4	1 9	2 4	3 0	0 0001	0 0001	0.0008
	0 118	0 084	0 034	0 397	0 280	0 117	0 121	0 298	0 300	0 293	1 963	0 143	0 00136	0 044	21 4	39 6	0 0236	3 6	0 252	3 21	0 55	0 58	0 61	0 65	0 70	0 75	0 82	0 24	0 23	0 22	0 22	0 21	0 20	0 19	0 7	1 3	2 4	4 8	10 4	22 0	50.0	2 2	2 8	3 4	4 3	5 3	6 5	7 9	0 0003	0 0002	0.0021
j	0 101	0 054	0 047	0 291	0 173	0 119	0 121	0 346	0 312	0 395	1 945	0 089	0 00136	0 034	31 5	35 9	0 0302	3 6	0 371	3 21	0 91	0 96	1 01	1 08	1 16	1 24	1 35	0 27	0 26	0 26	0 25	0 24	0 23	0 22	1 9	3 3	6 1	12 1	25 9	54 4	122.5	6 4	7 9	9 6	11 6	14 6	17 6	21 3	0 0008	0 0005	0 0040
k	0.090	0.057	0 033	0.327	0.208	0.119	0.121	0.274	0.274	0.274	1.896	0.110	0.00136	0.038	22.5	37.5	0.0229	3.6	0.284	3.21	0.59	0.62	0.65	0.70	0.75	0.80	0.87	0.24	0.23	0.23	0.22	0.21	0.21	0.20	0.2	0.5	1.0	2.3	5.5	12.8	31.6	0.7	1.1	1.5	2.2	3.0	4.0	5.3	0 0002	0 0001	0.0009
- o																																																			

Appendix 5: Flood Channel Facility Reference sheet

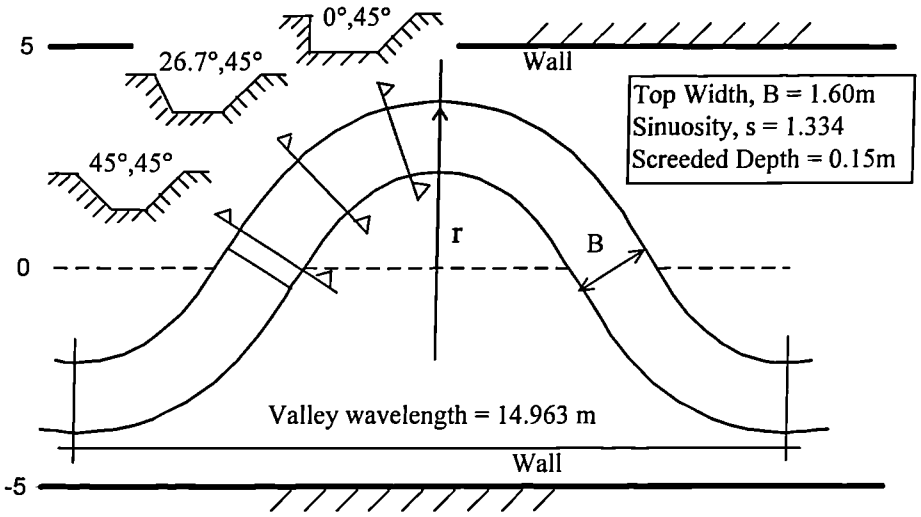

Figure A5. 1 Plan view of one wavelength of the Flood Channel Facility: Series C Mixed grain configuration with wide floodplains

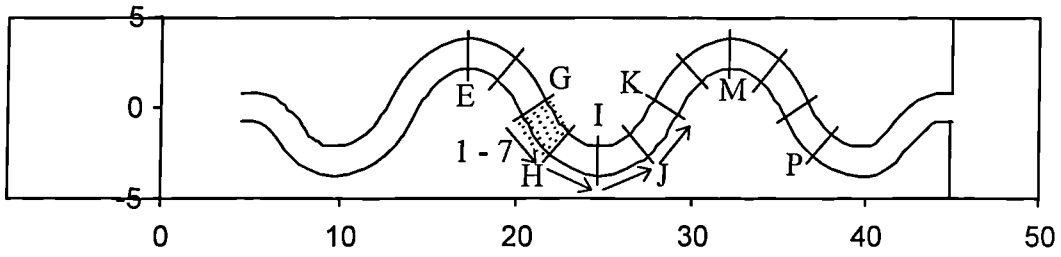

Figure A5. 2 Measuring positions: Velocities G - K, Bed profiles G, G1 - J7, K - N, Water surface slope E - P

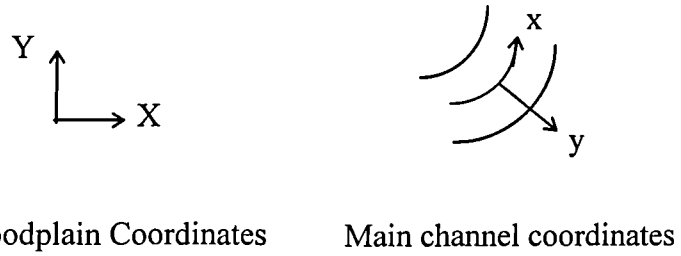

Figure A5. 3 Floodplain and main channel Co-ordinate Systems

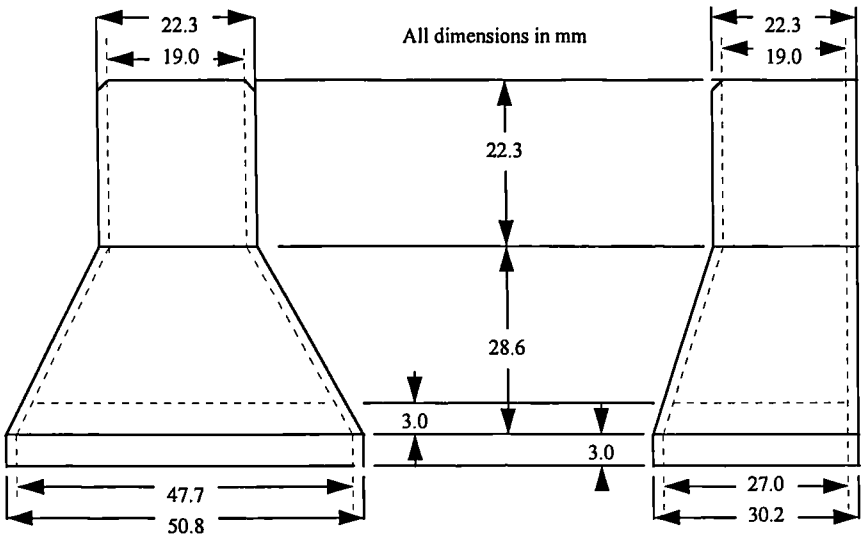

Figure A5. 4Dimensions of the Helley Smith sampler used in the channel.